# UNIVERSITÉ DU QUÉBEC À MONTRÉAL

DYNAMIQUES INTRA-ANNUELLES DES ISOTOPES DU CARBONE ET DE L'OXYGÈNE ET DE LA FORMATION DU BOIS CHEZ L'ÉPINETTE NOIRE DANS LA FORÊT BORÉALE D'AMÉRIQUE DU NORD

THÉSES

PRÉSENTÉE

COMME EXIGENCE PARTIELLE

DU DOCTORAT EN BIOLOGIE

PAR

SEPIDEH NAMVAR

# UNIVERSITÉ DU QUÉBEC À MONTRÉAL

# INTRA-ANNUAL DYNAMICS OF CARBON AND OXYGEN ISOTOPES AND WOOD FORMATION IN BLACK SPRUCE WITHIN NORTH AMERICA'S BOREAL FOREST

**THESIS** 

**PRESENTED** 

AS A PARTIAL REQUIREMENT

FOR THE DOCTORAL IN BIOLOGY

BY

SEPIDEH NAMVAR

# UNIVERSITÉ DU QUÉBEC À MONTRÉAL Service des bibliothèques

# Avertissement

La diffusion de cette thèse se fait dans le respect des droits de son auteur, qui a signé le formulaire *Autorisation de reproduire et de diffuser un travail de recherche de cycles supérieurs* (SDU-522 – Rév.12-2023). Cette autorisation stipule que «conformément à l'article 11 du Règlement no 8 des études de cycles supérieurs, [l'auteur] concède à l'Université du Québec à Montréal une licence non exclusive d'utilisation et de publication de la totalité ou d'une partie importante de [son] travail de recherche pour des fins pédagogiques et non commerciales. Plus précisément, [l'auteur] autorise l'Université du Québec à Montréal à reproduire, diffuser, prêter, distribuer ou vendre des copies de [son] travail de recherche à des fins non commerciales sur quelque support que ce soit, y compris l'Internet. Cette licence et cette autorisation n'entraînent pas une renonciation de [la] part [de l'auteur] à [ses] droits moraux ni à [ses] droits de propriété intellectuelle. Sauf entente contraire, [l'auteur] conserve la liberté de diffuser et de commercialiser ou non ce travail dont [il] possède un exemplaire.»

#### **ACKNOWLEDGMENTS**

I would like to express my deepest gratitude to my research supervisors for their invaluable support throughout this journey. I am especially thankful to Professor Étienne Boucher for his exceptional guidance, expertise, and unwavering support, which have been instrumental in shaping this work. I am also sincerely grateful to Professor Hubert Morin for his dedicated mentorship and invaluable contributions, particularly in fieldwork, which were essential to the successful completion of this research.

I extend my sincere appreciation to my advisors, Professor Annie Deslauriers and Professor Fabio Gennaretti, whose guidance, expertise, and continuous encouragement have been crucial throughout this journey. Their constructive feedback and insightful discussions have greatly enriched my research experience and helped me navigate challenges and refine my scientific perspective. Their unwavering support has not only strengthened this study but has also inspired me to push the boundaries of my knowledge and skills.

My heartfelt thanks also go to my colleagues at Université du Québec à Montréal (GEOTOP, Laboratoire de dendrochronologie, Laboratoire de géochimie des isotopes stables à la légers) and Université du Québec à Chicoutimi (Département des sciences fondamentales, Laboratoire d'écologie végétale et animale) for their collaboration, support, and dedication during fieldwork and laboratory analyses. Their technical assistance, thoughtful discussions, and shared commitment to scientific inquiry have been invaluable in shaping this research.

I would like to thank my jury members Professor Paolo Cherubini, Professor Annie Desrochers, and Dr. Jean-François Hélie, for taking the time to evaluate my work and for providing valuable insights, constructive comments, and encouragement that greatly improved the quality of this thesis.

Finally, I am profoundly grateful to my family, especially my husband, Hadi, as well as my friends, for their unwavering support, insightful conversations, and constant encouragement. Their generosity, kindness, and belief in me have been a source of strength throughout this journey. This thesis would not have been possible without their continuous support, patience, and inspiration.

# **DEDICATION**

"The important thing is not to stop questioning. Curiosity has its own reason for existence. One cannot help but be in awe when he contemplates the mysteries of eternity, of life, of the marvelous structure of reality. It is enough if one tries merely to comprehend a little of this mystery each day."

- Albert Einstein, *Life Magazine, May 2, 1955* 

#### **FOREWORD**

Trees in boreal forests are experiencing increased stress and altered growth dynamics due to rising temperatures and changing precipitation patterns driven by climate change. Understanding the physiological aspects of tree growth, wood formation dynamics, and its ability to acclimate to environmental constraints is crucial for predicting future changes in vegetation in this vast region. Stable isotope analysis combines precise and accurate dating with the sensitivity of isotope ratios to various physiological processes and environmental factors. Despite significant advancements in intra-annual stable isotope analyses, a suitable non-lethal method for real-time monitoring of seasonal carbon and oxygen isotopic fractionation in tree rings remains lacking. Developing such a method would enhance our understanding of post-photosynthetic processes and their interactions with isotopic signals, as well as the leaf-level physiological factors regulating wood formation dynamics during the growing season. This knowledge gap introduces uncertainties about the processes influencing isotopic signals, increasing the risk of misinterpretations in dendroclimatological studies.

This thesis aims to monitor weekly variations of carbon ( $\delta^{13}$ C) and oxygen ( $\delta^{18}$ O) stable isotopes in the growing cambium-xylem continuum of black spruce [*Picea mariana* (Mill.) BSP.] in the North American boreal forest. To achieve this, a suitable non-lethal sampling method is developed, and weekly  $\delta^{13}$ C and  $\delta^{18}$ O series are analysed. Wood formation dynamics are investigated by collecting microcores to track xylogenesis and cell traits during the growing season. The findings provide novel insights into carbon source-sink dynamics, plant hydrodynamics, and the primary factors constraining wood formation dynamics during the growing season in boreal forest ecosystems.

# **TABLE OF CONTENTS**

ACKNOWLEDGMENTS	iii
DEDICATION	iv
FOREWORD	ν
TABLE OF CONTENTS	Vi
LIST OF FIGURES	ix
LIST OF TABLES	Xi
LIST OF EQUATIONS	
LIST OF ABBREVIATIONS AND ACRONYMS	
LIST OF SYMBOLS AND UNITS	
RÉSUMÉ	
ABSTRACT	
CHAPTER 1 INTRODUCTION	
1.1 The context and current state of knowledge	
1.2 Objectives and hypothesis	
1.3 Experimental approach	
1.4 Structure of the thesis	
1.5 Figures Legend	
1.6 Figures	
CHAPTER 2 Monitoring weekly $\delta^{13}$ C variations along the cambium xy	
eastern boreal forest	
2.1 Abstract	
2.2 Introduction	
2.3 Materials and Methods	
2.3.1 Study area2.3.2 Sample preparation	
2.3.3 Sampling the cambial region	
2.3.4 Sampling the developing xylem (α-cellulose)	
2.3.5 Analysis of carbon stable isotope ratios	
2.3.6 Statistical analysis	
2.3.6.1 Climate response and $\delta^{13}C_{cam}$ and $\delta^{13}C_{xc}$ variations	21

2.4 Results	22
2.4.1 Intra-annual $\delta^{13}C_{cam}$ and $\delta^{13}C_{xc}$ variability	23
2.4.2 Inter-annual $\delta^{13}C_{cam}$ and $\delta^{13}C_{xc}$ variability	24
2.4.3 Relationships between $\delta^{13}C_{cam\_cor}$ and $\delta^{13}C_{xc\_cor}$ series and climate data	24
2.5 Discussion	25
2.6 Conclusions	30
2.7 Figures Legend	31
2.8 Tables Legend	32
2.9 Figures	33
2.10 Tables	39
CHAPTER 3 Weekly carbon and oxygen isotope dynamics in black spruce: a case str	udv in the
northeastern boreal forest of Quebec, Canada	
3.1 Abstract	45
3.2 Introduction	46
3.3 Materials and Methods	48
3.3.1 Study sites	48
3.3.2 Collection of cambial region and forming tree ring	49
3.3.3 Analysis of stable isotopes ratios	
3.3.4 Collection of rainwater	
3.3.5 Statistical analysis	51
3.4 Results	
3.4.1 Seasonal trends in $\delta^{13}C$ and $\delta^{18}O$ in the cambial region and developing tree ri	
3.4.2 Relationships between $\delta^{18}$ O and $\delta^{18}$ O <sub>rain</sub> series	
3.4.3 Relationships between $\delta^{13}$ C and $\delta^{18}$ O series and climate data	
3.4.4 Comparison between $\delta^{18}O_{cam}$ , $\delta^{18}O_{xc}$ , and $\delta^{18}O_{xc-sim}$ across $P_{ex}$ scenarios	56
3.5 Discussion	56
3.6 Conclusions	62
3.7 Figures Legend	63
3.8 Tables Legend	63
3.9 Figures	65
3.10 Tables	70
CHAPTER 4 Wood formation dynamics in black spruce: linking leaf-level physiologic	cal drivers and
environmental factors	
4.1 Abstract	76
4.2 Introduction	77
4.3 Materials and Methods	79
4.3.1 Study area	79

4.	3.2	Tree selection and sampling of microcores and wood strips	80
4.	3.3	Xylem formation	80
4.	3.4	Wood anatomy	
4.	3.5	Dynamics of xylem formation	
4.	3.6	Stable carbon isotope analysis	
	3.7	Calculation of iWUE	
	3.8	MODIS NDVI data	
	3.9	Meteorological data	
4.	3.10	Statistical analyses	85
4.4	Resu	ılts	85
4.5	Disc	ussion	87
4.6	Cond	clusions	92
4.7	Figu	res Legend	92
4.8	Tabl	es Legend	93
4.9	Figu	res	95
4.10	Tabl	es	101
GEN	ERAL	CONCLUSIONS	104
APP	ENDI)	( A	109
		$\Lambda.1$ Two step correction of $\delta^{13}C_{cam}$ and $\delta^{13}C_{xc}$ series for intra-seasonal variations in atmospherical contents of $\delta^{13}C_{cam}$	
$\delta^{13}C$	$(\delta^{13}C$		109
Met	hod A	$\Lambda.2$ Detrending the $\delta^{13}C_{xc\_cor}$ series	110
Арр	endix	A Figure legends	110
Арр	endix	A Table legends	111
APP	ENDI)	К.В	126
Met	hod E	$8.1$ Correction of $\delta^{13}C_{cam\_raw}$ and $\delta^{13}C_{xc\_raw}$ values for the Suess-effect	126
Арр	endix	B Figure Legend	126
Арр	endix	B Table Legend	126
APP	ENDI)	Κ C	139
		C Figure Legends	
		C Table Legends	
RFFI	FRFN	rfs	148

# **LIST OF FIGURES**

Figure 1.2.1 Schematic overview of the three main chapters of this thesis
Figure 1.3.1 Study sites: Simoncouche (SIM) and Bernatchez (BER), located in northeastern boreal forest of Quebec, Canada
Figure 2.1 Differentiation of cells in the xylem and cambial region during the growing season. CR refers to the cambial region (cambium and differentiating phloem and xylem cells)
Figure 2.2 Topography of the Saguenay-Lac-Saint-Jean area in eastern Quebec, Canada34
Figure 2.3 Collection techniques for the cambial region and developing tree ring
Figure 2.4 Intra-annual $\delta^{13}C_{cam}$ and $\delta^{13}C_{xc}$ profiles in SIM and BER. Both series are depicted for each site in every study year
Figure 2.5 Comparison of the $\delta^{13}C_{cam}$ and $\delta^{13}C_{xc}$ profiles between two sites, SIM and BER, over two study years of 2020 and 2021
Figure 2.6 Matrix of inter-trees' correlation between $\delta^{13}C_{xc}$ series for SIM and BER in different study years (Pearson's correlation)
Figure 3.1 Topography of the Saguenay-Lac-Saint-Jean region in Quebec, Canada
Figure 3.2 Intra-annual $\delta^{13}C_{cam}$ and $\delta^{18}O_{cam}$ profiles in SIM (a, b, c) and BER (d, e)
Figure 3.3 Intra-annual $\delta^{13}C_{xc}$ and $\delta^{18}O_{xc}$ profiles in SIM (a, b, c) and BER (d, e)
Figure 3.4 Scatterplots and regression lines of weekly $\delta^{18}O_{cam}$ and $\delta^{18}O_{xc}$ as a function of $\delta^{18}O_{rain}$ in SIM 2020 (a), SIM 2021 (b), and BER 2020 (c) and BER 2021 (d)
Figure 3.5 Comparison of the slopes between observed $\delta^{18}O_{cam}$ , $\delta^{18}O_{xc}$ , and simulated $\delta^{18}O_{xc}$ ( $\delta^{18}O_{xc-sim}$ ) under three $P_{ex}$ scenarios during the growing season
Figure 4.1 Topography of the Saguenay-Lac-Saint-Jean region in Quebec province (highlighted within the square on the left map), Canada95
Figure 4.2 Selected tree sample and sampling area in black spruce
Figure 4.3 Wood formation dynamics and cell traits analysis
Figure 4.4 Kinetics of cell formation in black spruce
Figure 4.5 Box plots of different variables including cell enlargement rate $(r_E)$ (a), wall deposition rate $(r_W)$ (b), cell production rate $(r_D)$ (c), iWUE (d), soil water content (VWC) (e), NDVI (f) in the two study sites and years

Figure 4.6 Principal component analysis (PCA) representing the variability of different factors explained by the first two dimensions and their relative contribution (%)
Figure A.1 $\delta^{13}C_{xc}$ profiles in each of the five tree samples in each site and study years
Figure A.3 Corrected $\delta^{13}C_{cam}$ profiles for the Suess-effect and seasonal atmospheric $\delta^{13}C_{atm}$ using the $\delta^{13}C_{atm}$ values collected from the Argyle station (AMT) in different study years at SIM (a, b, c) and BER (d, e)
Figure A.4 Corrected $\delta^{13}C_{xc}$ profiles for the Suess-effect and seasonal atmospheric $\delta^{13}C$ using the $\delta^{13}C$ values collected from the Argyle station (AMT), in different study years at SIM (a, b, c) and BER (d, e)
Figure A.5 Corrected $\delta^{13}C_{cam}$ profiles for the Suess-effect and seasonal atmospheric $\delta^{13}C_{atm}$ using the $\delta^{13}C_{atm}$ values collected from the Lac La Biche station (LLB) in different study years at SIM (a, b, c) and BEI (d, e)
Figure A.6 Corrected $\delta^{13}C_{xc}$ profiles for the Suess-effect and seasonal atmospheric $\delta^{13}C$ using the $\delta^{13}C$ values collected from the Lac La Biche station (LLB) in different study years at SIM (a, b, c) and BEI (d, e)
Figure A.7 Variations of $\delta^{13}C_{cam\_cor,}$ and $\delta^{13}C_{xc\_cor,}$ series (a), and climatic variables (Daytime averages (8h00 to 18h00) of $T_{max}$ (b), VPD (c), PAR (d), RH (c), P (f), VWC (g)) in SIM2019, SIM 2020, and SIM 2021
Figure A.8 Variations of $\delta^{13}C_{cam\_cor,}$ and $\delta^{13}C_{xc\_cor,}$ series (a), and climatic variables (Daytime averages (8h00 to 18h00) of $T_{max}$ (b), VPD (c), PAR (d), RH (c), P (f), VWC (g)) in BER 2020 and 2021119
Figure A.9 Matrix of correlations between $\delta^{13}C_{xc\_seq}$ values for each of five tree samples and differen climatic variables for SIM (a, b, c) and BER (d, e).
Figure B.1 Collection and analysis of rain samples in the field
Figure B.2 Comparison between global meteoric water line (blue solid line) with the SIM and BER meteoric water line (red dashed line) for the two growing seasons of 2020 and 2021
Figure C.1 (a) $\delta^{13}C_{atm\_AMT}$ and (b) $c_{a\_AMT}$ profiles during the two growing seasons of 2020 and 2021 140
Figure C.2 intrinsic Water Use Efficiency (iWUE) of black spruce in two different sites of SIM and BER during the two growing seasons of 2020 and 2021.
Figure C.3 Kinetics of cell formation and meteorological variables during the growing season 142

# **LIST OF TABLES**

Table 2.1 Location, tree characteristics, and climatic conditions at the two study sites
Table 2.2 The climatic variables, codes, and units
Table 2.3 Statistics of mean inter-trees correlation (Rbar) of $\delta^{13}C_{xc}$ and weekly EPS (EPS <sub>w</sub> ) in two sites 41
Table 2.4 Correlation coefficients for the relationships between $\delta^{13}C_{cam\_cor}$ and different climatic variables of daytime averages (8h00 to 18h00).
Table 2.5 Correlation coefficients for the relationships between $\delta^{13}C_{xc\_cor}$ and $\delta^{13}C_{xc\_seq}$ different climatic variables of daytime averages (8h00 to 18h00)43
Table 3.1 Location, tree characteristics, and climatic conditions at the two study sites. Latitude (Lat.) longitude (Long.), altitude (Alt, meters above sea level)
Table 3.2 Correlation coefficients and p-values between $\delta^{13}$ C and $\delta^{18}$ O values in the cambium and xylem cellulose in different study sites and years
Table 3.3 Correlation coefficients for the relationships between $\delta^{18}O_{cam}$ or $\delta^{18}O_{xc}$ values and $\delta^{18}O_{rain}$ ir different study sites and years.
Table 3.4 Correlation coefficients for the relationships between $\delta^{13}C_{cam}$ or $\delta^{18}O_{cam}$ values and different weekly meteorological variables of daytime averages (8h00 to 18h00) over the growing season 73
Table 3.5 Correlation coefficients for the relationships between $\delta^{13}C_{xc}$ or $\delta^{18}O_{xc}$ values and different weekly meteorological variables of daytime averages (8h00 to 18h00) over the growing season
Table 4.1 Location, tree characteristics, and climatic conditions at the two study sites
Table 4.2 Mean values (± SD) of different variables During the growing season
Table 4.3 Correlation between axes of the principal component analysis (PCA <sub>1</sub> and PCA <sub>2</sub> ) and different variables
Table A.1 Sample code, age, and stem diameter of five selected tree individuals in study years of 2019 (Justin SIM), 2020, and 2021, both in Simoncouche (SIM) and Bernatchez (BER)
Table A.2 Number of dates of sampling and/or wood strips collected from each of five tree samples during each of the growing seasons in SIM (2019-2021) and BER (2020-2021)
Table A.3 Propagation uncertainty (±standard deviation, ‰) associated with $\delta^{13}C$ values corrected for ai composition in xylem cellulose ( $\delta^{13}C_{xc\_cor}$ ) and cambial carbohydrate ( $\delta^{13}C_{cam\_cor}$ )
Table A.4 The time periods (day of year) to average $\delta^{13}C_{atm}$ data collected from the Argyle (AMT) and Lae La Biche (LLB) atmospheric $\delta^{13}C$ measurement stations

Table A.5 Regression analysis results for $\delta^{13}C_{xc}$ values in each tree sample in SIM and BER for each of the study years (the trees are different in each year of sampling)
Table B.1 Sample code, age, and stem diameter of the five selected tree individuals in study years of 2019 (Just in SIM), 2020, and 2021, both in Simoncouche (SIM) and Bernatchez (BER)
Table B.2 Number of wood strips collected from each of five tree samples during each of the growing seasons in SIM (2019-2021) and BER (2020-2021)
Table B.3 Mean values of $\delta^{13}C_{xc}$ and $\delta^{13}C_{cam}$ , mean inter-trees correlation (Rbar) of $\delta^{13}C_{xc}$ and weekly EPS (EPS <sub>w</sub> ) for the two sites: SIM (2019-2021) and BER (2020-2021)
Table B.4 Mean values of $\delta^{18}O_{xc}$ and $\delta^{18}O_{cam}$ , mean inter-trees correlation (Rbar) of $\delta^{18}O_{xc}$ and weekly EPS (EPS <sub>w</sub> ) for the two sites: SIM (2019-2021) and BER (2020-2021)
Table B.5 Regression slopes and significance level for $\delta^{13}C$ and $\delta^{18}O$ values in the cambial region ( $\delta^{13}C_{cam}$ , $\delta^{18}O_{cam}$ ) and developing tree ring ( $\delta^{13}C_{xc}$ , $\delta^{18}O_{xc}$ ) in SIM and BER for each of the study years 134
Table B.6 Correlation coefficients and p-values between pre-whitened detrended residuals of $\delta^{13}$ C and $\delta^{18}$ O in the cambium and xylem cellulose in different study sites and years
Table B.7 Correlation coefficients for the relationships between pre-whitened detrended residuals of $\delta^{13}C_{cam}$ or $\delta^{18}O_{cam}$ and residuals of different meteorological weekly variables of daytime averages (8h00 to 18h00)
Table B.8 Correlation coefficients for the relationships between pre-whitened detrended residuals of $\delta^{13}C_{xc}$ or $\delta^{18}O_{xc}$ and residuals of different meteorological weekly variables of daytime averages (8h00 to 18h00)
Table B.9 The mean $\delta^{18}O_{rain}$ values in SIM and BER for the growing seasons of 2020 and 2021. Sampling was done on a weekly basis at two study years during the sampling periods at each study year 138
Table C.1 Sample code, age, and stem diameter of five selected tree individuals in study years of 2020 and 2021, both in Simoncouche (SIM) and Bernatchez (BER)
Table C.2 Number of dates of sampling and/or wood strips and micro cores collected from each of five tree samples during each of the growing seasons in SIM (2020-2021) and BER (2020-2021)
Table C.3 Propagation of uncertainty ( $\pm$ SD) in carbon isotope discrimination ( $\Delta$ ) and relative sensitivities to $\delta^{13}$ C of atmospheric CO <sub>2</sub> ( $\delta^{13}$ C <sub>atm_AMT</sub> ) and $\delta^{13}$ C <sub>cam</sub>
Table C.4 Correlation coefficients for the relationships between iWUE <sub>cam</sub> and iWUE <sub>xc</sub> each site and study year (* $p$ < 0.1, ** $p$ < 0.05, *** $p$ < 0.01)
Table C.5 Mean Absolute Error (MAE, cells) and Model Efficiency (EF, %) from the GAMs model 147

# **LIST OF EQUATIONS**

Equation 2.1 Weekly Expressed Population Signal (EPS <sub>w</sub> )	20
Equation 2.2 Correction of $\delta^{13}C$ for seasonal $\delta^{13}C_{atm\_AMT}$ variations and Suess-effect	21
Equation 3.1 Calculation of Slope (rate per day) for P <sub>ex</sub> -effect	53
Equation 3. 2 Calculation of the $P_{ex}$ effect for daily linear increasing or decreasing trends	53
Equation 3.3 Calculation of simulated $\delta^{18}O_{xc}$ for different $P_{ex}$ scenarios	53
Equation 4.1 Calculation of carbon isotope discrimination against <sup>13</sup> C	83
Equation 4.2 Calculation of iWUE in the cambial region (iWUE cam)	84
Equation 4.3 Calculation of Normalized Difference Vegetation Index (NDVI)	84
Equation A.1 Calculation of Suess-effect corrected $\delta^{13}C_{xc}$	109
Equation A.2 Calculation of $\delta^{13}C_{xc}$ based on seasonal atmospheric carbon isotope composition	109
Equation A.3 Calculation of the detrended $\delta^{13}C_{xc\_cor}$ series	110
Equation B.1 Correction of $\delta^{13}$ C for seasonal $\delta^{13}$ C <sub>atm AMT</sub> variations and Suess-effect	126

# LIST OF ABBREVIATIONS AND ACRONYMS

NSC Non-Structural Carbohydrates

SIM Simoncouche

BER Bernatchez

PAR Photosynthetic Active Radiation

PP Photoperiod

iWUE intrinsic Water Use Efficiency

NDVI Normalized Difference Vegetation Index

VPD Vapour Pressure Deficit

RH Relative Humidity

VWC Soil Water Content

P Precipitation

GAMs Generalized Additive Models

DBH Diameter at Breast Height

#### **LIST OF SYMBOLS AND UNITS**

 $\delta^{13}C_{cam}$  Carbon stable isotope ratio in the cambial region

 $\delta^{13}C_{xc}$  Carbon stable isotope ratio in xylem cellulose

 $\delta^{18}O_{xc}$  Oxygen stable isotope ratio in xylem cellulose

 $g_s$  Stomatal conductance

A<sub>net</sub> Net photosynthesis

T<sub>max</sub> Maximum Temperature

°C Degrees Celsius

kPa Kilopascal

% Percentage

% Per mille (parts per thousand)

m<sup>3</sup>/m<sup>3</sup> Cubic meter per cubic meter

mm Millimeter

μmol/m²/s Micromoles per square meter per second

μmol/mol Micromoles per mole

r<sub>E</sub> Cell enlargement rate

r<sub>W</sub> Wall deposition rate

r<sub>D</sub> Cell production rate

Proportional exchange of oxygen isotopes between sugars and xylem water

#### RÉSUMÉ

Les analyses intra-annuelles des isotopes stables  $\delta^{13}$ C et  $\delta^{18}$ O dans différents compartiments de l'arbre sont des outils puissants pour étudier le stockage du carbone et les dynamiques hydriques à des échelles temporelles fines. Dans la tige, le continuum cambium-xylème constitue un site critique pour l'étude des dynamiques des isotopes stables. Cependant, les processus post-photosynthétiques peuvent introduire des différences entre la composition isotopique de ces deux tissus, en raison de l'utilisation de glucides stockés comme substrat pour la croissance, avec des signatures en  $\delta^{13}$ C distinctes. De plus, la formation du bois peut dépendre de différentes sources d'eau au cours de la saison de croissance, modifiant ainsi les signaux en  $\delta^{18}$ O provenant du niveau foliaire. Les avancées récentes dans l'analyse intra-annuelle du  $\delta^{13}$ C et du  $\delta^{18}$ O dans les cernes des arbres ont amélioré notre compréhension des cycles du carbone et de l'eau dans la tige des arbres. Toutefois, un cadre global permettant de suivre les isotopes stables tout au long de la saison de croissance fait encore défaut. Cette lacune limite notre compréhension du stockage du carbone et de l'oxygène dans les cernes des arbres à des échelles temporelles fines et contraint l'utilisation des données de  $\delta^{13}$ C et  $\delta^{18}$ O comme proxys fiables dans les études dendroclimatologiques. De plus, le suivi des valeurs des isotopes du carbone au cours de la saison de croissance offre une opportunité d'analyser l'efficacité intrinsèque d'utilisation de l'eau (intrinsic Water Use Efficiency, iWUE) chez les arbres. Cela permet d'obtenir des informations sur les processus physiologiques au niveau foliaire et les facteurs environnementaux qui régulent la formation du bois durant le développement du cerne annuel. Cette thèse vise à élucider comment les processus post-photosynthétiques influencent les signaux en  $\delta^{13}$ C et  $\delta^{18}$ O dans le continuum cambium-xylème de l'épinette noire (*Picea mariana*) dans la forêt boréale d'Amérique du Nord. Pour ce faire, une méthode non destructive a été développée afin de suivre le fractionnement cumulatif des isotopes du carbone et de l'oxygène au cours de la saison de croissance. L'étude vise également à identifier les principaux facteurs déterminant la dynamique de formation du bois, en mettant l'accent sur l'interaction entre la cinétique de formation des cellules et l'iWUE à des échelles saisonnières.

L'étude a été réalisée dans deux sites, Simoncouche (SIM) et Bernatchez (BER), tous deux situés dans la forêt boréale du Québec, au Canada. Les observations ont été menées au cours des saisons de croissance de 2019 à 2021 pour SIM et de 2020 à 2021 pour BER. Sur chaque site, cinq épinettes noires matures ont été sélectionnées chaque année. De la fin avril à octobre, des échantillons de bandes de bois rectangulaires ont été prélevés chaque semaine sur la tige des arbres afin de suivre la discrimination des isotopes du carbone et de l'oxygène dans le continuum cambium-xylème en croissance. Simultanément, des microcarottes ont été extraites de la zone d'échantillonnage pour surveiller la xylogenèse. Afin d'analyser les traits cellulaires, deux microcarottes supplémentaires ont été prélevées sur chaque arbre à la fin de la saison de croissance (mi-octobre), lorsque le cerne était complètement formé.

Cette étude a permis de développer une méthode innovante pour suivre le fractionnement hebdomadaire du  $\delta^{13}C$  et du  $\delta^{18}O$  dans le continuum cambium-xylème en croissance de l'épinette noire. Des profils hebdomadaires ont été établis pour les isotopes stables du carbone et de l'oxygène dans la région cambiale ( $\delta^{13}C_{cam}$  et  $\delta^{18}O_{cam}$ ) et dans le cerne en formation ( $\delta^{13}C_{xc}$  et  $\delta^{18}O_{xc}$ ). Les résultats suggèrent qu'un apport constant d'assimilats frais au continuum cambium-xylème est le principal moteur de la croissance secondaire sur les deux sites d'étude. Toutefois, le  $\delta^{13}C_{cam}$  et le  $\delta^{13}C_{xc}$  ont été peu influencés par la variabilité climatique, ce qui indique que les variations intra-annuelles de ces profils reflètent probablement des changements dans les stratégies d'allocation du carbone. Ces changements pourraient améliorer la résistance au gel et réduire l'absorption d'eau aux stades tardifs de la croissance, et sont

possiblement liés à la diminution saisonnière du rayonnement photosynthétiquement actif. La conductance stomatique a été identifiée comme le principal facteur physiologique influençant le fractionnement saisonnier du  $\delta^{13}C_{cam}$  et du  $\delta^{18}O_{cam}$ . Cependant, les échanges proportionnels entre l'eau du xylème et les sucres au site de synthèse de la cellulose (effet  $P_{\rm ex}$ ) ont masqué les tendances du  $\delta^{18}O_{\rm cam}$ . Cette découverte suggère que les signaux du  $\delta^{18}O_{xc}$  diffèrent de ceux d'origine dans le puits cambial initial. Alors que le cambium utilise principalement l'eau issue des feuilles, la cellulose du xylème en formation puise à la fois dans l'eau foliaire et dans l'eau du xylème provenant des racines durant la saison de croissance. Des liens négatifs forts entre la cinétique de formation cellulaire (taux d'élargissement des cellules et taux de dépôt pariétal) et l'iWUE suggèrent que les processus physiologiques au niveau foliaire régulent la formation du bois. Une photopériode plus longue et des niveaux de stress hydrique plus faibles ont favorisé des taux élevés d'élargissement cellulaire et de dépôt pariétal. En revanche, les taux de production cellulaire sont davantage influencés par la température et le déficit de pression de vapeur (VPD), avec une augmentation des taux de production cellulaire en réponse à des températures et à un VPD plus élevés dans notre région d'étude. Les résultats ont mis en évidence un découplage entre la dynamique de production cellulaire et l'iWUE chez l'épinette noire durant la saison de croissance, tout en soulignant le lien entre les processus physiologiques foliaires et les contraintes climatiques, telles que la disponibilité en eau du sol.

Les conclusions de cette étude apportent de nouvelles perspectives sur la dynamique saisonnière du carbone et de l'oxygène ainsi que sur les contraintes de croissance secondaire de l'épinette noire dans les écosystèmes de la forêt boréale. En introduisant une approche méthodologique novatrice pour le suivi des signaux isotopiques à des échelles temporelles fines, ce travail comble des lacunes essentielles dans la compréhension des processus d'allocation du carbone et de leurs déterminants environnementaux. Ces résultats mettent en évidence la nécessité d'interpréter avec précaution les signaux isotopiques afin d'éviter toute mauvaise représentation dans les études dendroclimatologiques. De plus, l'étude éclaire les facteurs environnementaux et physiologiques foliaires influençant la dynamique de formation du bois, fournissant ainsi des informations précieuses sur les réponses des arbres aux changements climatiques futurs.

Mots-clés: carbone, oxygène, iWUE, analyse hebdomadaire, forêt boréale

#### **ABSTRACT**

Intra-annual analyses of  $\delta^{13}$ C and  $\delta^{18}$ O stable isotopes in different tree compartments are powerful tools for studying carbon sequestration and water dynamics at finer temporal scales. In the stem, the cambiumxylem continuum serves as a critical site for investigating the dynamics of stable isotopes. However, postphotosynthetic processes can introduce temporal discrepancies, due to the utilization of stored carbohydrates as building blocks, with different  $\delta^{13}$ C signatures. Additionally, wood formation may rely on different water sources throughout the growing season, altering  $\delta^{18}$ O signals originating at the leaf level. Recent advancements in intra-annual  $\delta^{13}$ C and  $\delta^{18}$ O analysis in tree rings have enhanced our understanding of carbon and water cycles within tree stems. However, a comprehensive framework to track stable isotopes throughout the growing season remains lacking. This gap limits our understanding of carbon and oxygen sequestration in tree rings at finer temporal scales and constrains the use of  $\delta^{13}$ C and  $\delta^{18}$ O data as reliable proxies in dendroclimatological studies. Additionally, monitoring carbon isotopes values during the growing season provides an opportunity to analyse intrinsic water use efficiency (iWUE) in trees. This offers insights into the leaf-level physiological processes and environmental factors that regulate wood formation during tree ring development. This thesis aims to elucidate how post-photosynthetic processes influence  $\delta^{13}$ C and  $\delta^{18}$ O signals in the cambium-xylem continuum of black spruce in North America's boreal forest. To achieve this, a non-destructive method was developed to monitor cumulative carbon and oxygen isotope fractionation during the growing season. The study also aims to identify the primary drivers of wood formation dynamics, focusing on the interplay between cell formation kinetics and iWUE at seasonal scales.

The study was conducted at two sites, Simoncouche (SIM) and Bernatchez (BER), both located within the boreal forest of Quebec, Canada. Observations were conducted during the growing seasons of 2019-2021 for SIM and 2020-2021 for BER. At each site, five mature black spruce trees were selected annually. From late April to October, rectangular wood strip samples were collected from tree stem weekly to track carbon and oxygen isotope discrimination in the growing cambium-xylem continuum. Simultaneously, microcores were extracted from the sampling area to monitor xylogenesis. To analyze cell traits, two extra microcores were extracted from each tree sample at the end of the growing season (mid-October), when the tree ring was fully formed.

This study developed a novel method to track weekly  $\delta^{13}C$  and  $\delta^{18}O$  fractionation in the growing cambium-xylem continuum of black spruce. Weekly profiles were created for carbon and oxygen stable isotopes in the cambial region ( $\delta^{13}C_{cam}$  and  $\delta^{18}O_{cam}$ ) and forming tree ring (i.e., developing xylem cellulose;  $\delta^{13}C_{xc}$  and  $\delta^{18}O_{xc}$ ). Results suggest that a constant supply of fresh assimilates to the cambium-xylem continuum drives secondary growth in both study sites. However,  $\delta^{13}C_{cam}$  and  $\delta^{13}C_{xc}$  were minimally influenced by climate variability, indicating that intra-annual variations in these profiles likely reflect shifts in carbon allocation strategies. These shifts may enhance frost resistance and reduce water uptake in late growth stages and are possibly linked to seasonal decreases in photosynthetically active radiation. Stomatal conductance was identified as the dominant physiological factor influencing seasonal fractionation of  $\delta^{13}C_{cam}$  and  $\delta^{18}O_{cam}$ . However, proportional exchanges between xylem water and sugars at the sites of cellulose synthesis (i.e.,  $P_{ex}$  effect) obscured  $\delta^{18}O_{cam}$  trends. This finding suggests that  $\delta^{18}O_{xc}$  signals differ from those originating in the earlier cambium sink. While the cambium predominantly uses water sourced from leaves, developing xylem cellulose accesses both leaf water and root-sourced xylem water during the growing season. Strong negative links between cell formation kinetics (i.e., cell enlargement rate and wall deposition rate) and iWUE, suggest that leaf-level physiological processes regulate wood formation. Higher photoperiod and

lower water stress levels promoted rates of cell enlargement and wall deposition. Conversely, cell production rates are more influenced by temperature and vapour pressure deficit (VPD), with higher temperature and VPD, lead to more rate of cell production in our study region. The results highlighted the decoupling of cell production dynamics and iWUE in black spruce during the growing season while emphasizing the connection between leaf-level physiological processes and climatic constraints like soil water content.

The findings of this study provide novel insights into seasonal carbon and oxygen dynamics and secondary growth constraints of black spruce in boreal forest ecosystems. By introducing a new methodological approach for tracking isotopic signals at fine temporal scales, this work addresses critical gaps in understanding carbon allocation processes and their environmental drivers. These insights highlight the need to carefully interpret isotopic signals to avoid misrepresentation in dendroclimatological studies. Furthermore, the study sheds light on the environmental and leaf-level physiological factors influencing wood formation dynamics, offering valuable information on tree responses to future climate changes.

Keywords: carbon, oxygen, iWUE, weekly analysis, boreal forest

#### **CHAPTER 1**

#### **INTRODUCTION**

#### 1.1 The context and current state of knowledge

Boreal forests are among the largest terrestrial carbon reservoirs, with vast amounts of carbon stored in tree biomass including trunks, branches and foliage. These forests hold about one-third of the global forest carbon stock, with trees sequestering vast amounts of carbon through photosynthesis and biomass accumulation (Ameray et al., 2023; Pan et al., 2011). The longevity of boreal tree species contributes to sustained carbon storage over decades to centuries. This makes them essential components of the global carbon cycle (Bonan, 2008). However, tree carbon stocks in boreal forests are dynamic and influenced by environmental conditions and external disturbances such as wildfires, which can rapidly release stored carbon back into the atmosphere (Gauthier et al., 2015). While regrowth after disturbances enables carbon reaccumulation, the balance between carbon uptake and loss remains highly sensitive to climate change (Bonan, 2008). Global warming is expected to trigger earlier cambial resumption in cold climates like boreal forests (Rossi et al., 2014). This shift may extend the growing season, potentially affecting carbon uptake and the productivity of boreal tree species (Rossi et al., 2014). However, these changes may also alter the long-term role of boreal trees as carbon sinks (Bonan, 2008; Kurz et al., 2008). Given boreal forests' substantial contribution to global carbon storage, understanding carbon dynamics in boreal trees and the physiological constraints governing carbon sequestration in different tree compartments is crucial for predicting future carbon-climate feedback in this vast ecosystem.

Analysis of carbon isotope ratios ( $\delta^{13}$ C) provides valuable insights into tree eco-physiological processes and their responses to climate change (Farquhar et al., 1989; Gessler et al., 2014). Photosynthetic discrimination of  $^{13}$ CO<sub>2</sub> against  $^{12}$ CO<sub>2</sub> in C<sub>3</sub> plants is associated with the ratio of leaf internal to external CO<sub>2</sub> partial pressure ( $c_i/c_a$ ) which, itself, is regulated by stomatal conductance and influenced by the rate of CO<sub>2</sub> assimilation (Farquhar et al., 1982). The carbon signatures preserved in tree rings offer valuable records of past environmental conditions and are widely used for various applications, including the reconstruction of climatic variables such as temperature and precipitation (McCarroll & Loader, 2004), as well as the study of carbon allocation to stem growth in forest ecosystems (Gessler et al., 2014; Saurer et al., 2004). Furthermore, tree-ring carbon isotopes serve as indicators of physiological processes, such as intrinsic water use efficiency (iWUE) and photosynthetic performance. These indicators enable researchers to assess long-term ecological and climatic trends in boreal forests (Gessler et al., 2014).

Most studies on  $\delta^{13}$ C in tree-ring focus on annual timescales, which provide long-term environmental and physiological trends across different species and regions. For example, Bégin et al., (2015) developed the first dendroisotopic series for Canadian northeastern boreal forest, covering 1800 to 2003. In their research they aimed to evaluate the isotopes' sensitivity to climate variables and their potential as proxies for past climate conditions. A temperature reconstruction was developed for the study region based on a regression model that calibrated  $\delta^{13}$ C and  $\delta^{18}$ O against summer maximum temperatures. The research confirmed that carbon dendroisotopic series in high latitudes can adequately document past climatic conditions. The impact of rising CO<sub>2</sub> on tree physiology has also been investigated at annual scales, as demonstrated by Frank et al., (2015), who examined  $\delta^{13}$ C trends in tree rings across European forests and found widespread increases in intrinsic water use efficiency (iWUE), suggesting physiological adjustments to climate change. Furthermore, the effects of drought on carbon assimilation were assessed by Lévesque at al., (2014), who analyzed  $\delta^{13}$ C in annual rings of multiple coniferous species (e.g., *Pinus sylvestris*) in Alpine mountains. They observed strong  $\delta^{13}$ C signals in drought years, influenced by stomatal closure and reduced photosynthetic activity, at the cost of reduces carbon uptake and growth. These studies highlight the significance of annual tree-ring  $\delta^{13}$ C analysis in understanding past climate variations, physiological responses, and long-term carbon assimilation trends in different species.

Annual observations of  $\delta^{13}$ C signals in tree-rings represent the average environmental conditions and integrate the cumulative effects of various physiological processes involved in wood production throughout the entire growing season. However, this approach obscures short-term variations in tree responses to transient climatic events, such as droughts, rainfall episodes, heatwaves, and snowmelt. Moreover, the influence of short-term leaf-level physiological processes on  $\delta^{13}$ C fractionation remains poorly understood (Gessler et al., 2014). The impact and timing of these processes on tree productivity also remains insufficiently explored. To address this limitation, researchers have investigated intra-annual variations in carbon stable isotopes within tree rings (Fu et al., 2017; Porté & Loustau, 2001; Roden et al., 2009; Vaganov et al., 2009). These studies not only enhance our ability to identify external environmental and internal physiological factors influencing the isotopic composition of bulk wood or cellulose throughout the growing season but also provide valuable insights into the carbohydrate dynamics that sustain xylem cell development (Belmecheri et al., 2018; Ogée et al., 2009; Rinne et al., 2015).

Different methods have been used in dendroclimatology to study stable isotopes variations inside tree rings at intra-annual scales. One common method has been to divide wood segments or cores by cutting

tangential slices, using a fixed-blade sledge mounted on a sliding microtome (Ogée et al., 2009; Pons & Helle, 2011; Verheyden et al., 2004), or sampling of tree-rings by manual sub-division (whole ring, early wood /late wood, subdividing each ring into 6-10 sections) using scalpel or razor blades (Barçante Ladvocat Cintra et al., 2019; Brienen et al., 2011; Fu et al., 2017; Roden et al., 2009). For example, Roden et al., (2009) studied intra-annual variation in the stable carbon isotope ratios of cellulose in tree rings of coast redwood. For high-resolution stable isotopes fractionation analysis, they sub-divided each ring of the core into ten equal units and each section was cut out using a scalpel under a 20x dissecting microscope. As described by Schollaen et al., (2014) collecting wood dust from a series of small wood holes drilled in the radial direction with twist drills and sampling by robotic micro milling techniques, are two other methods for stable isotope analysis in high resolutions (Dodd et al., 2008; Fichtler et al., 2010; Gebrekirstos et al., 2009). Sampling tree-rings by laser ablation is another technique in isotope dendroclimatology and provides an essentially non-destructive means for accessing elemental and isotopic information from wood samples at high resolutions (Loader et al., 2017) first described in Schulze et al., (2004). They presented a new method for high-resolution online determination of  $\delta^{13}$ C in tree rings, combining laser ablation (LA), combustion (C), gas chromatography (GC) and isotope ratio mass spectrometry (IRMS) (LA-C-GC-IRMS). In this method sample material was extracted every 6 min with a UV-laser from a tree core, leaving 40-µm-wide holes. The use of laser-sampling has greatly facilitated the production of highresolution chronologies of stable isotopes and the potential for improved replication. Other studies have also been done based on laser ablation method to estimate stable isotope composition of wood at high resolutions (M. Fonti et al., 2018; Loader et al., 2017; Soudant et al., 2016; Vaganov et al., 2009).

While the information obtained by utilizing these methods provide valuable insights into complex interactions between climate and tree physiology over the seasonal scales (Offermann et al., 2011), they do not accurately identify the real-time fractionation of stable isotopes in tree rings. In fact, few of these methods allow to construct a time-integrated, accurately dated chronology of stable isotope fractionation inside tree ring during the growing season. Most intra-annual methods rely on cutting micro-slices from existing samples (i.e., previously formed tree ring) which does not yield an accurate dating which hampers the intercomparison with meteorological conditions, growth process, etc. Indeed, tree ring formation is the result of a complex succession of developmental processes, which rates and durations vary along the growing season (Cuny et al., 2014). Therefore, despite their relatively simple structure, not even conifer tree rings can be seen as a succession of cell rows formed during separate regular time intervals (Rathgeber et al., 2022). Rather, the successive cell rows of a tree ring are formed in highly overlapping time intervals

of variable durations (Cuny et al., 2014; M. Fonti et al., 2018). Thus, in order to take on this problem, a formal and fully integrated method is still needed to track seasonal variations of stable isotopes in the developing tree rings during the growing season. The high-resolution  $\delta^{13}$ C chronologies can be compared with external climatic constraints and internal physiological processes at seasonal scales and provide more accurate information about seasonal changes of internal physiological processes and their interactions with climatic variables.

Another layer of complexity arises from the role of non-structural carbohydrates (NSCs) in carbon source-sink dynamics, allocation, and remobilization within trees. During photosynthesis, plants absorb carbon dioxide (CO<sub>2</sub>) from the atmosphere and H<sub>2</sub>O from the soil and produce NSCs. Once assimilated, NSCs act as energy carriers and building blocks for different anabolic processes such as plant growth or may be stored for future utilization (Carbone et al., 2013). NSCs are transported to various sink tissues and serve as a critical link between photosynthetic carbon uptake and wood formation (Carbone et al., 2013; Richardson et al., 2013). However, uncertainties remain regarding the timing and extent of NSC allocation, storage, and remobilization, as well as the contribution of newly assimilated versus stored carbon to secondary growth (Sala et al., 2012; Wiley & Helliker, 2012). Recent studies suggest that the age and  $\delta^{13}$ C signatures of stored NSCs can vary significantly, leading to potential time lags and isotopic mixing during carbon allocation to developing xylem cells (Gessler et al., 2014; Offermann et al., 2011). Additionally, post-photosynthetic processes, such as carbon exchange during phloem transport and cellulose synthesis, further complicates the interpretation of  $\delta^{13}$ C signals in tree rings (Cernusak et al., 2016; Gessler et al., 2009). These complexities highlight the need for precisely dated intra-annual isotope chronologies as a tool for understanding NSCs origin, movement, and utilization throughout the growing season.

Previous studies have illustrated that deciduous species depend on stored NSCs during the initial stages of wood formation (Kagawa et al., 2006; Offermann et al., 2011; Simard et al., 2013), while evergreens are more capable of relying on recently assimilated resources (Barbour et al., 2002; Klein et al., 2005; Ogée et al., 2009; Soudant et al., 2016). However, a recent study on Mediterranean *Pinus pinea* L. illustrated significant reliance on stored carbon for the development of both earlywood and latewood (Castagneri et al., 2018). This indicates that xylem growth is sustained not only by most recent photosynthetic products but also by carbon that was accumulated for years previously (Von Arx et al., 2017). Despite progress in understanding NSC dynamics across tree species (Fajstavr et al., 2018; Piper, 2020; Rademacher et al., 2022; Richardson et al., 2013), key uncertainties persist regarding NSC allocation pathways, storage, and

time lags (Sala et al., 2012; Wiley & Helliker, 2012), especially in conifers (Schollaen et al., 2014). Since stored NSCs vary in age and  $\delta^{13}$ C composition, their contribution to tree-ring  $\delta^{13}$ C complicates dendroclimatological interpretations. Addressing these challenges requires seasonal monitoring of  $\delta^{13}$ C variations across tree compartments, from leaves to phloem, cambium, and xylem, to better trace the movement and utilization of NSCs for stem growth (Gessler et al., 2009).

The Lack of high-resolution data limits our ability to identify leaf-level physiological controls on carbon assimilation across species. One way to address this uncertainty is by tracking  $\delta^{13}$ C and  $\delta^{18}$ O signals in different tree sinks at seasonal scales. At high-resolution time scales, the decoupling of  $\delta^{13}C$  from  $\delta^{18}O$ variations provides critical insights into the physiological factors regulating carbon assimilation and sequestration at the leaf level (Scheidegger et al., 2000; Siegwolf et al., 2022). While  $\delta^{13}$ C signals primarily reflect changes in photosynthetic discrimination ( $A_{net}$ ) and stomatal conductance ( $q_s$ ) (Farguhar et al., 1989),  $\delta^{18}$ O signals are strongly influenced by evaporative  $^{18}$ O-enrichment in leaf water only controlled by  $q_s$  (Barbour, 2007). The dual-isotope approach leverages these relationships to disentangle the relative effects of stomatal regulation on carbon uptake (Scheidegger et al., 2000). Specifically,  $\delta^{18}$ O variation serves as a constraint on  $\delta^{13}$ C interpretation since  $\delta^{18}$ O enrichment is directly linked to transpiration, and  $q_s$  modulates both transpiration and photosynthetic discrimination (Grams et al., 2007; Scheidegger et al., 2000). For instance, under conditions of low humidity,  $\delta^{18}$ O enrichment in leaf water tends to increase due to intensified transpiration, which may coincide with elevated  $\delta^{13}$ C values if stomatal conductance decreases to mitigate water loss (Cernusak et al., 2016). In contrast, a decoupling of  $\delta^{13}$ C and  $\delta^{18}$ O signals may indicate changes in mesophyll conductance or post-photosynthetic effects on  $\delta^{13}$ C signals which may complicate the interpretation of stomatal limitations (Gessler et al., 2014).

A key assumption in the dual isotope model is that source water  $\delta^{18}$ O remains constant and thus the majority of organic matter  $\delta^{18}$ O variation is driven by evaporative enrichment (Roden & Farquhar, 2012). However, this assumption is not always valid. For example, a study by Offermann et al., (2011) on European beech (*Fagus sylvatica* L.) demonstrated that  $\delta^{18}$ O in tree-ring whole wood was not positively related to leaf water evaporative enrichment and  $\delta^{18}$ O of NSC pools. This highlights the important role of other water sources in modifying  $\delta^{18}$ O signals in tree ring (e.g.,  $P_{\rm ex}$  effect). The  $P_{\rm ex}$  effect refers to the proportion of carbonyl oxygen atoms that exchange between phloem sap and xylem water during cellulose biosynthesis in tree rings (Song, Farquhar, et al., 2014; Sternberg et al., 1986; Szejner et al., 2020). A study by Martínez-Sancho et al., (2022) demonstrated that source water (i.e., water uptake by roots) played a

dominant role in driving intra-annual  $\delta^{18}$ O variations in tree-ring cellulose of larch (*Larix decidua* L.) in the Swiss Alps, effectively masking leaf-level  $\delta^{18}$ O signals. Tracking real-time variations of  $\delta^{13}$ C and  $\delta^{18}$ O in different tree compartments provide insights into the shared physiological processes regulating  $\delta^{13}$ C and  $\delta^{18}$ O variations during the growing season. Additionally, it offers valuable information on the influence of different water sources (e.g. rainwater, underground water) that may alter leaf-level  $\delta^{18}$ O signatures while transporting NSCs from leaves to various sink tissues within the tree. This information is crucial when utilizing  $\delta^{13}$ C and  $\delta^{18}$ O data as proxies in dendroclimatological studies.

Significant uncertainties in intra-annual analysis of stable isotopes still remain regarding the interactions between external environmental constraints and internal physiological processes at seasonal scales (Savard & Daux, 2020; Silvestro et al., 2024). One key uncertainty involves the interplay between environmental drivers, such as temperature and precipitation, and internal needs for wood formation process (i.e., xylogenesis). Xylogenesis is regulated by a complex network of physiological and environmental factors, including temperature, soil moisture, and nutrient availability, which collectively influence cell division, enlargement, and wall thickening (Cuny et al., 2014; Rossi et al., 2014). These factors not only affect the timing and duration of xylem cell formation but also modulate the isotopic composition of carbon and oxygen in developing tree rings (M. Fonti et al., 2018; Gessler et al., 2014), which complicate the interpretation of isotopic signals as straightforward proxies for past environmental conditions (Gessler et al., 2014; Rossi et al., 2013). Consequently, precisely dated intra-annual measurements in different tree compartments (e.g., cambium, xylem) of stable isotope ratios are necessary to disentangle the relative contributions of external environmental factors and internal physiological processes influencing wood formation dynamics during the growing season.

High-resolution tree-ring carbon isotope data can be used to evaluate seasonal intrinsic water use efficiency (iWUE) at the leaf level, which provides a measure of how effectively trees use water to assimilate carbon during the growing season (Saurer & Voelker, 2022, and the literature therein). iWUE is determined by the ratio of photosynthesis to stomatal conductance and serves as a key indicator of how trees regulate carbon and water fluxes in response to environmental constraints (Farquhar et al., 1989). A comparison of intra-annual iWUE variations with wood formation dynamics provide insights into how trees balance carbon assimilation and growth processes under changing environmental conditions (Frank et al., 2015). Such comparisons are particularly valuable for understanding how trees' growth respond to climate change, as shifts in iWUE can indicate long-term adjustments in photosynthetic performance and stomatal

behavior in response to increasing atmospheric CO<sub>2</sub> levels and changing water availability (Voelker et al., 2016). For example, a sustained increase in iWUE over recent decades, as observed in many boreal and temperate forests, suggests that trees are acclimating to rising CO<sub>2</sub> by reducing stomatal conductance while maintaining or increasing photosynthesis (Peñuelas et al., 2011). However, the relationship between iWUE and tree growth is not always straightforward, as other factors, such as nutrient availability, hydraulic constraints, and shifts in carbon allocation, can influence how efficiently trees convert carbon into biomass. Integrating high-resolution iWUE data with xylogenesis and wood anatomical features at seasonal scales enhances our understanding of the interactions between carbon assimilation, water use, tree growth, and environmental constraints, which ultimately improve predictions of forest responses to future climate conditions.

The provided information will be important when using carbon and oxygen stable isotopes as proxies for reconstructing of meteorological variables in dendrochronology, as it enables researchers to more accurately disentangle environmental signals from internal physiological influences preserved within tree ring archives. Enhancing temporal resolution and capturing seasonal dynamics of  $\delta^{13}C$  and  $\delta^{18}O$  in developing tree rings helps bridge the gap between leaf-level physiology and long-term dendrochronological records. This approach strengthens the reliability of tree rings as climate proxies, enabling reconstructions that are more robust. Moreover, integrating isotope analyses with xylogenesis and wood anatomical traits, makes it possible to address the combined effects of climate, water availability, and carbon allocation strategies on tree growth. Ultimately, high-resolution isotope studies enhance the interpretative power of dendrochronology and advance our ability to reconstruct past climates while improving predictions of forest responses to ongoing climate change.

#### 1.2 Objectives and hypothesis

The present thesis is structured around the following objectives, each addressed in a distinct chapter (Figure 1.2.1). In the second chapter, I aim to explore the fluctuations of  $\delta^{13}$ C values in the cambium-xylem continuum throughout the growing season and examine how each tissue responds to the carbon demand for stem growth. I develop a non-lethal method for sampling on a weekly basis and develop weekly  $\delta^{13}$ C profiles for the cambial region and forming xylem cellulose. I hypothesize that  $\delta^{13}$ C values in xylem cellulose ( $\delta^{13}C_{xc}$ ) and cambium ( $\delta^{13}C_{cam}$ ) are either uncorrelated or exhibit temporal lags. This is due to the xylem's access to both newly assimilated carbohydrates and stored carbohydrates, the latter of which often have higher  $\delta^{13}$ C values. In the third chapter, my goal is to provide real-time insights into the dynamic

changes in  $\delta^{13}C$  and  $\delta^{18}O$  values within the vascular cambium-xylem continuum during the growing season. I hypothesize that  $\delta^{13}C$  and  $\delta^{18}O$  values are correlated within the cambial region and the developing tree ring, driven by shared physiological constraints on carbon and oxygen fractionation at the leaf level. Specifically, both  $\delta^{13}C$  and  $\delta^{18}O$  values are expected to increase following reductions in stomatal conductance during the growing season. These findings provide new insights into the processes influencing isotopic signals to avoid misinterpretations in dendroclimatological studies. Finally, in the fourth chapter, I aim to identify the primary drivers of wood formation dynamics in boreal trees. I focus on three key parameters including: cell enlargement rates ( $r_E$ ), wall deposition rates ( $r_W$ ), and cell production rates ( $r_D$ ), as indicators of wood formation in boreal spruce trees. Relationships between these parameters, intrinsic water use efficiency (iWUE), derived from  $\delta^{13}C_{cam}$  values, and meteorological factors are examined (Figure 1.2.1). Here, I hypothesize that iWUE has a direct influence on wood formation dynamics and is linked to environmental factors such as temperature and soil water content. Consequently, wood formation dynamics are expected to be primarily regulated by physiological processes at the leaf level and shaped by external environmental conditions.

#### 1.3 Experimental approach

The study was conducted in mature black spruce [*Picea mariana* (Mill.) BSP.] stands located in the Saguenay-Lac-Saint-Jean area within the boreal forest of Quebec, Canada (Figure 1.3.1). Two particular sites were selected: Simoncouche (SIM) and Bernatchez (BER), both featuring mature black spruce forests. SIM is within the Simoncouche research station of the "Université du Québec a Chicoutimi" (48°13′ N, 71°15′ W, 338 m a.s.l.), situated in the Laurentide Wildlife Reserve. BER is at a higher elevation near Lake Poulin de Courval (48°51′ N, 70°20′ W, 611 m a.s.l.). Black spruce is the dominant species at both sites. The undergrowth is a typical mixed vegetation with various herbaceous and ericaceous shrub species. The region has a continental climate, marked by long cold winters and short warm summers.

During the 2019-2021 study period, the mean annual air temperature in SIM was 3.2°C, while BER experienced a lower mean of 0.6°C. During the growing season, specifically from May to October (2019-2021), mean temperatures were 12.8°C in SIM and 10.3°C in BER, indicating a colder and shorter growing season in BER. This is further reflected in the number of days with minimum daily temperatures above 5°C, averaging 170±20 days in SIM and 139±15 days in BER. The two sites recorded similar mean precipitation levels during the growing season, with approximately 480 mm of rain each (average from May to October: 2019 to 2021). However, soil water content was higher at BER compared to SIM over the same period

(average from May to October 2019-2021: BER, 0.34 m³/m³; SIM, 0.22 m³/m³). Meteorological observations were available at each site using a 10-meter tower equipped with an automatic data acquisition system and several measuring devices. These stations recorded various meteorological variables, including maximum temperature ( $T_{max}$ , °C), vapor pressure deficit (VPD, kPa), photosynthetically active radiation (PAR,  $\mu$ mol/m²/s), relative humidity (RH, %), precipitation (P, mm), and soil water content (VWC, m³/m³), on an hourly basis. Photoperiod (PP, hour) was calculated for both sites as the difference between daily sunset and sunrise times.

Five mature black spruce trees with upright stems and relatively large diameters were selected in SIM and BER, during the three growing seasons of 2019 (just in SIM), 2020 and 2021. Trees showing reaction wood, dead crowns, or visible damage were excluded from selection. The selected trees had sufficiently large diameters to allow the collection of 13 to 22 wood strips for carbon and oxygen stable isotope analysis and microcores during the growing season. From late April to October, rectangular wood strip samples (~3 × 6 cm) were collected on a weekly basis from the selected trees' stem using a chisel and rubber hammer. To monitor xylogenesis, microcores were extracted from below of the cut area during the growing seasons of 2020 and 2021. Two additional microcores were extracted from each selected spruce tree during the last date of sampling (mid-October), once the tree ring was fully formed, to analyse cell anatomical features. The sampling was performed following the micro-core collection methodology introduced in previous studies. To analyze weekly oxygen signals in source water (i.e., precipitation), rain samples were collected weekly during the growing seasons of 2020 and 2021 at both sites, following the designated collection dates for strips and microcores.

#### 1.4 Structure of the thesis

This thesis is organized into three main chapters (Chapters 2, 3, and 4), each addressing one of the specific objectives outlined above. Chapter 2 has been published as a research article in *Tree Physiology* journal. Chapter 3 has been published in *Agricultural and Forest Meteorology*. Chapter 4 is currently being prepared for submission to a peer-reviewed journal. All images included in this document are copyright-free and used in compliance with usage rights.

# 1.5 Figures Legend

<u>Figure 1.2.1</u>: The figure illustrates the intra-annual dynamics of carbon and oxygen stable isotopes and wood formation in black spruce, highlighting potential sink limitation, leaf-level physiological processes

(source limitation) and environmental constraints on these dynamics. The objectives and order of studied subjects are shown by numbers on the figure: (1) develop a method for monitoring stable isotope fractionation in the cambium-xylem continuum (2) investigate dual isotope patterns both in the cambial region ( $\delta^{13}C_{cam}$  and  $\delta^{18}O_{cam}$ ) and developing xylem cellulose ( $\delta^{13}C_{xc}$  and  $\delta^{18}O_{xc}$ ) to understand physiological controls on carbon and water fluxes. (3) examine wood formation dynamics and their relationship with intrinsic water use efficiency (iWUE) and environmental constraints throughout the growing season.

<u>Figure 1.3.1</u>: The map displays two study sites: Simoncouche (SIM) and Bernatchez (BER). The study sites exhibit differences in altitude and annual mean temperature, with BER located at higher altitudes and experiencing lower annual temperatures, leading to shorter growing seasons. The map was created using ArcGIS Desktop.

# 1.6 Figures

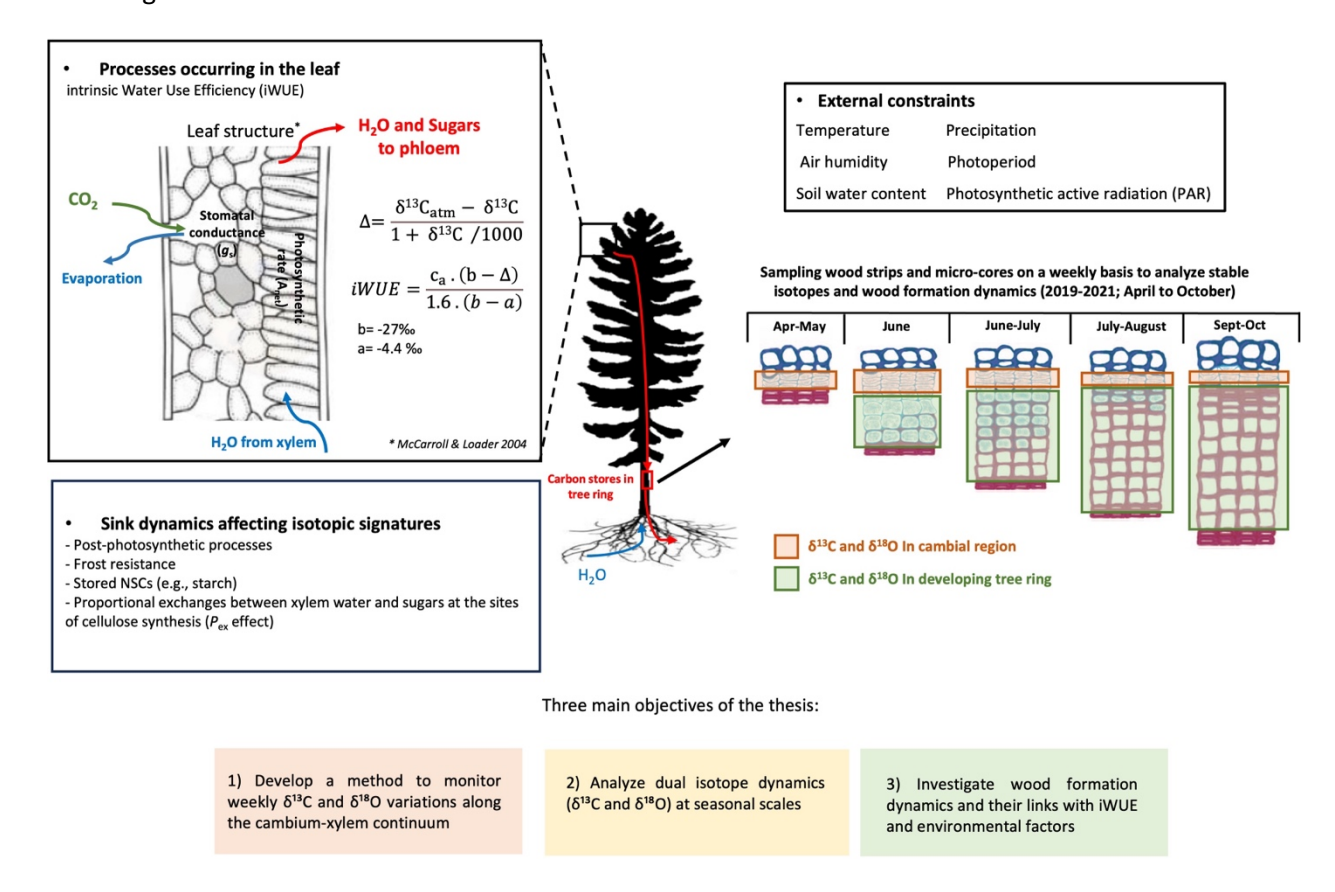


Figure 1.2.1 Schematic overview of the three main chapters of this thesis.

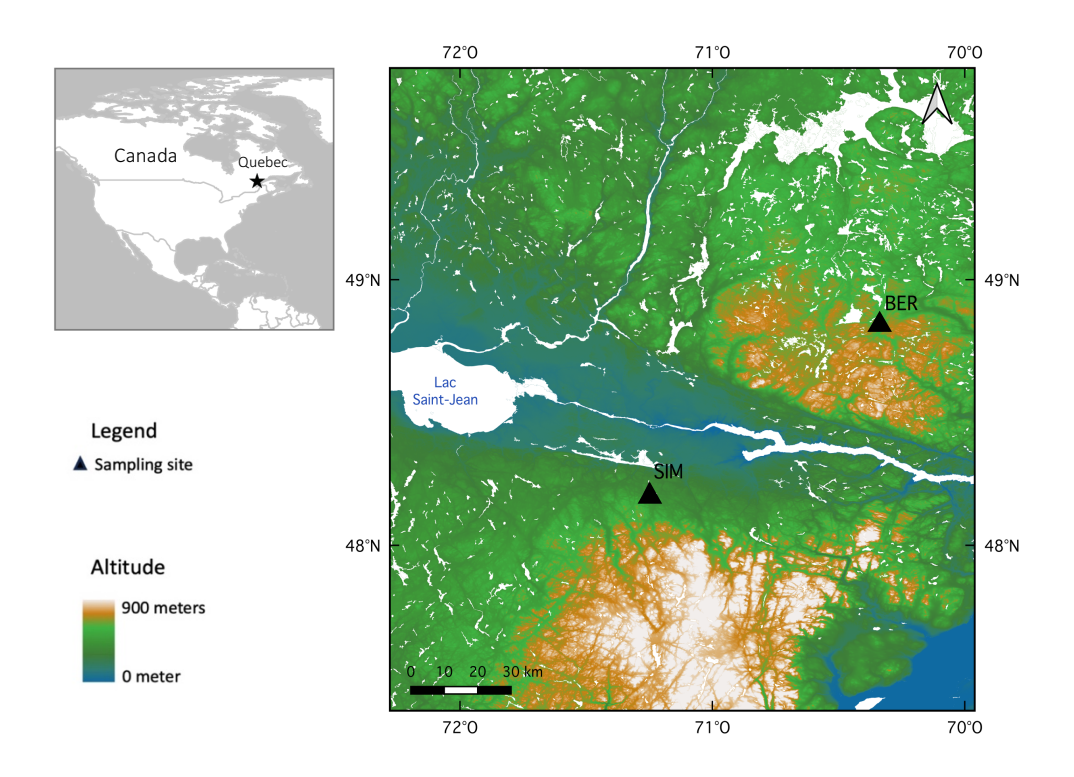


Figure 1.3.1 Study sites: Simoncouche (SIM) and Bernatchez (BER), located in northeastern boreal forest of Quebec, Canada.

#### **CHAPTER 2**

# Monitoring weekly $\delta^{13}\text{C}$ variations along the cambium xylem continuum in the Canadian eastern boreal forest

Sepideh Namvar<sup>1</sup>, Étienne Boucher<sup>2</sup>, Annie Deslauriers<sup>3</sup>, Hubert Morin<sup>3</sup>, Martine M. Savard<sup>4</sup>

- This article was published in Tree Physiology in October 2024
- Supplementary material is attached in Appendix A

<sup>&</sup>lt;sup>1</sup> Department of Biological Sciences and GEOTOP, Université du Québec à Montréal, 201, Président-Kennedy Ave, Montréal (QC), Canada H2X 3Y7

<sup>&</sup>lt;sup>2</sup> Department of Geography, GEOTOP and Centre d'études nordiques, Université du Québec à Montréal, Montréal (QC), Canada H2X 3R9

<sup>&</sup>lt;sup>3</sup> Departement des Sciences Fondamentales, Université du Québec à Chicoutimi, 555, boulevard de l'Université, Chicoutimi (QC), Canada G7H 2B1

<sup>&</sup>lt;sup>4</sup> Natural Resources Canada, Geological Survey of Canada, 490 de La Couronne, Québec (QC), Canada G1K 9A9

#### 2.1 Abstract

Intra-annual variations of carbon stable isotope ratios ( $\delta^{13}$ C) in different tree compartments could represent valuable indicators of plant carbon source-sink dynamics, at weekly time scale. Despite this significance, the absence of a methodological framework for tracking  $\delta^{13}$ C values in tree rings persists due to the complexity of tree ring development. To fulfill this knowledge gap, we developed a method to monitor weekly variability of  $\delta^{13}$ C in the cambium-xylem continuum of black spruce species [*Picea mariana* (Mill.) BSP.] during the growing season. We collected and isolated the weekly incremental growth of the cambial region and the developing tree ring from five mature spruce trees over three consecutive growing seasons (2019-2021) in Simoncouche and two growing seasons (2020-2021) in Bernatchez, both located in the boreal forest of Quebec, Canada. Our method allowed for the creation of intra-annual  $\delta^{13}\text{C}$  series for both the growing cambium ( $\delta^{13}C_{cam}$ ) and developing xylem cellulose ( $\delta^{13}C_{xc}$ ) in these two sites. Strong positive correlations were observed between  $\delta^{13}C_{cam}$  and  $\delta^{13}C_{xc}$  series in almost all study years. These findings suggest that a constant supply of fresh assimilates to the cambium-xylem continuum may be the dominant process feeding secondary growth in the two study sites. On the other hand, rates of carbon isotopic fractionation appeared to be poorly affected by climate variability, at an inter- weekly time scale. Hence, increasing  $\delta^{13}C_{cam}$  and  $\delta^{13}C_{xc}$  trends highlighted here possibly indicate shifts in carbon allocation strategies, likely fostering frost resistance and reducing water uptake in the late growth season. Additionally, these trends may be related to the black spruce trees' responses to the seasonal decrease in photosynthetically active radiation. Our findings provide new insights into the seasonal carbon dynamics and growth constraints of black spruce in boreal forest ecosystems, offering a novel methodological approach for studying carbon allocation at fine temporal scales.

Keywords: cambium, xylem, tree ring, carbon isotope composition, non-structural carbohydrates, boreal

#### 2.2 Introduction

Carbohydrate source-sink dynamics are fundamental aspects of tree growth and can modulate the response to environmental changes (Dietze et al., 2014). Nonstructural carbohydrates (NSCs) are the predominant products of photosynthesis occurring in the leaves (Carbone et al., 2013). Once produced, NSCs may be allocated to build structural components including cell walls in tree rings (e.g. cellulose), or can be stored in the form of starch for future utilization (Hartmann & Trumbore, 2016). A comprehensive body of knowledge on NSC dynamics has been generated from studies investigating carbohydrate concentrations in various tree sinks over time (Fajstavr et al., 2018; Piper, 2020; Rademacher et al., 2022; Rathgeber et al., 2022; Richardson et al., 2013). However, there are still uncertainties regarding the processes and pathways related to NSCs allocation in mature living trees (Wiley & Helliker, 2012).

In the stem, the cambium-xylem growing continuum is a critical site where carbohydrate dynamics can be tackled (Deslauriers et al., 2014). The cambial region (i.e., cambium and differentiating phloem and xylem cells), an important sink for NSCs synthesized in leaves, is at the origin of wood production (Giovannelli et al., 2011; Rossi et al., 2013; Simard et al., 2013). Cambium's NSC source is mostly limited to leaf-originating photosynthates unloaded from the phloem (Gessler et al., 2014). However, cambium-derived sinks such as earlywood or latewood are possibly fed synergistically from two different sources: cambial NSCs and NSCs stored in ray parenchyma cells (starches and soluble sugars) (Deslauriers et al., 2016; Dietze et al., 2014; Giovannelli et al., 2011). These variable source-sink dynamics may introduce significant time lags between the synthesis and fixation of photosynthates in xylem tissue, impeding our capacity to model and predict growth responses to a changing environment. The impact of storage on stem growth during the initial stages of wood formation has been proven for deciduous trees (Kagawa et al., 2006; Simard et al., 2013), where there is a larger number of wood parenchyma cells compared to conifers (Schweingruber et al., 2007). However, there are exceptions to this pattern, as some research on Mediterranean *Pinus pinea* L. demonstrated that both current and stored carbon sources are significant for development of tree rings in this conifer species (Castagneri et al., 2018).

Stable carbon isotope ratios in tree ring cellulose ( $\delta^{13}$ C) may greatly help trace different NSCs' origin, translocation and utilization by various plant growth sinks (Gessler et al., 2009). Photosynthetic discrimination of  $^{13}$ CO<sub>2</sub> against  $^{12}$ CO<sub>2</sub> in C<sub>3</sub> plants is associated with the ratio of leaf internal to external CO<sub>2</sub> partial pressure ( $c_i/c_a$ ) which, itself, is regulated by stomatal conductance ( $g_s$ ) and the rate of CO<sub>2</sub> assimilation (Farquhar et al., 1982). Hence, the  $\delta^{13}$ C value of current NSCs should, in theory, reflect the

interplay between such controlling factors at the time of synthesis in leaves. By contrast, the  $\delta^{13}$ C values of stored NSCs could diverge from that of current assimilates, particularly if storage includes carbohydrates in the form of <sup>13</sup>C-enriched starch (MacNeill et al., 2017), that were synthesized at different times of the year, and potentially during previous years. In boreal conifers for instance, a high amount of starch reserves is built during spring, especially in the needles, prior to growth activation and remobilized for both primary and secondary growth later during the growing season (Tixier et al., 2019; Cartenì et al., 2023; Deslauriers et al., 2019). If this holds true, then  $\delta^{13}$ C values in the cambial region ( $\delta^{13}$ C<sub>cam</sub>, mainly derived from current photosynthates) and the xylem cellulose ( $\delta^{13}C_{xc}$ , derived from a mixture of current + stored NSCs) should diverge in a manner that is somewhat proportional to the amount of stored assimilates involved in growth during xylogenesis, either coming from leaves or other woody parts of the tree. While more information is available on the chemical and isotopic properties of different wood constituents (Helle et al., (2022) and literature therein), few studies have examined the variations in sugars and chemical compounds in the cambium zone (Deslauriers et al., 2016; Giovannelli et al., 2011; Simard et al., 2013). Consequently,  $\delta^{13}C_{cam}$  values remain unknown. Therefore, differences in the  $\delta^{13}C$  values of NSCs from source (leaves-cambium) to sink (xylem) provide an ideal opportunity to track down the utilization and remobilization of NSCs by trees.

One of the most important obstacles that prevents tracking  $\delta^{13}$ C values from source to sink is the absence of a methodological framework enabling the construction of intra-annual  $\delta^{13}$ C chronologies along the growing cambium-xylem continuum. Recent improvements in dendro-isotopic analysis, such as dividing wood segments or cores by cutting tangential slices manually or using the microtome (Barçante Ladvocat Cintra et al., 2019; Belmecheri et al., 2018; Fu et al., 2017; Ogée et al., 2009; Pons & Helle, 2011; Roden et al., 2009; Verheyden et al., 2004; Xu et al., 2022) or by laser ablation techniques (Loader et al., 2017; Saurer et al., 2023; Schollaen et al., 2014) have greatly enhanced the possibility to study isotopic composition in tree rings at intra-annual resolution (Schollaen et al., 2014). In these studies, each ring sector is assumed to be associated with a specific time period based on its position within the previously developed ring. However, despite their seemingly straightforward structure, new anatomical studies suggest that tree rings cannot be reduced to a sequence of cell rows formed during distinct and regular time intervals (Buttò et al., 2019; Cuny et al., 2015). Instead, a given cell row within a tree ring results from multiple, largely successive, developmental processes (e.g., cell enlargement, cell wall thickening, etc., Figure 2.1) most of which overlap in timing, rate and duration (M. Fonti et al., 2018; Ziaco et al., 2016). Knowing this, an alternative option for tracking intra-annual variations would be the live  $\delta^{13}$ C monitoring in both cambium

and xylem, during the growing season. The method would be intrinsically cumulative (i.e., sampling during wood formation in current tree ring), rather than sequential (i.e., sampling after ring formation is complete). In other words, it would measure incremental changes in fractionation with a precise dating. A procedure developed by Giovannelli et al., (2011) overcame the challenge of separating the cambial region from other tissues, including phloem and xylem, for NSC determination (Deslauriers et al., 2014, 2016). The "scraping method" employed in this research offered the opportunity to collect samples from the cambial region throughout the year, enabling the examination of metabolic alterations during the process of tree-ring formation. However, to this date, no conductive method has been developed to analyze the intra-annual  $\delta^{13}$ C variations in the cambial region where the secondary growth occurs.

Here, we developed a method to investigate, at a weekly resolution, the co-evolution of  $\delta^{13}C$  values in the cambium and forming-mature xylem region of mature black spruce [*Picea mariana* (Mill.) BSP.] trees, in the eastern Canadian boreal forest. This study aims to provide insights into how  $\delta^{13}C$  values fluctuate in the cambium-xylem continuum over the entire growing season and how each tissue responds to the carbon demand for stem growth. We hypothesize that  $\delta^{13}C_{xc}$  and  $\delta^{13}C_{cam}$  either do not correlate or vary with some temporal lag. This is because xylem cellulose has access not only to newly formed assimilates but also to stored carbohydrates with relatively high  $\delta^{13}C$  values.

#### 2.3 Materials and Methods

# 2.3.1 Study area

The research was carried out in the Saguenay-Lac-Saint-Jean region, located in the boreal forest of Quebec, Canada (Figure 2.2). Two specific sites of Simoncouche (SIM, 338 m a.s.l.) and Bernatchez (BER, 611 m a.s.l.) with mature black spruce stands were selected. Black spruce is one of the most prevalent species in boreal forests of Northern America. This slow-growing conifer typically establishes after forest fires and has a shallow root system, primarily located within the upper 20 cm of organic soil (Belien et al., 2012). Monitoring was performed between May and October in 2019-2021, and in 2020-2021 for SIM and BER, respectively (Table 2.1). Meteorological stations were installed in each site, consisting of a 10-meter tower equipped with an automatic data acquisition system to which several measuring devices are attached. Various climatic variables including maximum temperature, vapour pressure deficit, photosynthetically active radiation, relative humidity, precipitation, and soil water content were recorded on an hourly basis (Table 2.2). The climatic data indicated a mean annual air temperature of 3.2°C in SIM (2019-2021) and 0.6°C in BER (2019-2021). During the growing season (May-Oct) mean temperatures decreased by

approximately 2.5°C, dropping from 12.8°C in SIM to 10.3°C in BER. This change reflects a colder and shorter growing season in BER (days with minimum daily temperature above 5°C on average: SIM 170±20 days, BER 139±15 days, mean± standard deviation) (Buttò et al., 2019; Rossi et al., 2011). Annual mean precipitation was higher in SIM compared to BER with 640.6 mm and 570.1 mm respectively (2019-2021). However, the mean precipitation during the growing season was similar with 484 mm of rain in both sites (Table 2.1).

#### 2.3.2 Sample preparation

In both sites, five mature black spruce trees were chosen for each growing season in 2019 (SIM only), 2020, and 2021 (Table A.1, see *Appendix A*). The selected trees were healthy, with over 50% of branches alive in the crown. To avoid reaction wood, the tree samples were grown on flat surfaces with upright stems. To estimate the average age of the black spruce stands at each site, we counted the tree rings in cores extracted from the trunk of each selected tree sample using an increment borer (Grissino-Mayer, 2003). The mean tree age was estimated to be 78±7.7 years in SIM and 133±4 years in BER with a mean stem diameter of 24.8 ±3.8 cm in SIM and 23.6±1.8 cm in BER (Table 2.1). The diameter of the selected trees was large enough to support the sampling of 13 to 22 wood strips during the growing season (Table A.2). To provide high-quality weekly samples and sufficient mass for IRMS analysis, the strips were collected on the selected trunks starting at the beginning of the growing seasons (late April) up to the end of the growing seasons in October. To reduce possible damage to the tree's cambium layer and its growth, sampling was done on different parts of the stem, preferably at breast height (1.35 m), in accordance with the micro-core collection methodology outlined in previous studies (Buttò et al., 2019; Rossi et al., 2011).

Rectangle wood strips of  $\sim 3 \times 6$  cm, including the bark (phloem) and wooden part (xylem), were separated from the trunk using a wood chisel and a mallet. In the laboratory, the samples were divided in two parts along the tangential plane in the cambial region, either manually or with a surgical scalpel (Figure 2.1) (Giovannelli et al., 2011). The two separated parts (Figure 2.3a) were plunged into liquid nitrogen for one minute to stop any enzymatic activity followed by lyophilisation for 5 days at a constant temperature of  $-50^{\circ}$ C under vacuum (0.05 mbar or less). The wood strip separation between phloem and xylem was more problematic at the growing season's beginning (May) and ending (October), because of the absence of dividing cambium and elastic tissues linked with enlarging phloem and xylem cells. For these samples, separation after freeze-drying was more efficient. The loss of intra and intercellular water in the cambial

region during the drying process caused the shrinkage of the developing elastic tissues, leading to an easier separation of the two parts (Giovannelli et al., 2011).

#### 2.3.3 Sampling the cambial region

The cambial region, probably including a few enlargement cells (Deslauriers et al., 2016), was collected by gently scraping the bark's inner part (Figure 2.3b) and the xylem's outermost part, according to Giovanelli et al. (2011). The cambial region was clearly identifiable as a thin dark brown layer on the phloem (light brown area) and as a thin transparent layer on the outermost part of the xylem sample. To reduce the costs of stable isotope analysis, pooling of the cambial region material was done for each sampling date including all five trees (Table A.2). To maximize homogenization, the pooled samples were ground using a two-bladed mixer mill (Retsch MM 400, Haan, Germany) at 30 Hz for 30 seconds.

#### 2.3.4 Sampling the developing xylem ( $\alpha$ -cellulose)

The separation of the currently forming ring was done from the last date of the growing season (mid-October) when the tree ring was formed completely. To do so, the transverse section was sanded and moisturized, and the forming ring was cut using a razor blade under a binocular microscope with 10 × magnifying lenses and LED ring light (Figure 2.3c). For narrower rings, at the beginning of the growing season, cutting from the transverse section was not possible because of a very low number of cells. Therefore, the tangential area was moisturized, and the cells were scraped (in the form of fibre) with a surgical scalpel (Figure 2.3d) down to the previous year's tree ring. The difference in colour and brightness between the previous year's tree ring (light brown and bright) and newly produced cells (white and opaque) facilitated the scraping process and its intensity.

The collected xylem samples for each date of sampling were ground into fine particles (≤0.1mm) in the mixer mill at 30 Hz frequency each for 3 minutes. Pooling was done for a few of the xylem samples from the beginning dates of the growing season when there was not enough mass to perform the cellulose extraction separately (Table A.2). The samples weighing less than 5 milligrams, acquired from the beginning dates of wood formation (early June), were excluded due to the small amount of cellulose extraction material.

Cellulose was extracted from xylem samples following a modification of the method described by Epstein et al., (1976). The extraction involved three consecutive steps to eliminate soluble organic compounds,

lignin, and hemicellulose respectively. Between 15 to 20 mg of ground sample was loaded in Teflon/polyester filter bags (ANKOM® XT4) and heat-sealed for cellulose extraction. The filter bags were placed into a 1:1 solution of toluene: ethanol (to extract lipids and resins) and placed into the ultrasonic bath for 90 minutes, followed by a period of 80 minutes in acetone. The bags were boiled for one hour to extract soluble organic compounds. A sodium chlorite/acetic acid solution was used to 'bleach' the samples over a 3-hour extraction in heated (80°C) demineralized water to remove lignin. To obtain pure  $\alpha$ -cellulose, the samples were placed in a strong (17% w/v) NaOH solution followed by an acetic acid solution (10%) to neutralize the pH, with each step followed by extensive rinsing with double-distilled water. The  $\alpha$ -cellulose was dried under the hood at room temperature for 24 hours.

#### 2.3.5 Analysis of carbon stable isotope ratios

All isotopic measurements were performed at the light-stable isotope geochemistry laboratory at the University of Quebec (Geotop, Montreal, Canada). Between 0.5 and 0.8 mg of cellulose (for xylem samples,  $\delta^{13}C_{xc}$ ) or pooled bulk material (for the cambial samples,  $\delta^{13}C_{cam}$ ) were weighed into tin capsules to obtain the same amount of  $CO_2$  for all samples and reference materials. The samples were then analyzed with a Micromass model Isoprime 100 isotope ratio mass spectrometer coupled to an Elementar Vario MicroCube elemental analyzer in continuous flow mode. The overall analytical uncertainty was better than  $\pm 0.1\%$ . This uncertainty was based on the propagation of uncertainties of the normalization of the internal reference materials and the samples but did not include the homogeneity nor the representativity of the sample (Hélie & Hillaire-Marcel, 2021).

## 2.3.6 Statistical analysis

The Weekly Expressed Population Signal (EPS<sub>w</sub>) is an adaptation of regular EPS defined by Wigley et al., (1984) and Briffa and Jones (1990) calculating as bellow:

$$EPS_w = \frac{Nr}{(1 + (N-1)r)}$$

Equation 2.1 Weekly Expressed Population Signal (EPSw)

Where r is the mean correlation coefficient among all tree samples for each study year (Rbar), and N is the number of trees that are measured at each study site (N=5). The EPS $_w$ >0.85 was defined as a reasonable albeit objective value for an acceptable level of chronology confidence (Wigley et al., 1984). The analysis of covariance (ANCOVA) was used to compare the two regression lines of  $\delta^{13}C_{cam}$  and  $\delta^{13}C_{xc}$  in the sites and

study years. ANCOVA demonstrates whether the regression lines were different from each other in either slope or intercept. A two-sided t-test (Welch test) was applied to the distribution of the means to determine significant differences among  $\delta^{13}C_{cam}$  and  $\delta^{13}C_{xc}$  in different sites and study years. Pearson's correlations between the two chronologies ( $\delta^{13}C_{xc}$ ,  $\delta^{13}C_{cam}$ ) were calculated to evaluate whether the two profiles shared a similar variation during the growing season.

# 2.3.6.1 Climate response and $\delta^{13}C_{cam}$ and $\delta^{13}C_{xc}$ variations

In order to compare our weekly values with meteorological variability, the  $\delta^{13}C_{cam}$  and  $\delta^{13}C_{xc}$  values were first corrected to account for changes in atmospheric  $\delta^{13}C$  ( $\delta^{13}C_{atm}$ ). This has two benefits. First, it corrects for the Suess effect, which is the progressive decline in  $\delta^{13}C_{atm}$ , due to fossil emissions, since 1850 (Pre-Industrial reference,  $\delta^{13}C_{atm\_Pl}$  = -6.61%) (Belmecheri & Lavergne, 2020; McCarroll & Loader, 2004). Second, it accounts for the seasonal variability in  $\delta^{13}C_{atm}$ , attributable to the preferential sequestration of <sup>12</sup>C during photosynthesis, leaving a progressively enriched atmosphere as photosynthesis increases (Ballantyne et al., 2010). Unfortunately, on site measurements of  $\delta^{13}C_{atm}$  were unavailable. In order to perform these corrections, we used the  $\delta^{13}C_{atm}$  data collected from the NOAA-ESRL tall tower at Argyle, Maine, United States (AMT, 45.03°N, 68.68°W,  $\delta^{13}C_{atm\_AMT}$ , <a href="https://gml.noaa.gov/dv/iadv">https://gml.noaa.gov/dv/iadv</a>) in conformity with our sampling dates. The Argyle site is the closest  $\delta^{13}C_{atm}$  measurement station to our study region. The tower is located in a mixed (deciduous and evergreen) forest in rural central Maine, north of Bangor, at 50 m above sea level. For each sampling date (date=n), we corrected our isotopic values as follows (example for xylem, same for cambium):

$$\delta^{13}\mathsf{C}_{xc\_cor(date=n)} = \delta^{13}\mathsf{C}_{\mathsf{xc\_(date=n)}} - \left(\delta^{13}\mathsf{C}_{\mathsf{atm\_AMT\ (date=n)}} - \delta^{13}\mathsf{C}_{\mathsf{atm\_PI}}\right)$$

Equation 2.2 Correction of  $\delta^{13}C$  for seasonal  $\delta^{13}C_{atm\ AMT}$  variations and Suess-effect

In the *Appendix A*, we provide further illustrated examples on how  $\delta^{13}C_{xc\_cor}$  and  $\delta^{13}C_{cam\_cor}$ , corrected using equation 2.2, account for both: i) the change in mean  $\delta^{13}C_{atm}$  attributable to the long-term Suess effect, and ii) the trends in  $\delta^{13}C_{xc}$  or  $\delta^{13}C_{cam}$  resulting from intra-seasonal variations in  $\delta^{13}C_{atm\_AMT}$  (Method A.1, see Appendix *A*). Propagation uncertainty was calculated for  $\delta^{13}C_{xc\_cor}$  values (Table A.3). Uncertainties were propagated using first-order partial derivatives (Taylor expansion method). The Argyle site is the closest site, but it is quite a different ecosystem from the one studied here. We therefore also performed a similar correction using comparable, although remotely located, boreal forest  $\delta^{13}C_{atm}$  data. Indeed, we performed the same calculations, this time using the  $\delta^{13}C_{atm}$  Lac La Biche, Alberta, Canada. (LLB, 54.95°N, 112.47°W,  $\delta^{13}C_{atm\_LLB}$ ), This site is located at slightly the same altitude as our study region (540 m above sea level) and

is dominated by *Picea mariana* and *Larix laricina*, two species found locally in our study region. However, the  $\delta^{13}C_{atm}$  data for this site was only available between 2008-2013 (<a href="https://gml.noaa.gov/dv/iadv">https://gml.noaa.gov/dv/iadv</a>), so we only considered the average  $\delta^{13}C_{atm}$  seasonal cycle for the LLB site and applied it uniformly to all years (Table A.4).

Pearson correlations were employed to assess the relationships between  $\delta^{13}C_{cam\_cor}$  and  $\delta^{13}C_{xc\_cor}$  values corrected using the AMT dataset and the different climatic parameters. The weekly daytime (8h00 to 18h00) values of six different climate parameters: maximum temperature, vapour pressure deficit, photosynthetically active radiation, relative humidity, precipitation, and soil volumetric water content, were averaged on time periods (day of year) matching those of sampling intervals for each year and site (Table 2.2). The climate data were obtained from *in situ* meteorological stations at each site.

The cumulative sampling method developed here, may induce time discrepancies when weekly  $\delta^{13}C_{xc\_cor}$  values are compared with weekly climatic variables. This is because values measured using our method are intrinsically additive rather than "instantaneous". Specifically, the  $\delta^{13}C_{xc\_cor}$  values measured at week t represents the fractionation during week t which adds up to the fractionation of the preceding weeks. To minimize these discrepancies and remove the associated autocorrelation in  $\delta^{13}C_{xc\_cor}$  measurements, we weighted and isolated the fractionation at week t and subtracted it from that of previous weeks ( $\delta^{13}C_{xc\_seq}$ ; Method A.2). Pearson correlations were then used to analyze the relationships between the detrended series of  $\delta^{13}C_{xc\_seq}$  and climatic variables at tree level and site level.

# 2.4 Results

Our method facilitated the acquisition of varying quantities of materials from the cambial region and developing tree ring depending on the date of sampling and the size of the strips, both in SIM and BER. At the beginning (Late April-May) and end (Sep-Oct) of the growing season, 5-10 mg of scraped tissues from the cambial region were obtained only from the inner side of the bark. However, during the xylem differentiation phase (June-August), the amounts increased to 15-30 mg in each tree sample. Moreover, we obtained sufficient masses of xylem cells to perform weekly  $\delta^{13}C_{xc}$  analysis on individual trees in both sites. At the beginning of wood formation (June to early July), 10-20 mg of materials were obtained using the scraping technique. The cutting of the widening ring (July-Oct) yielded masses over 20 mg per tree. Pooling of xylem cells was only necessary in SIM 2020 and BER 2020 at the earliest dates of wood formation (mid-June), at times when xylogenesis was beginning (Figure 2.4b and 2.4d).

# 2.4.1 Intra-annual $\delta^{13}C_{cam}$ and $\delta^{13}C_{xc}$ variability

During the full growing season, all  $\delta^{13}C_{cam}$  profiles showed an increasing trend, with a slight decrease observed at the very end of the growing season in most profiles (Figure 2.4). SIM and BER sites showed comparable increasing  $\delta^{13}C_{cam}$  trends (F=1.0, p=0.3 for 2020, F=0.5, p=0.5 for 2021) although with different intercepts (F=71.4, p<0.0001 for 2020, F=14.3, p<0.001 for 2021) (Figure 2.5a and 2.5b). Compared to BER, the  $\delta^{13}C_{cam}$  mean in SIM was significantly higher by +0.8 and +0.2 ‰, in 2020 and 2021, respectively (p<0.001) (Table 2.3).

A consistent seasonal pattern of increasing  $\delta^{13}C_{xc}$  was observed in most replicates from the first sampling date to the last for all sites and years investigated (Figure A.1, see *Appendix A*). In SIM, nine out of fifteen trees presented a significant positive  $\delta^{13}C_{xc}$  trend (average slope parameter,  $\beta$ = 0.008, p<0.05). In BER, the  $\delta^{13}C_{xc}$  series depicted similar patterns: seven out of ten trees also presented significant positive trends ( $\beta$ = 0.009, p<0.05) (Table A.5).

Inter-tree  $\delta^{13}C_{xc}$  correlations were relatively high in each study year ranging between -0.4 to +0.9 in SIM 2019-2021 (Figure 2.6a, 2.6b, and 2.6c) and +0.1 to +0.8 in BER 2020-2021 (Figure 2.6d, 2.6e). In SIM, Rbar varied between 0.1 and 0.5 over the three growing seasons (Table 2.3). The inter-tree statistics were improved once tree no.1 in SIM 2019 and tree no.5 in SIM 2021 were removed. These trees showed negative correlations with some of other individuals (Figure 2.6a and 2.6c). This removal boosted the Rbar to 0.6 (2019) and 0.3 (2021). The EPS<sub>w</sub> also increased to 0.9 and 0.7 once these trees were removed. In SIM 2020, the Rbar and EPS<sub>w</sub> were 0.5 and 0.8 respectively. In BER, Rbar was 0.4 and EPS<sub>w</sub> was 0.8 both in 2020 and 2021. Despite the high variability in inter-tree correlation, inter-tree  $\delta^{13}$ C variability remained quite low in both sites (standard deviations of averages for trees were lower than 0.5‰, Table 2.3).

Averaged  $\delta^{13}C_{xc}$  series showed increasing trends at each site and for all study years (Figure 2.4). Both sites presented average  $\delta^{13}C_{xc}$  trends with comparable increasing trends (F=0.3, p=0.6 for 2020, F=3.8, p=0.1 for 2021), but with different intercepts (F=83.7, p<0.0001 for 2020, F=45.2, p<0.0001 for 2021) (Figure 2.5c and 2.5d). SIM displayed significantly higher  $\delta^{13}C_{xc}$  values compared to BER, during both growing seasons (+1.1 and +0.4 % for 2020 and 2021, respectively, p<0.001) (Table 2.3). Furthermore, similar increasing trends were observed in all  $\delta^{13}C_{xc\_seq}$  series across the different study years (Figure A.2). Both sites exhibited  $\delta^{13}C_{xc\_seq}$  profiles with similar increasing trends (F=0.7, p=0.4 for 2020, F=0.2, p=0.7 for 2021) and intercepts (F=0.7, p=0.4 for 2020, F=0.1, p=0.8 for 2021).

# 2.4.2 Inter-annual $\delta^{13}C_{cam}$ and $\delta^{13}C_{xc}$ variability

During each of the investigated growing seasons,  $\delta^{13}C_{cam}$  and  $\delta^{13}C_{xc}$  covaried in both sites (Figure 2.4): positive correlations in SIM for 2019 (r=+0.8, p<0.01), 2020 (r=+0.9, p<0.001) and 2021 (r=+0.4, p<0.2), and in BER for 2020 (r=+0.8, p<0.01) and 2021 (r=+0.8, p<0.01) (Table 2.3). Increasing trends in  $\delta^{13}C_{cam}$  and  $\delta^{13}C_{xc}$  are comparable for all study years and both sites (F=1.1, p=0.5), except for SIM 2021 (F=8.8, p<0.05), but intercepts for these slopes differed (F= 136.6, p<0.0001) (Figure 2.4). Indeed, the mean  $\delta^{13}C_{xc}$  was systematically higher than the mean value of  $\delta^{13}C_{cam}$  in SIM (+0.8, +1.3 and +1% differences in 2019-2021) and in BER (+1 and +0.8% in 2020-2021, p<0.001) (Table 2.3).

# 2.4.3 Relationships between $\delta^{13}C_{cam\_cor}$ and $\delta^{13}C_{xc\_cor}$ series and climate data

Both  $\delta^{13}C_{cam\_cor}$  and  $\delta^{13}C_{xc\_cor}$  series similarly responded to climate factors such as  $T_{max}$ , VPD, RH, and PAR (Table 2.4 and 2.5). In both study sites, negative correlations were observed when comparing mean daytime (8h00 to 18h00)  $T_{max}$  and VPD with  $\delta^{13}C_{cam\_cor}$  and  $\delta^{13}C_{xc\_cor}$  profiles across most study years, ranging from -0.6 to -0.1 (p<0.1, p>0.1) and -0.7 to -0.3 (p<0.05, p>0.1), respectively. In SIM 2021 however, weaker positive correlations were observed between VPD and  $\delta^{13}C_{cam\_cor}$  series (r=+0.01). Significant negative correlations were shown between PAR and  $\delta^{13}C_{cam\_cor}$  and  $\delta^{13}C_{xc\_cor}$  series in most study years, ranging from -0.8 to -0.6 when significant (p<0.01, p<0.1), except in SIM 2021, where positive correlation was shown between  $\delta^{13}C_{cam\_cor}$  and PAR (r=+0.3, p>0.1). In contrast, significant positive correlations were observed between  $\delta^{13}C_{cam\_cor}$  and  $\delta^{13}C_{xc\_cor}$  profiles and RH in most of the study years at both sites ranging between +0.5 to +0.8 (p<0.1, p<0.05). The  $\delta^{13}C_{cam\_cor}$  and  $\delta^{13}C_{xc\_cor}$  profiles were not related to the mean daytime P and VWC in most of the sites and study years except in SIM 2019 where significant positive relationships were observed between the P and  $\delta^{13}C_{cam\_cor}$  (r=+0.8, p<0.01) and  $\delta^{13}C_{xc\_cor}$  (r=+0.9, p<0.01) (Table 2.4 and 2.5). Moreover, significant positive correlations were shown between mean soil VWC and  $\delta^{13}C_{cam\_cor}$  in SIM 2021 (r=+0.6, p<0.05).

Negative correlations were observed between  $\delta^{13}C_{xc\_seq}$  series and  $T_{max}$ , VPD, and PAR across all study years and in both sites, ranging between -0.7 to -0.2 (p<0.05, p>0.1), -0.6 to -0.1 (p<0.05, p>0.1), and -0.8 to -0.2 (p<0.05, p>0.1) respectively (Table 2.5). In contrast, positive correlations were calculated between RH and  $\delta^{13}C_{xc\_seq}$  series in both sites, significant only in SIM 2019 and SIM 2021 (r=+0.7, p<0.05, r=+0.6, p<0.05 respectively). Additionally, significant positive correlations were observed between  $\delta^{13}C_{xc\_seq}$  values and P only in SIM 2019 (r=+0.8, p<0.01).

## 2.5 Discussion

The linkages between cambial merismatic activity and stem growth are essential for an accurate understanding of source-sink dynamics of NSCs in plants. Although high-resolution studies using manual cutting or laser-based systems are becoming more frequent to analyze intra-ring isotopic composition profiles (Barçante Ladvocat Cintra et al., 2019; Belmecheri et al., 2018; Fu et al., 2017; Ogée et al., 2009; Pons & Helle, 2011; Roden et al., 2009; Saurer et al., 2023; Verheyden et al., 2004; Xu et al., 2022), a specific technical procedure is still required for sampling and analysing both the cambial region and the developing tree ring. This procedure is necessary to produce precisely dated samples that could link tree-ring formation and, at the same time, isotopic values of both tissues as they are forming. In this paper, we presented a suitable and non-lethal method to collect these two tissues from mature black spruce trees. This developed method can be used to monitor the weekly  $\delta^{13}$ C evolution of the cambium-xylem continuum.

Our strategy for collecting the cambial cells and developing tree ring was primarily based on the plant water status and stage of tree-ring formation at the sampling date (Giovannelli et al., 2011). During the dormant phases and at the beginning or ending of the growing season, smaller quantities of scraped tissues were obtained in the cambial region (i.e., cambium initial cells) because of narrow cell population in this zone during those periods. On the contrary, during the xylem differentiation phase, the quantity of scraped tissues (i.e., initial cambial cells with differentiating xylem and phloem cells on both sides) increased notably in each tree samples. The higher availability of scrapped tissue coincided with an enhanced hydration and a lack of lignification in the developing area of the cambial region (Deslauriers et al., 2016; Giovannelli et al., 2011). Our method consistently provided sufficient masses of tissue (mg) for  $\delta^{13}$ C analysis on a weekly basis throughout the growing seasons. Both the scraping of the narrower developing ring at the onset of wood formation and the cutting of the widening ring, yielded ample masses per tree. However, black spruce, being a slow-growing species, exhibits less total cell production during the growing season. In contrast, a study conducted on fast-growing poplar yielded greater quantities of material both in cambium and xylem tissues (Deslauriers et al., 2009). To ensure that enough mass is sampled, cutting bigger strips (> 3×6 cm) from the tree trunk during earlier phases of secondary growth (June) could be considered in future monitoring studies.

In both sites, our method generated isotopically lighter  $\delta^{13}C_{cam}$  (by ~1‰) compared to  $\delta^{13}C_{xc}$  (Figure 2.4, Table 2.3). This most likely reflects the difference in isotopic values of the material analyzed along the

continuum (Gessler et al., 2014). Intra-annual  $\delta^{13}C_{xc}$  profiles were measured on  $\alpha$ -cellulose isolated from the developing tree ring. In contrast,  $\delta^{13}C_{cam}$  measurements were performed on raw material, without cellulose extraction because of the lower mass of collected tissue. In conifers, different types of NSCs along with other compounds including polyols and the raffinose family of oligosaccharides are transport from phloem to the cambial region (Dominguez & Niittylä, 2022; Simard et al., 2013). The presence of isotopically less enriched substances such as pinitol, and soluble sugars like fructose in the cambial region of black spruce (Rinne et al., 2015; Simard et al., 2013) may contribute to the observed more negative  $\delta^{13}C_{cam}$  values. Indeed, extracting  $\alpha$ -cellulose on cambial cells would otherwise have resulted in drastic mass losses on these already extra light samples, which would be incompatible with IRMS analysis. Indeed, hemi- and  $\alpha$ -cellulose are polymers only present in low amounts in the cambial region. Thus, the multiple source (i.e., different substances and sugars in the cambial region) versus single sink ( $\alpha$ -cellulose in tree rings) approach we used here may not fully unveil the subtle source-sink interactions that impact  $\delta^{13}C$  ratios in these two tissues. To achieve a deeper understanding of those interactions, comparing isotopic signature of  $\delta^{13}C$  in the cambial region with  $\delta^{13}C$  in whole wood may provide further insights into  $\delta^{13}C$  ratios within the growing cambium-xylem continuum (Helle G et al., 2022; Rathgeber et al., 2022).

However, regardless of the chemical composition of the tissues analyzed, our study highlighted a notable coherence both in the seasonal trends and weekly variations of  $\delta^{13}C_{cam}$  and  $\delta^{13}C_{xc}$  mean profiles (Figure 2.4, Table 2.3). This suggests that cambium and xylem share carbohydrates that originate from similar sources and that were synthesized at the same time during the growing season. These sources can be either: i) newly assimilated NSCs unloaded from the phloem alone (Vaganov et al., 2009), or ii) newly assimilated NSCs unloaded from the phloem along with carbohydrates stored in ray cells (Soudant et al., 2016).

Evidence from studies focalizing on NSC concentration in the cambial zone and xylem indicate that the first scenario (i) is more credible (Deslauriers et al., 2016; Simard et al., 2013), especially for conifer species of boreal zones. In these studies, mobile sugars in the cambial zone were shown to originate predominantly from recently fixed NSCs unloaded from the phloem. These sugars then supply the xylem sink during the growing season (Deslauriers et al., 2016), amplifying the coherence between the  $\delta^{13}$ C values of both tissues. Complementarily, low variations in  $^{13}$ C-enriched starch were observed in the cambium of larch and spruce trees during the growing season, suggesting that a constant supply of fresh assimilates to the cambium-xylem continuum may be the dominant process feeding secondary growth

(Rinne et al., 2015; Simard et al., 2013). Thus, the high level of correspondence between  $\delta^{13}C_{cam}$  and  $\delta^{13}C_{xc}$  revealed in our study does not support our initial hypothesis. We initially assumed that, if stored NSCs were to be used by xylem and not by cambium, divergences in  $\delta^{13}C$  variations between the two tissues would necessarily emerge, reflecting a mixture of NSC sources synthesized at different time periods.

Our novel method helps supporting the fact that conifers are less prompt than deciduous broadleaves species to exhibit a sharp transition in NSC source from stored NSCs to current assimilates during the growing season (Klein et al., 2005; Sarris et al., 2013; Schollaen et al., 2014). On the contrary, our study provides additional isotopic evidence that the secondary growth of evergreens relies primarily on current assimilates (Hansen & Beck, 1990; Klein & Hoch, 2015; Ogée et al., 2009; Rinne et al., 2015). Indeed, a recent study on black spruce showed very strong correlations in the  $\delta^{13}$ C ratios of latewood and whole rings over 70 years, suggesting that both earlywood and latewood were constructed from current-year photosynthates (Alvarez et al., 2018). These results are compatible with the coherence of intra-annual  $\delta^{13}C_{cam}$  and  $\delta^{13}C_{xc}$  profiles shown in our study. The isotopic signature of starch, a major stored carbohydrate during spring in conifers' needles, is influenced by metabolic processes during its synthesis in the chloroplast. During daylight, starch is produced and accumulates in the chloroplasts of leaves, originating from fructose-6-phosphate via fructose 1,6-bisphosphate. The aldolase enzyme, acting during the regeneration phase of the Calvin Cycle, favors <sup>13</sup>C during production of fructose 1,6bisphosphate, leading to a relative <sup>13</sup>C enrichment of starch as an end product (Gleixner & Schmidt, 1997). Therefore, if <sup>13</sup>C-enriched, starch-derived NSCs would contribute significantly to earlywood and less to latewood formation, then, a negative slope contrary to the one observed here would be expected.

Intra-annual increasing trends in  $\delta^{13}C_{cam}$  and  $\delta^{13}C_{xc}$  in our sites may, on the contrary, partially reflect the  $\delta^{13}C$  signature of the local atmosphere. Indeed, photosynthesis is well known to use lighter  $^{12}CO_2$  preferentially, resulting in an atmosphere that becomes progressively enriched in  $^{13}CO_2$  as the growing season comes to an end (Ballantyne et al., 2010). However, accounting for seasonal  $\delta^{13}C_{atm}$  values at AMT and LLB, does not entirely remove the trends in  $\delta^{13}C_{cam}$  (Figure A.3 and A.5) and  $\delta^{13}C_{xc}$  series (Figure A.4 and A.6). We observed that the increasing pattern in the two profiles remained even after the correction for seasonal  $\delta^{13}C_{atm}$  variations in almost all intra-annual series. While recognizing that the trends in  $\delta^{13}C_{atm}$  might be both smoothed and conservative, one could argue that the residual trends in  $\delta^{13}C_{xc}$  and  $\delta^{13}C_{cam}$  may reflect either climate-induced stress responses, changes in carbon allocation strategies, or a combination of both.

Our analysis reveals that the increasing  $\delta^{13}$ C trends in the cambium-xylem continuum are unlikely to be entirely driven by climatic conditions. A vast body of knowledge in dendroclimatology exists, which suggests that increasing moisture stress towards the end of the growing season may result in higher  $\delta^{13}$ C values in the tree ring (Barbour et al., 2002; Castagneri et al., 2018; Sarris et al., 2013; Xu et al., 2022). For instance, a decline in precipitation and soil water content, excessively high temperatures and a lower relative humidity may all contribute to the limitation of  $g_s$  in the needles of evergreen conifers. In turn, this could lead to increasing  $\delta^{13}C_{cam}$  and  $\delta^{13}C_{xc}$  trends. However, our detailed micro-meteorological analysis suggests that all these variables ( $T_{max}$ , VPD, RH, P, VWC) are not indicative of trees growing in conditions that become increasingly cold and wet towards the end of the growing season (Figure A.7 and A.8), neither at the tree level (Figure A.9), nor at the site level (Table 2.4 and 2.5). In this context, it is unlikely that the increase in  $\delta^{13}C_{cam}$  and  $\delta^{13}C_{xc}$  reflects a seasonally-integrated  $g_s$  response to water stress.

In absence of detrimental climatic effects, we speculate on three alternative causes that may individually or jointly explain the residual increasing trends in  $\delta^{13}C_{cam}$  and  $\delta^{13}C_{xc}$ . These upward trends remain evident even after detrending the  $\delta^{13}C_{xc}$  series ( $\delta^{13}C_{xc}$  seq) (Figure A.2). First, as the growing season advances, trees may shift allocation strategies, from a secondary growth priority (in the early to mid-season) to a frost resistance priority (in the late season). As this shift operates, trees would then allocate less enriched NSCs (e.g., pinitol and lipids) for frost resistance purposes (Rinne et al., 2015; Sleptsov et al., 2023). This strategy is commonly adopted by trees that need to maintain tissue functional integrity despite prolonged freezing winters (Lipavská et al., 2000). Consequently, the unreacted, <sup>13</sup>C-enriched residual sugars like sucrose (Rinne et al., 2015) may be loaded into the phloem and ultimately used for wood formation, mostly in the form of latewood. Trees like spruce may be particularly susceptible to frost damage due to their thin bark (Simard et al., 2013). Thus, they probably need an effective resource allocation strategy to resist frost damages specifically in the cambial region (Gurskaya & Shiyatov, 2006). The observed slight decrease in  $\delta^{13}C_{cam}$  values towards the season's end (Figure 2.4) could be attributed to an increase in the concentration of <sup>13</sup>C-depleted sugars, possibly raffinose (Deslauriers et al., 2016; Simard et al., 2013), unloaded from phloem into the cambial region (Simard et al., 2013), as a response to the dropping temperatures in the study region. A second cause could be that, in early autumn, trees gradually reduce water content and increase residual evaporation through the needles to prevent frost damages due to ice crystal formation (Bozonnet et al., 2024; Charrier & Améglio, 2024). Although this is not a response to a typical atmospherically-induced drought stress, less water uptake could result in a lower q<sub>s</sub> which, in turn, could yield NSCs that are systematically enriched in <sup>13</sup>C as the growing season comes to its end. The third cause

could be related to the reduced PAR as the growing season ends (Figure A.7d and A.8d), leading to a gradual decline in the photosynthesis rate. This decline forces a proportional reduction in  $g_s$ , leading to the observed increasing trends in the  $\delta^{13}C_{cam}$  and  $\delta^{13}C_{xc}$  profiles (Siegwolf et al., 2023). In this context, a dual-isotope analysis of weekly variations in carbon and oxygen isotopes can provide deeper insights into the physiological processes affecting tree growth on a seasonal scale.

While the sampling approach proposed here enables to capture similarities between  $\delta^{13}C_{\text{cam}}$  and  $\delta^{13}C_{\text{xc}}$ profiles, it also underlines several differences at the inter-site scale. For example, we found that the mean  $\delta^{13}$ C levels in SIM, for both the cambial zone and the xylem, are systematically more enriched by about 0.6% compared to BER. Longer growing seasons along with higher soil temperatures in SIM (Balducci et al., 2021), may contribute to an increase in the rate of carboxylation at the leaf level at this site. This leads to a decrease in  $c_i/c_a$ , resulting in less negative  $\delta^{13}$ C values at this site compared to the colder site of BER (Siegwolf et al., 2023). This difference cannot be explained by other confounding factors such as stand age or altitude. Indeed, stand age usually has the opposite effect:  $\delta^{13}$ C is known to increase with tree age (M. Fonti et al., 2018; Helama et al., 2018; Marchand et al., 2020). Here, BER presents the oldest individuals (Table 2.1), but reveals the lowest  $\delta^{13}$ C values. Altitude could also have a positive effect on  $\delta^{13}$ C composition in tree rings (Helama et al., 2018; Hultine & Marshall, 2000; Li et al., 2009). Warren et al., (2001) indicated that the  $\delta^{13}$ C values of conifer stem wood increased by +2.5% per km of rising altitude. Applying this rate to our  $\delta^{13}$ C data for the two study sites of SIM and BER with a 273 m altitudinal difference (Table 2.1) could result in a potential increase of +0.7%, while we observed a decrease in  $\delta^{13}C_{xc}$  and  $\delta^{13}C_{cam}$ values in BER, suggesting that altitude does not act as a direct single factor in the region of study (C. Warren et al., 2001).

The method we developed also underlines significant differences in  $\delta^{13}C_{xc}$  profiles at the intra-site scale. In about all sites and years, most individual trees share a common increasing pattern (Figure A.1), but that there is also a notable amount on inter-tree weekly variability, reflected in EPS<sub>w</sub> that remain quite low (Table 2.3). High inter-individual variability in  $\delta^{13}C$  profiles have also been observed, at inter-annual time scales, for black spruce (Bégin et al., 2015) and various other deciduous and coniferous species (Raffalli-Delerce et al., 2004; Roden et al., 2011). This may suggest that, just like for inter-annual time scales, microenvironmental conditions surrounding each sampled tree may have a large influence on the weekly carbon isotopic fractionation (Bégin et al., 2015). Genetic factors and nutritional stress from inter-tree competition may also contribute to the variability in  $\delta^{13}C$  series among tree samples (Bégin et al., 2015;

McCarroll & Loader, 2004). Furthermore, our findings align with previous research indicating that sampling from different parts of the stem contributes to the variability in  $\delta^{13}C_{xc}$  values, due to incoherent intra-ring  $\delta^{13}C$  variability (i.e., circumferential variability) (Leavitt, 2010; Tans & Mook, 1980). One way to improve the current method, for black spruce at the very least, would be to increase sampling depth to about ten individuals per site, so to converge towards EPS<sub>w</sub> > 0.85.

#### 2.6 Conclusions

Overall, our study unveils the first *in situ* monitoring of carbon isotope fractionation in trees, at a weekly time scale. Its main contribution lies in the ability to perform  $\delta^{13}C$  analysis on newly formed cambium and xylem cells, separately. Performing  $\delta^{13}C$  analysis on these two tissues has the potential to reduce knowledge gaps that persist on the timing of NSC synthesis in leaves, their subsequent transport / remobilization through phloem / cambium, and ultimately, their incorporation in tree-ring cellulose. In the present case, our method has clearly demonstrated that the weekly construction of black spruce's cambium and xylem cells are formed by shared NSC pools, originating predominantly from current photoassimilates. While this method has proven effective for monitoring the weekly  $\delta^{13}C$  evolution of the cambium-xylem continuum in black spruce, further research is recommended to evaluate its applicability to species with different growth characteristics.

However, to better ascertain the variations in the rate of production of such assimilates, the ecophysiological processes involved, and how they relate to external (e.g., climate-related) or internal drivers (e.g., sink dynamics) additional data are required. Fortunately, the method is most likely also suitable for oxygen stable isotopes ( $\delta^{18}$ O), opening the way for multi-isotope analysis at a weekly resolution. Coupling such isotopic analysis to high precision xylogenesis monitoring, anatomical features and phenological changes, for example, would represent a means to refine current state-of-the-art eco-physiological models (Guiot et al., 2014) and better predict the short-term response of boreal forests to environmental changes.

Additionally, a study comparing weekly variations of  $\delta^{13}C$  series in cellulose and whole wood within developing tree ring could provide further insights into the use of whole wood versus  $\alpha$ -cellulose for weekly monitoring of carbon stable isotopes and help optimize sample collection and analysis. Lastly, while our multiple-source ( $\delta^{13}C_{cam}$ ), single-sink ( $\delta^{13}C_{xc}$ ) analysis approach provided insights into carbon dynamics in black spruce, a compound-specific monitoring of carbon stable isotopes in the cambium-xylem

continuum (e.g.,  $\delta^{13}$ C in different sugars found in the two tissues) could offer further information on seasonal carbon allocation strategies in boreal trees.

#### 2.7 Figures Legend

<u>Figure 2.1:</u> Within the tree ring, ENL denotes enlargement cells, CWT represents cell wall thickening and M indicates mature cells. PH refers to phloem. The horizontal dashed line represents the separation area between xylem and bark in the strips. Our method enabled weekly monitoring of  $\delta^{13}$ C variation in the cambial region ( $\delta^{13}$ C<sub>cam</sub>) and developing xylem ( $\delta^{13}$ C<sub>xc</sub>) both in SIM and BER across different study years.

<u>Figure 2.2:</u> The map displays two study sites: Simoncouche (SIM) and Bernatchez (BER). The study sites exhibit differences in altitude and annual mean temperature, with BER located at higher altitudes and experiencing lower annual temperatures, leading to shorter growing seasons. The map was created using ArcGIS Desktop.

Figure 2.3: (a) bark (left) and xylem (right) strips approximate sized 3 × 6 cm. (b) Scraping the cambial region into the form of powder from the inner side of the bark. (c) Cutting the last ring from the transverse section of the xylem sample with razor blade. (d) Scraping the narrower rings (onset of early wood formation) from the tangential area of the xylem sample. Our method for collecting cambium and xylem cells was efficient, providing enough mass for isotope ratio mass spectrometry (IRMS) and developing  $\delta^{13}$  C<sub>cam</sub> and  $\delta^{13}$ C<sub>xc</sub> series at both sites.

Figure 2.4: SIM 2019 (a), SIM 2020 (b), SIM 2021 (c), BER 2020 (d) and BER 2021 (e). The lower lines represent the  $\delta^{13}$  C<sub>cam</sub> profiles for the full growing season in each study year. The dashed part is related to the dates before the beginning of early wood formation (EW), while the solid part represents the dates after the onset of early wood formation. Thin lines represent each individual's seasonal  $\delta^{13}$ C<sub>xc</sub> profiles and the upper bold lines are the mean  $\delta^{13}$ C<sub>xc</sub> profiles. Regression lines are shown for each of the profiles. The insets represent the difference between the mean values of  $\delta^{13}$ C in xylem cellulose (xc) and  $\delta^{13}$ C cambial region (cam). The asterisks in SIM 2020 (b) and BER 2020 (d) represent the dates that pooling was done for the xylem samples. Strong positive correlations were observed between the  $\delta^{13}$ C<sub>cam</sub> and  $\delta^{13}$ C<sub>xc</sub> profiles in almost all study years at both sites.

Figure 2.5: The  $\delta^{13}C_{cam}$  series are compared between SIM and BER in 2020 (a) and 2021 (b), while the  $\delta^{13}C_{xc}$  series are compared between SIM and BER in 2020 (c) and 2021 (d). Dashed and solid lines represent the regression lines. Increasing trends are evident in all series from the beginning to the end of the growing season. Compared with BER, mean values of  $\delta^{13}C_{cam}$  and  $\delta^{13}C_{xc}$  in SIM were significantly higher (more enriched in  $^{13}C$ ) both in 2020 and 2021.

Figure 2.6: Inter-tree correlations in SIM 2019 (a), SIM 2020 (b), SIM 2021 (c), BER 2020 (d) and BER 2021 (e). Tree samples vary in each study year. Inter-tree  $\delta^{13}C_{xc}$  correlations were positive and relatively high in each study year. However, negative correlations were observed between tree no.1 and trees no. 2 and 4 in SIM 2019 (a) and tree no.5 and trees no. 1, 3 and 4 in SIM 2021 (c). Asterisks denote the significance of the correlation coefficient (\*\*\*p< 0.01, \*\*p< 0.05, \*p< 0.1).

#### 2.8 Tables Legend

<u>Table 2.1</u>: Latitude (Lat.), longitude (Long.), altitude (Alt, meters above sea level). DBH (diameter at breast height) was calculated by averaging all selected individuals' DPH measurements for each site. The average age of trees at each site. Annual statistics for temperature (average) and precipitation (sum) were calculated values from 2019-2021 for SIM and BER.

<u>Table 2.2</u>: The analyzed periods for different study years at SIM and BER are shown as day of year periods.

Table 2.3: The mean  $\delta^{13}C_{cam}$  and  $\delta^{13}C_{xc}$  and standard deviations (SD) at each site, and study year. Pearson's correlation analysis between  $\delta^{13}C_{xc}$  and  $\delta^{13}C_{cam}$  profiles.

<u>Table 2.4</u>: Maximum temperature ( $T_{max}$ ), vapour pressure deficit (VPD), photosynthetically active radiation (PAR), relative humidity (RH), precipitation (P), soil volumetric water content (VWC), (\* p<0.1, \*\* p<0.05, \*\*\* p<0.01).

<u>Table 2.5</u>: Maximum temperature ( $T_{max}$ ), vapour pressure deficit (VPD), photosynthetically active radiation (PAR), relative humidity (RH), precipitation (P), soil volumetric water content (VWC), (\* p<0.1, \*\* p<0.05, \*\*\* p<0.01).

# 2.9 Figures

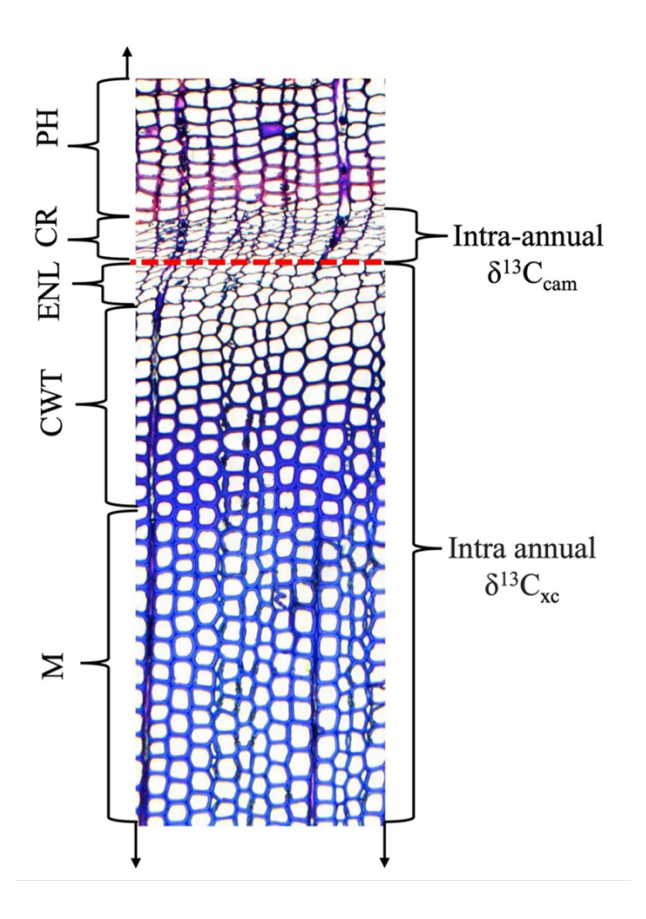


Figure 2.1 Differentiation of cells in the xylem and cambial region during the growing season. CR refers to the cambial region (cambium and differentiating phloem and xylem cells).

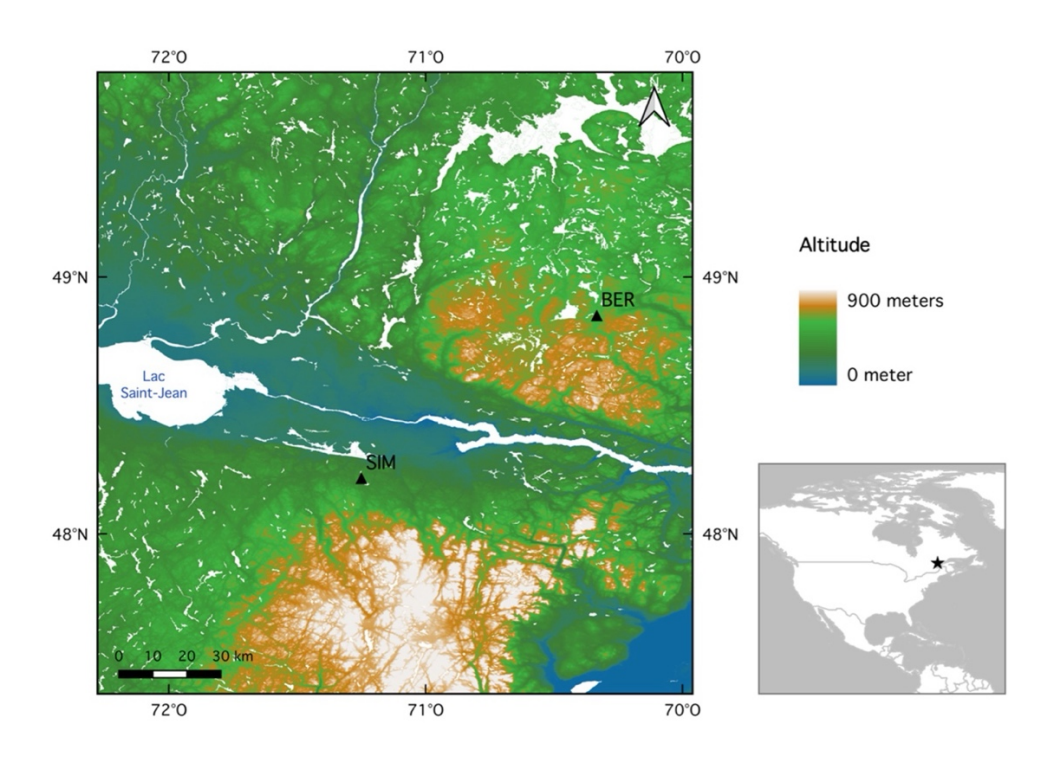


Figure 2.2 Topography of the Saguenay-Lac-Saint-Jean area in eastern Quebec, Canada.

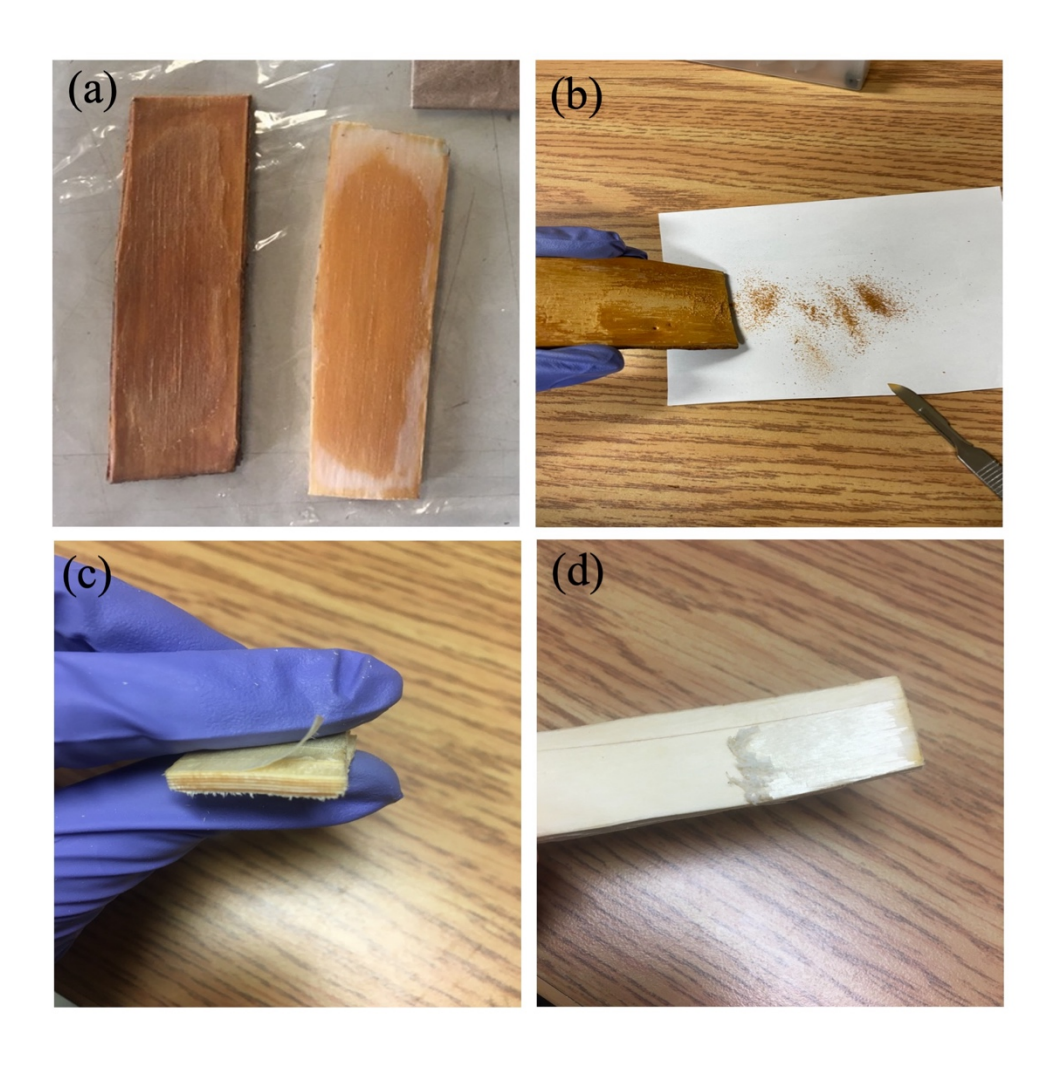


Figure 2.3 Collection techniques for the cambial region and developing tree ring.

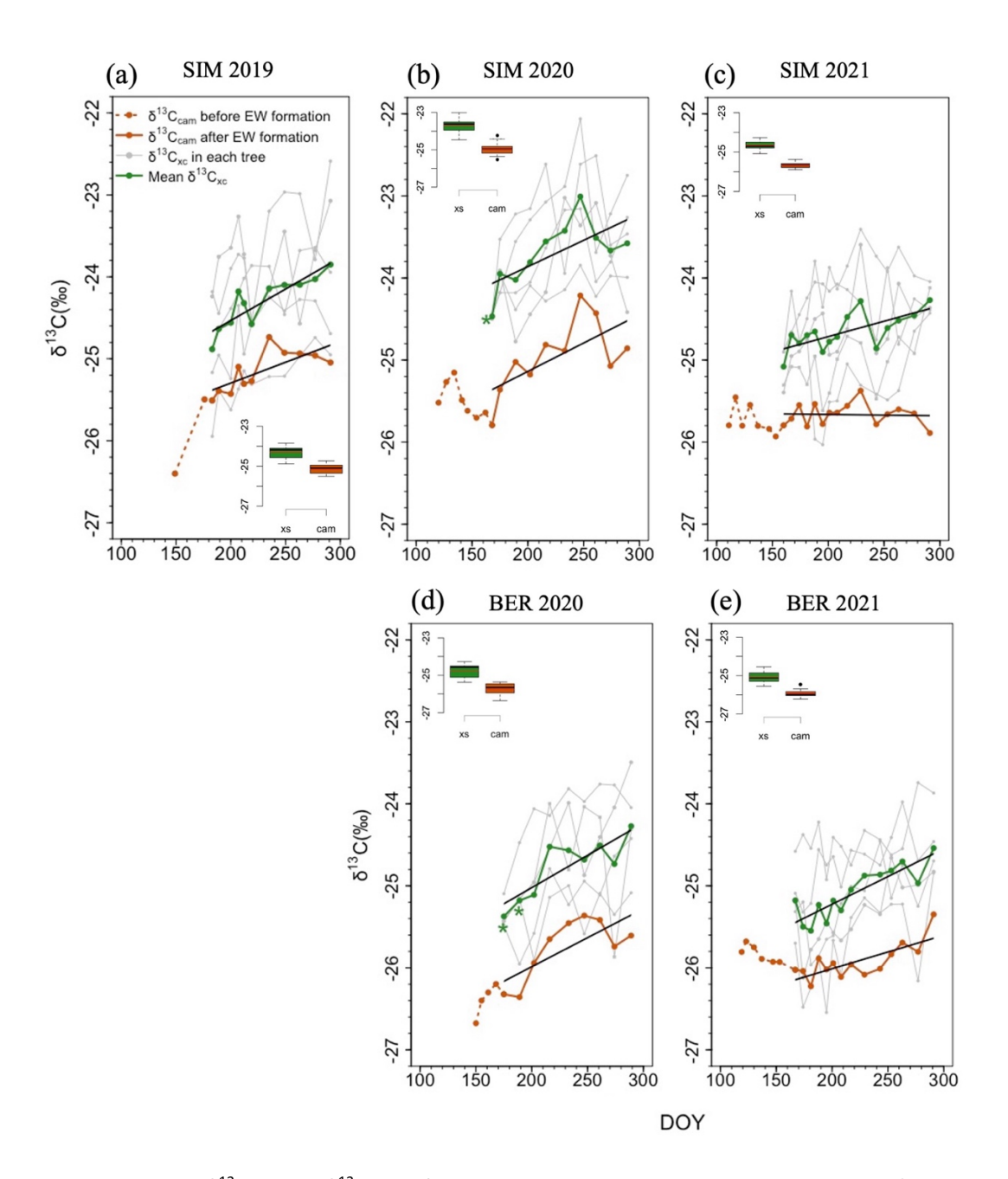


Figure 2.4 Intra-annual  $\delta^{13}C_{cam}$  and  $\delta^{13}C_{xc}$  profiles in SIM and BER. Both series are depicted for each site in every study year.

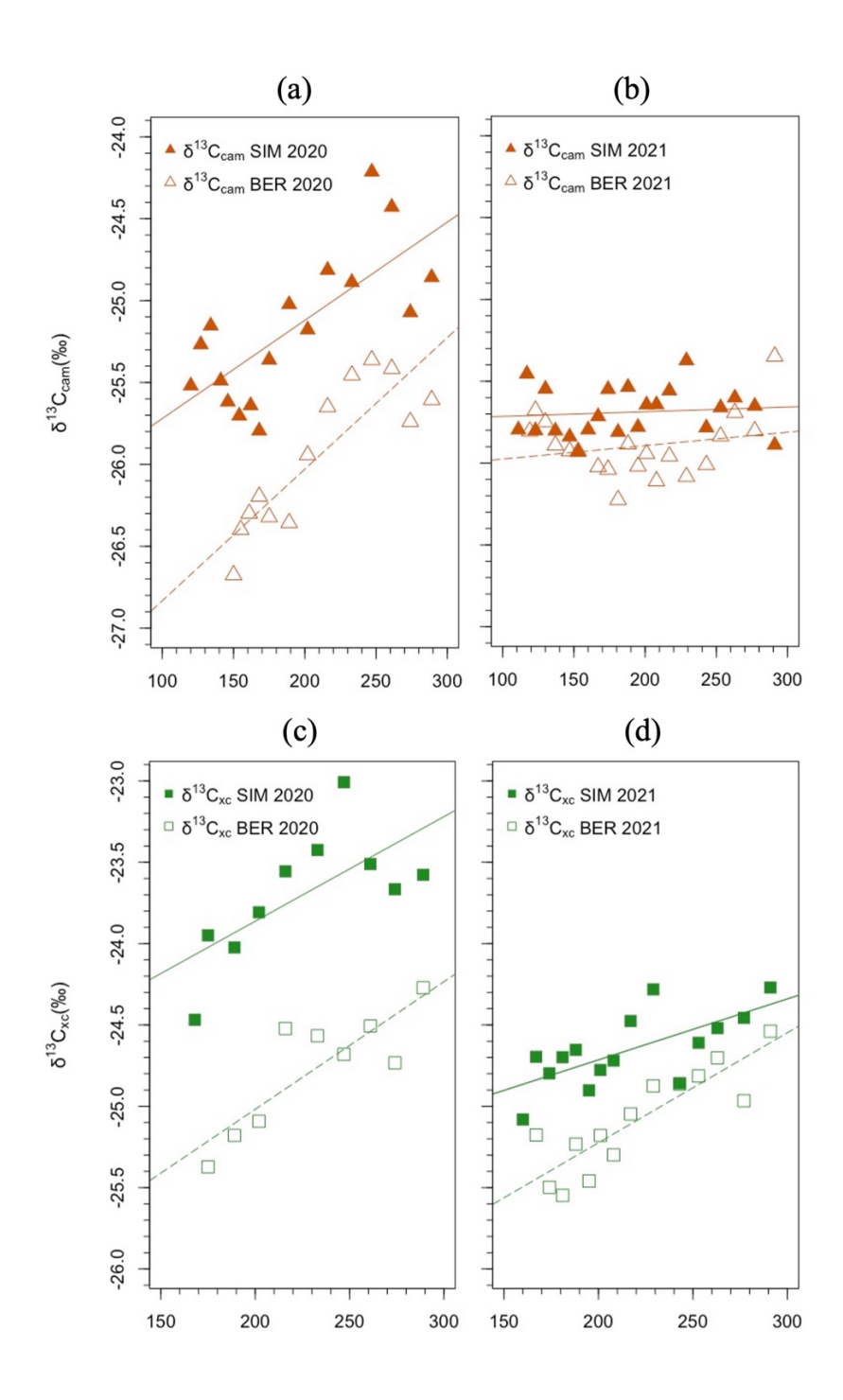


Figure 2.5 Comparison of the  $\delta^{13}C_{cam}$  and  $\delta^{13}C_{xc}$  profiles between two sites, SIM and BER, over two study years of 2020 and 2021.

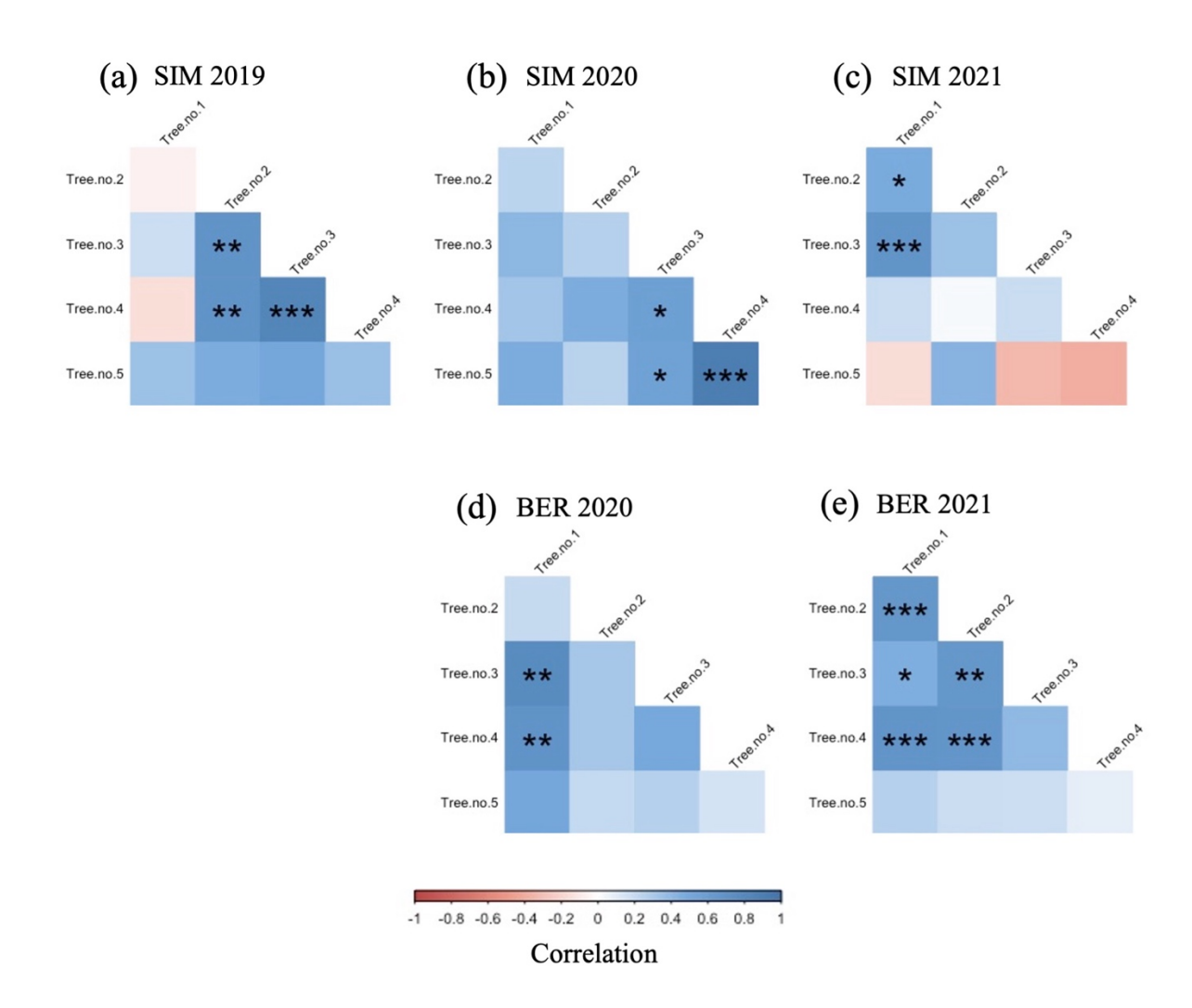


Figure 2.6 Matrix of inter-trees' correlation between  $\delta^{13}C_{xc}$  series for SIM and BER in different study years (Pearson's correlation).

# 2.10 Tables

Table 2.1 Location, tree characteristics, and climatic conditions at the two study sites.

Code	Lat.	Long.	Alt (m a.s.l.)	DBH (cm)	Mean age	May-Oct temperature (°C)	Annual temperat ure (°C)	May-Oct Precipitati on (mm)	Annual Precipita tion(mm )
SIM	48°13′	71°15′	338	24.8 ±3.8	78±7.7	12.8	3.2	484.3	640.6
BER	48°51′	70°20′	611	23.6 ±1.8	133±4	10.3	0.6	483	570.1

Table 2.2 The climatic variables, codes, and units.

Climatic	Code	Unit	SIM	SIM	SIM	BER	BER
Variables	Code	Oilit	2019	2020	2021	2020	2021
Maximum temperature	T <sub>max</sub>	°C	183-291	168-289	160-291	175-289	167-291
Vapour pressure deficit	VPD	kPa					
Photosyntheti cally active radiation	PAR	μmol/m²/s					
Relative humidity	RH	%					
Precipitation	Р	mm					
Soil volumetric water content	VWC	m³/m³					

Table 2.3 Statistics of mean inter-trees correlation (Rbar) of  $\delta^{13}C_{xc}$  and weekly EPS (EPS<sub>w</sub>) in two sites.

Site/year	SIM 2019	SIM 2020	SIM 2021	BER 2020	BER 2021
Rbar	0.4	0.5	0.1	0.4	0.4
EPS <sub>w</sub>	0.8	0.8	0.5	0.8	0.8
Mean δ <sup>13</sup> C <sub>cam</sub> (‰±SD) full growing season	-25.3±0.4	-25.2±0.4	-25.7±0.1	-26.0±0.4	-25.9±0.2
Mean $\delta^{13}C_{cam}$ (%±SD) after onset of wood formation	-25.1±0.2	-25.0±0.4	-25.7±0.1	-25.8±0.4	-25.9±0.2
Mean δ <sup>13</sup> C <sub>xc</sub> (‰±SD)	-24.3±0.3	-23.7±0.4	-24.7±0.2	-24.8±0.4	-25.1±0.3
Correlation coefficient between $\delta^{13}C_{\text{cam}}$ and $\delta^{13}C_{\text{xc}}$	0.8 (p<0.01)	0.9 (p<0.001)	0.4 (p<0.2)	0.8 (p<0.01)	0.8 (p<0.01)

Table 2.4 Correlation coefficients for the relationships between  $\delta^{13}C_{cam\_cor}$  and different climatic variables of daytime averages (8h00 to 18h00).

Site/year	SIM 2019	SIM 2020	SIM 2021	BER 2020	BER 2021	
δ <sup>13</sup> C	$\delta^{13}C_{\text{cam\_cor}}$	$\delta^{13}C_{\text{cam\_cor}}$	$\delta^{13}C_{\text{cam\_cor}}$	$\delta^{13}C_{\text{cam\_cor}}$	$\delta^{13}C_{\text{cam\_cor}}$	
T <sub>max</sub>	-0.5	-0.3	-0.1	-0.6*	-0.6**	
VPD	-0.6*	-0.5	0.0	-0.7**	-0.5	
PAR	-0.8***	-0.6*	0.3	-0.7*	-0.4	
RH	0.7**	0.7**	-0.1	0.8**	0.3	
Р	0.8***	0.2	0.0	0.5	-0.2	
VWC	-0.3	0.3	0.6**	0.3	0.1	

Table 2.5 Correlation coefficients for the relationships between  $\delta^{13}C_{xc\_cor}$  and  $\delta^{13}C_{xc\_seq}$  different climatic variables of daytime averages (8h00 to 18h00).

Site/	SIM		SIM		SIM		BER		BER	
year	2019		2020		2021		2020		2021	
δ <sup>13</sup> C	$\delta^{13}C_{xc\_c}$	$\delta^{13}C_{xc}$	$\delta^{13}C_{xc\_c}$	$\delta^{13}C_{xc}$	$\delta^{13}C_{xc\_c}$		$\delta^{13}C_{xc\_c}$	$\delta^{13}C_{xc\_s}$	$\delta^{13}C_{xc\_c}$	$\delta^{13}C_{xc\_s}$
	or	_seq	or	_seq	or	eq	or	eq	or	eq
$T_{max}$	-0.5	-0.6*	-0.2	-0.2	-0.5*	-0.7**	-0.6*	-0.6*	-0.5**	-0.4
VPD	-0.6*	-0.6*	-0.3	-0.1	-0.5*	-0.6**	-0.7*	-0.4	-0.5*	-0.4
PAR	-0.7**	- 0.8**	-0.5	-0.2	-0.4	-0.5**	-0.7**	-0.4*	-0.6**	-0.5*
RH	0.7**	0.7**	0.6*	0.2	0.5*	0.6**	0.8**	0.5	0.5	0.4
Р	0.9***	0.8**	0.1	-0.5	0.1	0.1	0.4	0.1	-0.4	-0.3
VWC	-0.2	-0.2	0.3	0.2	0.0	-0.1	0.2	0.2	-0.4	-0.2

#### **CHAPTER 3**

# Weekly carbon and oxygen isotope dynamics in black spruce: a case study in the northeastern boreal forest of Quebec, Canada

Sepideh Namvar<sup>1</sup>, Étienne Boucher<sup>2</sup>, Annie Deslauriers<sup>3</sup>, Fabio Gennarettid<sup>4,5</sup>, Hubert Morin<sup>3</sup>

- This article was published in Agricultural and Forest Meteorology in August 2025
- Supplementary material is attached in Appendix B

<sup>&</sup>lt;sup>1</sup> Department of Biological Sciences and GEOTOP, Université du Québec à Montréal, 201, Président-Kennedy Ave, Montréal (QC), Canada H2X 3Y7

<sup>&</sup>lt;sup>2</sup> Department of Geography, GEOTOP and Centre d'études nordiques, Université du Québec à Montréal, Montréal (QC), Canada H2X 3R9

<sup>&</sup>lt;sup>3</sup> Departement des Sciences Fondamentales, Université du Québec à Chicoutimi, 555, boulevard de l'Université, Chicoutimi (QC), Canada G7H 2B1

<sup>&</sup>lt;sup>4</sup> Institut de Recherche sur les Forêts, Groupe de Recherche en Écologie de la MRC Abitibi, Université du Québec en Abitibi-Témiscamingue, 341, rue principale Nord, Amos (QC), Canada J9T 2L8

<sup>&</sup>lt;sup>5</sup> Department of Agricultural, Food and Environmental Sciences, Università Politecnica delle Marche, Piazza Roma, 22, 60121, Ancona, Italy

## 3.1 Abstract

The stable isotopic composition of carbon ( $\delta^{13}$ C) and oxygen ( $\delta^{18}$ O) in tree rings is widely used to explore tree eco-physiological dynamics across various time scales. However, interpreting these isotopic signals is challenging due to multiple interacting factors, including gas exchange at the leaf level, stored carbohydrate reserves, and xylem water, whose timing and interactions during the growing season remain poorly understood. In this study weekly  $\delta^{13}$ C and  $\delta^{18}$ O signals were tracked within the cambial region and forming xylem of black spruce [Picea mariana (Mill.) BSP.] in boreal forests of Quebec, Canada. The study covered three consecutive growing seasons (2019–2021) at two forest sites with differing temperature and soil water content. Weekly isotopic profiles were developed for the cambial region ( $\delta^{13}C_{cam}$  and  $\delta^{18}O_{cam}$ ) and developing xylem cellulose ( $\delta^{13}C_{xc}$  and  $\delta^{18}O_{xc}$ ). Strong positive correlations were observed between  $\delta^{13}C_{cam}$  and  $\delta^{18}O_{cam}$ , with an increasing trend along the growing season. Conversely, negative relationships were observed between  $\delta^{13}C_{xc}$  and  $\delta^{18}O_{xc}$ , characterized by an increasing trend in  $\delta^{13}C_{xc}$  and a decreasing trend in  $\delta^{18}O_{xc}$ . The results illustrated that stomatal conductance is the dominant physiological factor controlling seasonal fractionation of  $\delta^{13}C_{cam}$  and  $\delta^{18}O_{cam}$ . Increasing proportional exchanges between xylem water and sugars at the sites of cellulose synthesis (i.e.,  $P_{\rm ex}$  effect) are thought to be strong enough to completely blur the trends visible in  $\delta^{18}O_{cam}$ . This suggests that  $\delta^{18}O_{xc}$  signals differ from those originating in the earlier cambium sink. These findings highlight the need to carefully consider the processes influencing isotopic signals to avoid misinterpretations in dendroclimatological studies.

Keywords: dual-isotope approach, carbon, oxygen, weekly monitoring, tree ring,  $P_{\rm ex}$  effect

#### 3.2 Introduction

Trees acclimate on daily to weekly time scales to ever-changing meteorological, environmental, and ecological conditions. To do this, they continuously adjust key processes like net photosynthesis ( $A_{net}$ ) and stomatal conductance ( $g_s$ ) to balance  $CO_2$  uptake with  $H_2O$  losses while meeting sink demands (Buckley, 2017; Flexas et al., 2013). These adjustments have critical impacts on gas and energy exchanges at the vegetation-atmosphere interface, ultimately providing important ecological services such as carbon sequestration and climate mitigation, for example through the regulation of transpiration rates (Beer et al., 2010). Despite considerable advances at the ecosystem level, derived from eddy-covariance data (Baldocchi, 2020), the rate and synchronicity of  $A_{net}$  and  $g_s$  adjustments at the individual tree level remain poorly understood (Buckley, 2017).

At the tree level, dendrochronological studies have predominantly utilized carbon and oxygen stable isotopes of tree ring to retrospectively document changes in  $A_{net}$  and  $g_s$ , linking these changes to shifting environmental conditions at the interannual scale (Bégin et al., 2015; Danis et al., 2006; Hilasvuori et al., 2009; Naulier et al., 2014; Raffalli-Delerce et al., 2004; Sass-Klaassen et al., 2005; Szymczak et al., 2012; Young et al., 2011). More specifically, the dual-isotope approach leverages the fact that carbon and oxygen stable isotopes are modified by gas exchanges at the leaf level, through processes such as  $A_{net}$  and  $g_s$  (Grams et al., 2007; Scheidegger et al., 2000). Tree ring stable isotope values, therefore, provide valuable insights into metabolic adjustments under stress conditions. However, because measurements are made at the tree ring level, they yield only one isotopic value for an entire growing season, making it challenging to monitor adjustments on finer timescales (Rinne-Garmston et al., 2023). Moreover, this approach struggles to disentangle leaf-level physiological responses from other contributing factors (e.g., stored carbon reserves) that influence isotopic signals in tree rings.

Significant gaps persist in our mechanistic understanding of how physiological and climatic signals are transmitted into tree rings, particularly with regard to  $\delta^{18}$ O (Martínez-Sancho et al., 2023). One of the main processes influencing the final  $\delta^{18}$ O signature in tree rings is related to the synthesis of wood constituents in the xylem (Gessler et al., 2014; Offermann et al., 2011; Treydte et al., 2014). Proportional exchanges of oxygen occur with unenriched xylem (source) water during the conversion of sucrose to cellulose within the stem (Hill et al., 1995). This exchange of oxygen is known as " $P_{\rm ex}$  effect" and is largely determined by the rate of cycling of hexose phosphates through triose phosphate before incorporation into cellulose, which exposes more carbonyl oxygen to the xylem water prior to its incorporation into cellulose (Hill et

al., 1995; Waterhouse et al., 2002). Consequently, a portion of carbonyl oxygen atoms (from enriched sugars) is exchanged with unenriched xylem water, thereby impairing the subsequent biochemical processes at the leaf level (Martínez-Sancho et al., 2023).

Previous studies proposed that  $P_{\rm ex}$  represents a constant exchange rate during cellulose formation (Roden et al. 2000, Sternberg 2009). However, more recent research has shown that  $P_{\rm ex}$  can vary from 0.29 to 0.77, depending on different factors such as species (Gessler et al. 2013) and environmental conditions (Luo and Sternberg 1992, Cernusak et al. 2005, Gessler et al. 2009, Song et al. 2014a, Belmecheri et al. 2018). Additionally, a recent study by Szejner et al. (2020) found that in two coniferous species, *Pinus ponderosa* (Douglas ex C. Lawson) and *Pseudotsuga menziesii* (Mirb.) Franco,  $P_{\rm ex}$  increased across the tree ring. This increase was strongly associated with changes in wood anatomical features, particularly a reduction in lumen area as observed in latewood, suggesting a link between  $\delta^{18}$ O exchange during cellulose synthesis and xylem structure in coniferous species.

Recent advances have enabled the generation of intra-annual isotope profiles through techniques such as sequential cutting of fully formed tree ring sections followed by IRMS analysis (Belmecheri et al., 2018; Fu et al., 2017; Ogée et al., 2009; Pons & Helle, 2011; Xu et al., 2022), or laser ablation methods (Loader et al., 2017; Saurer et al., 2023; Schollaen et al., 2014). Despite their important role in studying the isotopic composition of tree rings at intra-annual timescales, these methods encounter several challenges. Specifically, xylem cell formation is a predominantly successive developmental process (e.g., cell enlargement, cell wall thickening, etc.), with significant overlap in timing, rate, and duration (M. Fonti et al., 2018). This overlap restricts the ability of these sequential methods to detect short-term physiological and environmental impacts on carbon and oxygen isotope signals in tree rings. Furthermore, accurately identifying the source and timing of isotope fractionation at the leaf level and tracing the influence of previously synthesized carbohydrates (e.g., starch) on xylem development remain unclear (Helle & Schleser, 2004; Rinne-Garmston et al., 2023). Additionally, estimating post-carboxylation processes introduces significant uncertainties (Gessler et al., 2014; Schiestl-Aalto et al., 2019).

To address these limitations and capture finer temporal dynamics, Namvar et al., (2024) developed a new method to monitor stable isotope fractionation in the growing cambium-xylem continuum as the tree ring forms. This method was initially applied to examine the dynamics of non-structural carbohydrates (NSCs) in the cambium and xylem of black spruce (Deslauriers et al., 2016), hybrid poplar (Deslauriers et al., 2009;

Giovannelli et al., 2011) and Norway spruce (Simard et al., 2013). The findings confirmed that both the cambium and xylem derive carbohydrates from the same sources, most likely originating from the leaves throughout the growing season, with a minimal reliance on stored carbohydrates for stem growth (Deslauriers et al., 2016). Comparing these findings with oxygen isotope signals in the cambial region and developing xylem cellulose could provide new insights into the physiological processes driving seasonal carbon and oxygen stable isotope fractionation in the cambium-xylem continuum.

Here, we monitor weekly fluctuations of  $\delta^{13}C$  and  $\delta^{18}O$  within the cambial region ( $\delta^{13}C_{cam}$  and  $\delta^{18}O_{cam}$ ) and developing xylem cellulose ( $\delta^{13}C_{xc}$  and  $\delta^{18}O_{xc}$ ) of black spruce [*Picea mariana* (Mill.) BSP.] trees growing in two boreal forests of eastern Canada, using the method proposed by Namvar et al (2024). Our analysis aims to provide insights into the dynamic shifts in  $\delta^{13}C$  and  $\delta^{18}O$  values within the vascular cambium-xylem continuum during the growing season in almost real time. We hypothesize that  $\delta^{13}C$  and  $\delta^{18}O$  values correlate within the cambial region and developing tree ring due to shared physiological constraints on carbon and oxygen fractionation originating at the leaf level. Indeed, both are expected to increase following the reduction in stomatal conductance during the growing season.

#### 3.3 Materials and Methods

#### 3.3.1 Study sites

The study was conducted in mature black spruce stands located in the Saguenay-Lac-Saint-Jean area within the boreal forest of Quebec, Canada (Figure 3.1). We used two particular sites: Simoncouche (SIM) and Bernatchez (BER), both featuring mature black spruce forests (Table 3.1). SIM is within the Simoncouche research station of the "Université du Québec a Chicoutimi" (48°13′ N, 71°15′ W, 338 m a.s.l.), situated in the Laurentide Wildlife Reserve. BER is at a higher elevation near Lake Poulin de Courval (48°51′ N, 70°20′ W, 611 m a.s.l.). Black spruce is the dominant species at both sites. The undergrowth is a typical mixed vegetation with various herbaceous and ericaceous shrub species (Dao et al., 2015). The region has a continental climate, marked by long cold winters and short warm summers (Balducci et al., 2021). Meteorological observations were available at each site using a tower equipped with an automatic data acquisition system and several measuring devices. These stations recorded various meteorological variables, including maximum temperature ( $T_{max}$ , °C), vapor pressure deficit (VPD, kPa), photosynthetically active radiation (PAR,  $\mu$ mol/m²/s), relative humidity (RH, %), precipitation (P, mm), and soil water content (VWC, m³/m³), on an hourly basis.

During the 2019-2021 study period, the mean annual air temperature in SIM was 3.2°C, while BER experienced a lower mean of 0.6°C (Table 3.1). During the growing season, specifically from May to October (2019-2021), mean temperatures were 12.8°C in SIM and 10.3°C in BER, indicating a colder and shorter growing season in BER. This is further reflected in the number of days with minimum daily temperatures above 5°C, averaging 170±20 days in SIM and 139±15 days in BER (Buttò et al., 2019; Rossi et al., 2011). The two sites recorded similar mean precipitation levels during the growing season, with approximately 480 mm of rain each (average from May to October: 2019 to 2021). However, soil water content was higher at BER compared to SIM over the same period (average from May to October 2019-2021: BER, 0.34 m³/m³; SIM, 0.22 m³/m³) (Table 3.1). The difference in altitude, mean annual air temperature, and soil moisture (Table 3.1), between the two sites provided a framework to assess  $\delta^{13}$ C and  $\delta^{18}$ O dynamics under contrasting environmental conditions, thereby enriching the comparative dimension of this study.

#### 3.3.2 Collection of cambial region and forming tree ring

Observations were conducted from late April to October in the years 2019-2021 for SIM and 2020-2021 for BER. For each growing season, five mature black spruce trees with relatively similar stem diameters were selected at each site (Table B.1, see *Appendix B*). The selected trees were healthy, with over 50% of branches alive in the crown. To avoid reaction wood, the tree samples were grown on flat surfaces with upright stems. From late April to October, we collected 13 to 22 rectangular strip samples, each measuring  $3 \times 6$  cm, for each tree and study year using a chisel and rubber hammer (Table B.2). The difference in sampling times (or number of samples) between the sites is attributed to variations in the length of the growing season. BER is located at a higher elevation and experiences cooler temperatures, which lead to a shorter growing season compared with SIM. As a result, fewer sampling times were possible at BER than at SIM. Moreover, BER is not accessible by road until the snow melts, which varies from year to year, further contributing to difference in the sampling period.

The strips, which included both bark and wood, were separated tangentially (Giovannelli et al., 2011), then frozen in liquid nitrogen and lyophilized at –50°C for five days (Namvar et al., 2024). The cambial region, including some enlargement cells, was collected by scraping the inner bark and outermost xylem (Giovannelli et al., 2011). To reduce the costs of stable isotope analysis and ensure sufficient sample mass, cambial region material from all five trees was pooled for each sampling date. The samples were homogenized using a two-bladed mixer mill (Retsch MM 400, Haan, Germany) at 30 Hz for 30 seconds.

The forming tree ring was collected by cutting the transverse section under a binocular microscope with  $10 \times \text{magnifying}$  lenses and LED ring light. For narrower rings early in the growing season, the tangential area was scraped, the difference in color and brightness between the new cells and the previous year's ring facilitates scrapping the target cells (Namvar et al., 2024). Collected xylem samples were ground into fine particles for analysis, with pooling exclusively done for a few early-season samples lacking sufficient mass. Cellulose was extracted from xylem samples through a multi-step process to remove soluble organic compounds, lignin, and hemicellulose (Epstein et al., 1976). Samples placed in Teflon/polyester filter bags (ANKOM® XT4), were treated with a 1:1 solution of toluene and ethanol in an ultrasonic bath for 90 minutes, followed by an 80-minute treatment in acetone. The bags were then boiled for one hour to extract soluble organic compounds and subsequently bleached with sodium chlorite and acetic acid to remove lignin. Finally, pure  $\alpha$ -cellulose was obtained by treating the samples with NaOH (17% w/v) and acetic acid (10%), followed by extensive rinsing and drying (Namvar et al., 2024).

#### 3.3.3 Analysis of stable isotopes ratios

All isotopic measurements were conducted at the light-stable isotope geochemistry lab at the University of Quebec's Geotop facility in Montreal, Canada. For carbon isotope analysis, 0.5 to 0.8 mg of cellulose ( $\delta^{13}C_{xc}$  for xylem samples) or pooled bulk material ( $\delta^{13}C_{cam}$  for cambial samples) was weighed into tin capsules to ensure consistent  $CO_2$  amounts across all samples and reference materials. These were analyzed using a Micromass Isoprime 100 isotope ratio mass spectrometer connected to an Elementar Vario MicroCube elemental analyzer in continuous flow mode, with an overall analytical uncertainty of  $\pm 0.1\%$ , excluding sample homogeneity and representativity. Two internal reference materials were used to normalize the results on the NBS19-LSVEC scale, and a third was analyzed as an unknown to assess the accuracy of the normalization. The total analytical uncertainty was within  $\pm 0.1\%$  (Hélie & Hillaire-Marcel, 2021).

For oxygen isotope analysis, 0.3 mg of cellulose from xylem ( $\delta^{18}O_{xc}$ ) and pooled cambial samples ( $\delta^{18}O_{cam}$ ) was placed in silver cups to standardize mass amounts across samples. The analysis was performed using an Isoprime Vision isotope ratio mass spectrometer coupled to an Elementar Vario PyroCube elemental analyzer in continuous flow mode. Results were normalized using two internal references on the VSMOW-SLAP scale, and a third reference was tested as an unknown to verify the accuracy of the process. The total analytical uncertainty was within  $\pm 0.3\%$  (Hélie & Hillaire-Marcel, 2021).

The weekly  $\delta^{13}$ C and  $\delta^{18}$ O profiles for the forming xylem cellulose were calculated by averaging the values from the five tree samples for each study year (Table B.3 and B.4). Inter-tree correlations for the  $\delta^{13}$ C<sub>xc</sub> series were previously analyzed by Namvar et al. (2024). The same analysis was performed here for  $\delta^{18}$ O<sub>xc</sub> profiles (Table B.4, Figure B.1). The differences in carbon and oxygen isotopic values between the cambial region and xylem cellulose (Table B.3 and B.4) likely reflect variations in the isotopic composition of the materials analyzed along the cambium-xylem continuum (see Namvar et al. 2024 for more details). The averaged  $\delta^{13}$ C<sub>cam</sub> and  $\delta^{13}$ C<sub>xc</sub> values were corrected to account for changes in atmospheric  $\delta^{13}$ C ( $\delta^{13}$ C<sub>atm</sub>) and Suess effect (Method B.1). These corrected values are referred as  $\delta^{13}$ C<sub>cam</sub> and  $\delta^{13}$ C<sub>xc</sub> throughout the text.

#### 3.3.4 Collection of rainwater

The rain samples were collected on a weekly basis, following the designated collection dates for the strips, during the growing seasons of 2020 and 2021 at both sites. To achieve this, a rain collector was mounted on the ground with no slope, ensuring that the funnel was approximately 30 cm above the ground to minimize wind turbulence (Figure B.1a and B.1b, see *Appendix B*). The collector was positioned around 20 m away from the sampled trees in an open area. Each week, the collected rain samples were transferred into an accumulation bottle with a double cap, sealed with parafilm, and stored in the fridge for further analysis (Figure B.1c).

To conduct the oxygen isotope analysis on rain samples, 1 ml of water was pipetted into a 2 ml vial and sealed with a septum cap. The samples were analyzed using a Picarro L2130-i Cavity Ring Down Spectroscopy (CRDS) system, with an overall analytical uncertainty of ±0.1‰. To ensure accuracy, three internal standards were used to adjust results to the VSMOW2-SLAP2 scale, and a fourth standard was tested as an unknown to verify the normalization accuracy. The reported standard deviations (1 sigma) reflect the variation among three replicate injections per sample.

## 3.3.5 Statistical analysis

Regression analysis was conducted to examine the seasonal trends of  $\delta^{13}C$  and  $\delta^{18}O$ , as well as their significance, in both the cambial region and the developing tree ring (Table B.5). The analysis of covariance (ANCOVA, VassarStats.net website, Vassar College Poughkeepsie, NY, USA) was used to compare the two regression lines of  $\delta^{13}C$  and  $\delta^{18}O$  in the cambial region and forming xylem cellulose across sites and study years. Pearson's correlations between the two chronologies ( $\delta^{13}C$  and  $\delta^{18}O$ ) were calculated to assess whether the profiles exhibited similar variations in the cambial region and developing xylem cellulose

during the growing season as observed in other studies (Ballantyne et al., 2010; Belmecheri & Lavergne, 2020; McCarroll & Loader, 2004). This method was selected because the data met the key assumptions of normality and linearity. Normality was confirmed using the Shapiro-Wilk test (Table B.6). To mitigate potential autocorrelation in the  $\delta^{13}$ C and  $\delta^{18}$ O time series, we performed an extra analysis by prewhitening the data and fitting linear models as a function of the day of sampling (day of year; DOY). The obtained residuals of  $\delta^{13}$ C and  $\delta^{18}$ O were used for correlation analysis. This process removed time-dependent trends, allowing us to evaluate the correlation between  $\delta^{13}$ C and  $\delta^{18}$ O independently of temporal autocorrelation (Table B.6).

Pearson's correlations were also employed to assess the relationships between  $\delta^{13}$ C,  $\delta^{18}$ O, and various meteorological parameters, as all series exhibited linear trends and met the assumption of linearity (Figure S3 and S4) and normality, as confirmed by Shapiro-Wilk test (Table B6). The same pre-whitening method was applied to the meteorological variables to perform correlations between the residuals of the isotopic data and the climate variables (Table B.7 and B.8). The weekly daytime (8h00 to 18h00) values of six different climate parameters: maximum temperature, vapour pressure deficit, photosynthetically active radiation, relative humidity, and soil volumetric water content, were averaged, and precipitation values were summed for the corresponding time periods (DOY) matching the sampling intervals for each year and site. Meteorological data were collected from on-site weather stations at each location. A comparison between the Global Meteoric Water Line (GMWL) and the local meteoric water lines derived for SIM and BER during the 2020 and 2021 growing seasons was performed (Figure B.2).

To simulate the seasonal dynamics of the fraction of oxygen atoms exchanged with xylem water, known as  $P_{\rm ex}$  effect,  $P_{\rm ex}$  was modeled under three scenarios: a constant value of 0.4, a linear increasing  $P_{\rm ex}$  from 0.3 to 0.5, and a linear decrease from 0.5 to 0.3 (Szejner et al. 2020). To represent seasonal variation,  $P_{\rm ex}$  was modeled as a linear function of the day of year (DOY), starting from an initial value ( $P_{\rm ex}^{\rm start}$ ) at the beginning of the growing season and changing gradually to a final value ( $P_{\rm ex}^{\rm end}$ ) by the end of the season. The rate of change in  $P_{\rm ex}$  (Slope, rate per day) was calculated from the beginning (DOY<sub>start</sub>) to the end of the growing season (DOY<sub>end</sub>), using the following equation:

$$Slope = \frac{P_{ex}^{end} - P_{ex}^{start}}{DOY_{end} - DOY_{start}}$$

Equation 3.1 Calculation of Slope (rate per day) for  $P_{ex}$ -effect

The  $P_{\rm ex}$  values were then generated to increase or decrease linearly over the DOY range, either from 0.3 to 0.5 (increasing trend) or from 0.5 to 0.3 (decreasing trend) as follows:

$$P_{ex(date=n)} = P_{ex}^{start} + Slope \left(DOY_{(date=n)} - DOY_{start}\right)$$

Equation 3. 2 Calculation of the  $P_{\rm ex}$  effect for daily linear increasing or decreasing trends

To test the effect of  $P_{\rm ex}$  on  $\delta^{18}O_{xc}$  signals during the growing season, a model was developed to simulate  $\delta^{18}O_{xc}$  ( $\delta^{18}O_{xc-sim}$ ), using the following equation (Szejner et al. 2020):

$$\delta^{18}O_{xc-sim\,(date=n)}\\ =P_{ex(date=n)}\left(\delta^{18}O_{xw\,(date=n)}+\varepsilon_{c}\right)+\left(1-P_{ex(date=n)}\right)\left(\delta^{18}O_{lw(date=n)}+\varepsilon_{c}\right)$$

Equation 3.3 Calculation of simulated  $\delta^{18}O_{xc}$  for different  $P_{ex}$  scenarios

Where  $\varepsilon_c$  represents the average biochemical fractionation between water and organic materials, which was set to a constant value of 27‰. The isotopic composition of source water,  $\delta^{18}O_{xw}$ , was represented by  $\delta^{18}O_{rain}$  values.  $\delta^{18}O_{lw}$  refers to the isotopic composition of water at the leaf evaporation sites, here approximated by  $\delta^{18}O_{cam}$ . The  $P_{ex}$  values were obtained from equation (2) for linear variability or assumed constant during the growing season ( $P_{ex}$ =0.4). To evaluate the influence of  $P_{ex}$  on  $\delta^{18}O_{xc-sim}$ , regression analyses (ANCOVA) were performed using standardized  $\delta^{18}O_{cam}$  and  $\delta^{18}O_{xc-sim}$  series. The resulting regression slopes were then compared across different sites and years to determine which  $P_{ex}$  scenario best reflects the observed  $\delta^{18}O_{xc}$  patterns.

#### 3.4 Results

# 3.4.1 Seasonal trends in $\delta^{13}$ C and $\delta^{18}$ O in the cambial region and developing tree ring

During the full growing season, both  $\delta^{13}C_{cam}$  and  $\delta^{18}O_{cam}$  profiles showed increasing trends with varying significance levels across almost all study years, except in SIM 2021 where  $\delta^{13}C_{cam}$  and  $\delta^{18}O_{cam}$  profiles showed downward trends ( $\beta$ =-0.003, p<0.01;  $\beta$ =-0.002, p>0.1, respectively) (Figure 3.2, Table B.5). A non-significant decreasing trend was also observed in BER 2021  $\delta^{13}C_{cam}$  series ( $\beta$ =-0.002, p>0.1). The  $\delta^{13}C_{cam}$  increasing series were significant in SIM 2019 ( $\beta$ =+0.006, p<0.001) and BER 2020 ( $\beta$ =+0.005, p<0.001), while the  $\delta^{18}O_{cam}$  rising patterns were significant in SIM 2020 ( $\beta$ =+0.006, p<0.05), BER 2020 ( $\beta$ =+0.011, p<0.001) and BER 2021 ( $\beta$ =+0.007, p<0.01) (Table B.5). In SIM, slopes in  $\delta^{13}C_{cam}$  were similar to those of

 $\delta^{18}O_{cam}$  across three years of 2019 (F=0.9, p=0.4), 2020 (F=2.5, p=0.1), and 2021 (F=0.1, p=0.7), although with different intercepts (2019: F=140730.7, p<0.0001; 2020: F=87473.4, p<0.0001, 2021: F=174720.8, p<0.0001). However, in BER, significant differences were observed between  $\delta^{13}C_{cam}$  and  $\delta^{18}O_{cam}$  profiles both in terms of slopes (2020: F=12.0, p<0.01; 2021: F=11.4, p<0.01) and intercepts (2020: F=233382.24, p<0.0001; 2021: F=81335, p<0.0001).

From the perspective of intra-annual variability, consistent and significant intra-annual covariations between  $\delta^{13}C_{cam}$  and  $\delta^{18}O_{cam}$  profiles were observed at both sites and during all study years (Table 3.2, Figure 3.2). In SIM, positive correlations were evident between the two series during study years of 2019 (r=+0.58, p<0.05), 2020 (r=+0.73, p<0.001) and 2021 (r=+0.38, p<0.1). Similarly, in BER, positive relationships were observed for the years 2020 (r=+0.76, p<0.01) and 2021 (r=+0.35, p>0.1). The strong positive relationships remained between the pre-whitened detrended residuals of  $\delta^{13}C_{cam}$  and  $\delta^{18}O_{cam}$  series in SIM 2019 (r=+0.60, p<0.05), SIM 2020 (r=+0.76, p<0.01), and BER 2021 (r=+0.70, p<0.01) (Table B.6).

In contrast to the stable isotope profiles in the cambial region,  $\delta^{13}C_{xc}$  and  $\delta^{18}O_{xc}$  series in the developing tree rings displayed opposite seasonal trends (Table B.5, Figure 3.3). Specifically,  $\delta^{13}C_{xc}$  series showed significant increasing trends both in SIM (2019:  $\beta$ =+0.008, p<0.01; 2020:  $\beta$ =+0.004, p<0.1), and BER (2020:  $\beta$ =+0.005, p<0.1, 2021:  $\beta$ =+0.006, p<0.01). In contrast,  $\delta^{18}O_{xc}$  series exhibited decreasing trends at both study sites, while significant only in SIM 2019 ( $\beta$ =-0.019, p<0.01), and BER 2020 ( $\beta$ =-0.008, p<0.05) (Table B.5). We observed significant differences between the regression slopes of  $\delta^{13}C_{xc}$  and  $\delta^{18}O_{xc}$  series both in SIM (2019: F=38.3, p<0.001; 2020: F=15.1, p<0.01) and BER (2020: F=12.9, p<0.01; 2021: F=10.8, p<0.01) (Figure 3.3).

Concerning intra-annual variability,  $\delta^{13}C_{xc}$  and  $\delta^{18}O_{xc}$  showed negative correlations across the three study years in SIM 2019 (r=-0.60, p<0.1), 2020 (r=-0.36, p>0.1) and 2021 (r=-0.07, p>0.1), as well as in BER 2020 (r=-0.45, p>0.1) and BER 2021 (r=-0.26, p>0.1) (Table 3.2). The pre-whitened detrended residuals of  $\delta^{13}C_{xc}$  and  $\delta^{18}O_{xc}$  exhibited non-significant positive correlations in SIM during 2019 (r=+0.26, p>0.1), 2020 (r=+0.24, p>0.1), and 2021 (r=+0.02, p>0.1), while weak negative correlations were observed in BER for 2020 and 2021 (r=-0.01, p>0.1; r=-0.25, p>0.1 respectively) (Table B.6).

## 3.4.2 Relationships between $\delta^{18}$ O and $\delta^{18}$ O<sub>rain</sub> series

Significant negative relationships were observed between  $\delta^{18}O_{cam}$  and  $\delta^{18}O_{rain}$  (r =-0.45, p<0.1) and  $\delta^{18}O_{xc}$  and  $\delta^{18}O_{rain}$  (r =-0.53, p<0.05) in SIM 2021. All other relationships between  $\delta^{18}O$  in the cambium or xylem and  $\delta^{18}O_{rain}$  were non-significant in both sites and study years (Figure 3.4, Table 3.3).

# 3.4.3 Relationships between $\delta^{13}$ C and $\delta^{18}$ O series and climate data

Negative correlations were identified when comparing  $\delta^{13}C_{cam}$  and  $\delta^{18}O_{cam}$  series with meteorological variables of  $T_{max}$ , VPD, and PAR, across almost all study years, though they were only significant in certain cases (Table 3.4). Conversely, positive links were detected between  $\delta^{13}C_{cam}$  and  $\delta^{18}O_{cam}$  profiles and RH both in SIM and BER, with significant values in a few series in both sites (Table 3.4). In both sites and most study years, no significant relationships were found between the sum of daytime P and mean daytime VWC and either  $\delta^{13}C_{cam}$  or  $\delta^{18}O_{cam}$  profiles, except in SIM 2019, where strong positive interactions were observed between P and  $\delta^{13}C_{cam}$  (r=+0.84, p<0.01). Similar positive links were found between VWC and  $\delta^{13}C_{cam}$  in SIM 2021 (r=+0.59, p<0.05),  $\delta^{18}O_{cam}$  in SIM 2020 (r=+0.71, p<0.05) and  $\delta^{18}O_{cam}$  in BER 2020 (r=+0.68, p<0.05) (Table 3.4). In terms of pre-whitened detrended residuals, significant relationships between  $\delta^{13}C_{cam}$  or  $\delta^{18}O_{cam}$  and meteorological variables varied across sites and years (Table B.7).  $T_{max}$ , VPD, and PAR were particularly influential in 2020 and 2021, showing strong negative correlations with both  $\delta^{13}C_{cam}$  and  $\delta^{18}O_{cam}$  in both sites. In contrast, RH, P and VWC had more sporadic, site-specific effects, indicating a less consistent influence (Table B.7).

 $\delta^{13}C_{xc}$  and  $\delta^{18}O_{xc}$  profiles exhibited divergent associations with various meteorological variables (Table 3.5). Negative relationships were consistently noted between  $\delta^{13}C_{xc}$  and  $T_{max}$ , VPD, and PAR across all study years, though they were only significant in certain cases. In contrast, positive correlations were observed between  $T_{max}$ , VPD, and PAR and  $\delta^{18}O_{xc}$  in SIM 2019, SIM 2020, and BER 2020. Strong negative relationships were detected between  $\delta^{18}O_{xc}$  and RH in SIM 2019 (r=-0.64, p<0.05), and BER 2020 (r=-0.66, p<0.1). In SIM 2019, significant positive relationships were evident between  $\delta^{18}O_{xc}$  and VWC (r=+0.72, p<0.05) (Table 3.5). Additionally, the pre-whitened detrended residuals of  $\delta^{13}C_{xc}$  or  $\delta^{18}O_{xc}$  exhibited variable responses to meteorological factors (Table B.8), with VWC and RH generally showing more consistent positive effects, while  $T_{max}$  and VPD played a more site- and year-specific role in shaping the isotopic dynamics of the developing xylem (Table B.8).

# 3.4.4 Comparison between $\delta^{18}O_{cam}$ , $\delta^{18}O_{xc}$ , and $\delta^{18}O_{xc-sim}$ across $P_{ex}$ scenarios

In the decreasing  $P_{\rm ex}$  scenario, the slopes of  $\delta^{18}{\rm O}_{\rm xc-sim}$  were similar to those of observed  $\delta^{18}{\rm O}_{\rm cam}$  across SIM 2020 (ANCOVA test between standardized values, F=0.2, p=0.7), BER 2020 (F=0.3, p=0.6), and BER 2021 (F=0.5, p=0.5) (Figure 3.5a, 3.5c, and 3.5d respectively). The only exception was SIM 2021, where a significant difference was found between the two slopes (F=6.02, p<0.05) (Figure 3.5b). Similarly, the constant  $P_{\rm ex}$  scenario had little influence on the  $\delta^{18}{\rm O}_{\rm cam}$  slope in 2021, with no significant differences observed in SIM (F=0.2, p>0.1) and BER (F=0.9, p>0.1). However, in 2020, the effect was more pronounced, as significant differences were detected in both SIM (F=12.6, p<0.01) and BER (F=13.4, p<0.01) (Figure 3.5).

The increasing  $P_{\rm ex}$  scenario induced a clear shift on the slope of  $\delta^{18}{\rm O}_{\rm cam}$  (Figure 3.5). It transformed the observed increasing  $\delta^{18}{\rm O}_{\rm cam}$  slope into a decreasing trend in  $\delta^{18}{\rm O}_{\rm xc\text{-}sim}$ , consistent with the pattern observed in measured  $\delta^{18}{\rm O}_{\rm xc}$  (i.e., decreasing trends  $\delta^{18}{\rm O}_{\rm xc}$ ). Under this condition, significant differences emerged between the  $\delta^{18}{\rm O}_{\rm cam}$  and  $\delta^{18}{\rm O}_{\rm xc\text{-}sim}$  slopes in both SIM (2020: F=42.5, p<0.01; 2021: F=13.1, p<0.01) and BER (2020: F=83.6, p<0.01; 2021: F=64.3, p<0.01) (Figure 3.5). In contrast, comparison between the slopes of  $\delta^{18}{\rm O}_{\rm xc}$  and  $\delta^{18}{\rm O}_{\rm xc\text{\_}sim}$  under increasing  $P_{\rm ex}$  (from 0.3 to 0.5) revealed no significant differences in SIM 2020 (F=0.4, p>0.1), SIM 2021 (F=1.6, p>0.1), and BER 2020 (F=0.8, p>0.1) (Figure 3.5a, 3.5b, 3.5c respectively), except for BER 2021 (F=3.1, p=0.09) (Figure 3.5d).

#### 3.5 Discussion

This study represents the first attempt to monitor weekly variations in carbon and oxygen stable isotopes within the cambial region ( $\delta^{13}C_{cam}$  and  $\delta^{18}O_{cam}$ ) and developing xylem cellulose ( $\delta^{13}C_{xc}$  and  $\delta^{18}O_{xc}$ ) in black spruce trees. These data allowed us to distinguish between the processes driving isotope variation in the cambial region and those affecting developing xylem cellulose. Our findings underscore the importance of accounting for these processes to avoid misinterpretation of isotopic signals in dendroclimatological studies.

Our initial hypothesis proposed that  $\delta^{13}C$  and  $\delta^{18}O$  values in the cambial region would correlate due to shared physiological constraints on stable isotopes fractionation originating at the leaf level. The results of this study confirm this hypothesis and suggest that stomatal conductance  $(g_s)$  regulation in the needles of black spruce is likely the dominant factor controlling the seasonal fractionation of  $\delta^{13}C_{cam}$  and  $\delta^{18}O_{cam}$  in our study region. Both  $\delta^{13}C_{cam}$  and  $\delta^{18}O_{cam}$  series exhibited consistent seasonal enrichment patterns during the growing season in nearly all study years and sites (Figure 3.2), with no strong relationships observed

between  $\delta^{18}O_{rain}$  and  $\delta^{18}O_{cam}$  (Table 3.3). This pattern aligns with the dual-isotope theory (Scheidegger et al., 2000; Siegwolf et al., 2023), which attributes such enrichment to the concurrent influence of  $q_s$  on the fractionation of both isotopes. Indeed, the observed enrichment cannot be explained by changes in photosynthesis, as photosynthesis declines toward the end of the growing season. A previous study on European beech (Fagus sylvatica L.) reported similar findings, showing strong positive correlations between  $\delta^{13}$ C and  $\delta^{18}$ O in the organic matter of phloem sap, further underscoring the dominant influence of  $q_s$  on both carbon and oxygen isotopic signals (Keitel et al., 2003). Furthermore, if  $\delta^{13}C_{cam}$  variations were driven by changes in  $A_{net}$ ,  $\delta^{18}O_{cam}$  series would diverge from those of  $\delta^{13}C_{cam}$ . This was not the case here, as we observed strong positive correlations between  $\delta^{13}C_{cam}$  and  $\delta^{18}O_{cam}$  profiles in almost all study years (Table 3.2), a pattern related to stomatal and not photosynthetic control of  $\delta^{13}C_{cam}$  (Farguhar et al., 1998; Scheidegger et al., 2000). However, SIM 2021 appears to be an exception. In this year, both  $\delta^{13}C_{cam}$ and  $\delta^{18}O_{cam}$  showed trends distinct from those observed in other years (Figure 2c), and a significant correlation between  $\delta^{18}O_{cam}$  and  $\delta^{18}O_{rain}$  was detected (Table 3). This suggests that source water may play a larger role in influencing  $\delta^{18}O_{\text{cam}}$  values in SIM 2021. This anomaly indicates that the dual-isotope approach may not reliably capture stomatal conductance limitations in all years, particularly when external environmental conditions, such as changes in source water composition, exert a stronger influence.

The dual isotope theory primarily addresses leaf-level fractionations, but it can be applied to carbon and oxygen in other tissues, provided that post-carboxylation processes are minimal (Gessler et al., 2009; Siegwolf et al., 2021, 2023). The strong similarity observed in  $\delta^{13}C_{cam}$  and  $\delta^{18}O_{cam}$  variations in this study further supports the notion that post-carboxylation processes played a minor role, if any, in the overall fractionation of carbon isotopes, up to its fixation in tree-ring cellulose (Barbour et al., 2002; Gessler et al., 2008, 2009; Klein et al., 2005). If such processes were to dominate, notable differences between  $\delta^{13}C_{cam}$  and  $\delta^{18}O_{cam}$  would arise, both in terms of their trends and inter-weekly variability. This is because only carbon isotopes are affected by post-carboxylation processes, while the  $\delta^{18}O$  signature of NSCs is unlikely to be altered during phloem transport of assimilates to the cambial region (Gessler et al., 2009; Roden et al., 2000; Siegwolf et al., 2023). Indeed, sucrose which is the main sugar exported from the leaves, carries no free carbonyl group that could exchange oxygen atoms with water during its movement from the leaves to the cambial region (Gessler et al., 2014). These findings are in conformity with a study by Gessler et al., (2009), who found rather consistent transfer of  $\delta^{13}C$  and  $\delta^{18}O$  signals from canopy to the trunk phloem organic matter and cellulose or wood in *P. sylvestris*, during the entire growing season. In addition, previous studies indicate that the  $\delta^{18}O$  in leaf water is reflected in the oxygen isotope signature of organic

matter synthesized in the leaves and potentially transported in the phloem (Barbour et al., 2000; Roden & Ehleringer, 1999), suggesting minimal changes in  $\delta^{18}$ O in phloem sap during transport through the tree trunk.

The neglectable effect of post-carboxylation processes, combined with a strong correlation between  $\delta^{13}C_{cam}$  and  $\delta^{13}C_{xc}$  as evidenced by Namvar et al (2024), finally supports the fact that both cambium and xylem cells derive carbohydrates from the same resources during the growing season. Indeed, NSCs most likely derive from recently produced photo assimilates incoming from the leaves, with minimal contribution from stored NSCs, mostly in the form of  $^{13}C$ -enriched starch, for growth purposes in our spruce species (Deslauriers et al., 2016; Gessler et al., 2014; Simard et al., 2013). This aligns with the recent findings of Rinne-Garmston et al., (2023) who observed that intra-seasonal dynamics of  $\delta^{13}C$  in primary photosynthates were clearly reflected in the tree ring  $\delta^{13}C$  signals of 7-year-old *Pinus sylvestris*, suggesting a negligible impact of reserve use on tree ring  $\delta^{13}C$  values. Additionally, lower variations in  $^{13}C$ -enriched starch were observed in the cambium of larch and spruce trees during the growing season. This suggests that a constant supply of fresh assimilates to the cambium-xylem continuum may be the dominant process feeding secondary growth in our spruce trees (Simard et al. 2013, Rinne et al. 2015).

Increasing  $\delta^{13}C_{cam}$  and  $\delta^{18}O_{cam}$  trends do not exclusively originate from changing meteorological conditions, during the growing season (Table 3.4). Indeed, most studies in dendroclimatology indicate that increasing moisture stress towards the end of the growing season may lead to elevated  $\delta^{13}C$  values in tree rings (Castagneri et al., 2018; Sarris et al., 2013; Xu et al., 2022). For instance, reduced precipitation and soil water content, excessively high temperatures and a lower relative humidity may all contribute to the limitation of  $g_s$  in the needles of evergreen conifers. In turn, this could lead to increasing  $\delta^{13}C$  and  $\delta^{18}O$  trends in different tissues of trees. Conversely, in our study region, growing seasons become increasingly cold and wet towards their end. Such conditions are unlikely to trigger a typical water-stress-induced  $g_s$  reduction, which would increase  $\delta^{13}C_{cam}$  and  $\delta^{18}O_{cam}$  (Namvar et al., 2024).

In the absence of climate conditions conductive to a moisture stress response of  $g_s$ , three alternative causes are proposed that individually or jointly explain the observed cumulative increasing trends in  $\delta^{13}C_{cam}$  and  $\delta^{13}O_{cam}$  in almost all study year and sites (Figure 3.2). First, reduced light intensity (PAR) and temperature ( $T_{max}$ ) toward the end of the growing season may lead to a gradual decline in net photosynthesis ( $A_{net}$ ), which in turn may force a greater reduction in  $g_s$  resulting in increasing  $\delta^{13}C_{cam}$  values

(Farquhar & Sharkey, 1982; Siegwolf et al., 2023). Additionally, increasingly limited light conditions may lead to higher  $\delta^{18}$ O values in leaf water due to lower transpiration rates. This effect is further compounded by a progressive decline in black spruce water content and reduced turnover of leaf water from soil water toward the end of the growing season (Péclet effect) (Barbour & Farquhar, 2000; Farquhar & Lloyd, 1993; Turcotte et al., 2011). Indeed, black spruce trees gradually dehydrate their stem tissues in response to decreasing autumn temperatures, leading to maximum stem shrinkage in winter (Turcotte et al., 2009). The second alternative involves mechanisms of preparation for overwintering to minimize potential damage to tree hydraulic functions and living cells (Arora, 2018; Burke et al., 1976; Charrier et al., 2013). To mitigate such damage, trees reduce water content and enhance residual evaporation through their needles to prevent ice crystal formation in living cells (Bozonnet et al., 2024; Charrier & Améglio, 2024). Reduced water uptake in early autumn also leads to less discrimination against <sup>13</sup>C at the leaf level. This produces non-structural carbohydrates (NSCs) enriched in <sup>13</sup>C, which could be used in the cambium pool during the last months of the growing season (September-October), corresponding with cell wall deposition in the last latewood tracheid (Namvar et al. 2024). Consequently, unreacted 13C-enriched residual sugars such as sucrose (Rinne et al. 2015) may be transported through the phloem and ultimately used for wood formation, mostly for the production of latewood (Namvar et al. 2024), while less enriched NSCs (e.g., pinitol and lipids) are allocated to frost protection in various parts of tree (Rinne et al. 2015, Sleptsov et al. 2023). In this regard, a compound-specific monitoring of carbon stable isotopes in the cambium-xylem continuum (e.g.,  $\delta^{13}$ C in different sugars found in the two tissues) may offer deeper insights into seasonal carbon allocation strategies in boreal trees. Lastly, it is also possible that the behavior of  $q_s$  is driven by shifts in sink demand rather than by external factors such as climatic variations. For example, a reduction in  $q_s$  can be driven by a shift from primary to secondary growth during xylogenesis, which would require adjustments in tradeoffs between carbon assimilated and water losses through stomata. To investigate this, linking weekly  $\delta^{13}$ C-derived intrinsic water use efficiency (iWUE) data with wood anatomy and seasonal xylogenesis dynamics would offer deeper insights into such ecophysiological interactions (Cartenì et al., 2018).

Eastern Canada's black spruces' cambial and developing xylem display contrasting  $\delta^{18}O$  trends which suggests that the two tissues may be fed by differing water sources (Barbour et al., 2004). Indeed, this is highlighted by a marked increase in  $\delta^{18}O_{cam}$  which contrasts with a decreasing pattern in  $\delta^{18}O_{xc}$  (Figure 3.3). The  $\delta^{18}O_{cam}$  is expected to reflect the  $\delta^{18}O$  signals in leaf water transferred to NSCs, the primary photosynthetic products, unloaded from the phloem into the cambial region. By contrast,  $\delta^{18}O_{xc}$  signals

seem to partially derive from the isotopically depleted (i.e., lower  $\delta^{18}O_{rain}$  values) upward-moving xylem water from the soil (Barbour et al., 2004; Barbour & Farquhar, 2000; Roden et al., 2000; Song, Clark, et al., 2014).

Proportional exchanges between the un-enriched xylem water (i.e., lower  $\delta^{18}O_{rain}$  values) and sugars during the formation of cellulose in the developing xylem (i.e.,  $P_{ex}$  effect) may explain the depletion of  $\delta^{18}O_{xc}$  (i.e., lower  $\delta^{18}O_{xc}$  values) (Gessler et al., 2009; Roden et al., 2000; Song, Clark, et al., 2014; Sternberg et al., 1986). In support of our finding, a study by Offermann et al., (2011) on European beech (*Fagus sylvatica* L.) demonstrated that  $\delta^{18}O$  in tree-ring whole wood was not positively related to leaf water evaporative enrichment and  $\delta^{18}O$  of NSC pools, highlighting the important role of  $P_{ex}$  effect in modifying  $\delta^{18}O$  signals in tree ring. Similar findings were reported by Martínez-Sancho et al., (2023), where source water had dominant influence on intra-annual  $\delta^{18}O$  variations in tree-ring cellulose of larch (*Larix decidua* L.) in the Swiss Alps, masking signals from needle-level processes. Our results indicate a strong  $P_{ex}$  effect, capable of altering the oxygen isotopic signature of cellulose in the xylem cells (Martínez-Sancho et al., 2023). This effect likely represents the largest modification of  $\delta^{18}O$  signal between the leaves and tree rings (Siegwolf et al., 2023).

Increasing proportional oxygen isotope exchange between xylem water (source water) and NSCs during the growing season can transform the rising  $\delta18$ Ocam signal into a decreasing trend in  $\delta18$ Oxc in black spruce (Figure 3.5). This divergence is likely driven by intensified post-photosynthetic exchange ( $P_{ex}$ ) processes that progressively replace the  $\delta^{18}$ O signature acquired at the leaf level with that of local water during cellulose synthesis (Gessler et al. 2014). Oxygen isotopic composition in tree-ring cellulose reflects both the evaporative enrichment of leaf water and the degree of exchange between sugars and ambient water during transport and metabolism (Roden et al. 2000, Cernusak et al. 2005). When  $P_{ex}$  increases, due to higher metabolic turnover, prolonged carbohydrate residence time, or increased cellular hydration in summer, the  $\delta^{18}$ O signal from enriched leaf water becomes increasingly overwritten by the more depleted isotopic signature of xylem water (Barbour et al. 2004, Cernusak et al. 2005, Gessler et al. 2009, Gessler et al. 2014). As a result,  $\delta^{18}$ O<sub>xc</sub> can decline, even while  $\delta^{18}$ O<sub>cam</sub> continues to rise due to leaf level physiological processes.

This mechanism has been further supported by recent work from Szejner et al. (2020), who demonstrated that post-photosynthetic fractionation processes, including exchange with water during cellulose

biosynthesis, can substantially alter the  $\delta^{18}$ O signal inherited from leaf water. Their results across coniferous tree species (Pinus ponderosa and Pseudotsuga menziesii) and environmental conditions confirmed that intra-seasonal and inter-annual  $\delta^{18}$ O patterns in tree-ring cellulose are strongly influenced by  $P_{\rm ex}$  dynamics, mostly when increasing during the growing season, which may vary with phenology, water availability, and tissue-specific metabolic activity. In our spruce stands,  $\delta^{18}$ O<sub>xc-sim</sub> under increasing  $P_{\rm ex}$  values (i.e., from 0.3 to 0.5) mirrored these findings, showing decreasing trends that contrasted with the increasing  $\delta^{18}$ O<sub>cam</sub> signal. The effect was particularly evident during late-season wood formation, when extended sugar residence times, likely related to increased sugar concentrations for frost resistance and prevent cellular lysis (Charrier and Améglio 2011), may have enhanced opportunities for exchange. This pattern is consistent with previous studies emphasizing the role of seasonal dynamics in carbohydrate transport and cellulose synthesis (Barbour et al. 2004, Gessler et al. 2009, Offermann et al. 2011).

Previous studies indicated that  $\delta^{18}O_{rain}$  varies with temperature, latitude and altitude, showing greater depletion (i.e., lower  $\delta^{18}O_{rain}$  values) at higher altitudes with lower temperatures (Bortolami et al., 1979; Poage & Chamberlain, 2001). The location of BER site, at a higher latitude and altitude with a lower annual mean temperature compared to SIM, likely contributes to the more depleted  $\delta^{18}O_{rain}$  signals (i.e., lower  $\delta^{18}O_{rain}$  values) at this site (Table B.9). The  $\delta^{18}O$  values in different tree compartments are influenced by  $\delta^{18}O_{rain}$  signals, leading to lower  $\delta^{18}O_{cam}$  and  $\delta^{18}O_{xc}$  values in BER compared to SIM (Table B.4, mean  $\delta^{18}O_{cam}$  and  $\delta^{18}O_{xc}$  in SIM were significantly more enriched (i.e., higher  $\delta^{18}O_{xc}$  values) compared to BER by 1.1% ( $\rho$ <0.01) for 2020 and 0.7% for 2021 ( $\rho$ <0.01), not shown in the results section). Additionally, warmer summers in SIM may contribute to an increased soil water evaporation rate, resulting in an increased enrichment in source water, leading to the more enriched  $\delta^{18}O_{cam}$  and  $\delta^{18}O_{xc}$  values observed at this site compared to BER.

Comparing the Global Meteoric Water Line (GMWL) with the local meteoric water lines for SIM and BER in the 2020 and 2021 growing seasons shows slopes  $\approx 8$  (consistent with equilibrium fractionation) indicating little to no evaporative enrichment (Figure B.2). However, the  $\delta^{18}O_{xc}$  series do not fully reflect the signature of  $\delta^{18}O_{rain}$  during the growing season at our sites (Table 3.3). This discrepancy may be attributed to two main factors. First, because the exchange of oxygen isotopes between xylem water and NSCs occurs in a proportional manner (i.e., increasing  $P_{ex}$ ) during the growing season, strong links between weekly  $\delta^{18}O_{rain}$  and  $\delta^{18}O_{xc}$  signals are not evident. Second, complex environmental processes may alter  $\delta^{18}O_{rain}$  signals before it is incorporated into tree tissues. For example, only a portion of total precipitation

infiltrates the soil, reaches the roots, and is ultimately absorbed by trees. As water infiltrates the soil, further fractionation can occur, especially during periods of high evaporative demand like summers. Consequently,  $\delta^{18}O$  of soil water ( $\delta^{18}O_{sw}$ ) may vary with depth depending on soil structure, season, and climate (Sprenger et al., 2016). Since roots can access water from a range of soil depths, the  $\delta^{18}O$  of source water (and of xylem water) may differ from the initial meteoric water inputs (Siegwolf et al., 2023). The discrepancy between weekly  $\delta^{18}O_{xc}$  signals and  $\delta^{18}O_{rain}$  variations observed here, underscores the need for further investigation into the relationships between weekly  $\delta^{18}O_{sw}$  and  $\delta^{18}O_{xc}$  signals in spruce stands, potentially shedding light on the hydrodynamics of source water affecting  $\delta^{18}O_{xc}$  at seasonal scales (Thomas et al., 2018).

#### 3.6 Conclusions

Overall, our findings underscore the complexities inherent in using the isotopic signature of xylem cellulose, a common tool in dendroclimatology. This signature results from a multifaceted and cumulative array of processes affecting the end signal. Both carbon and oxygen isotopes in the cambium were influenced by  $g_s$ . Xylem carbon isotopes also appeared to derive directly from the leaf and cambial region. This finding is in accordance with previous studies demonstrating strong correlations between isotope composition of new assimilates and tree rings in evergreen coniferous species (Gessler et al., 2009; Rinne-Garmston et al., 2023). In contrast, xylem oxygen isotopes were more complex and the  $P_{\rm ex}$  effect, with increasing trend during the growing season, seemed strong enough to obscure the  $g_s$  signal. This complexity cautioned against oversimplistic assumptions that oxygen isotopes in xylem cellulose serve as a reliable proxy for  $g_s$  signals, particularly in boreal forests. Our findings highlighted the need for careful consideration of the processes influencing isotopic signals to avoid misinterpretations in dendroclimatological studies.

Moving forward, further research is needed to understand the role of  $\delta^{18}O_{sw}$  dynamics in influencing oxygen isotope signals in forming tree rings. Additionally, linking weekly  $\delta^{13}C$ -derived iWUE data with wood anatomy and seasonal xylogenesis dynamics may offer deeper insights into interactions among physiological factors, such as sink-driven influences on  $g_s$ , in tree species. Expanding this research to other regions, climatic contexts, and species with different growth dynamics and characteristics such as stem diameter (i.e., distance from pith), crown condition, and root depth will enhance our understanding of these processes and improve the robustness of dendroclimatological models across diverse ecosystems. Such interdisciplinary approaches are crucial for understanding how environmental changes may affect tree physiology and xylem hydraulic conductivity over seasonal and decadal scales.

#### 3.7 Figures Legend

<u>Figure 3.1</u>: Locations of the two study sites: Simoncouche (SIM) and Bernatchez (BER). The map was designed in QGIS.

<u>Figure 3.2:</u> The red lines represent the  $\delta^{13}C_{cam}$  values for the full growing season in each study year. The blue lines represent  $\delta^{18}O_{cam}$  values for the same period during the growing season. Solid lines denote regression lines with significant slopes, and dashed lines indicate non-significant slopes. The insets represent standardized  $\delta^{13}C_{cam}$  and  $\delta^{18}O_{cam}$  profiles (z-scores) in each site and study year.

<u>Figure 3.3</u>: The orange lines represent the  $\delta^{13}C_{xc}$  values over the growing season in each study year. The light blue lines represent  $\delta^{18}O_{xc}$  values for the same period during the growing season. Solid lines denote regression lines with significant slopes, and dashed lines indicate non-significant slopes. The insets represent standardized  $\delta^{13}C_{xc}$  and  $\delta^{18}O_{xc}$  profiles (z-scores) in each site and study year.

<u>Figure 3.4</u>: Solid lines denote regression lines with significant slopes, and dashed lines indicate non-significant slopes. The two points highlighted with a red circle in Figure (c) correspond to rainwater samples that were likely affected by post-depositional evaporation.

<u>Figure 3.5</u>: Three  $P_{\text{ex}}$  scenarios: Increasing  $P_{\text{ex}}$  (from 0.3 to 0.5), decreasing  $P_{\text{ex}}$  (from 0.5 to 0.3), and constant  $P_{\text{ex}}$  (0.4), across different sites and study years.

#### 3.8 Tables Legend

<u>Table 3.1</u>: Annual and seasonal statistics for temperature (average), precipitation (sum), and soil water content (only seasonal, average) were calculated for the study years 2019-2021 at the two sites SIM and BER.

<u>Table 3.4</u>: Maximum temperature ( $T_{max}$ ), vapour pressure deficit (VPD), photosynthetically active radiation (PAR), relative humidity (RH), precipitation (P), soil volumetric water content (VWC), (\* p< 0.1, \*\* p< 0.05, \*\*\* p< 0.01).

<u>Table 3.5</u>: Maximum temperature ( $T_{max}$ ), vapour pressure deficit (VPD), photosynthetically active radiation (PAR), relative humidity (RH), precipitation (P), soil volumetric water content (VWC), (\* p< 0.1, \*\* p< 0.05, \*\*\* p< 0.01).

# 3.9 Figures

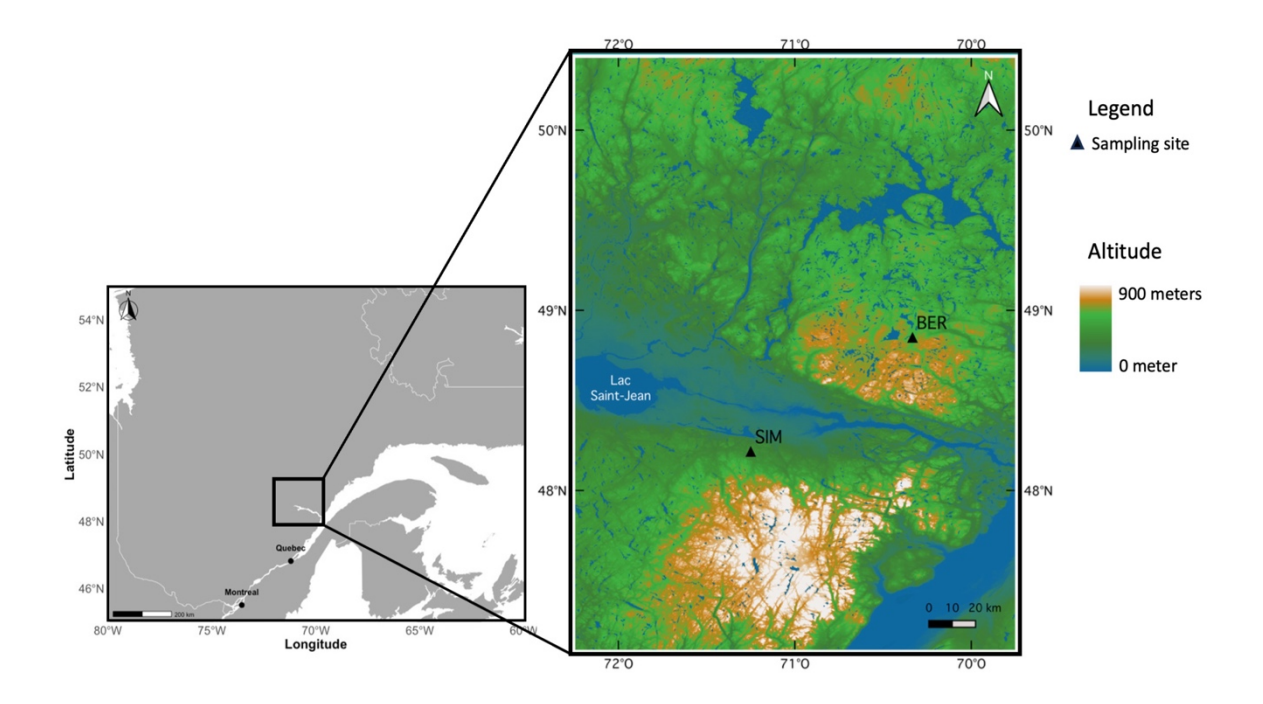


Figure 3.1 Topography of the Saguenay-Lac-Saint-Jean region in Quebec, Canada.

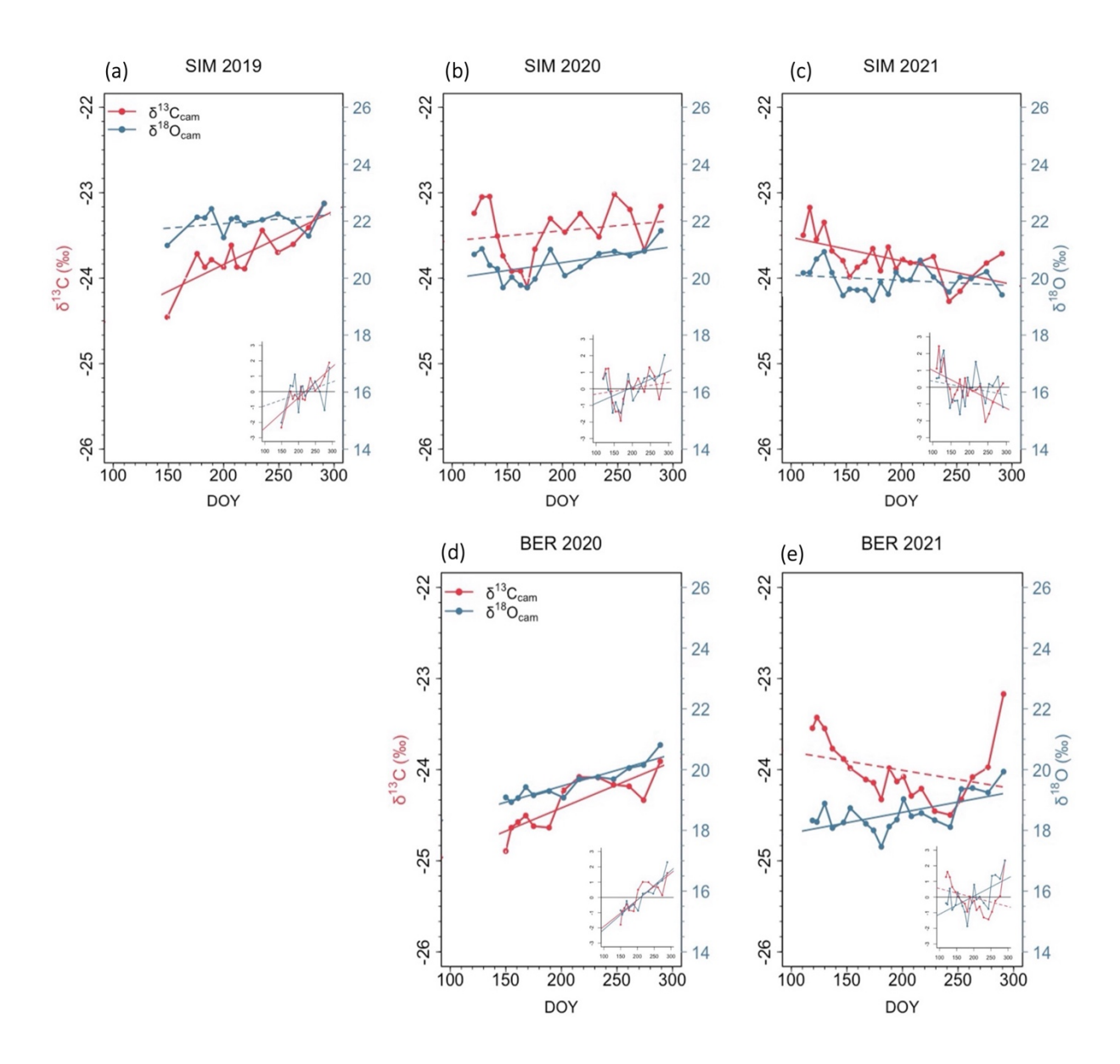


Figure 3.2 Intra-annual  $\delta^{13}C_{cam}$  and  $\delta^{18}O_{cam}$  profiles in SIM (a, b, c) and BER (d, e).

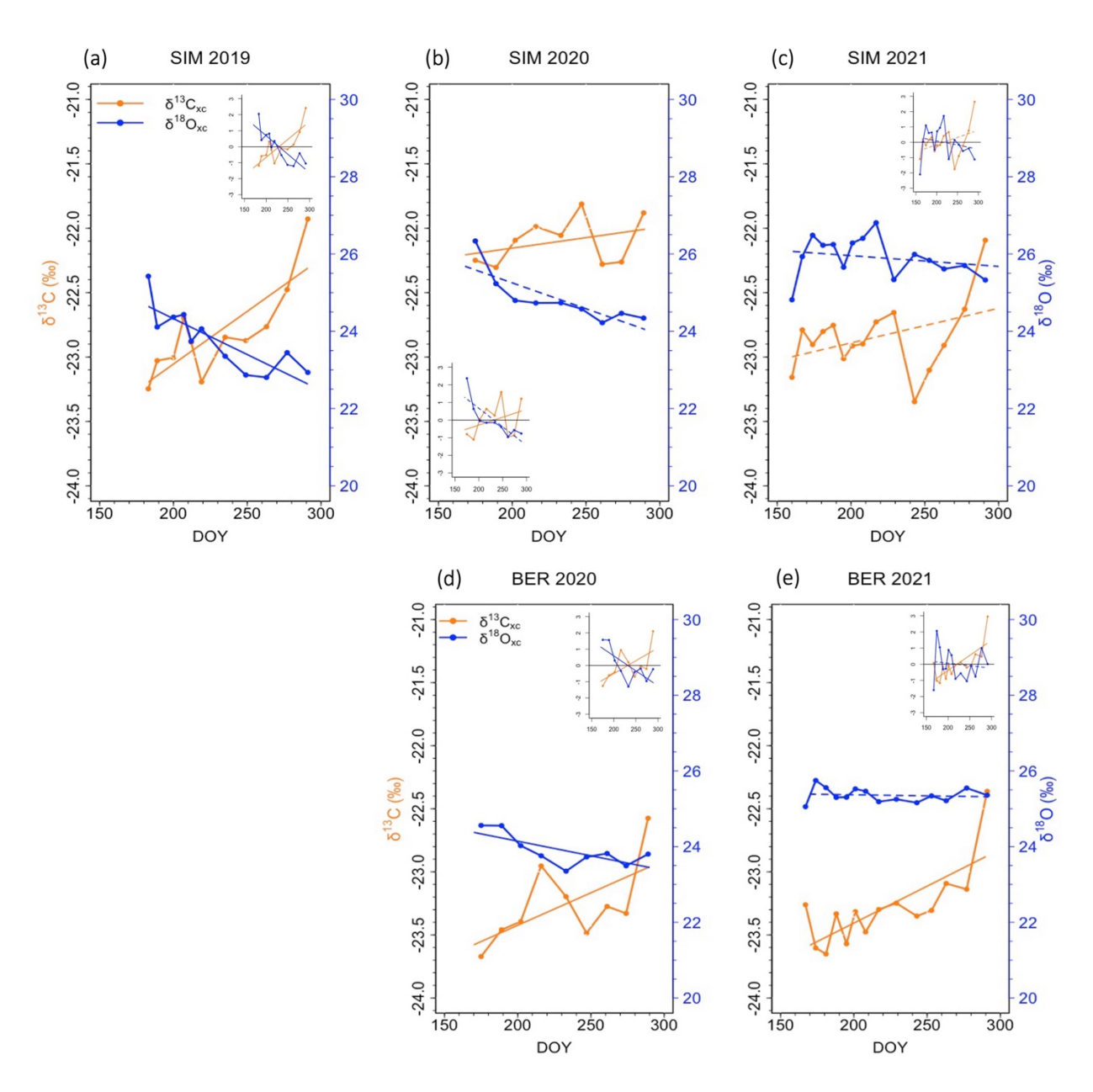


Figure 3.3 Intra-annual  $\delta^{13}C_{xc}$  and  $\delta^{18}O_{xc}$  profiles in SIM (a, b, c) and BER (d, e).

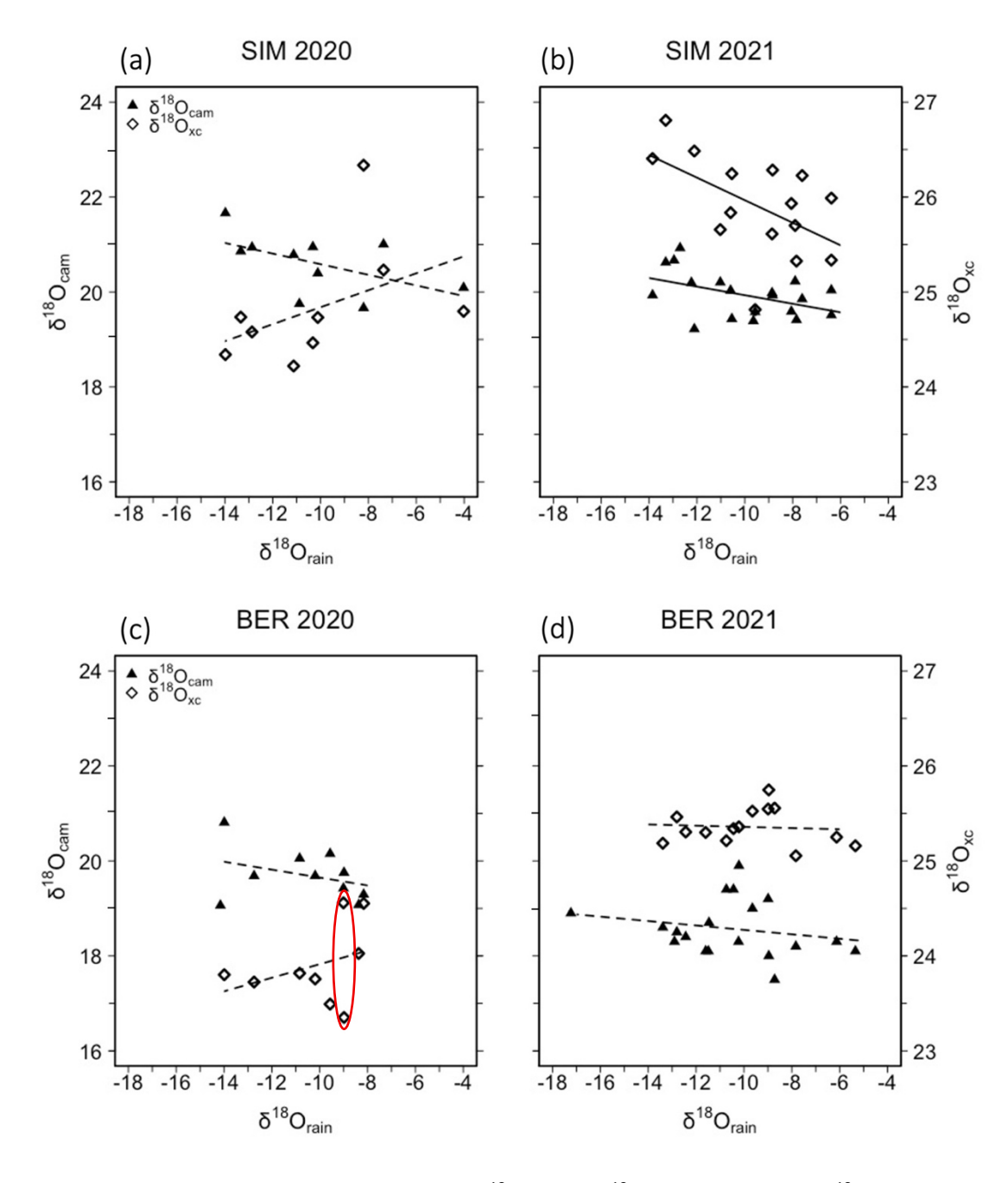


Figure 3.4 Scatterplots and regression lines of weekly  $\delta^{18}O_{cam}$  and  $\delta^{18}O_{xc}$  as a function of  $\delta^{18}O_{rain}$  in SIM 2020 (a), SIM 2021 (b), and BER 2020 (c) and BER 2021 (d).

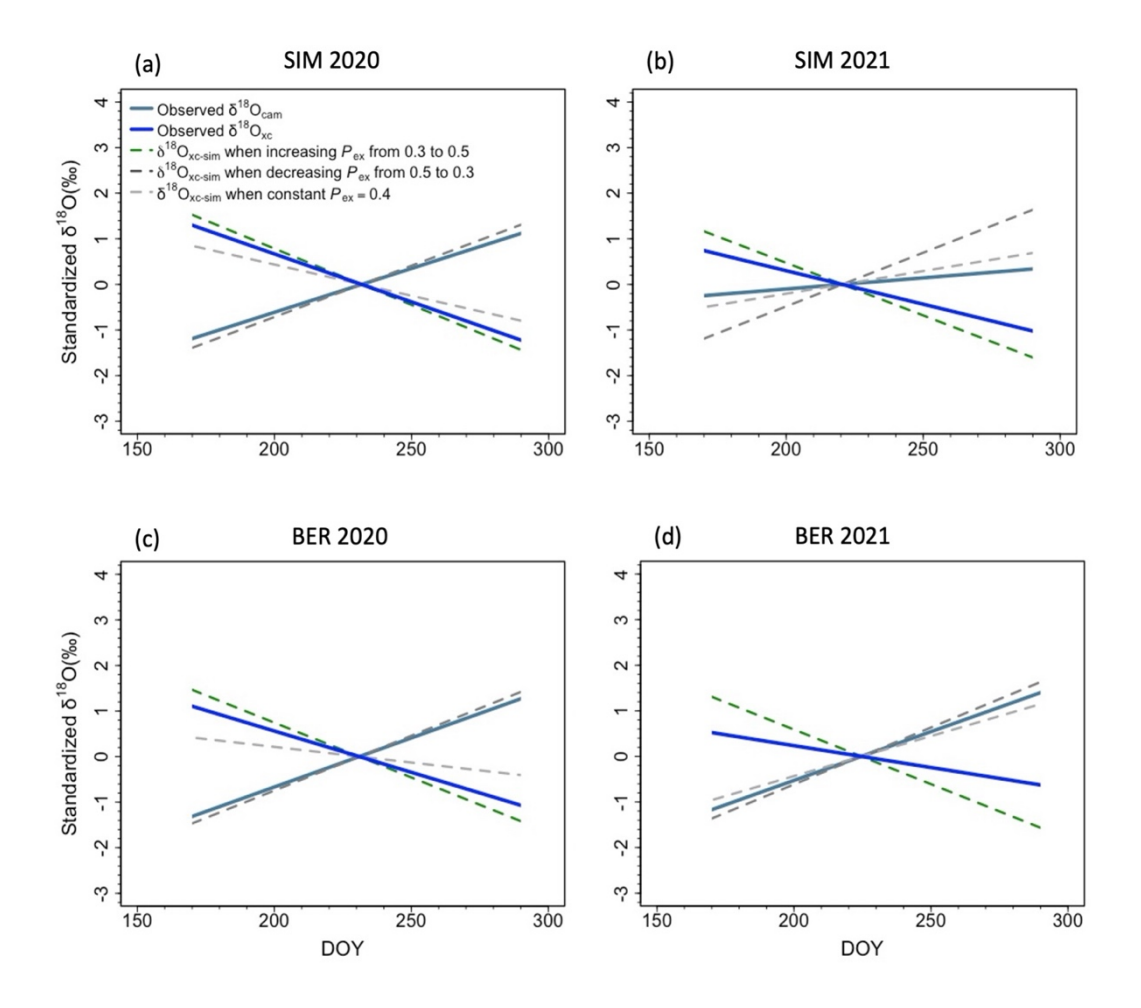


Figure 3.5 Comparison of the slopes between observed  $\delta^{18}O_{cam}$ ,  $\delta^{18}O_{xc}$ , and simulated  $\delta^{18}O_{xc}$  ( $\delta^{18}O_{xc-sim}$ ) under three  $P_{ex}$  scenarios during the growing season.

# 3.10 Tables

Table 3.1 Location, tree characteristics, and climatic conditions at the two study sites. Latitude (Lat.), longitude (Long.), altitude (Alt, meters above sea level).

Code	Lat.	Long.	Alt (m a.s.l.)	May-Oct temperatu re (°C)	Annual temperat ure (°C)	May-Oct Precipitati on (mm)	Annual Precipitati on (mm)	May-Oct Soil water content (m³/m³)
SIM	48°13′	71°15′	338	12.8	3.2	484.3	640.6	0.22
BER	48°51′	70°20′	611	10.3	0.6	483	570.1	0.34

Table 3.2 Correlation coefficients and p-values between  $\delta^{13}C$  and  $\delta^{18}O$  values in the cambium and xylem cellulose in different study sites and years.

Pearson's correlation	SIM 2019	SIM 2020	SIM 2021	BER 2020	BER 2021
Between $\delta^{13}C_{\text{cam}}$ and $\delta^{18}O_{\text{cam}}$	0.58	0.73	0.38	0.76	0.35
	(p<0.05)	(p<0.001)	(p<0.1)	(p<0.01)	(p>0.1)
Between $\delta^{13}C_{xc}$ and $\delta^{18}O_{xc}$	-0.60	-0.36	-0.07	-0.45	-0.26
	(p<0.1)	(p>0.1)	(p>0.1)	( <i>p</i> >0.1)	(p>0.1)

Table 3.3 Correlation coefficients for the relationships between  $\delta^{18}O_{cam}$  or  $\delta^{18}O_{xc}$  values and  $\delta^{18}O_{rain}$  in different study sites and years.

Pearson's correlation	SIM 2020	SIM 2021	BER 2020	BER 2021	
Between $\delta^{18} O_{\text{cam}}$ and $\delta^{18} O_{\text{rain}}$	-0.54	-0.45	-0.35	-0.21	
	( <i>p</i> >0.1)	(p<0.1)	(p>0.1)	(p>0.1)	
Between $\delta^{18} O_{xc}$ and $\delta^{18} O_{rain}$	0.45	-0.53	0.34	-0.08	
	(p>0.1)	(p<0.05)	(p>0.1)	(p>0.1)	

Table 3.4 Correlation coefficients for the relationships between  $\delta^{13}C_{cam}$  or  $\delta^{18}O_{cam}$  values and different weekly meteorological variables of daytime averages (8h00 to 18h00) over the growing season.

Site/year	SIM 2019		SIM 2020		SIM 2021		BER 2020		BER 2021	
	$\delta^{13}C_{\text{cam}}$	$\delta^{18}O_{\text{cam}}$								
T <sub>max</sub>	-0.49	-0.12	-0.33	-0.68**	-0.13	-0.05	-0.62*	0.92***	- 0.59**	- 0.64**
VPD	-0.61*	-0.14	-0.49	-0.67**	0.01	-0.11	- 0.71**	-0.77**	-0.45	- 0.59**
PAR	- 0.79***	-0.24	-0.56*	0.81***	0.27	-0.10	-0.65*	0.92***	-0.42	- 0.64**
RH	0.73**	0.18	0.71**	0.69**	-0.10	0.21	0.81**	0.72**	0.34	0.49*
Р	0.84***	0.48	0.16	-0.23	0.03	-0.06	0.54	0.07	-0.21	-0.46
VWC	-0.31	0.23	0.30	0.71**	0.59**	-0.30	0.29	0.68**	0.07	-0.45

Table 3.5 Correlation coefficients for the relationships between  $\delta^{13}C_{xc}$  or  $\delta^{18}O_{xc}$  values and different weekly meteorological variables of daytime averages (8h00 to 18h00) over the growing season.

Site/year	SIM 2019		SIM 2020		SIM 2021		BER 2020		BER 2021	
	$\delta^{13}C_{xc}$	$\delta^{18}O_{xc}$								
T <sub>max</sub>	-0.51	0.22	-0.18	0.57*	-0.48*	-0.02	-0.64*	0.51	-0.54**	-0.11
VPD	-0.58*	0.51	-0.34	0.55	-0.48*	-0.17	-0.66*	0.67*	-0.51*	-0.24
PAR	-0.71**	0.67**	-0.48	0.24	-0.44	0.13	-0.71**	0.56	-0.63**	-0.17
RH	0.69**	-0.64**	0.63*	-0.25	0.46*	0.09	0.76**	-0.66*	0.45	0.36
Р	0.85***	-0.47	0.10	-0.29	0.12	0.16	0.42	-0.46	-0.37	0.37
VWC	-0.19	0.72**	0.30	-0.39	0.01	0.24	0.19	-0.48	-0.44	0.42

## **CHAPTER 4**

# Wood formation dynamics in black spruce: linking leaf-level physiological drivers and environmental factors

Sepideh Namvar<sup>1</sup>, Étienne Boucher<sup>2</sup>, Annie Deslauriers<sup>3</sup>, Hubert Morin<sup>3</sup>

<sup>1</sup> Department of Biological Sciences and GEOTOP, Université du Québec à Montréal, 201, Président-Kennedy Ave, Montréal (QC), Canada H2X 3Y7

<sup>2</sup> Department of Geography, GEOTOP and Centre d'études nordiques, Université du Québec à Montréal, Montréal (QC), Canada H2X 3R9

<sup>3</sup> Departement des Sciences Fondamentales, Université du Québec à Chicoutimi, 555, boulevard de l'Université, Chicoutimi (QC), Canada G7H 2B1

- Supplementary information is attached in Appendix C

#### 4.1 Abstract

Understanding the drivers of xylem formation dynamics is essential for interpreting tree growth responses to environmental and physiological constraints. In conifers, secondary growth is influenced by external factors, such as temperature and water availability, as well as internal sink limitations that regulate carbon allocation. However, the relative contributions of these factors at seasonal scales remain unclear. Examining the relationships between wood formation dynamics and leaf-level physiological processes, specifically intrinsic water use efficiency (iWUE), can offer valuable insights into the main drivers of wood formation during the growing season. In this study, we analysed the kinetics of cell formation, including cell enlargement rates, and wall deposition rates, as well as stem growth rates in black spruce [Picea mariana (Mill.) BSP.] in boreal forests of Quebec, Canada. Sampling was conducted over two growing seasons (2020 and 2021) at two study sites, Simoncouche and Bernatchez which exhibit distinct differences in temperature and soil water content. The results indicated that cell enlargement and wall deposition rates were primarily regulated by iWUE at the leaf level, while cell production rate was more influenced by environmental factors such as temperature and vapor pressure deficit. This suggested that stomatal regulation played a key role in controlling cell enlargement rates and carbon deposition in black spruce, with stomatal conductance modulated by soil water content. Higher soil moisture lowered iWUE, enhancing cell enlargement and wall deposition, whereas higher temperatures and a drier atmosphere promoted greater cell production. Our findings highlight the influence of leaf-level physiological processes and environmental factors on wood formation dynamics throughout the growing season. This information offers new insights into how future climate change may impact forest productivity in boreal ecosystems.

Keywords: wood formation dynamics, cell enlargement, wall deposition, iWUE, temperature, black spruce, boreal forest

#### 4.2 Introduction

Recent studies on xylem formation dynamics have significantly enhanced our understanding of how cell growth processes (i.e., cell production, enlargement and wall formation) shape the anatomical structure of tree rings (Rossi, Deslauriers, & Anfodillo, 2006). These processes influence water transport efficiency, carbon sequestration within the xylem cells, and the mechanical strength of the stem (Chave et al., 2009). Xylem formation dynamics are driven by two primary factors, including environmental conditions (e.g., temperature, soil water content, and photoperiod) and resource availability defined by sink demands (e.g., carbon and nutrition) (Fonti et al., 2010). However, the relative roles of external environmental factors and internal constraints in controlling xylem growth patterns remain poorly understood (Cartenì et al., 2018).

Wood formation dynamics are influenced by external factors, particularly meteorological conditions. In boreal forests, temperature plays an important role in regulating the cambial activity of conifer species, influencing the phenology of wood formation (Rossi et al., 2011) and the rate of cellular division (Gričar et al., 2014), with a predominant effect on cell wall-related characteristics (Wang et al., 2002). The formation of tracheids responsible for water conduction is shaped by the water availability at the time of their development, making the xylem hydraulic architecture a valuable archive for reconstructing past hydroclimatic variability (Von Arx et al., 2012). While ring-widths generally reflect the cumulative growth of an entire growing season, cellular structures, such as cell cross-sectional area, are more sensitive to short-term climatic conditions (Deslauriers & Morin, 2005; Martin-Benito et al., 2013). These cellular features are particularly effective in capturing extreme climatic events. As a result, seasonal variations in climatic conditions influence the anatomical properties of tree rings, providing insights into how trees respond to environmental constraints over time (Carrer et al., 2015).

While external factors are crucial in shaping wood formation dynamics, internal sink limitations could also exert a significant influence. Once the activity of primary and secondary meristems begins in the early spring, sink competition for carbon allocation is unavoidable (Cartenì et al., 2018). In conifers, the onset of stem growth activity (i.e., cambium) and canopy development (i.e., buds) occurs at the same time (Antonucci et al., 2015). Such synchronization has been observed in previous studies, where early bud flushing exhibited early xylem formation in black spruce. This indicates a close correlation between the reactivation dates of cambium and buds in this coniferous species (Perrin et al., 2017). Despite being an active sink, the xylogenesis process in the stem receives a minor portion of the recently assimilated C when

shoots and needles in the canopy are actively growing (Heinrich et al., 2015). Accordingly, primary growth in the tree canopy could influence the sugar/carbon availability for xylogenesis and contribute to the xylem anatomical changes throughout the tree ring (Cartenì et al., 2018; Vieira et al., 2020). In addition, in boreal forest with harsh winters, trees may shift carbon allocation strategies, from a secondary growth priority (in the early to mid-season) to a frost resistance priority (in the late season). As this shift operates, trees would then allocate more NSCs for frost resistance purposes (Chave et al., 2009; P. Fonti et al., 2010), inducing carbon limitation for wood formation specially, latewood formation. Thus, tree ring patterns and dynamics of wood formation in conifers, may be controlled/influenced by sink limitations on carbon allocation during the growing season.

A key approach to assessing the relative influence of environmental constraints and sink limitations on wood formation dynamics is to examine leaf-level physiological processes (Körner, 2003; Steppe et al., 2015). Xylem formation acts as a carbon sink and is influenced by leaf level physiological processes providing energy sources (i.e., carbon-enriched assimilates) for stem growth (Körner, 2003). Zuidema et al., (2018) highlighted that the extent to which tree growth is constrained by the availability of sugars produced through photosynthesis (source limitation) versus the conditions that regulate cell enlargement and division during wood formation (sink limitation) remains poorly understood. If growth is primarily source-limited, climatic variability (e.g., temperature fluctuations, rising atmospheric CO<sub>2</sub> levels) may significantly enhance tree growth. In contrast, when tissue formation is sink-limited, tree biomass accumulation may be less responsive to environmental changes (Zuidema et al., 2018).

Stable carbon isotope analysis provides a powerful tool for examining leaf level physiological constraints on wood formation (Verlinden et al., 2015). Trees regulate stomatal conductance to balance carbon dioxide uptake for photosynthesis and water loss through transpiration (Farquhar & Sharkey, 1982). The trade-off between carbon gain and water loss can be quantified as intrinsic water use efficiency (iWUE), defined as the ratio of net assimilation rate to stomatal conductance (Farquhar & Ehleringer, 1989). Studies have demonstrated that the interplay between carbon assimilation and water loss at the leaf level significantly influences the quantity and quality of xylem cells produced during the growing season (Steppe et al., 2015). Environmental factors affect iWUE, as demonstrated in a study on *Populus euphratica*, which identified relative humidity and vapor pressure deficit as key drivers of iWUE (Ye et al., 2023). Thus, comparing iWUE data with wood formation dynamics can help identify the primary drivers of xylem formation in developing tree rings. Indeed, if relationships exist between xylem formation dynamics and

iWUE, and if iWUE is influenced by climatic factors, it suggests that wood formation is primarily driven by external environmental conditions. On the other hand, if iWUE shows no relationship with external factors but correlates with wood formation rates, this would indicate that wood formation dynamics modulate iWUE independently of climate and are predominantly controlled by sink limitations. This comparative approach offers crucial insights into the interactions between climate, source, and sink processes in tree ring formation.

Here, we investigate real time wood formation dynamics and iWUE in the developing tree rings of mature black spruce ( $Picea\ mariana\ [Mill.]\ BSP)$  in the eastern Canadian boreal forest. This study aims to identify the main drivers of wood formation dynamics in boreal trees. Specifically, we focus on cell enlargement rates ( $r_E$ ), wall deposition rates ( $r_W$ ), and cell production rates ( $r_D$ ) as indicators of wood formation dynamics. We then examine the relationships between these parameters, iWUE, and various meteorological factors. We hypothesize that iWUE directly influences these three parameters (i.e.,  $r_E$ ,  $r_W$ ,  $r_D$ ) and is associated with meteorological factors such as temperature and soil water content. Consequently, wood formation dynamics are primarily regulated by leaf-level physiological processes and shaped by environmental factors. This research advances our understanding of how physiological and environmental factors interact to influence wood anatomical features in boreal forests, providing insights into their implications for tree growth under changing climatic conditions.

#### 4.3 Materials and Methods

#### 4.3.1 Study area

The research was carried out in mature black spruce stands within Quebec's boreal forest, Canada (Figure 4.1). The study focused on two distinct locations in the Saguenay-Lac-Saint-Jean area: Simoncouche (SIM) and Bernatchez (BER), both characterized by mature black spruce stands (Table 4.1). SIM is situated at the Simoncouche research station (48°13′ N, 71°15′ W, 338 m a.s.l.) within the Laurentide Wildlife Reserve, managed by Université du Québec à Chicoutimi. BER is located at higher elevations near Lake Poulin de Courval (48°51′ N, 70°20′ W, 611 m a.s.l.). Black spruce is the dominant tree species at both sites, accompanied by a typical undergrowth of mixed vegetation (Dao et al., 2015). The climate in this region is continental, characterized by long, cold winters and brief, warm summers (Balducci et al., 2021). During the 2020-2021 study period, the mean annual air temperature in SIM was 3.9°C, while BER experienced a lower mean of 1.4°C. During the growing season, specifically from May to October (2020-2021), mean temperatures were 13.2°C in SIM and 10.8°C in BER, indicating a colder and shorter growing season in BER

(number of days with minimum daily temperatures above 5°C, SIM: 174±27 days, BER: 144±15 days; mean 2020-2021) (Buttò et al., 2019; Rossi et al., 2011). Mean annual precipitation (2020-2021) was higher in BER compared to SIM with 528.6 mm and 490.6 mm annual rainfalls respectively. However, during the growing season SIM received higher amounts of precipitation compared to BER (mean 2020-2021; 694.4 mm, 641.9 mm respectively) (Table 4.1). Higher values of soil water content were observed in BER compared to SIM during the growing season (BER: 0.34 m³/m³; SIM: 0.23 m³/m³; mean values from May to October 2020-2021).

#### 4.3.2 Tree selection and sampling of microcores and wood strips

Five mature black spruce trees with upright stems and relatively large diameters were selected in SIM and BER, during the two study years, 2020 and 2021 (Figure 4.2a, Table C.1, see *Appendix C*). Trees showing reaction wood, dead crowns, or visible damage were excluded from selection. The selected trees had sufficiently large diameters to allow the collection of 13 to 22 microcores for monitoring xylogenesis and wood strips for carbon stable isotope analysis during the growing season (Table C.2). From late April to October (2020-2021), microcores were extracted weekly from the stems of selected trees using a Trephor, to monitor xylogenesis (Buttò et al., 2019; Rossi et al., 2011). Simultaneously, rectangular wood strip samples (~3 × 6 cm) were collected from above the coring area to track weekly carbon isotope fractionation (Figure 4.2b, for more information see Namvar et al., (2024)). The sampling was performed following the micro-core collection methodology introduced in previous studies (Buttò et al., 2019; Rossi et al., 2011).

#### 4.3.3 Xylem formation

Section slides were prepared from each microcore to monitor xylem formation (i.e., xylogenesis) in the sampled spruce stands (Figure 4.3a). The microcores were first dehydrated through a series of successive immersions in ethanol and d-limonene. Once dehydrated, they were embedded in paraffin, and 7  $\mu$ m transverse sections were cut using a rotary microtome (Leica RM2245, Leica Biosystems, Nussloch, Germany). The sections were then stained with a 0.16% cresyl violet acetate solution in water. Cells were classified in three different phases of enlarging (primary cell walls, absence of glistening under polarized light) (Figure 4.3b), wall thickening and lignifying (formation of secondary cell wall, glistened under polarized light) (Figure 4.3c), and mature cells (cell walls were entirely blue under the polarized light) (Buttò et al., 2019; Deslauriers et al., 2003; Rossi, Deslauriers, & Anfodillo, 2006). For each section, the radial number of enlarging ( $n_E$ ), wall thickening ( $n_W$ ) and mature cells ( $n_M$ ) were counted along three radial

files with a microscope at X400-500, under polarized light (Deslauriers et al., 2003). The total number of xylem cells was calculated as the sum of differentiating and mature cells for different dates of sampling  $(n_{Total}=n_E+n_W+n_M)$ .

#### 4.3.4 Wood anatomy

To analyse tracheid's anatomical features, two additional microcores were collected from each sampled tree when the ring was fully formed on the last sampling date (mid-October, 2020-2021). These samples were prepared according to the previously described protocol, stained with a 1% safranin solution in water, and mounted on slides using a mounting medium. Digital images of the cross-sections were captured using a camera attached to an optical microscope at 10X magnification (Buttò et al., 2019). Various cell traits were measured, including: (1) cell radial diameter (CRD, cell length), (2) lumen tangential diameter (LTD, lumen width), (3) wall radial thickness (WRT), and (4) lumen cross-sectional area (LCA) of the fully formed rings (Figure 4.3d) (Cuny et al., 2014). Measurements were taken for each cell along five radial files using Wincell™ software (Regent Instruments Inc., Canada).

#### 4.3.5 Dynamics of xylem formation

To represent variation in tracheid dimensions along the tree ring, cell traits' measurements were grouped by radial file in profiles called tracheidograms (Vaganov, 1990). However, due to the variability in the number of cells among radial files within and between trees at each site and study year, tracheidograms were standardized following Vaganov's method using a dedicated function in SAS software. The asymptotes (maximum number of cells) were obtained by fitting the total number of cells (n<sub>Total</sub>) for each tree sample to a Gompertz function in R statistical software (R Development Core Team, 2011). The standardized tracheidograms were then mean values for the five tree samples to obtain tree-ring structures for each site and study year.

During the enlargement phase, cells grow mainly in the radial direction, while their tangential diameter and length stay mostly unchanged (Cuny et al., 2014; Skene, 1972). Therefore, we utilized the cell radial diameter (CRD,  $\mu$ m) as an indicator of the final result of the enlargement phase in our tree samples at each site and study year. Moreover, although cell volume is constant after enlargement, the deposition of carbon-rich compounds on the inner side of the cell wall reduces the volume of the lumen and hence the surface of deposition (Cuny et al., 2014). Therefore, we used the wall cross-sectional area (WCA), a direct estimate of the amount of deposited material per cell, as the final outcome of the wall-thickening phase

(Cuny et al., 2014). The wall cross-sectional area (WCA,  $\mu$ m<sup>2</sup>) was calculated by subtracting the lumen cross sectional area from the cell cross-sectional area, assuming a rectangular shape for the tracheid cells (Figure 4.3d).

To accurately characterize the dynamics of wood formation, a statistical approach based on Generalized Additive Models (GAMs) was employed, using the mgcv package (Wood, 2006) in the R statistical software (RStudio 2024 by Posit Software, PBC), following the methodology developed by Cuny et al., (2013). A GAM is an extension of Generalized Linear Models (GLMs) that incorporates smooth functions to capture nonlinear and non-monotonic relationships between response and explanatory variables, offering flexibility and a data-driven approach (Balducci et al., 2016). GAMs were applied to smooth temporal trends in cell growth variables (mean values for five trees;  $n_E$ ,  $n_W$ ,  $n_M$ ), generating predictions at each site and study year. Corrections were applied to the predictions using Gompertz-derived asymptotes, incorporating site- and year-specific growth dynamics.

Growth rates, defined by cell production rates or  $(r_D, cells \, day^{-1})$ , were derived from the corrected data to capture critical periods of change, calculated as the difference in total cell numbers  $(n_{Total})$  predicted by GAMs over two consecutive days. Durations of specific growth phases of cell enlargement  $(d_E, days)$  and wall thickening/lignification  $(d_W, days)$  were estimated using mean cell numbers and by identifying the day of year thresholds (DOY,  $t_E$  and  $t_W$ ). These durations were integrated with anatomical data, including cell radial diameter (CRD,  $\mu$ m) and wall cross-sectional area (WCA,  $\mu$ m<sup>2</sup>), to compute developmental rates per day  $(r_E$  in  $\mu$ m day<sup>-1</sup> and  $r_W$  in  $\mu$ m<sup>2</sup> day<sup>-1</sup>, respectively). This was achieved by dividing each cell's final dimension (CRD and WCA) by the time spent in the corresponding growth phases  $(d_E$  or  $d_W$ ).

#### 4.3.6 Stable carbon isotope analysis

The collected wood strips containing bark and wood were separated from the tangential area (Giovannelli et al., 2011), frozen in liquid nitrogen, and lyophilized at  $-50^{\circ}$ C for five days. The cambial region was scraped from the inner bark and outermost xylem, pooled across all trees for each date, and homogenized. Tree rings were collected by cutting transverse sections or scraping cells in narrow rings, at the beginning of the growing season, under a microscope. Cellulose was extracted from xylem samples following a modification of the method described by Epstein et al., (1976). The analysis of carbon stable isotopes was conducted at the light-stable isotope geochemistry lab at the University of Quebec's Geotop facility in Montreal, Canada. To do so, 0.5 to 0.8 mg of cellulose ( $\delta^{13}C_{xc}$  for xylem samples) or pooled bulk material

 $(\delta^{13}C_{cam})$  for cambial samples) was weighed into tin capsules to ensure consistent CO<sub>2</sub> amounts across all samples and reference materials. These were analyzed using a Micromass Isoprime 100 isotope ratio mass spectrometer connected to an Elementar Vario MicroCube elemental analyzer in continuous flow mode, with an overall analytical uncertainty of  $\pm 0.1\%$ , excluding sample homogeneity and representativity as described by Hélie and Hillaire-Marcel (2021).

#### 4.3.7 Calculation of iWUE

In order to define intrinsic water use efficiency (iWUE) in our spruce stands, first we needed to calculate carbon isotope discrimination against  $^{13}$ C ( $\Delta$ ). We calculated the  $\Delta$  using the  $\delta^{13}$ C values obtained for the cambial region ( $\delta^{13}C_{cam}$ ) and forming xylem cellulose ( $\delta^{13}C_{xc}$ ). The raw  $\delta^{13}C_{cam}$  and  $\delta^{13}C_{xc}$  values (uncorrected values) can be used to calculate these parameters (Farquhar et al., 1982; Leland et al., 2023) as follows (example for  $\delta^{13}C_{cam}$ , same for  $\delta^{13}C_{xc}$ ):

$$\Delta_{cam} = \frac{\delta^{13} C_{atm_{AMT}} - \delta^{13} C_{cam}}{1 + \frac{\delta^{13} C_{cam}}{1000}}$$

Equation 4.1 Calculation of carbon isotope discrimination against <sup>13</sup>C

Where  $\delta^{13}C_{atm}$  is the isotopic value of atmospheric CO<sub>2</sub>. These data were conducted using the mean  $\delta^{13}C_{atm}$  values collected from the NOAA-ESRL tall tower at Argyle, Maine, United States (AMT, 45.03°N, 68.68°W,  $\delta^{13}C_{atm\_AMT}$ , the plot is available in *Appendix C*, Figure C.1a) in conformity with our sampling dates (Namvar et al., 2024). The propagation of uncertainty ( $\pm$  SD) in carbon isotope discrimination ( $\Delta$ ) and relative sensitivities to  $\delta^{13}C$  of atmospheric CO<sub>2</sub> ( $\delta^{13}C_{atm\_AMT}$ ) and  $\delta^{13}C_{cam}$  was calculated. Uncertainties were propagated using first-order partial derivatives (Taylor expansion method), and sensitivities were normalized to reflect the relative contribution of each input to  $\Delta$  (Table C.3).  $\delta^{13}C_{cam}$  values were derived from the pooled  $\delta^{13}C$  values of the cambium bulk material for each sampling date. The weekly  $\delta^{13}C_{xc}$  data were calculated by averaging the  $\delta^{13}C$  values for the forming xylem cellulose from the five tree samples for each study year (Namvar et al., 2024). We then calculated the intrinsic water-use efficiency iWUE as follows (Martin-Benito et al., 2017) (example for iWUE<sub>cam</sub>, same for iWUE<sub>xc</sub>):

$$iWUE_{cam} = \frac{c_{a\_AMT} \cdot (b - \Delta)}{1.6 \cdot (b - a)}$$

Equation 4.2 Calculation of iWUE in the cambial region (iWUE cam)

Where  $c_{a\_AMT}$  represents the mean atmospheric CO<sub>2</sub> data (Figure C.1b). These data were conducted using the mean CO<sub>2</sub> values collected from Argyle site in conformity with our sampling dates for the two growing seasons of 2020 and 2021. The  $\Delta$  represents carbon isotope discrimination against <sup>13</sup>C and was calculated using the equation (4.1). The constant a represents fractionation associated with diffusion of CO<sub>2</sub> through stomata (4.4‰), and b is the discrimination against <sup>13</sup>CO<sub>2</sub> by Rubisco during carboxylation (~27‰). 1.6 is the ratio between the diffusivities of water vapor and CO<sub>2</sub> in air.

The  $iWUE_{cam}$  and  $iWUE_{xc}$  profiles were developed for the two sites and study years (Figure C.2). Our previous research indicated that both  $\delta^{13}C_{cam}$  and  $\delta^{13}C_{xc}$  are mostly regulated by leaf-level physiological processes, with strong correlations between the two profiles in almost all sites and study years (Namvar et al., 2024). Strong positive correlations were also observed between  $iWUE_{cam}$  and  $iWUE_{xc}$  profiles (Table C.4). Therefore, in this research we considered  $iWUE_{cam}$  (here after iWUE) as the indicator of leaf-level physiological processes.

#### 4.3.8 MODIS NDVI data

The NDVI data for the two study sites were sourced from the Bhoomicam.com website. Satellite technology and AI were utilized by Bhoomicam to provide actionable insights for monitoring and managing agricultural and natural ecosystems. Among its core offerings was the provision of NDVI (Normalized Difference Vegetation Index) data, a critical metric for assessing vegetation health and dynamics. A time series of daily NDVI data was generated using 250-meter MODIS atmospherically corrected surface reflectance imagery. NDVI was calculated as:

$$NDVI = \frac{\rho(NIR) - \rho(Red)}{\rho(NIR) + \rho(Red)}$$

Equation 4.3 Calculation of Normalized Difference Vegetation Index (NDVI)

Where  $\rho$  (Red) and  $\rho$  (NIR) represented reflectance values in the red (620–670 nm) and near-infrared (841–871 nm) bands, respectively. For the Simoncouche site, the analysis was focused on undisturbed black spruce-dominated forests (>75% canopy cover) within a 5 km buffer zone, with a minimum 30-year history. Daily maximum composite NDVI values were extracted specifically from areas overlapping with black spruce stands, allowing for precise monitoring of greenness dynamics and phenological trends.

#### 4.3.9 Meteorological data

Meteorological variables, including maximum temperature ( $T_{max}$ ,  $^{\circ}$ C), vapour pressure deficit (VPD, kPa), relative humidity (RH, %) and soil water content (VWC,  $m^3/m^3$ ), were recorded hourly at both study sites and over both study years. The data were collected using a tower equipped with an automated data acquisition system and various measurement devices. Photoperiod (PP, hour) was calculated for SIM and BER 2020 and 2021, as the difference between daily sunset and sunrise times, computed as proposed by Teets (2003).

#### 4.3.10 Statistical analyses

The goodness of fit of the GAMs was evaluated using the Mean Absolute Error (MAE). Additionally, the Model Efficiency (EF, %) was calculated to assess the model's ability to explain the variability in the observed data (Balducci et al., 2016; Cuny et al., 2013; Willmott & Matsuura, 2005) (Table C.5). To minimize time discrepancies between different variables: cell enlargement ratio ( $r_E$ ), wall deposition ratio ( $r_W$ ), and cell production rate ( $r_D$ ), along with values for iWUE, NDVI, and meteorological parameters (8h00 to 18h00 daytime values:  $T_{max}$ , VPD, RH, VWC, PP), were interpolated into uniform five-day intervals during the growing season (Figure C.3 a-j). Principal component analysis (PCA) was then performed to explore the links between all variables. This analysis enabled the construction of a PCA biplot to identify the factors influencing/controlling the  $r_E$ ,  $r_W$ , and  $r_D$  in our spruce stands at seasonal scales. The t-tests was conducted to compare the mean rates of cell differentiation ( $r_E$ ,  $r_W$ , and  $r_D$ ), iWUE, and meteorological variables between the two study sites in 2020 and 2021.

#### 4.4 Results

The GAMs generally demonstrated strong goodness of fit, with high EF values ranging from 86% to 99% and low MAE values across most cases (Table C.5). This demonstrates the models' capability to capture the intrinsic complexity and variability of wood formation dynamics in our spruce trees (Cuny et al., 2013). The results indicate that the model was robust and reliable enough to be used for further calculations as explained earlier. The timing of the onset of the differentiation phases ( $t_E$  and  $t_W$ ) varied between the two sites. The first cell enlargement activities started earlier in SIM compared with BER in both growing seasons of 2020 (Day of Year; DOY=157, DOY=162, respectively) and 2021 (DOY=146, DOY=151, respectively) (Figure 4.4a). Cell wall formation began earlier in SIM than in BER during the two growing seasons, with a difference of four days in 2020 (DOY=170 and DOY=174, respectively) and one day in 2021 (DOY=162 and DOY=163, respectively) (Figure 4.4b). Cells completed their maturation phase earlier in SIM than in BER in

2020 (DOY= 270 and DOY=284, respectively), whereas in 2021, maturation took longer in SIM compared to BER (DOY=284 and DOY=277, respectively).

Similar decreasing patterns were observed in cell enlargement rates and wall deposition rates across both study sites and years (Figure 4.4a and 4.4b). Rates of cell division during cell differentiation followed a bell-shaped pattern in both sites and years (Figure 4.4c). No significant differences were observed between the mean  $r_E$  values in 2020, while mean  $r_E$  showed significantly higher ratios in BER compared to SIM in 2021 (2.96±0.27 and 2.11±0.35  $\mu$ m day<sup>-1</sup>, respectively, p<0.01) (Figure 4.5a, Table 4.2). In 2020, mean wall deposition rates were significantly higher in SIM compared to BER (25.82±9.95 and 17.21±8.58  $\mu$ m<sup>2</sup> day<sup>-1</sup>, respectively, p<0.1), while no significant differences were observed between the mean  $r_W$  values in 2021 (Figure 4.5b, Table 4.2). Mean cell production was significantly higher in SIM compared to BER in 2020 (0.31±0.05 and 0.21±0.07 cell d<sup>-1</sup>, respectively, p<0.01), while it was significantly higher in BER compared to SIM 2021 (SIM: 0.18±0.05 and BER: 0.23±0.06 cell d<sup>-1</sup>, p<0.05) (Figure 4.5c, Table 4.2).

Both iWUE and NDVI were significantly higher in SIM compared to BER in both study years of 2020 (iWUE in SIM:  $109.29\pm2.45$ ; BER:  $98.63\pm1.89$ , p<0.01; NDVI in SIM:  $0.43\pm0.09$ ; BER:  $0.31\pm0.09$ , p<0.01) and 2021 (iWUE in SIM:  $105.10\pm1.18$ ; BER: $102.41\pm1.76$ , p<0.01; NDVI in SIM:  $0.39\pm0.10$ ; BER:  $0.29\pm0.08$ , p<0.05) (Figure 4.5d and 4.5e, Table 4.2). In contrast, soil water content (VWC) showed significantly higher values in BER compared to SIM in both 2020 (SIM:  $0.19\pm0.03$  and BER:  $0.38\pm0.01$  m<sup>3</sup>/m<sup>3</sup>, p<0.01) and 2021 (SIM:  $0.22\pm0.06$  and BER:  $0.30\pm0.02$  m<sup>3</sup>/m<sup>3</sup>, p<0.01) (Figure 4.5f, Table 4.2), indicating BER being wetter site with lower iWUE and photosynthesis rate in growing seasons of 2020 and 2021. No significant differences were observed between the mean  $T_{max}$ , RH, and PP at SIM and BER over the two study years of 2020 and 2021. Similarly, VPD showed no significant differences between the sites in 2020, while it was significantly higher in SIM 2021 than BER 2021 ( $1.01\pm0.17$  kPa and  $0.90\pm0.13$  kPa respectively, p<0.1) (Table 4.2).

The first two principal components of the PCA explained 32.9% and 25.4% of the variation in the variables, explaining a total of 58.3% of the overall data variation (Figure 4.6). Higher  $r_E$  and  $r_W$  were associated with longer photoperiods (r=0.82 with PCA<sub>2</sub>) and lower iWUE (r=-0.58 with PCA<sub>2</sub>), indicating that cell enlargement and wall deposition rates were more active when trees experienced minimal water and light stress during the growing season (Table 4.3). In contrast, higher  $r_D$  were observed under higher temperatures (r=0.59 with PCA<sub>1</sub>) and drier atmospheric conditions (i.e., higher VPD) (r=0.86 with PCA<sub>1</sub>). Weak relationship was found between iWUE and  $r_D$  (Figure 4.6, Table 4.3). iWUE showed a strong negative

relationship with soil water content (both well correlated with  $PCA_2$ , r=-0.58 and r=0.71 respectively) suggesting that lower soil moisture levels resulted in higher iWUE in black spruce. NDVI exhibited positive links with temperature ( $T_{max}$ ) and VPD, indicating that hot and dry conditions promoted higher photosynthetic activity in our study region and higher cell production rates in black spruce (Figure 4.6, Table 4.3).

The PCA highlighted site-specific links between iWUE, and meteorological factors influencing wood the confidence regions of the PCA scores, indicating distinct site-specific differences in influencing variables. The BER site showed a stronger association with factors like VWC, PP, and  $r_E$  and  $r_W$ , suggesting that water availability and light duration were the key drivers at this site. In contrast, SIM was more closely linked to  $r_D$ , VPD,  $T_{max}$  and NDVI, highlighting the influence of atmospheric stressors and physiological processes on cell formation rates.

#### 4.5 Discussion

This research emphasized the relationships between the kinetics of cell formation (i.e., rates of cell enlargement, wall deposition), cell production rates during xylogenesis and the leaf-level physiological processes mediated by iWUE in black spruce. The findings provide insights into how leaf-level physiological processes shape wood formation and their interactions with environmental constraints. This approach enhances our ability to understand the extent to which wood formation in boreal black spruce is regulated by external environmental factors, offering new insights into tree behavior in a changing climate.

Our initial hypothesis suggested that cell enlargement rates and wall deposition rates (i.e., cell formation kinetics) are primarily influenced by iWUE, driven by the physiological regulation of cell formation kinetics in the leaves. A previous study has shown that under water deficit conditions, plants reduce transpiration of water, leading to higher water use efficiency. This improved efficiency is associated with physiological adjustments, such as stomatal closure, which can influence cell expansion and wall deposition by altering turgor pressure and the availability of resources necessary for cell wall synthesis (Yang et al., 2016). The results of this study confirm this hypothesis and highlight that rates of cell enlargement and wall deposition are closely related to iWUE, and therefore to gas exchange processes at the leaf level (Table 4.3). Lower iWUE, probably caused by an increase in stomatal conductance ( $g_s$ ), promotes higher evaporation and consequently more water transport from the roots to the leaves (Farquhar et al., 1982). Higher water transport provides sufficient water for cell enlargement, thereby increasing its rate during the early

months of the growing season. Favorable water status results in positive turgor pressure, which promotes cell enlargement during this period (Hsiao, 1973; Ortega, 2010; Steppe et al., 2015). In addition, lower iWUE is associated with higher  $g_s$ , which enhances  $CO_2$  diffusion into the leaf, promoting greater photosynthetic rates and carbon assimilation (Farquhar & Sharkey, 1982). Increased carbon assimilation provides more sugars, which are essential building blocks for cell wall formation (Saurer et al., 2004). The relationship between iWUE and wall deposition rates is further supported by previous studies that emphasize the role of intra-seasonal carbon allocation and nitrogen-driven photosynthetic activity in secondary growth (Helle & Schleser, 2004; C. R. Warren & Adams, 2004). Increased photosynthate availability under conditions of higher  $g_s$  and lower iWUE facilitates cell wall thickening by providing the essential substrates for cell wall synthesis (Helle & Schleser, 2004).

In the studied sites, black spruce's iWUE is directly controlled by the dynamics of soil water content. This was shown by strong negative link with soil water content and iWUE in our spruce trees (Figure 4.6, Table 4.3). This finding aligns with the observed positive effect of soil water content on the rates of cell enlargement and wall deposition in our black spruce trees. This relationship can be explained by physiological factors, including water requirements during cell enlargement and its role in sugar allocation and biomass production in black spruce (Buttò et al., 2021; Deslauriers et al., 2016; Martínez-Sancho et al., 2022). Cell enlargement requires a substantial amount of water, making its rate highly sensitive to water availability at the beginning of the growing season (Cabon et al., 2020; Castagneri et al., 2017; Martínez-Sancho et al., 2022). Additionally, enhanced soil water availability not only boosts nitrogen uptake but also increases the dry mass and retention of needles, thereby improving photosynthetic efficiency and carbon sequestration (Buttò et al., 2021; Nilsson, 1997), which may contribute to a higher wall deposition rate in spruce trees. This relationship is further supported by studies indicating that increased nitrogen availability enhances photosynthetic capacity and growth rates in coniferous species (Durzan & Steward, 1967).

Longer photoperiod (i.e., longer daylight) promotes rates of cell enlargement and wall deposition in tree rings of black spruce. Research indicates that photoperiod influences the dynamics of cell enlargement and secondary wall deposition in conifers. A study by Buttò et al., (2021) on black spruce demonstrated that longer photoperiods are associated with increased cell-wall thickness and reduced cell diameter, leading to higher wood micro-density. Their structural equation model revealed a direct effect of photoperiod on micro-density, suggesting that extended daylight periods enhance secondary wall deposition. Additionally, Drew and Downes (2015), developed a model indicating that as day length

increases, carbon allocation is preferentially directed toward cell division and enlargement, while the process of cell-wall thickening is prioritized after the summer solstice. This suggests that photoperiod directly controls the transition from earlywood to latewood in conifers. In addition, a study by Cuny and Rathgeber (2016) found that cell enlargement rates and final tracheid sizes were not directly influenced by seasonal climatic variations. However, a decrease in temperature due to shorter day light during latewood formation constrained cell wall deposition rates. The influence of temperature was permanently recorded in the tree-ring structure only for the last latewood cells. This suggests that developmental controls, potentially linked to photoperiod, play a crucial role in wood formation dynamics particularly cell enlargement and wall deposition rates. Furthermore, research by Rossi et al., (2006) demonstrated that conifers in cold environments synchronize the maximum growth rate of tree-ring formation with day length. This synchronization allows plants to complete secondary cell wall deposition and lignification before the end of the growing season. Therefore, longer photoperiods can lead to higher rates of cell enlargement and wall deposition in boreal conifers.

While other factors like photoperiod and soil water content showed stronger impacts on kinetics of cell formation (i.e., cell enlargement rate, wall deposition rate), temperature (and consequently VPD) had a positive and direct influence on cell production rates (cell per day). This indicate that higher iWUE did not necessarily limit cell production rates in black spruce. We therefore rejected our initial hypothesis, stating that iWUE controls cell production rates in spruce trees. Indeed, our observations showed that not iWUE, but other meteorological factors like temperature and VPD have stronger influences on cell production rates. Previous studies illustrated that improved iWUE did not necessarily lead to growth increases owing to the complex response of trees to drought stress in temperate forests (Fernández-de-Uña et al., 2017; Frank et al., 2015; Lévesque et al., 2014). Additionally, weak correlations observed between iWUE and stem growth, defined by tree ring width, in boreal forest indicate that water availability does not constraint cell production rates in coniferous species and other factors such as temperature and nutrient availability, may play more significant roles in influencing tree growth in this region (Giguère-Croteau et al., 2019). In boreal spruce trees, cambial activity and xylem cell production are closely linked to temperature (Rossi et al., 2007). Warm conditions in late spring and early summer can enhance cell production, provided that water stress is minimal. Warmer temperatures enhance photosynthesis and promote carbon assimilation by increasing the rate of carboxylation of Rubisco and electron transport (Way & Oren, 2010). This intensified activity has different effects on the cambium depending on the moment of the growing season. Early in the growing season, warming temperatures cause snow melt and thereby increase water and

nutrient availability for roots, leading to the onset of stem rehydration (Turcotte et al., 2009). The increased supply of sugars linked to these warmer temperatures promotes water conduction by increasing the number of earlywood tracheids (Castagneri et al., 2017). Later during the growing season, the increase in carbon availability, induced by early warming, can have a carry-over effect on the radial growth of trees because of increased carbon assimilation during latewood formation.

The links between iWUE and wood formation dynamics must be interpreted with respect to the differences in altitude between the BER and SIM sites (Table 4.1). Soil water content and photoperiod were observed to be the dominant factors on wood formation dynamics in BER site, which is located at a higher altitude. This indicates that wetter conditions and longer photoperiods dominate in this site, favoring cell enlargement and wall deposition rates (Steppe et al., 2015). However, in the southern site (i.e., SIM) temperature and VPD were observed to influence cell production rates more strongly. This suggests that SIM experiences drier and warmer conditions, promoting higher iWUE and reduced relative humidity. Higher temperatures lead to higher photosynthesis and consequently higher cell production rates in SIM compared to BER. A nine-year study by Rossi et al., (2014) examined the effects of temperature on wood formation dynamics in black spruce across a thermal gradient in Quebec, Canada. Warmer temperatures led to an earlier onset of cambial activity in spring, thereby extending the growing season. This lengthening of the growing season resulted in a significant increase in cell production. Specifically, a 14-day extension in the period of xylogenesis corresponded to an increase of 33 cells, which is a 109% rise in cell production. These findings suggest that higher temperatures can enhance cell production in black spruce specially in southern site of SIM, by prolonging the duration of wood formation. This aligns with the positive links between NDVI and temperature, which is most clearly visible at the warmer site of SIM.

Our findings illustrated that future climatic changes would impact forest productivity in boreal ecosystems (Ameray et al., 2023). In particular, soil drought stress alters leaf-level physiological processes in spruce trees by increasing water use efficiency (i.e., higher iWUE). This shift affects growth dynamics, leading to reduced cell enlargement and wall deposition rates, ultimately lowering wood density in boreal spruce trees (Buttò et al., 2021; Martínez-Sancho et al., 2022). In contrast, warmer temperatures extend the growing season and enhance cell production rates in spruce trees, which result in an increase in growth rates while reducing potential cold temperature injuries (Ameray et al., 2023; D'Orangeville et al., 2018). However, longer growing seasons do not necessarily accumulate more biomass in the wood. This suggests

that while climate change may extend the growing season in boreal forests, it may not enhance carbon sequestration or consequently increase biomass accumulation through increased wood production. A recent study on balsam fir (*Abies balsamea* (L.) Mill.) in Quebec's boreal forest revealed that more productive trees allocated a greater proportion of their growth to earlywood formation with larger cells, meaning that while trees with longer growing seasons produced more cells, this did not necessarily lead to increased biomass accumulation in the wood (Silvestro et al., 2023).

While our findings provide insights into source limitations on wood formation dynamics through iWUE controls on different cell traits, sink limitations during the growing season should not be overlooked. A recent study by Silvestro et al., (2024) examined the seasonal relationship between carbon uptake and its allocation to woody biomass in Northern Hemisphere coniferous forests. The findings showed that while the peaks of carbon assimilation (Gross Primary Production, GPP) and wood cell differentiation are temporally aligned, these processes are notably decoupled during off-peak periods. Additionally, the study observed that peaks in cambial activity occur earlier than those in GPP. This suggests that non-structural carbohydrates may buffer the timing between carbon assimilation and its allocation to wood. While the prioritization of certain uses of newly formed photo assimilates remains unclear, evidence suggests that survival-related processes supersede structural biomass accumulation (Silvestro et al., 2024; Andreu-Hayles et al., 2022; Palacio et al., 2014), especially in boreal forests with harsh winters (Namvar et al., 2024). As the growing season progresses, trees may shift their carbon allocation strategies, from prioritizing secondary growth in the early to mid-season to enhancing frost resistance in the late season. During this shift, trees may allocate more carbon (e.g., pinitol and lipids) for frost resistance, a strategy commonly adopted by species that must maintain tissue functionality through prolonged freezing winters (Lipavská et al., 2000). Therefore, beyond direct influence of temperature on cell production rate, the weaker links between cell production rates and iWUE observed here, may translate into sink limitations on stem growth specially at higher altitudes. This is consistent with lower stem diameter (Diameter at Breast Height; DBH) observed in older black spruce trees in BER compared to SIM with younger spruce trees (Table C.1). To disentangle the interplay between environmental factors (source limitations), wood formation dynamics, and sink constraints, an intra-annual analysis of carbon stable isotopes and/or sugar concentrations across different tissues (needles, phloem, cambium, and xylem), bud phenology, alongside wood formation data would provide deeper insights into carbon source-sink dynamics in boreal forests. Such an approach would refine our understanding of the seasonal drivers of wood formation in these ecosystems.

### 4.6 Conclusions

The results of the present study highlighted the strong links between kinetics of cell formation, iWUE, and environmental constraints (i.e., soil water content and photoperiod) in black spruce. Wood formation dynamics are shown to be linked to environmental constraints, and controlled by leaf-level physiological process, with cell kinetics reflecting stomatal regulation and cell production rates serving as indicators of temperature and vapor pressure deficit. Future changes in boreal forests ecosystems such as lower soil water content, may induce higher iWUE, constraining the rates of cell enlargement and wall deposition. This may lead to decreased cell wall thickness and wood density especially in the latewood cells at higher latitudes (Buttò et al., 2021). Additionally, an increase in temperature may enhance cell production rates in boreal spruce trees, particularly in lower altitudes. Warmer temperatures influence cambium phenology, allowing longer duration and higher intensity of growth and resulting in proportionally increased xylem cell production (Rossi et al., 2014). However, this temperature increase should not exceed the optimal range for growth, as extreme warming could negatively impact tree physiology and xylem formation (Ameray et al., 2023; Piao et al., 2019; Xi et al., 2024). Longer growing seasons do not necessarily accumulate more biomass in the wood, suggesting that while climate change may extend the growing season in boreal forests, it may not enhance carbon sequestration through increased wood production (Silvestro et al., 2023).

Given the study's limited duration, further research across multiple seasons, sites, and species is needed to refine our understanding of these dynamics. Expanding this work to different climatic contexts will improve eco-physiological studies and help predict how environmental changes will shape tree growth and xylem formation over seasonal and long-term scales. Additionally, real-time analysis of carbon stable isotopes and/or sugar concentrations across tissues (needles, phloem, cambium, xylem), combined with wood formation dynamics, could provide deeper insights into sink limitations, if any, in boreal forests and refine our understanding of seasonal controls on wood formation.

### 4.7 Figures Legend

<u>Figure 4.1</u>: Locations of the two study sites: Simoncouche (SIM) and Bernatchez (BER). The map was designed in QGIS.

<u>Figure 4.2</u>: (a) Black spruce tree at the Simoncouche study site. (b) Sampling process for stable isotope analysis: separation of xylem and bark with a chisel (top), and extraction of microcores using a Trephor to monitor xylogenesis (bottom; the Trephor is shown inserted into the stem to extract microcores).

<u>Figure 4.3</u>: (a) cross section of forming tree ring in the stem of black spruce including cells in different phases of growth as enlargement cells, secondary wall thickening cells and mature cells, (b) Enlarging cells observed under a polarized light microscope (without glistening), (c) wall thickening cells glistened under the polarized light, (d) cell traits measurement using Wincell software, list of measured variables, and derived anatomical parameters.

<u>Figure 4.4</u>: Cell production rate  $(r_E)$ , wall deposition rate  $(r_W)$ , and cell production rate  $(r_D)$  during two consecutive growing seasons of 2020 and 2021 in *Picea mariana* at two site SIM and BER.

<u>Figure 4.5</u>: The horizontal lines represent the median of the variable at each box.

<u>Figure 4.6</u>: The PCA projects the variables related to cell enlargement rate  $(r_E)$ , wall deposition rate  $(r_W)$ , cell production rate  $(r_D)$ , temperature (maximum temperature;  $T_{max}$ ), vapour pressure deficit (VPD), relative humidity (RH), photoperiod (PP), and soil water content (VWC), NDVI, and intrinsic water use efficiency (iWUE) of *Picea mariana* at the sampling sites along a latitudinal gradient. The data represents the recorded variables both in SIM and BER (2020-2021).

### 4.8 Tables Legend

<u>Table 4.1</u>: Latitude (Lat.), longitude (Long.), altitude (Alt, meters above sea level). Annual and May-October statistics for temperature (mean), precipitation (sum), and soil water content (mean, only May-Oct) were calculated values from 2020-2021 for SIM and BER.

<u>Table 4.2</u>: The variables include cell enlargement rate  $(r_E)$ , wall deposition rate  $(r_W)$ , cell production rate  $(r_D)$ , iWUE, soil water content (VWC), NDVI, maximum temperature  $(T_{max})$ , vapour pressure deficit (VPD), relative humidity (RH), and photoperiod (PP) in the two study sites and years.

<u>Table 4.3</u>: The variables are environmental factors, iWUE, NDVI, cell anatomy ratios ( $r_E$  and  $r_W$ ), and cell production rate ( $r_D$ ) in *Picea mariana*, used in the PCA with their contribution to the axis definition (%).

## 4.9 Figures

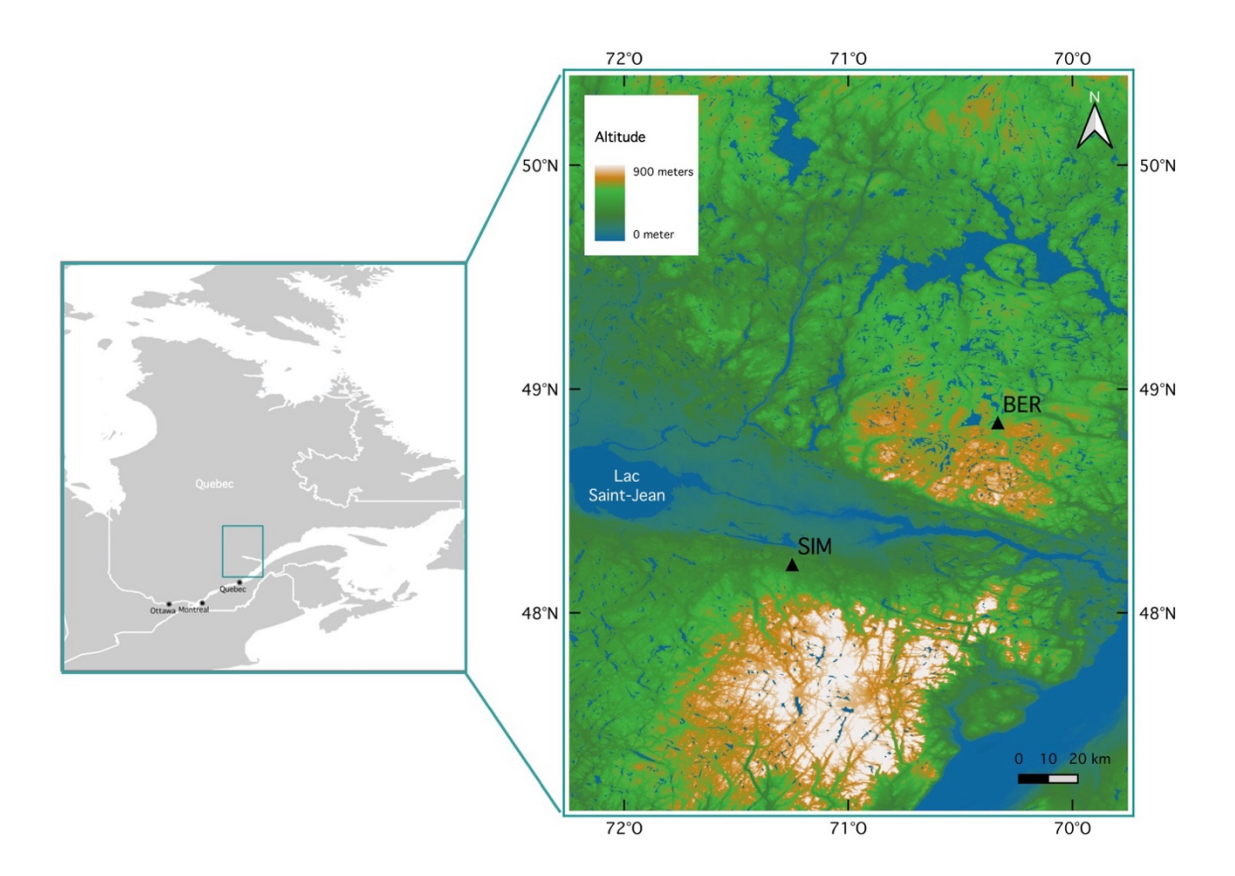


Figure 4.1 Topography of the Saguenay-Lac-Saint-Jean region in Quebec province (highlighted within the square on the left map), Canada.

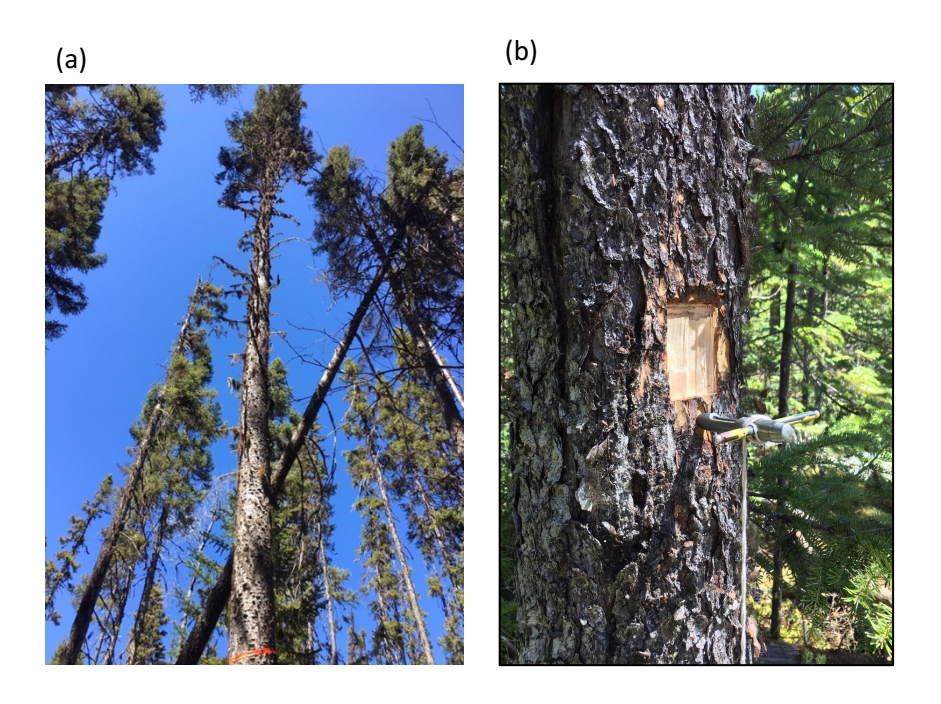


Figure 4.2 Selected tree sample and sampling area in black spruce.

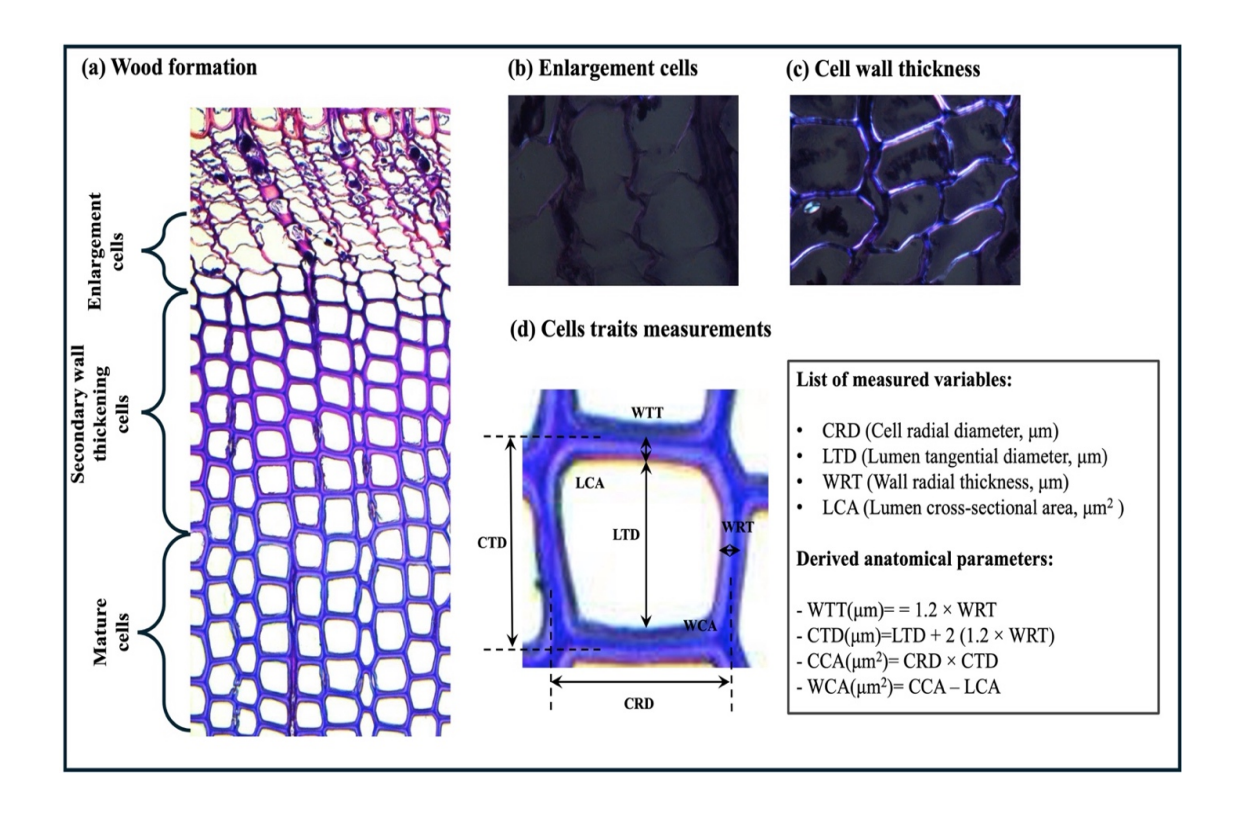


Figure 4.3 Wood formation dynamics and cell traits analysis.

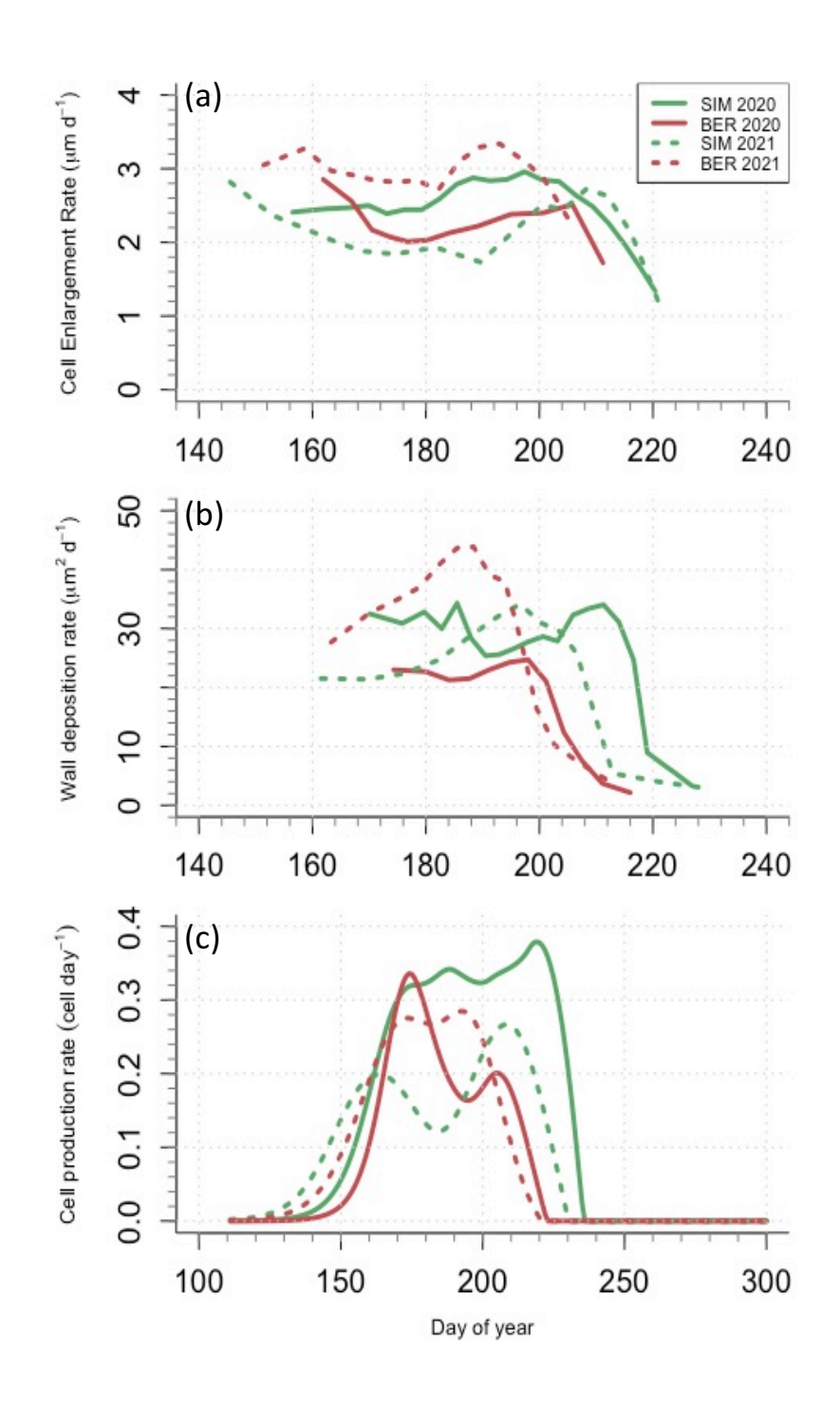


Figure 4.4 Kinetics of cell formation in black spruce

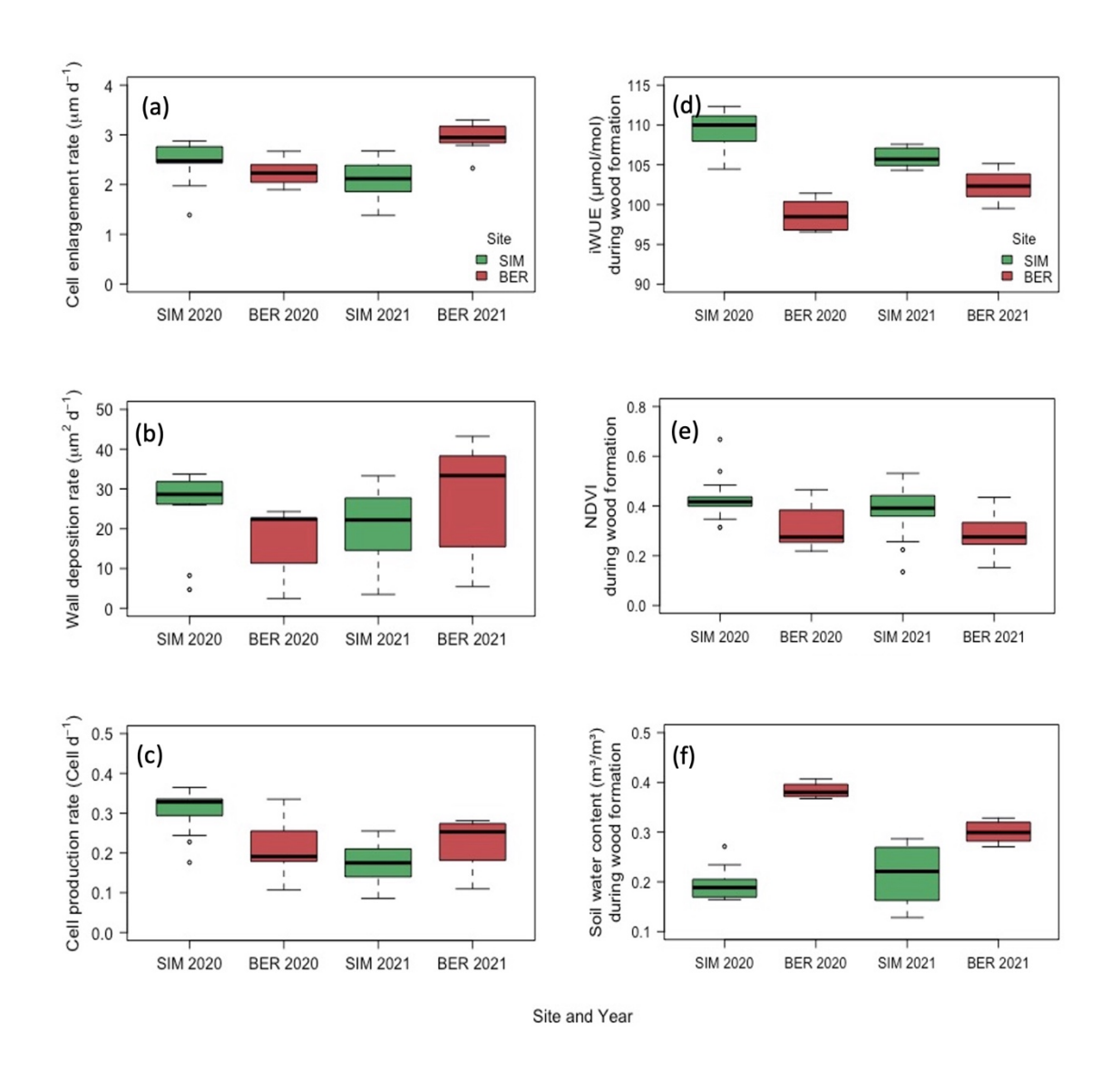


Figure 4.5 Box plots of different variables including cell enlargement rate  $(r_E)$  (a), wall deposition rate  $(r_W)$  (b), cell production rate  $(r_D)$  (c), iWUE (d), soil water content (VWC) (e), NDVI (f) in the two study sites and years.

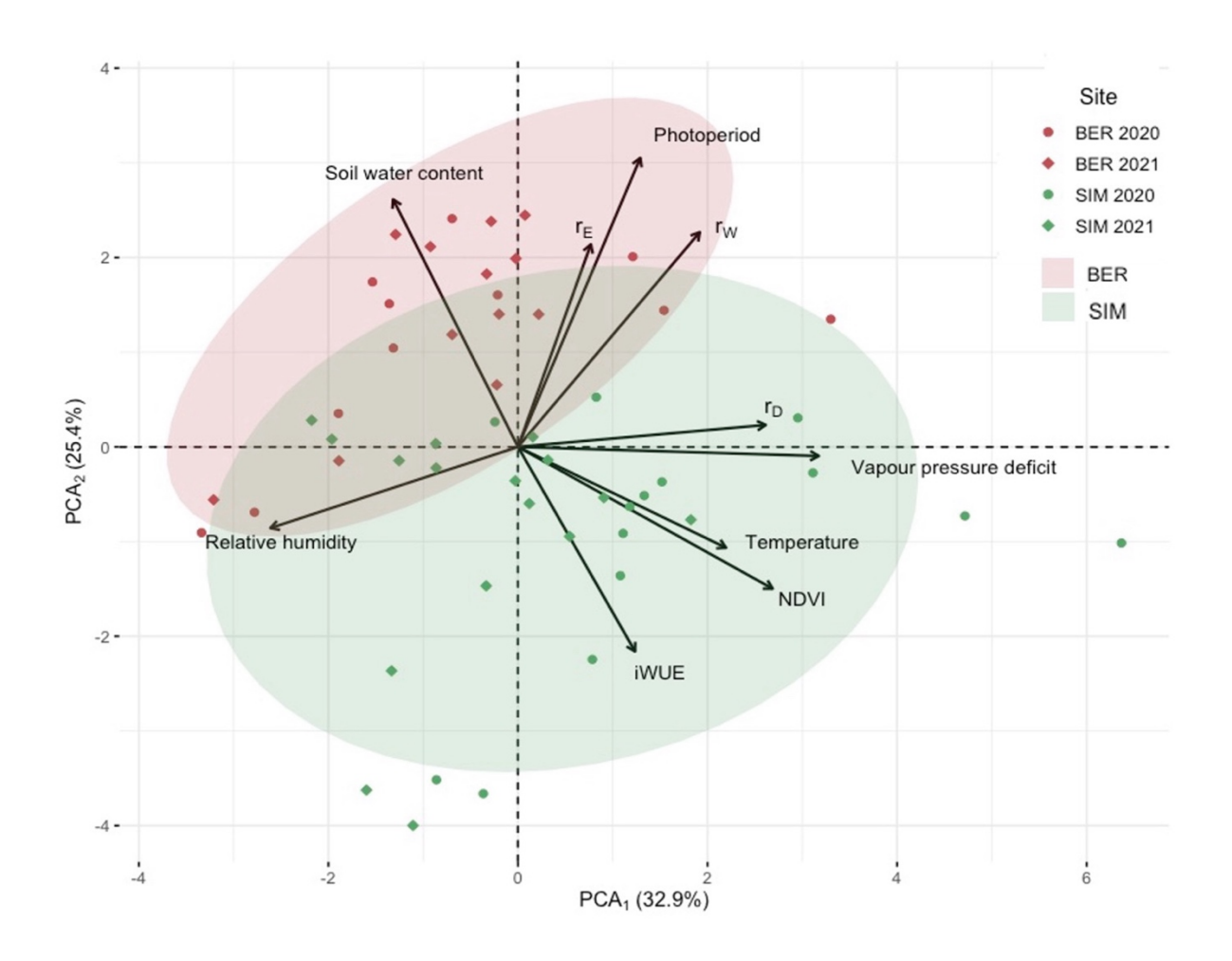


Figure 4.6 Principal component analysis (PCA) representing the variability of different factors explained by the first two dimensions and their relative contribution (%).

# 4.10 Tables

Table 4.1 Location, tree characteristics, and climatic conditions at the two study sites.

Code	Lat.	Long.	Alt (m a.s.l.)	May-Oct Temperature (°C)	Annual Temperature (°C)	May-Oct Precipitati on (mm)	Annual Precipita tion (mm)	Soil water content (m³/m³)
SIM	48°13′	71°15′	338	13.2	3.9	694.4	490.6	0.23
BER	48°51′	70°20′	611	10.8	1.4	641.9	528.6	0.34

Table 4.2 Mean values ( $\pm$  SD) of different variables During the growing season.

	SIM 2020	BER 2020	SIM 2021	BER 2021	
r <sub>E</sub>	2.48±0.41	2.25±0.24	2.11±0.35	2.96±0.27	
r <sub>W</sub>	25.82±9.95	17.21±8.58	20.41±10.44	28.28±13.57	
r <sub>D</sub>	0.31±0.05	0.21±0.07	0.18±0.05	0.23±0.06	
iWUE	109.29±2.45	98.63±1.89	105.10±1.18	102.41±1.76	
VWC	0.19±0.03	0.38±0.01	0.22±0.06	0.30±0.02	
NDVI	0.43±0.09	0.31±0.09	0.39±0.10	0.29±0.08	
T <sub>max</sub>	22.47±3.25	21.59±3.05	19.21±2.13	17.84±2.25	
VPD	1.20±0.49	1.20±0.42	1.01±0.17	0.90±0.13	
RH	57.41±10.02	58.72±9.39	59.04±5.68	59.88±5.88	
PP	15.70±0.41	15.87±0.29	15.64±0.43	15.87±0.24	

Table 4.3 Correlation between axes of the principal component analysis ( $PCA_1$  and  $PCA_2$ ) and different variables.

	PCA <sub>1</sub>	PCA <sub>2</sub>	PCA <sub>1</sub>	PCA <sub>2</sub>	
	Correlation	Correlation	Contribution	Contribution	
r <sub>E</sub>	0.21	0.58***	1.32	13.18	
r <sub>W</sub>	0.52**	0.61***	8.18	14.81	
rD	0.71**	0.06	15.20	0.15	
iWUE	0.33**	-0.58***	3.39	13.45	
VWC	-0.36**	0.71***	3.86	19.69	
NDVI	0.73***	-0.40***	16.05	6.46	
T <sub>max</sub>	0.59***	-0.29**	10.71	3.27	
VPD	0.86***	-0.03	22.40	0.03	
RH	-0.71***	-0.23	15.17	2.12	
PP	0.35**	0.82***	3.71	26.83	

### **GENERAL CONCLUSIONS**

In this study, I investigated the intra-annual fractionation of carbon and oxygen stable isotopes in black spruce within North America's boreal forests. Weekly monitoring was conducted to track carbon and oxygen stable isotope fractionation in secondary growth, specifically in the growing cambial region ( $\delta^{13}C_{cam}$ and  $\delta^{18}O_{cam}$ ) and developing tree ring ( $\delta^{13}C_{xc}$  and  $\delta^{18}O_{xc}$ ). The  $\delta^{13}C$  and  $\delta^{18}O$  profiles were developed for both tissues, and their relationships with leaf-level physiological processes and environmental constraints were investigated. Additionally, wood formation dynamics of black spruce were analyzed at two sites, and their association with iWUE, derived from weekly  $\delta^{13}C_{cam}$  values, were examined. My main objectives of this thesis were: (i) Developing a method to explore the fluctuations of  $\delta^{13}$ C and  $\delta^{18}$ O values within the vascular cambium-xylem continuum throughout the growing season and examine how each tissue responds to the carbon demand for stem growth. (ii) to provide real-time insights into the dynamic changes in weekly  $\delta^{13}$ C and  $\delta^{18}$ O values in the cambial region and developing xylem cellulose (iii) to identify the primary drivers of wood formation dynamics in boreal trees, focusing on three key parameters as indicators of wood formation: cell enlargement rates (r<sub>E</sub>), wall deposition rates (r<sub>W</sub>), and cell production rates (r<sub>D</sub>). Relationships between these parameters, intrinsic water use efficiency (iWUE), and meteorological factors were examined. Each chapter of this thesis explored a distinct aspect of secondary growth dynamics in black spruce and provided novel insights into carbon source-sink dynamics, plant hydrodynamics, and the key factors regulating wood formation rates during the growing season in boreal forest ecosystems.

The sampling technique I employed for collection of the cambial region and forming xylem was efficient and allowed for creation of  $\delta^{13}C_{cam}$  and  $\delta^{13}C_{xc}$  series (chapter 2). Strong positive correlations were observed between  $\delta^{13}C_{cam}$  and  $\delta^{13}C_{xc}$  series at the two sites, with an increasing trend from the beginning to the end of the growing season in almost all study years. Additionally, no strong correlations were observed between the two series and meteorological parameters at seasonal scales. Performing  $\delta^{13}C_{cam}$  and  $\delta^{13}C_{xc}$  series and analysis on these two tissues has the potential to reduce knowledge gaps that persist on the timing of NSC synthesis in leaves, their subsequent transport through phloem, cambium tissue, and ultimately, their incorporation in tree-ring cellulose. The implemented method in this thesis clearly demonstrated that the weekly construction of black spruce's cambium and xylem cells are formed by shared NSC pools, originating predominantly from current photo-assimilates. The high level of correspondence between  $\delta^{13}C_{cam}$  and  $\delta^{13}C_{xc}$  challenged our initial hypothesis, which assumed that if stored

NSCs were to be used by xylem and not by cambium, divergences in  $\delta^{13}C$  variations between the two tissues would necessarily emerge, reflecting a mixture of NSC sources synthesized at different time periods. While the strong links between the two profiles rejected this hypothesis and imply that a constant supply of fresh assimilates feed stem growth dynamics in our spruce trees. Therefore, weekly  $\delta^{13}C_{cam}$  and  $\delta^{13}C_{xc}$  values may provide reliable information about physiological processes (i.e., stomatal conductance) that occur at the leaf level during the growing season, with minor incorporation of stored NSCs with different  $\delta^{13}C$  signals. On the other hand, in absence of detrimental climate constraints, the increasing  $\delta^{13}C_{cam}$  and  $\delta^{13}C_{xc}$  trends observed here possibly indicate shifts in carbon allocation strategies, likely fostering frost resistance and reducing water uptake in the late growth season. Additionally, these trends may be related to the black spruce trees' responses to the seasonal decrease in photosynthetically active radiation.

For our second objective, weekly isotopic profiles for the cambial region ( $\delta^{13}C_{cam}$  and  $\delta^{18}O_{cam}$ ) and developing xylem cellulose ( $\delta^{13}C_{xc}$  and  $\delta^{18}O_{xc}$ ) were analysed (Chapter 3). Strong positive correlations were observed between  $\delta^{13}C_{cam}$  and  $\delta^{18}O_{cam}$ , with an increasing trend along the growing season. Conversely, negative relationships were observed between  $\delta^{13}C_{xc}$  and  $\delta^{18}O_{xc}$ , characterized by an increasing trend in  $\delta^{13}C_{xc}$  and a decreasing trend in  $\delta^{18}O_{xc}$ . Our initial hypothesis proposed that  $\delta^{13}C$  and  $\delta^{18}O$  values in the cambial region would correlate due to shared physiological constraints on stable isotopes fractionation originating at the leaf level. The results of this study confirm this hypothesis and suggest that stomatal conductance  $(g_s)$  regulation in the needles of black spruce is likely the dominant factor controlling the seasonal fractionation of  $\delta^{13}C_{cam}$  and  $\delta^{18}O_{cam}$  in our study region. Both  $\delta^{13}C_{cam}$  and  $\delta^{18}O_{cam}$  series exhibited consistent seasonal <sup>13</sup>C-enrichment patterns during the growing season in nearly all study years and sites, with no strong relationships observed between  $\delta^{18}O_{rain}$  and  $\delta^{18}O_{cam}$ . This pattern aligns with the dualisotope theory (Scheidegger et al., 2000; Siegwolf et al., 2023), which attributes such enrichment to the concurrent influence of  $g_s$  on the fractionation of both isotopes. However, proportional exchanges between xylem water and sugars at the sites of cellulose synthesis (i.e., Pex effect) are thought to be strong enough to completely blur the trends visible in  $\delta^{18}O_{cam}$ . This suggests that  $\delta^{18}O_{xc}$  signals differ from those originating in the earlier cambium sink. Therefore, our hypothesis was rejected for  $\delta^{18}O_{xc}$  series, illustrating that  $\delta^{18}O_{xc}$  does not entirely correlates with leaf-level physiological processes during the growing season. This complexity cautioned against oversimplistic assumptions that oxygen isotopes in xylem cellulose serve as a reliable proxy for  $g_s$  signals, particularly in boreal forests. Our findings highlighted the need for careful consideration of the processes influencing isotopic signals to avoid misinterpretations in dendroclimatological studies.

In the fourth chapter, we analyzed wood formation dynamics by monitoring the xylogenesis process and measuring cell traits in fully formed tree rings. Specifically, we assessed the rates of cell enlargement, wall deposition, and cell production. Intrinsic water use efficiency (iWUE) was derived from  $\delta^{13}C_{cam}$  data. To examine the relationships between cell trait rates, cell production rate, iWUE, and various environmental parameters, we conducted a principal component analysis (PCA) and visualized the results using a biplot. The results demonstrated that while the rates of cell enlargement and wall deposition are primarily regulated by iWUE at the leaf level (confirming our hypothesis), cell production is more influenced by environmental factors such as temperature and vapor pressure deficit (VPD), contradicting our primary hypothesis that iWUE directly controls cell production rates in black spruce. This finding suggests that stomatal regulation plays a key role in controlling cell growth rates and carbon deposition in the secondary cell wall of black spruce, with  $g_s$  itself being modulated by soil water content (Cuny et al., 2015; Rossi et al., 2016). Higher soil water content results in lower iWUE, which leads to increased rates of cell enlargement and wall deposition specifically at higher altitudes. Conversely, higher temperatures and a drier atmosphere promote higher rates of cell production in black spruce more likely in southern site of SIM.

These findings indicate that while cell enlargement and wall deposition rates are directly controlled by leaf-level physiological constraints, cell production rates are predominantly influenced by environmental factors (i.e., temperature and VPD). This distinction highlights that cell production data derived from xylogenesis analysis may serve as a more reliable proxy for climatic variables like temperature and VPD (Gričar et al., 2015; Korpela et al., 2021). In contrast, the rates of cell traits are better indicators of leaf-level physiological factors regulating wood formation dynamics during the growing season (Cuny et al., 2019; Cabon et al., 2020; Rathgeber et al., 2016). This aligns with our findings from the previous chapters, demonstrating that leaf-level physiological constraints, particularly stomatal conductance, regulate carbon isotopes fractionation in both the cambial region and developing tree ring, suggesting that the ratios of carbon isotopes in the xylem cellulose are more closely linked to the rates of cell enlargement and carbon sequestration in the secondary cell wall during tree ring formation, while cell production rate is more influenced by external climatic constraints.

Our findings confirm that future climatic changes will impact forest productivity in boreal ecosystems (Ameray et al., 2023). Soil drought stress alters leaf-level physiological processes in spruce trees by increasing water use efficiency (i.e., higher iWUE). This shift affects growth dynamics, leading to reduced

cell enlargement and wall deposition rates, ultimately lowering wood density and biomass production in boreal spruce trees (Buttò et al., 2021; Martínez-Sancho et al., 2022). In contrast, warmer temperatures extend the growing season and enhance cell production rates in spruce trees, which result in an increase in growth rates (Ameray et al., 2023; D'Orangeville et al., 2018). This study highlights the link between growth dynamics and iWUE in black spruce during the growing season while emphasizing the strong connection between leaf-level physiological processes and climatic constraints. Our findings underscore how wood formation dynamics are influenced by environmental factors (i.e., soil water content, photoperiod, and temperature) throughout the growing season. However, our results also highlight the importance of sink limitations, such as constraints on carbon allocation and cell differentiation, in shaping seasonal growth patterns (i.e., cell production rates) in boreal black spruce.

Although no significant correlations were found between  $\delta^{13}C$  and  $\delta^{18}O$  series and climatic variables during the growing season (Chapters 2 and 3), significant relationships emerged between iWUE (derived from  $\delta^{13}C_{cam}$  values) and soil water content, temperature, and VPD (Chapter 4). This discrepancy likely reflects differences in the scale of comparison: in the first two chapters,  $\delta^{13}C$  and  $\delta^{18}O$  series were analyzed against meteorological variables over time within the growing season (temporal scale), whereas in Chapter 4, iWUE was assessed in relation to climatic variables across the two sites (spatial scale). Such scale dependency may therefore explain the contrasting outcomes when comparing  $\delta^{13}C$ ,  $\delta^{18}O$ , and iWUE with climatic drivers in this study.

Limits and perspectives: In this thesis, I aimed to monitor weekly fractionation of  $\delta^{13}$ C and  $\delta^{18}$ O isotopes in the growing cambium-xylem continuum in black spruce, by developing a new non-lethal method. However, the multiple source (i.e., different substances and sugars in the cambial region) versus single sink ( $\alpha$ -cellulose in tree rings) approach we used here for monitoring  $\delta^{13}$ C ratios in the cambial region and xylem cellulose may not fully unveil the subtle source-sink interactions that impact  $\delta^{13}$ C ratios in these two tissues. To achieve a deeper understanding of those interactions, comparing isotopic signature of  $\delta^{13}$ C in the cambial region with  $\delta^{13}$ C in whole wood may provide further insights into  $\delta^{13}$ C ratios within the growing cambium-xylem continuum. Additionally, a compound-specific monitoring of carbon stable isotopes in the cambium-xylem continuum (e.g.,  $\delta^{13}$ C in different sugars found in the two tissues) could offer further information on seasonal carbon allocation strategies in boreal trees. Moreover, a study comparing weekly variations of  $\delta^{13}$ C series in cellulose and whole wood within developing tree ring could provide further insights into the use of whole wood versus  $\alpha$ -cellulose for weekly monitoring of carbon stable isotopes

and help optimize sample collection and analysis. While the developed method in this thesis has proven effective for monitoring the weekly  $\delta^{13}C$  evolution of the cambium-xylem continuum in black spruce, further research is recommended to evaluate its applicability to species with different growth characteristics.

To better understand the dynamics  $\delta^{18}O_{xc}$  signals during the growing season, further research is needed to understand the role of soil water  $\delta^{18}O$  dynamics in influencing oxygen isotope signals in forming tree rings. Additionally, extending this research to longer sampling periods (for isotopes analysis and monitoring xylogenesis and cell traits), will deepen our understanding of these processes and enhance the reliability of dendroclimatological models across boreal ecosystems. Such interdisciplinary approaches are essential for assessing how environmental changes influence tree physiology, xylem hydraulic conductivity and factors controlling/influencing wood formation dynamics on seasonal to decadal scales. Moreover, real-time analysis of carbon stable isotopes and/or sugar concentrations across tissues (needles, phloem, cambium, xylem), combined with wood formation dynamics, could provide deeper insights into sink limitations, if any, in boreal forests and refine our understanding of seasonal controls on wood formation.

### **APPENDIX A**

Method A.1 Two step correction of  $\delta^{13}C_{cam}$  and  $\delta^{13}C_{xc}$  series for intra-seasonal variations in atmospheric  $\delta^{13}C$  ( $\delta^{13}C_{atm}$ )

In order to gain better insights into the effect of changes in seasonal atmospheric  $\delta^{13}C$  ( $\delta^{13}C_{atm}$ ) on our weekly  $\delta^{13}C_{cam}$  and  $\delta^{13}C_{xc}$  values, we disentangled the Suess-effect and intra-seasonal variations in  $\delta^{13}C_{atm}$  in two steps. First, we corrected  $\delta^{13}C_{cam}$  and  $\delta^{13}C_{xc}$  series for the Suess effect, which is the progressive decline in  $\delta^{13}C_{atm}$ , due to fossil emissions, since 1850 (Pre-Industrial reference,  $\delta^{13}C_{atm\_Pl} = -6.61\%$ ) (Belmecheri & Lavergne, 2020; McCarroll & Loader, 2004). To do so, we used the seasonal averaged values of  $\delta^{13}C_{atm}$  data from Argyle station (AMT,  $\delta^{13}C_{atm\_AMT\_average}$ ) in accordance with the time periods of  $\delta^{13}C_{cam}$  and  $\delta^{13}C_{xc}$  series in each study year (Table A.2). We calculated the Suess-effect corrected values for each date of sampling ( $\delta^{13}C_{xc\_suess\_cor(date=n)}$ , blue curves on figure A.3) as follows (example for xylem, same for cambium):

$$\delta^{13}\mathsf{C}_{xc_{suess}_{cor(date=n)}} = \delta^{13}\mathsf{C}_{xc(date=n)} - \left(\delta^{13}\mathcal{C}_{atm_{AMT_{average}}} - \delta^{13}\mathcal{C}_{atm_{PI}}\right)$$

Equation A.1 Calculation of Suess-effect corrected  $\delta^{13}C_{xc}$ 

Second, we refined the Suess-effect corrected carbon isotope values ( $\delta^{13}C_{xc\_suess\_cor}$ ) by accounting for the intra-seasonal variability in atmospheric carbon isotope composition in our study region. To achieve this, we subtracted the difference in  $\delta^{13}C_{atm\_AMT}$  between two specific dates of sampling (date=n and date=n-1) from the Suess-effect corrected carbon isotope values as is shown below ( $\delta^{13}C_{xc\_seasonal\_cor}$ , red curves on Figure A.3):

$$\delta^{13}\mathsf{C}_{xc_{seasonal_{cor(date=n)}}} = \delta^{13}\mathsf{C}_{xc_{suess_{cor(date=n)}}} - \left(\delta^{13}C_{atm_{AMT(date=n)}} - \delta^{13}C_{atm_{AMT(date=n-1)}}\right)$$

Equation A.2 Calculation of  $\delta^{13}C_{xc}$  based on seasonal atmospheric carbon isotope composition

The resulting  $\delta^{13}C_{xc\_seasonal\_cor}$  series allow for a more precise understanding of carbon isotope dynamics independent of changes in intra-seasonal  $\delta^{13}C_{atm}$  variations within our study region (Figure A.3 and A.4). We also performed a similar correction using comparable, although remotely located, boreal forest  $\delta^{13}C_{atm}$  data. Indeed, we performed the same calculations, this time using the  $\delta^{13}C_{atm}$  Lac La Biche station (LLB,  $\delta^{13}C_{atm\_LLB}$ ) (Figure A.5 and A.6). However, the  $\delta^{13}C_{atm}$  data for this site was only available between 2008-2013, so we only considered the average  $\delta^{13}C_{atm}$  seasonal cycle for the LLB site and applied it uniformly to all years (Table A.4).

### Method A.2 Detrending the $\delta^{13}C_{xc}$ cor series

$$\delta^{13}C_{xc_{seq(t)}} = \frac{\delta^{13}C_{xc_{cor(t)}} \cdot \sum_{0}^{t} m_{(t)} - \delta^{13}C_{xc_{cor(t-1)}} \cdot \sum_{0}^{t-1} m_{(t-1)}}{\sum_{0}^{t} m_{(t)} - \sum_{0}^{t-1} m_{(t-1)}}$$

Equation A.3 Calculation of the detrended  $\delta^{13}C_{xc}$  cor series

Where  $\delta^{13}C_{xc\_seq}$  is the average weight of  $\delta^{13}C_{xc\_cor}$  during the t=t-1 to t=t interval. We detrended the  $\delta^{13}C_{xc\_cor}$  series at the tree level and site level and for all different study years (detrended series at site level; Figure A.2).

### Appendix A Figure legends

<u>Figure A.1</u>: SIM at each study year of 2019 (a-e), 2020 (f-j), and 2021 (k-o), and BER at the study years of 2020 (p-t) and 2021 (u-y), the black solid line represents the regression line for each of  $\delta^{13}C_{xc}$  profiles.

<u>Figure A.2</u>: The solid lines represent the regression line for each of  $\delta^{13}C_{xc}$  and  $\delta^{13}C_{xc}$  are profiles.

<u>Figure A.3</u>: The orange curves represent the raw  $\delta^{13}C_{cam}$  profiles at each study year. The dashed lines in different colors are related to the dates before the beginning of early wood formation, and the solid parts represents the dates after the onset of early wood formation. The thick green curves represent the seasonal variation of Argyle  $\delta^{13}C_{atm}$  ( $\delta^{13}C_{atm\_AMT}$ , daily values). The solid lines represent the regression line for each of  $\delta^{13}C_{cam}$  profiles.

<u>Figure A.4</u>: The green curves are the raw  $\delta^{13}C_{xc}$  profiles. The thick green curve represents the seasonal variation of Argyle  $\delta^{13}C_{atm}$  ( $\delta^{13}C_{atm\_AMT}$ , daily values). The solid lines represent the regression line for each of  $\delta^{13}C_{xc}$  profiles.

Figure A.5: The orange curves represent the raw  $\delta^{13}C_{cam}$  profiles at each study year. The dashed lines in different colors are related to the dates before the beginning of early wood formation, and the solid parts represents the dates after the onset of early wood formation. The thick blue curves represent the seasonal variation of Lac La Biche  $\delta^{13}C_{atm}$  ( $\delta^{13}C_{atm}$ , daily values). The solid lines represent the regression line for each of  $\delta^{13}C_{cam}$  profiles.

<u>Figure A.6</u>: The green curves are the raw  $\delta^{13}C_{xc}$  profiles. The thick blue curves represent the seasonal variation of Lac La Biche  $\delta^{13}C_{atm}$  ( $\delta^{13}C_{atm\_LLB}$ , daily values). The solid lines represent the regression line for each of  $\delta^{13}C$  profiles.

Figure A.7: The solid black lines represent the regression line for each of profiles.

Figure A.8: The solid black lines represent the regression line for each of profiles.

<u>Figure A.9</u>: Daytime averages (8h00 to 18h00) for maximum temperature ( $T_{max}$ ), vapour pressure deficit (VPD), photosynthetically active radiation (PAR), relative humidity (RH), precipitation (P), soil volumetric water content (VWC), (\* p< 0.1, \*\* p< 0.05, \*\*\* p< 0.01).

Appendix A Table legends

<u>Table A.2</u>: Pooling was done for each date of sampling for five trees for cambial region. For xylem samples, pooling was done only in SIM 2020 (day of year=168) and BER 2020 (day of year=175 and day of year=189).

<u>Table A.4</u>: The full growing season periods are in accordance with the periods in full growing season  $\delta^{13}C_{cam}$  series. The periods after onset of early wood formations (EW) are in accordance with  $\delta^{13}C_{cam}$  and  $\delta^{13}C_{xc}$  series.

<u>Table A.5</u>: The parameter  $\beta$  represents the regression slope of  $\delta^{13}C_{xc}$  values in each tree sample and p represents the significance level of the regression slope (\*\*\* p< 0.001, \*\* p< 0.05).

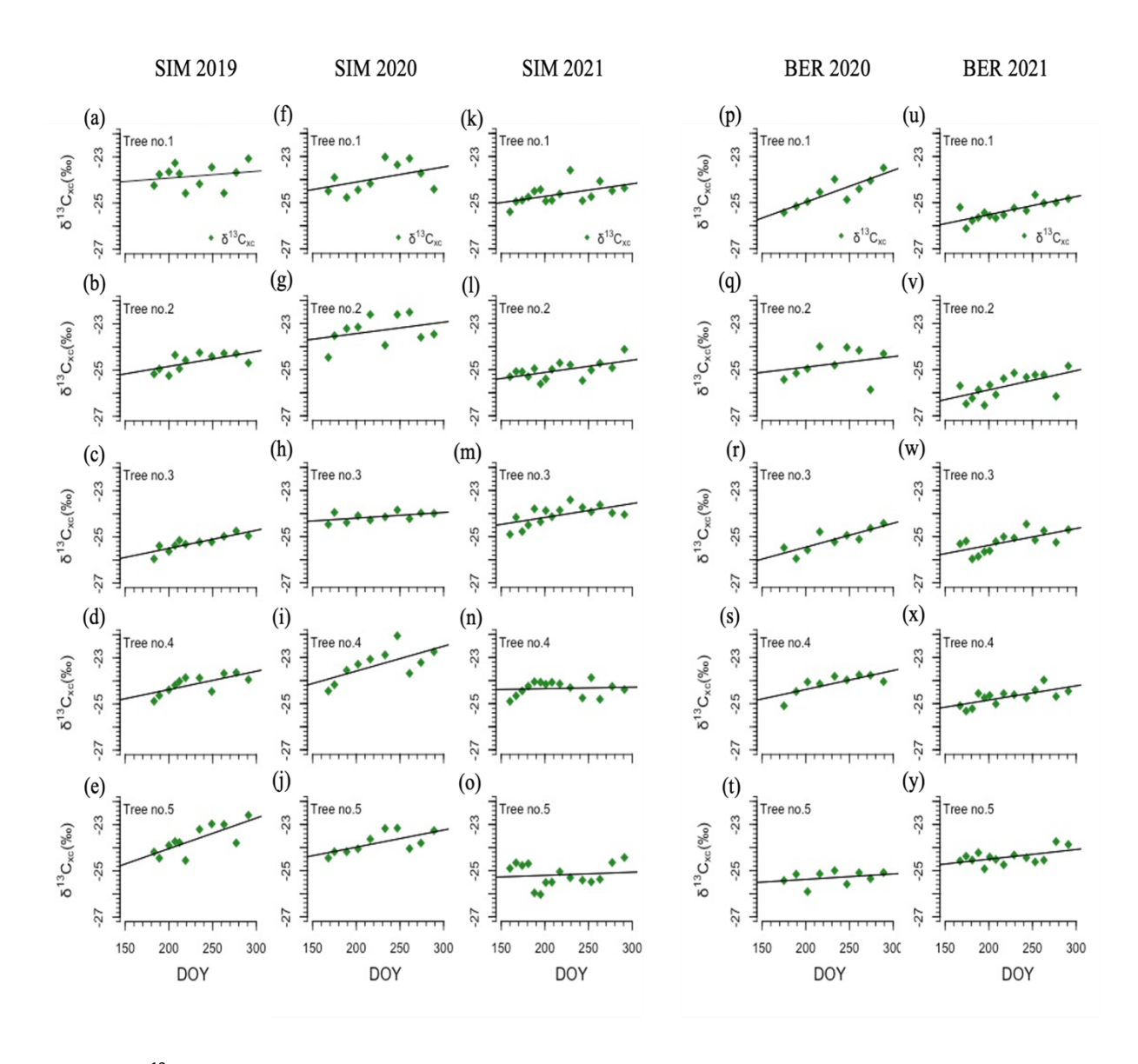


Figure A.1  $\delta^{13}C_{xc}$  profiles in each of the five tree samples in each site and study years.

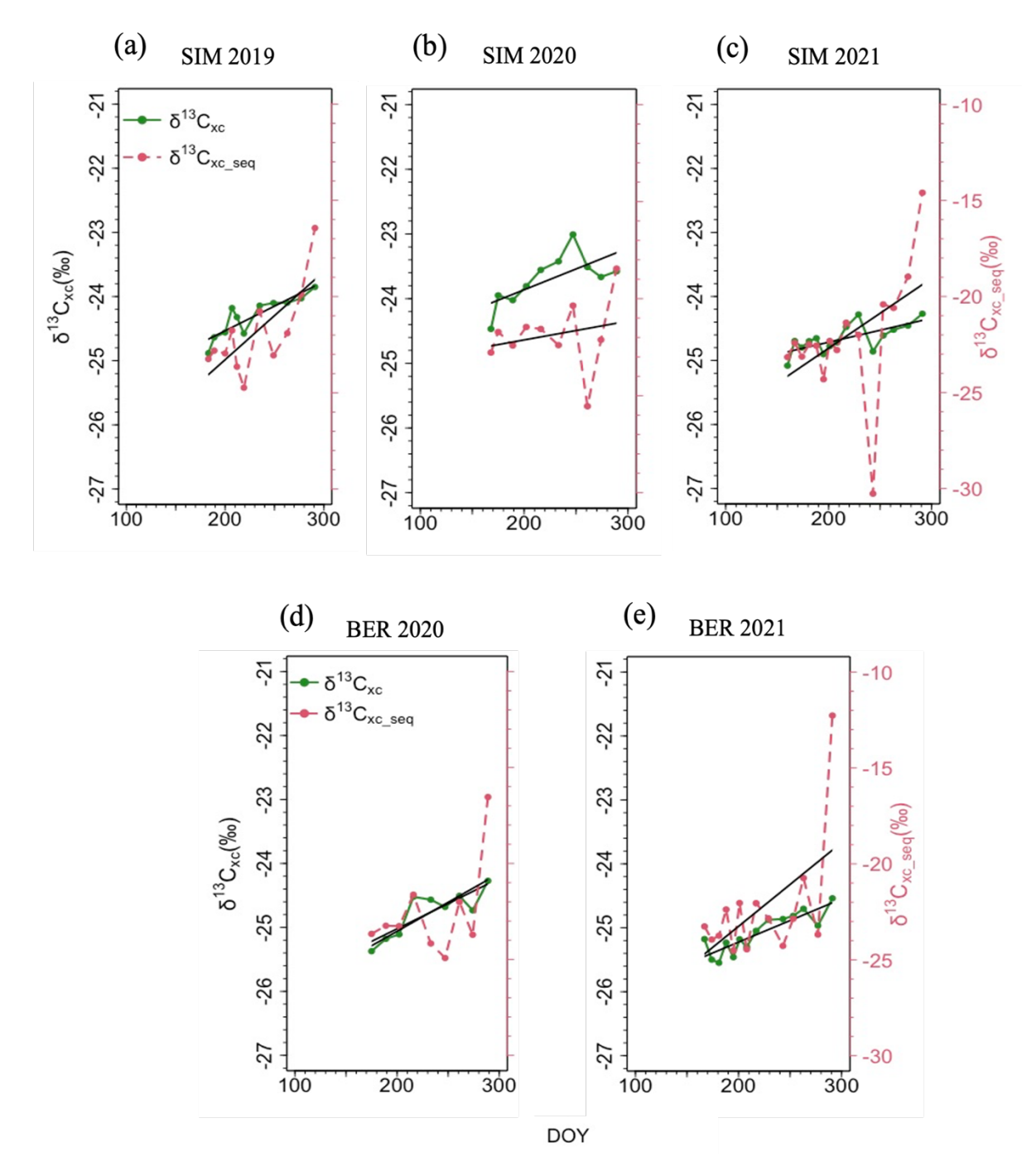


Figure A.2  $\delta^{13}C_{xc}$  and  $\delta^{13}C_{xc\_seq}$  profiles in different study years at SIM (a, b, c) and BER (d, e).

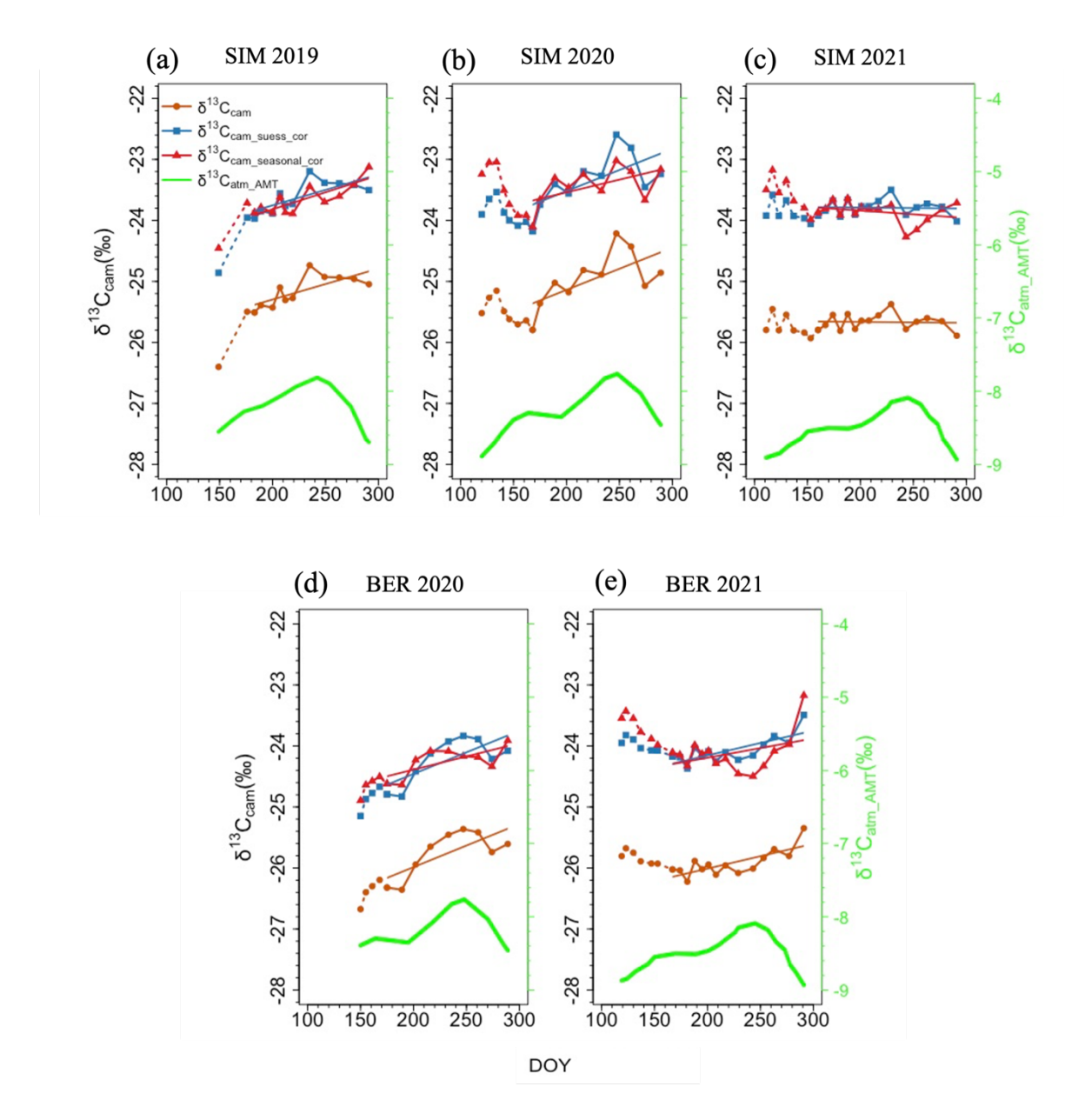


Figure A.3 Corrected  $\delta^{13}C_{cam}$  profiles for the Suess-effect and seasonal atmospheric  $\delta^{13}C_{atm}$  using the  $\delta^{13}C_{atm}$  values collected from the Argyle station (AMT) in different study years at SIM (a, b, c) and BER (d, e).

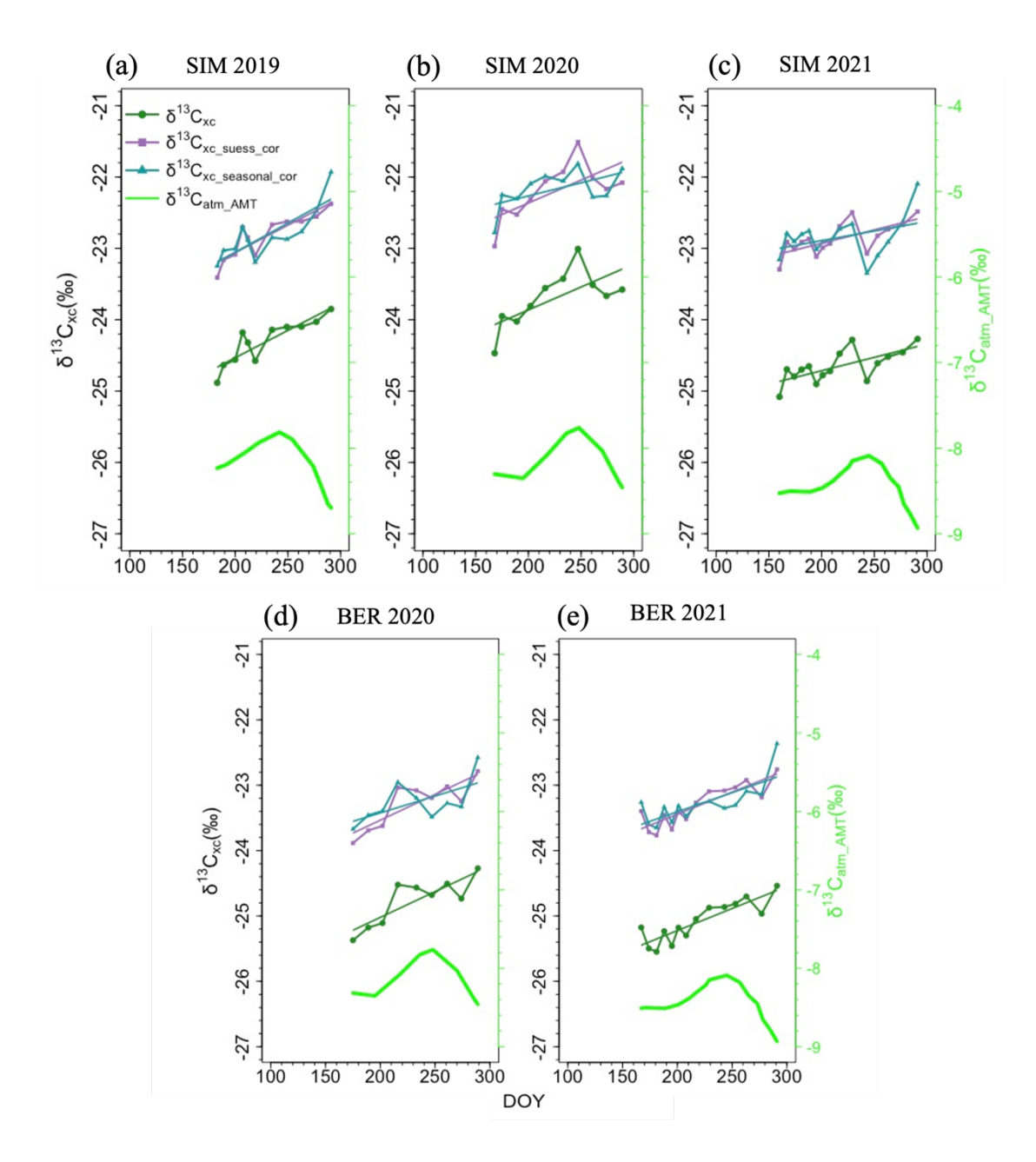


Figure A.4 Corrected  $\delta^{13}C_{xc}$  profiles for the Suess-effect and seasonal atmospheric  $\delta^{13}C$  using the  $\delta^{13}C$  values collected from the Argyle station (AMT), in different study years at SIM (a, b, c) and BER (d, e).

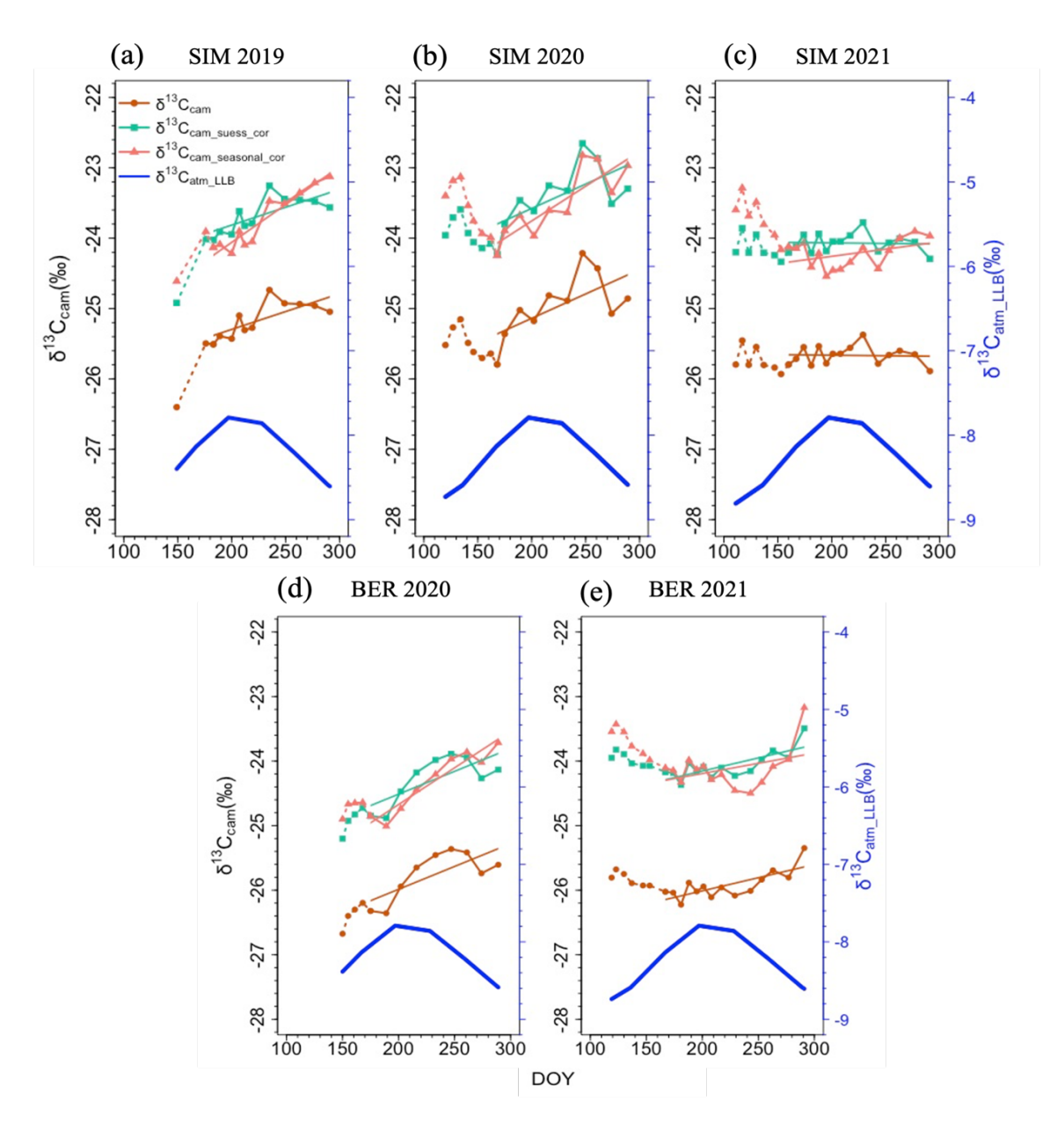


Figure A.5 Corrected  $\delta^{13}C_{cam}$  profiles for the Suess-effect and seasonal atmospheric  $\delta^{13}C_{atm}$  using the  $\delta^{13}C_{atm}$  values collected from the Lac La Biche station (LLB) in different study years at SIM (a, b, c) and BER (d, e).

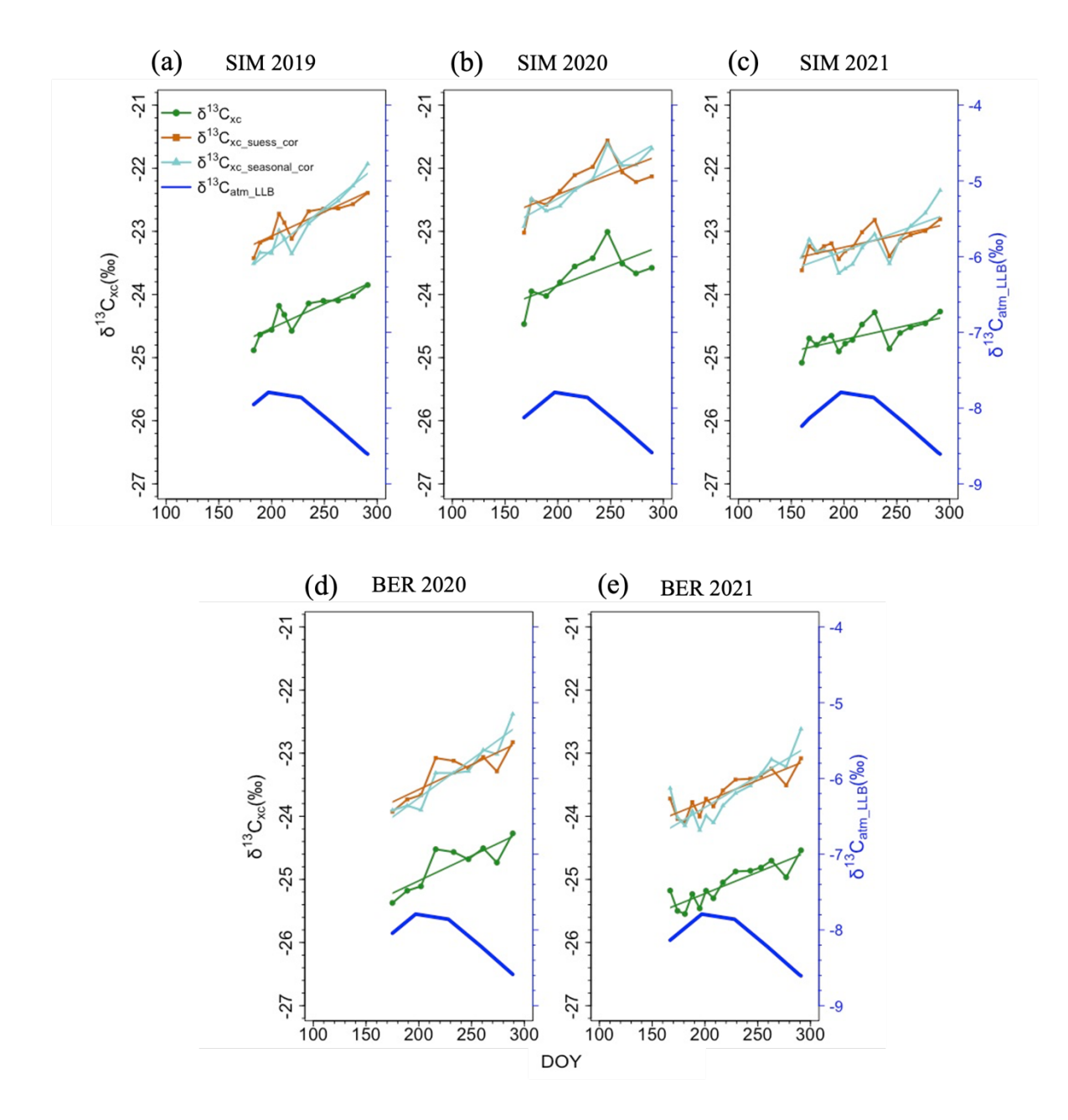


Figure A.6 Corrected  $\delta^{13}C_{xc}$  profiles for the Suess-effect and seasonal atmospheric  $\delta^{13}C$  using the  $\delta^{13}C$  values collected from the Lac La Biche station (LLB) in different study years at SIM (a, b, c) and BER (d, e).

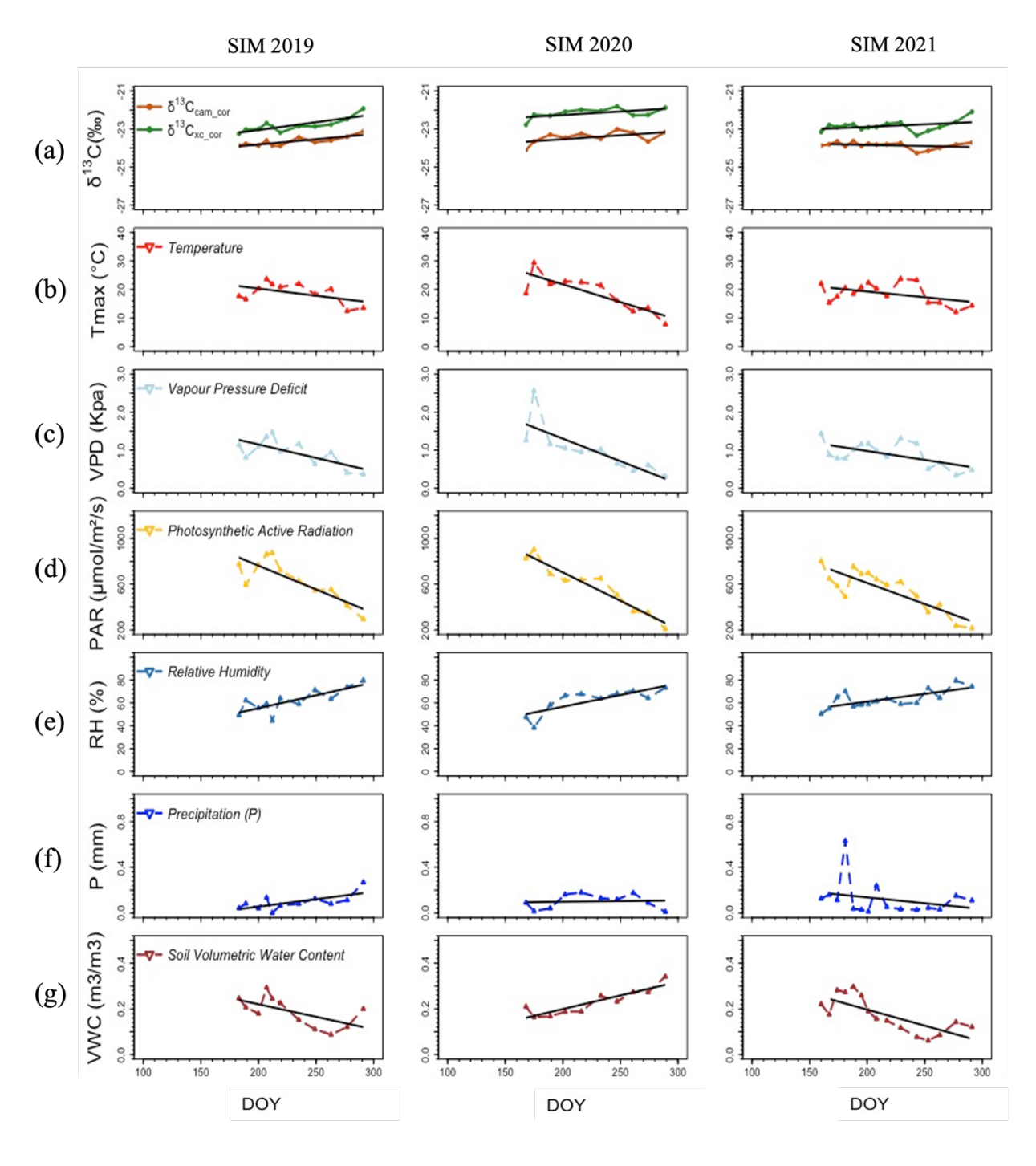


Figure A.7 Variations of  $\delta^{13}C_{cam\_cor}$ , and  $\delta^{13}C_{xc\_cor}$ , series (a), and climatic variables (Daytime averages (8h00 to 18h00) of  $T_{max}$  (b), VPD (c), PAR (d), RH (c), P (f), VWC (g)) in SIM2019, SIM 2020, and SIM 2021.

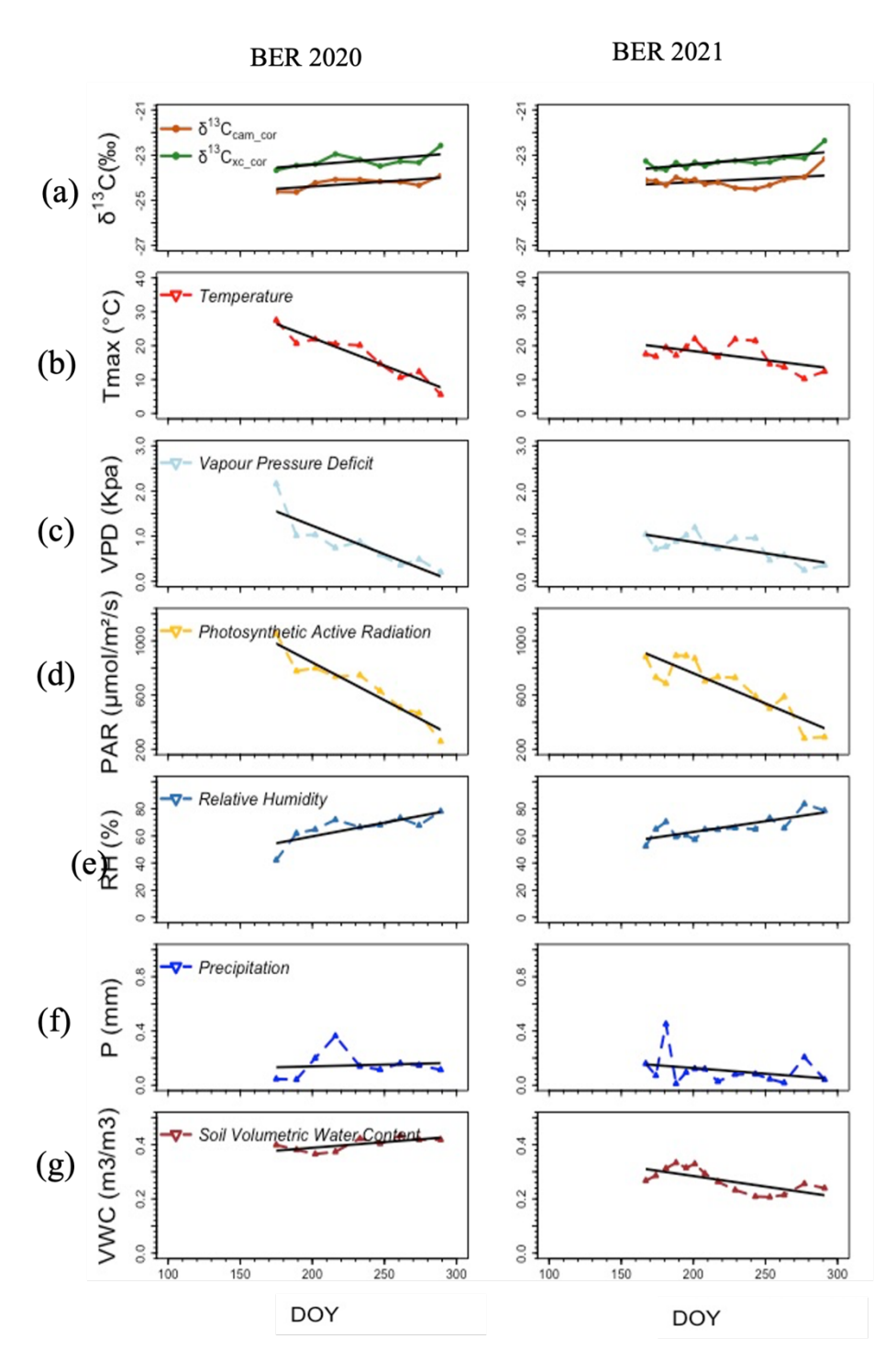
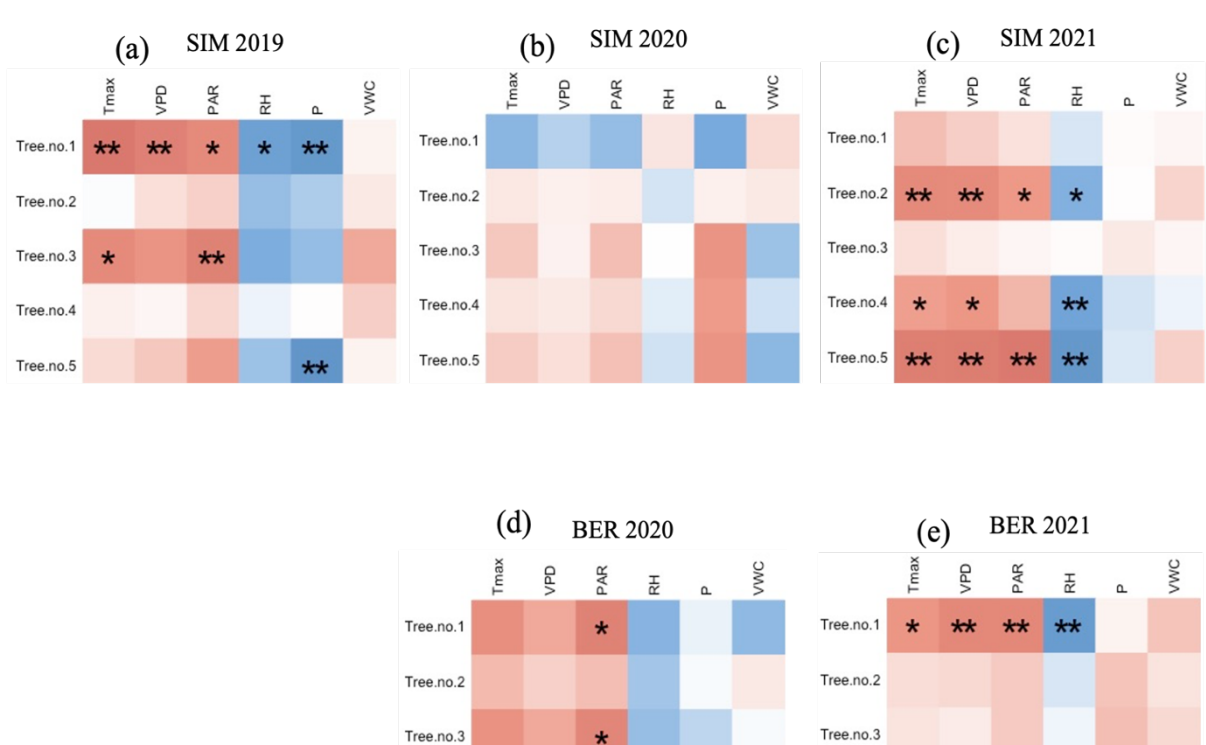


Figure A.8 Variations of  $\delta^{13}C_{cam\_cor}$ , and  $\delta^{13}C_{xc\_cor}$ , series (a), and climatic variables (Daytime averages (8h00 to 18h00) of  $T_{max}$  (b), VPD (c), PAR (d), RH (c), P (f), VWC (g)) in BER 2020 and 2021.



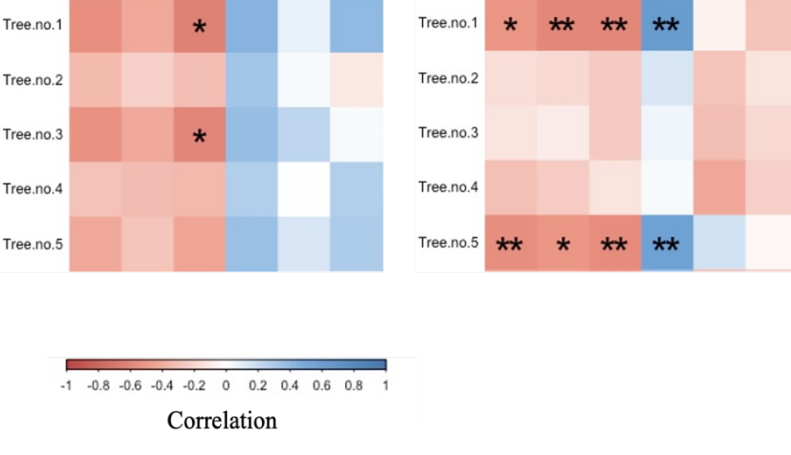


Figure A.9 Matrix of correlations between  $\delta^{13}C_{xc\_seq}$  values for each of five tree samples and different climatic variables for SIM (a, b, c) and BER (d, e).

Table A.1 Sample code, age, and stem diameter of five selected tree individuals in study years of 2019 (Just in SIM), 2020, and 2021, both in Simoncouche (SIM) and Bernatchez (BER).

Site code/year	Tree no.	Tree code	Age	DBH (cm)
	Tree no.1	SIM2019E1	-	32
	Tree no.2	SIM2019E2	-	23
SIM 2019	Tree no.3	SIM2019E3	-	21.5
	Tree no.4	SIM2019E4	-	27.5
	Tree no.5	SIM2019E5	-	31.5
	Tree no.1	SIM2020E1	77	25
	Tree no.2	SIM2020E2	72	21
SIM 2020	Tree no.3	SIM2020E3	63	23.5
	Tree no.4	SIM2020E4	70	22.5
	Tree no.5	SIM2020E5	84	28.5
	Tree no.1	SIM2021E1	87	26
	Tree no.2	SIM2021E2	78	23.5
SIM 2021	Tree no.3	SIM2021E3	83	21.2
	Tree no.4	SIM2021E4	80	26.5
	Tree no.5	SIM2021E5	86	19.2
	Tree no.1	BER2020E1	132	25
	Tree no.2	BER2020E2	130	20
BER 2020	Tree no.3	BER2020E3	134	22
	Tree no.4	BER2020E4	131	24.5
	Tree no.5	BER2020E5	139	24.5
	Tree no.1	BER2021E1	136	24.3
	Tree no.2	BER2021E2	125	22.5
BER 2021	Tree no.3	BER2021E3	131	26
	Tree no.4	BER2021E4	136	25
	Tree no.5	BER2021E5	136	22.5

Table A.2 Number of dates of sampling and/or wood strips collected from each of five tree samples during each of the growing seasons in SIM (2019-2021) and BER (2020-2021).

	SIM 2019	SIM 2020	SIM 2021	BER 2020	BER 2021
Tree no.1	13	17	22	13	20
Tree no.2	13	17	22	13	20
Tree no.3	13	17	22	13	20
Tree no.4	13	17	22	13	20
Tree no.5	13	17	22	13	20
Number of pooled samples for cambial region	13	17	22	13	20
Number of pooled samples for xylem	-	1	-	2	-

Table A.3 Propagation uncertainty (±standard deviation, ‰) associated with  $\delta^{13}C$  values corrected for air composition in xylem cellulose ( $\delta^{13}C_{xc\_cor}$ ) and cambial carbohydrate ( $\delta^{13}C_{cam\_cor}$ ).

Sites/Years	δ <sup>13</sup> C Propagation Uncertainty (±SD, ‰)	δ <sup>13</sup> C Propagation Uncertainty (±SD, ‰)	
SIM 2019	±0.58	±0.13	
SIM 2020	±0.52	±0.12	
SIM 2021	±0.55	±0.12	
BER 2020	±0.58	±0.12	
BER 2021	±0.57	±0.12	

Table A.4 The time periods (day of year) to average  $\delta^{13}C_{atm}$  data collected from the Argyle (AMT) and Lac La Biche (LLB) atmospheric  $\delta^{13}C$  measurement stations.

δ <sup>13</sup> C <sub>atm</sub> measurement sites	δ <sup>13</sup> C <sub>atm</sub>	SIM 2019	SIM 2020	SIM 2021	BER 2020	BER 2021
Argyle	$\delta^{13}C_{atm\_AMT}$ (full growing season)	149-291	120-289	111-291	150-289	119-291
(AMT)	$\delta^{13} C_{atm\_AMT}$ (after onset of EW formation)	183-291	168-289	160-291	175-289	167-291
Lac La Biche	$\delta^{13}C_{atm\_LLB}$ (full growing season)	149-291	120-289	111-291	150-289	119-291
(LLB)	$\delta^{13}C_{atm\_LLB}$ (after onset of EW formation)	183-291	168-289	160-291	175-289	167-291

Table A.5 Regression analysis results for  $\delta^{13}C_{xc}$  values in each tree sample in SIM and BER for each of the study years (the trees are different in each year of sampling).

Site/Year	SIM 2019		SIM 2020		SIM 2021		BER 2020		BER 2021	
	β	Р	β	р	β	Р	β	Р	β	Р
Tree 1	0.003	0.5	0.007	0.2	0.005	0.04*	0.014	0.003 **	0.008	0.001 **
Tree 2	0.006	0.04 *	0.005	0.3	0.005	0.02 *	0.005	0.5	0.008	0.02 *
Tree 3	0.008	0.0007	0.002	0.1	0.006	0.02 *	0.010	0.005 **	0.007	0.01 *
Tree 4	0.008	0.01 *	0.011	0.04 *	0.001	0.8	0.008	0.02*	0.006	0.006 **
Tree 5	0.013	0.007	0.007	0.03 *	0.001	0.7	0.002	0.4	0.004	0.05

#### **APPENDIX B**

Method B.1 Correction of  $\delta^{13}C_{cam\_raw}$  and  $\delta^{13}C_{xc\_raw}$  values for the Suess-effect

The  $\delta^{13}C_{cam}$  and  $\delta^{13}C_{xc}$  raw values were corrected to account for changes in atmospheric  $\delta^{13}C$  ( $\delta^{13}C_{atm}$ ) (Namvar et al., 2024). This has two benefits. First, it corrects for the Suess effect, which is the progressive decline in  $\delta^{13}C_{atm}$ , due to fossil emissions, since 1850 (Pre-Industrial reference,  $\delta^{13}C_{atm_p} = -6.61\%$ ) (Namvar et al., 2024). Second, it accounts for the seasonal variability in  $\delta^{13}C_{atm}$ , attributable to the preferential sequestration of  $^{12}C$  during photosynthesis, leaving a progressively enriched atmosphere as photosynthesis increases (Ballantyne et al., 2010). Unfortunately, on site measurements of  $\delta^{13}C_{atm}$  were unavailable. In order to perform these corrections, we used the  $\delta^{13}C_{atm}$  data collected from the NOAA-ESRL tall tower at Argyle, Maine, United States (AMT, 45.03°N, 68.68°W,  $\delta^{13}C_{atm_pAMT}$ , https://gml.noaa.gov/dv/iadv) in conformity with our sampling dates. The Argyle site is the closest  $\delta^{13}C_{atm}$  measurement station to our study region. The tower is located in a mixed (deciduous and evergreen) forest in rural central Maine, north of Bangor, at 50 m above sea level. For each sampling date (date=n), we corrected our isotopic values as follows (example for xylem, same for cambium):

$$\delta^{13}\mathsf{C}_{\textit{xc (date=n)}} = \delta^{13}\mathsf{C}_{\mathsf{xc raw (date=n)}} - \left(\delta^{13}\mathsf{C}_{\mathsf{atm\_AMT (date=n)}} - \delta^{13}\mathsf{C}_{\mathsf{atm\_Pl}}\right)$$

Equation B.1 Correction of  $\delta^{13}C$  for seasonal  $\delta^{13}C_{atm\_AMT}$  variations and Suess-effect Where  $\delta^{13}C_{xc}$  is the Suess-effect corrected values for each date of sampling. The  $\delta^{13}C_{xc\_raw}$  is the raw values of carbon stable isotopes at each date of sampling, provided by IRMS analysis.

#### Appendix B Figure Legend

<u>Figure B.1</u>: (a) Rain collector mounted on the ground on a flat surface, positioned around 20 m away from the sampled trees in an open area. (b) collection of rain samples on a weekly basis during the growing season. (c) collected rain samples into accumulation bottles with a double cap.

## Appendix B Table Legend

<u>Table B.1</u>: The average age of the black spruce stands was achieved by counting the tree rings in cores extracted from the trunk of each selected tree sample using an increment borer. The DBH was measured using a diameter tape at breast height.

<u>Table B.7</u>: Maximum temperature ( $T_{max}$ ), vapour pressure deficit (VPD), photosynthetically active radiation (PAR), relative humidity (RH), precipitation (P), soil volumetric water content (VWC), (\* p< 0.1, \*\* p< 0.05, \*\*\* p< 0.01).

<u>Table B8</u>: maximum temperature ( $T_{max}$ ), vapour pressure deficit (VPD), photosynthetically active radiation (PAR), relative humidity (RH), precipitation (P), soil volumetric water content (VWC), (\* p< 0.1, \*\* p< 0.05, \*\*\* p< 0.01).

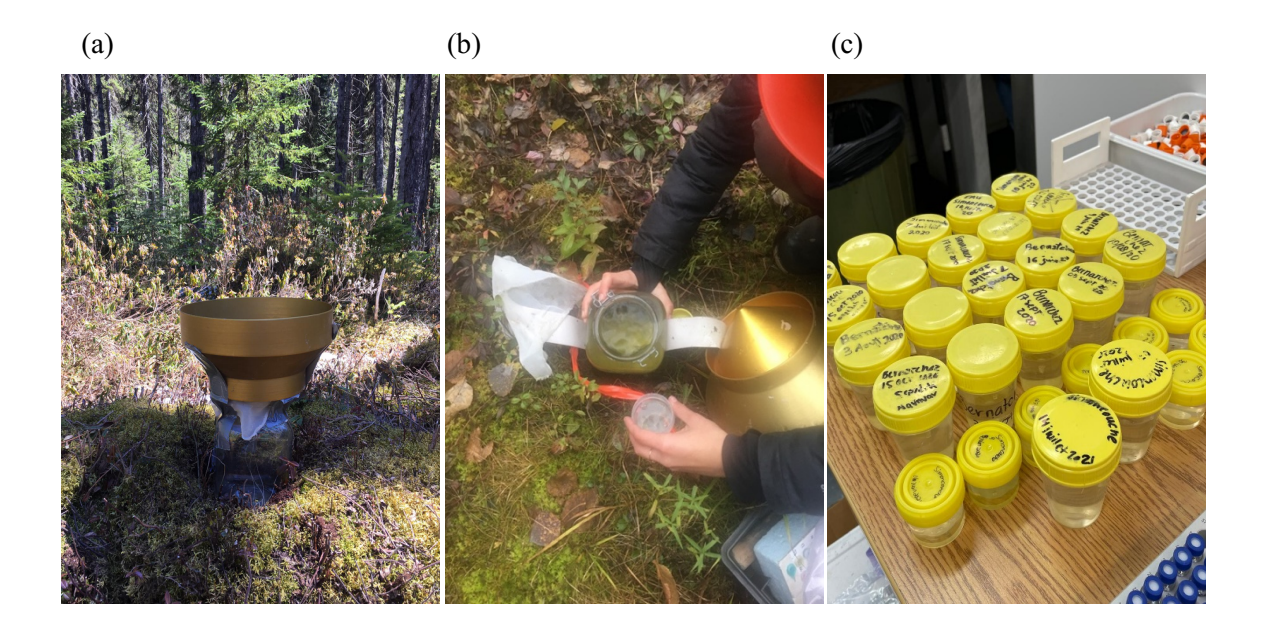


Figure B.1 Collection and analysis of rain samples in the field

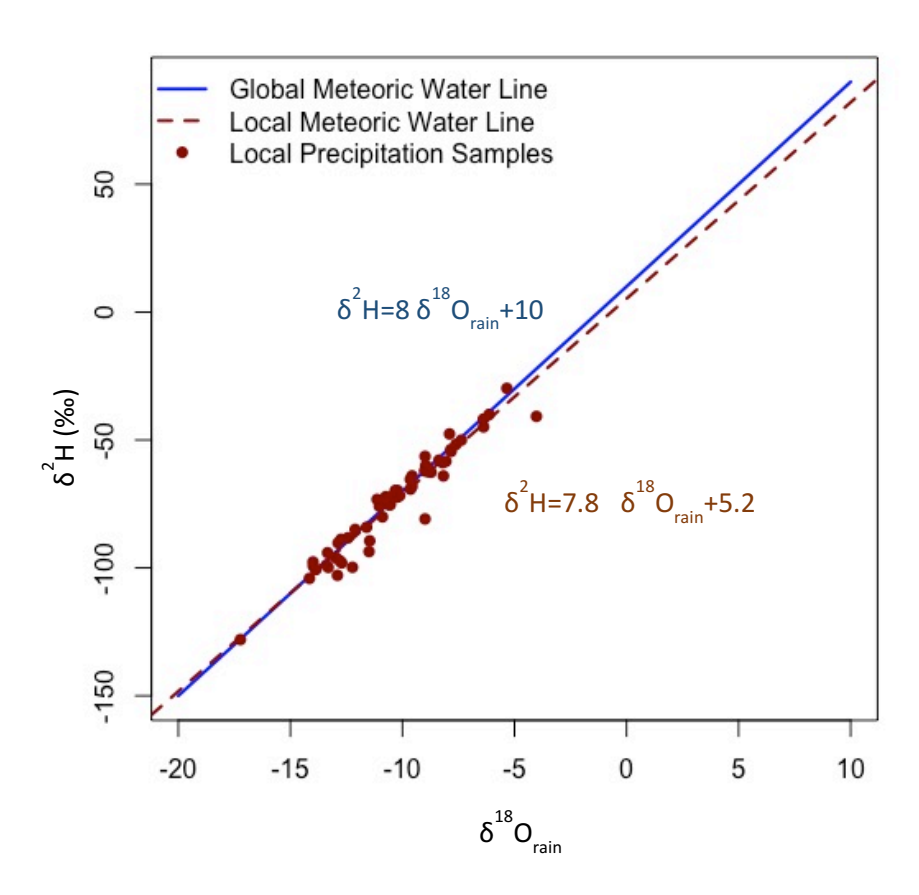


Figure B.2 Comparison between global meteoric water line (blue solid line) with the SIM and BER meteoric water line (red dashed line) for the two growing seasons of 2020 and 2021.

Table B.1 Sample code, age, and stem diameter of the five selected tree individuals in study years of 2019 (Just in SIM), 2020, and 2021, both in Simoncouche (SIM) and Bernatchez (BER).

Site/year	Tree no.	Tree code	Age	DBH (cm)
	Tree no.1	SIM2019E1	-	32
	Tree no.2	SIM2019E2	-	23
SIM 2019	Tree no.3	SIM2019E3	-	21.5
	Tree no.4	SIM2019E4	-	27.5
	Tree no.5	SIM2019E5	-	31.5
	Tree no.1	SIM2020E1	77	25
	Tree no.2	SIM2020E2	72	21
SIM 2020	Tree no.3	SIM2020E3	63	23.5
	Tree no.4	SIM2020E4	70	22.5
	Tree no.5	SIM2020E5	84	28.5
	Tree no.1	SIM2021E1	87	26
	Tree no.2	SIM2021E2	78	23.5
SIM 2021	Tree no.3	SIM2021E3	83	21.2
	Tree no.4	SIM2021E4	80	26.5
	Tree no.5	SIM2021E5	86	19.2
	Tree no.1	BER2020E1	132	25
	Tree no.2	BER2020E2	130	20
BER 2020	Tree no.3	BER2020E3	134	22
	Tree no.4	BER2020E4	131	24.5
	Tree no.5	BER2020E5	139	24.5
	Tree no.1	BER2021E1	136	24.3
	Tree no.2	BER2021E2	125	22.5
BER 2021	Tree no.3	BER2021E3	131	26
	Tree no.4	BER2021E4	136	25
	Tree no.5	BER2021E5	136	22.5

Table B.2 Number of wood strips collected from each of five tree samples during each of the growing seasons in SIM (2019-2021) and BER (2020-2021).

Site/Year	SIM 2019	SIM 2020	SIM 2021	BER 2020	BER 2021
Number of strips	13	17	22	13	20

Table B.3 Mean values of  $\delta^{13}C_{xc}$  and  $\delta^{13}C_{cam}$ , mean inter-trees correlation (Rbar) of  $\delta^{13}C_{xc}$  and weekly EPS (EPS<sub>w</sub>) for the two sites: SIM (2019-2021) and BER (2020-2021).

Site/year	SIM 2019	SIM 2020	SIM 2021	BER 2020	BER 2021
Rbar (δ <sup>13</sup> C <sub>xc</sub> series)	0.39	0.45	0.14	0.40	0.43
EPS <sub>w</sub> (δ <sup>13</sup> C <sub>xc</sub> series)	0.76	0.80	0.45	0.77	0.79
Mean δ <sup>13</sup> C <sub>cam</sub> (‰±SD) full growing season	-25.3±0.4	-25.2±0.4	-25.7±0.1	-26.0±0.4	-25.9±0.2
Mean $\delta^{13}C_{cam}$ (‰ $\pm$ SD) after onset of wood formation	-25.1±0.2	-25.0±0.4	-25.7±0.1	-25.8±0.4	-25.9±0.2
Mean δ <sup>13</sup> C <sub>xc</sub> (‰±SD)	-24.3±0.3	-23.7±0.4	-24.7±0.2	-24.8±0.4	-25.1±0.3

Table B.4 Mean values of  $\delta^{18}O_{xc}$  and  $\delta^{18}O_{cam}$ , mean inter-trees correlation (Rbar) of  $\delta^{18}O_{xc}$  and weekly EPS (EPS<sub>w</sub>) for the two sites: SIM (2019-2021) and BER (2020-2021).

Site/Year	SIM	SIM	SIM	BER	BER
Site, rear	2019	2020	2021	2020	2021
Rbar (δ <sup>18</sup> O <sub>xc</sub> series)	0.63	0.77	0.36	0.33	-0.06
EPS <sub>w</sub> (δ <sup>18</sup> O <sub>xc</sub> series)	0.90	0.94	0.74	0.71	-0.39
Mean δ <sup>18</sup> O <sub>cam</sub> (‰±SD) full growing season	22.0±0.4	20.5±0.6	19.9±0.4	19.6±0.5	18.6±0.6
Mean $\delta^{18}O_{cam}$ (‰±SD) after onset of wood formation	22.0±0.4	20.7±0.5	19.8±0.4	19.7±0.5	18.6±0.7
Mean δ <sup>18</sup> O <sub>xc</sub> (‰±SD)	23.8±0.8	24.8±0.6	25.9±0.5	23.9±0.4	25.4±0.2

Table B.5 Regression slopes and significance level for  $\delta^{13}C$  and  $\delta^{18}O$  values in the cambial region  $(\delta^{13}C_{cam},\,\delta^{18}O_{cam})$  and developing tree ring  $(\delta^{13}C_{xc},\,\delta^{18}O_{xc})$  in SIM and BER for each of the study years.

Site/Year		IM )19		IM 020		IM 021		ER 20	BE 202	
Regression coefficient and sig.	β	Р	β	Р	β	Р	β	Р	β	Р
δ <sup>13</sup> C <sub>cam</sub> (full growing season)	0.00	0.000	0.00	0.465	- 0.00 3	0.003	0.00 5	0.00 04	0.0020	0.19
δ <sup>18</sup> O <sub>cam</sub> (full growing season)	0.00	0.281	0.00 6	0.0307	- 0.00 2	0.328	0.01	0.00	0.007	0.00 48
δ <sup>13</sup> C <sub>cam</sub> (after onset of wood formation)	0.00 6	0.001 9	0.00	0.099	- 0.00 1	0.294	0.00	0.03 64	0.003	0.16
δ <sup>18</sup> O <sub>cam</sub> (after onset of wood formation)	0.00	0.840	0.01	0.0038	0.00	0.372	0.01	0.00 03	0.014	0.00 04
$\delta^{13}C_{xc}$	0.00	0.002	0.00	0.0886	0.00	0.15	0.00 5	0.07 45	0.006	0.00 24
$\delta^{18} O_{xc}$	- 0.01 9	0.001	- 0.00 3	0.6950	- 0.00 3	0.430	- 0.00 8	0.02 77	- 0.0006	0.68 00

Table B.6 Correlation coefficients and p-values between pre-whitened detrended residuals of  $\delta^{13}C$  and  $\delta^{18}O$  in the cambium and xylem cellulose in different study sites and years.

Site/Year	SI 20			M 20	SI 20			ER 20		BER 021
	r	Р	r	р	r	Р	r	Р	r	Р
Between $\delta^{13}C_{\text{cam}}$ and $\delta^{18}O_{\text{cam}}$	0.60	0.03	0.76	0.000	0.33	0.1398	-0.04	0.8928	0.70	0.0006
Between $\delta^{13}C_{xc}$ and $\delta^{18}O_{xc}$	0.26	0.443	0.24	0.346 5	0.02	0.9482	-0.01	0.9894	-0.25	0.3847

Table B.7 Correlation coefficients for the relationships between pre-whitened detrended residuals of  $\delta^{13}C_{cam}$  or  $\delta^{18}O_{cam}$  and residuals of different meteorological weekly variables of daytime averages (8h00 to 18h00).

	SIM 2019		SIM 2020		SIM 2021		BER 2020		BER 2021	
	$\delta^{13}C_{\text{cam}}$	$\delta^{18}O_{\text{cam}}$	$\delta^{13}C_{\text{cam}}$	$\delta^{18}O_{\text{cam}}$	$\delta^{13}C_{\text{cam}}$	$\delta^{18}O_{\text{cam}}$	$\delta^{13}C_{\text{cam}}$	$\delta^{18}O_{\text{cam}}$	$\delta^{13} C_{\text{cam}}$	$\delta^{18}O_{ca}$
T <sub>max</sub>	0.12	0.24	-0.53**	-0.66***	- 0.57**	-0.39*	0.14	-0.39	-0.76***	- 0.66** *
VPD	0.06	0.14	-0.55**	-0.64**	- 0.51**	-0.32	-0.11	-0.17	-0.64***	- 0.50**
PAR	-0.29	-0.21	-0.51**	-0.66***	- 0.46**	-0.11	0.09	-0.35	-0.49**	-0.27
RH	0.34	0.23	0.45*	0.45*	0.45**	0.06	0.57**	-0.10	0.19	0.00
Р	0.66**	0.52*	0.33	0.16	0.07	-0.07	0.69**	-0.08	-0.15	-0.26
VWC	0.31	0.18	0.32	0.50**	0.52**	-0.01	-0.46	0.39	0.41*	0.15

Table B.8 Correlation coefficients for the relationships between pre-whitened detrended residuals of  $\delta^{13}C_{xc}$  or  $\delta^{18}O_{xc}$  and residuals of different meteorological weekly variables of daytime averages (8h00 to 18h00).

Site/year	SIM 2019		SIM 2020		SIM 2021		BER 2020		BER 2021	
	$\delta^{13}C_{xc}$	$\delta^{18}O_{xc}$	$\delta^{13}C_{xc}$	$\delta^{18}O_{xc}$	$\delta^{13}C_{xc}$	$\delta^{18}O_{xc}$	$\delta^{13}C_{xc}$	$\delta^{18}O_{xc}$	$\delta^{13}C_{xc}$	$\delta^{18} O_{xc}$
T <sub>max</sub>	-0.18	-0.44	0.12	0.18	-0.37	-0.15	-0.21	-0.80**	-0.20	-0.23
VPD	-0.01	-0.22	-0.14	0.62*	-0.34	-0.39	-0.30	0.13	0.05	-0.48*
PAR	-0.12	-0.09	0.17	0.28	-0.22	-0.12	-0.50	-0.60*	0.05	-0.58**
RH	0.12	0.10	0.34	-0.63*	0.28	0.35	0.57	-0.22	-0.27	0.71***
Р	0.69**	0.26	0.06	-0.52	0.26	0.10	0.46	-0.55	-0.23	0.35
VWC	0.69**	0.46	0.01	0.25	0.50*	0.11	-0.42	0.04	0.16	0.47*

Table B.9 The mean  $\delta^{18}O_{rain}$  values in SIM and BER for the growing seasons of 2020 and 2021. Sampling was done on a weekly basis at two study years during the sampling periods at each study year.

Site/Year	SIM 2020	SIM 2021	BER 2020	BER 2021
Sampling period	June-Oct	May-Oct	June-Oct	May-Oct
Mean $\delta^{18} O_{\text{rain}}$	-10.2±3	-10.02± 2	-10.6± 2	-10.6± 3

### **APPENDIX C**

# Appendix C Figure Legends

<u>Figure C.3</u>: Variations of cell enlargement rate;  $r_E$  (a), cell wall deposition rate;  $r_W$  (b), cell production rate,  $r_D$  (c), iWUE (d), soil water content; VWC (e), NDVI (f), maximum temperature;  $T_{max}$  (g), vapour pressure deficit; VPD (h), relative humidity; RH (i) and photoperiod; PP(j) in SIM and BER 2020 and 2021.

# Appendix C Table Legends

<u>Table C3</u>: Uncertainties were propagated using first-order partial derivatives (Taylor expansion method), and sensitivities were normalized to reflect the relative contribution of each input to  $\Delta$ .

<u>Table C5</u>: GAM fittings on the number of cells in the enlargement ( $n_E$ ), wall thickening ( $n_W$ ), and mature zones ( $n_M$ ) of black spruce at the SIM and BER sites during the 2020 and 2021 growing seasons.

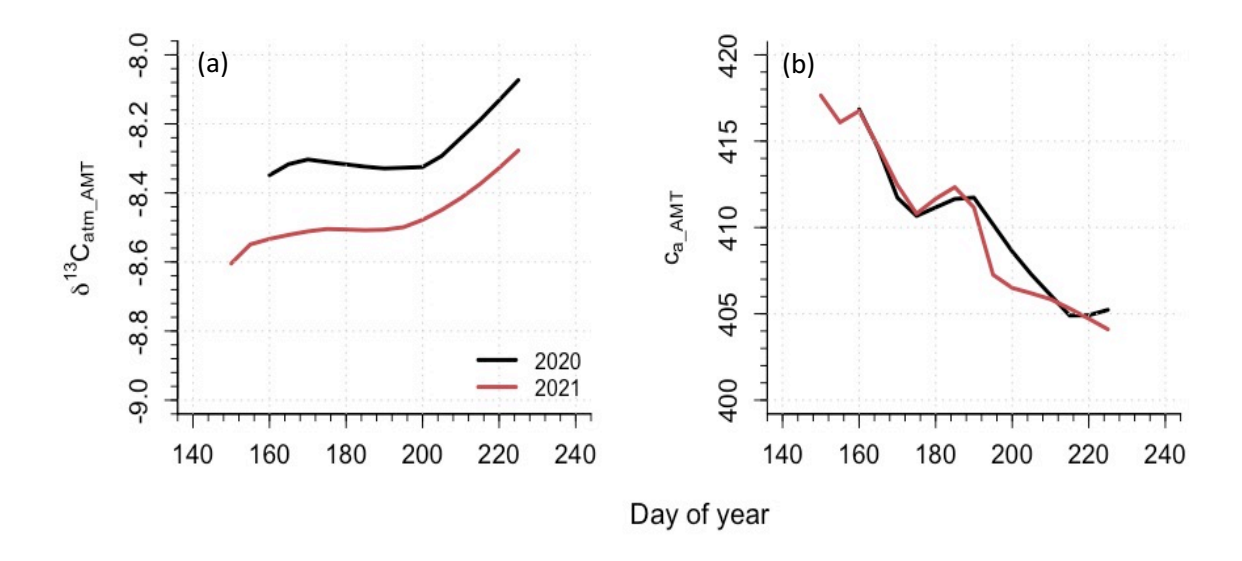


Figure C.1 (a)  $\delta^{13}C_{atm\_AMT}$  and (b)  $c_{a\_AMT}$  profiles during the two growing seasons of 2020 and 2021.

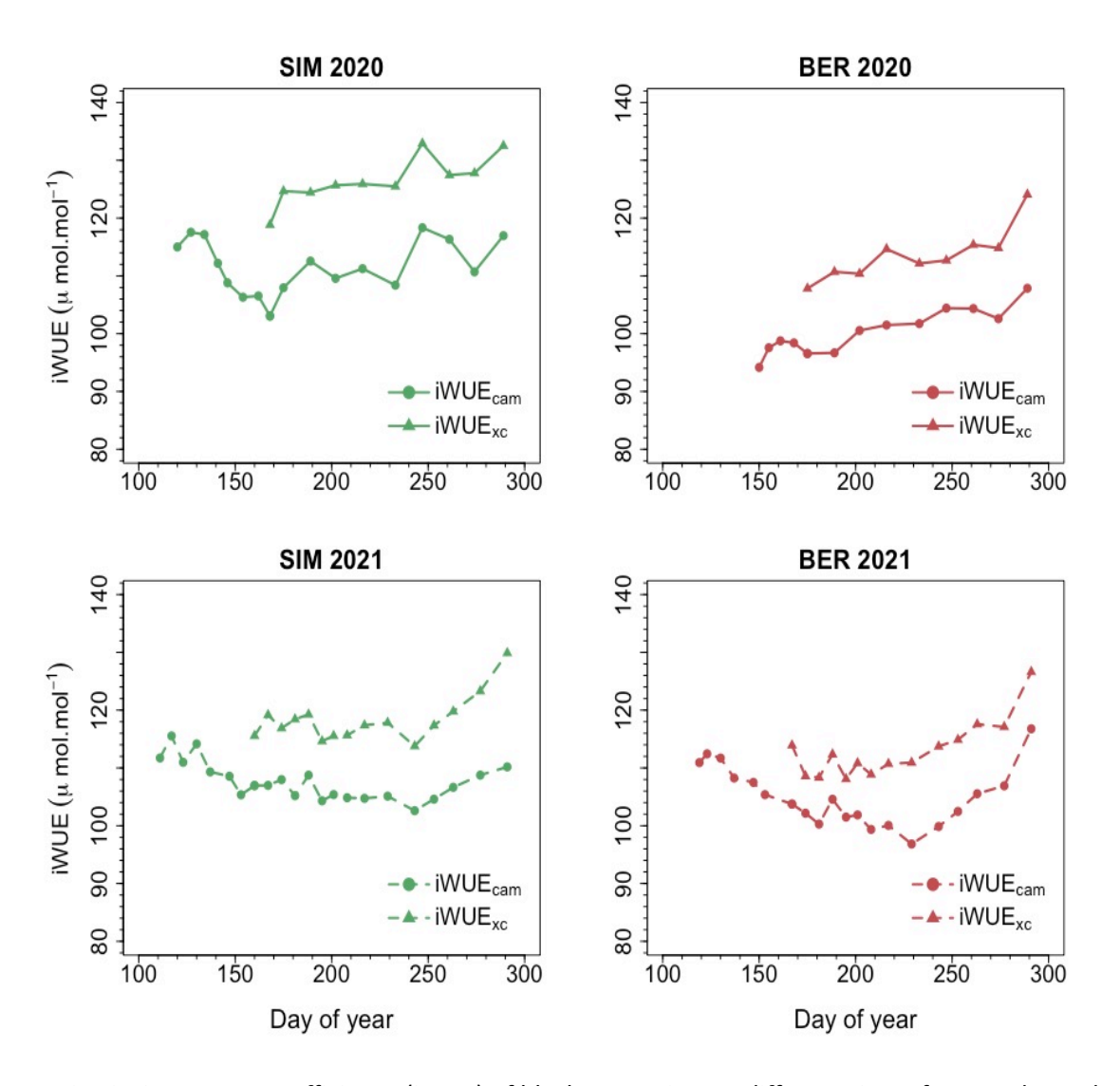


Figure C.2 intrinsic Water Use Efficiency (iWUE) of black spruce in two different sites of SIM and BER during the two growing seasons of 2020 and 2021.

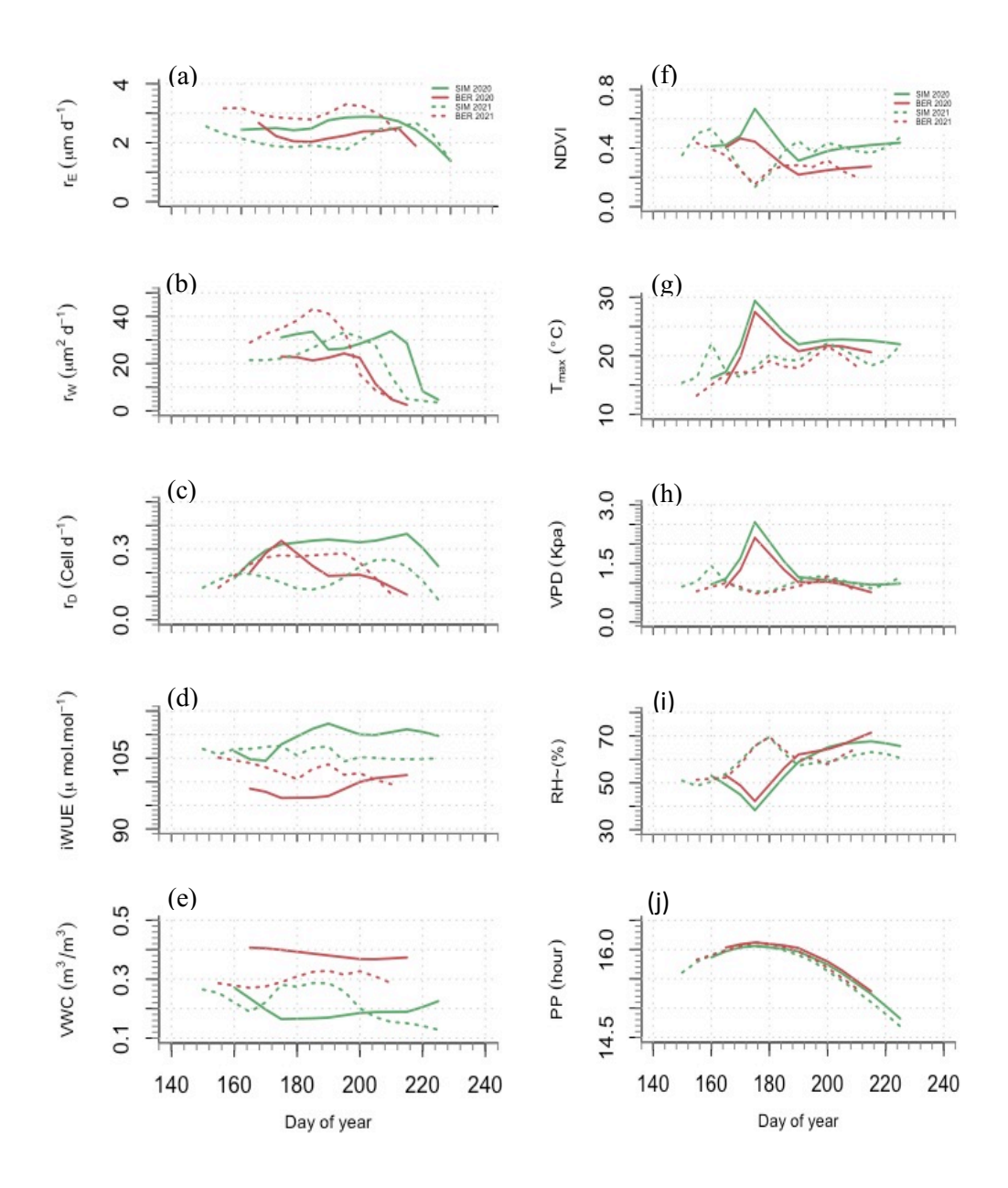


Figure C.3 Kinetics of cell formation and meteorological variables during the growing season.

Table C.1 Sample code, age, and stem diameter of five selected tree individuals in study years of 2020 and 2021, both in Simoncouche (SIM) and Bernatchez (BER).

Site code/year	Tree no.	Tree code	Age	DBH (cm)
	Tree no.1	SIM2020E1	77	25
	Tree no.2	SIM2020E2	72	21
SIM 2020	Tree no.3	SIM2020E3	63	23.5
	Tree no.4	SIM2020E4	70	22.5
	Tree no.5	SIM2020E5	84	28.5
	Tree no.1	SIM2021E1	87	26
	Tree no.2	SIM2021E2	78	23.5
SIM 2021	Tree no.3	SIM2021E3	83	21.2
	Tree no.4	SIM2021E4	80	26.5
	Tree no.5	SIM2021E5	86	19.2
	Tree no.1	BER2020E1	132	25
	Tree no.2	BER2020E2	130	20
BER 2020	Tree no.3	BER2020E3	134	22
	Tree no.4	BER2020E4	131	24.5
	Tree no.5	BER2020E5	139	24.5
	Tree no.1	BER2021E1	136	24.3
	Tree no.2	BER2021E2	125	22.5
BER 2021	Tree no.3	BER2021E3	131	26
	Tree no.4	BER2021E4	136	25
	Tree no.5	BER2021E5	136	22.5

Table C.2 Number of dates of sampling and/or wood strips and micro cores collected from each of five tree samples during each of the growing seasons in SIM (2020-2021) and BER (2020-2021).

Tree samples	SIM 2020	SIM 2021	BER 2020	BER 2021
Tree no.1	17	22	13	20
Tree no.2	17	22	13	20
Tree no.3	17	22	13	20
Tree no.4	17	22	13	20
Tree no.5	17	22	13	20

Table C.3 Propagation of uncertainty ( $\pm$  SD) in carbon isotope discrimination ( $\Delta$ ) and relative sensitivities to  $\delta^{13}C$  of atmospheric CO<sub>2</sub> ( $\delta^{13}C_{atm\_AMT}$ ) and  $\delta^{13}C_{cam}$ .

Site/Year	Δ Propagation Uncertainty (±SD, ‰)	Sensitivity $\delta^{13}C_{\text{atm-AMT}}$	Sensitivity $\delta^{13} C_{\text{cam}}$
SIM 2019	±0.12	0.0026	-0.0061
SIM 2020	±0.12	0.0024	-0.0062
SIM 2021	±0.11	0.0016	-0.0061
BER 2020	±0.12	0.0023	-0.0059
BER 2021	±0.11	0.0017	-0.006

Table C.4 Correlation coefficients for the relationships between iWUE<sub>cam</sub> and iWUE<sub>xc</sub> each site and study year (\* p< 0.1, \*\* p< 0.05, \*\*\* p< 0.01).

Site/year	Correlation coefficient between iWUE <sub>cam</sub> and iWUE <sub>xc</sub>	
SIM 2020	0.90***	
SIM 2021	0.79***	
BER 2020	0.86***	
BER 2021	0.88***	

Table C.5 Mean Absolute Error (MAE, cells) and Model Efficiency (EF, %) from the GAMs model.

Site/Year	Number of cells in different phases of growth	MAE	EF (%)
SIM 2020	n <sub>E</sub>	0.34	88
	n <sub>W</sub>	0.34	95
	n <sub>M</sub>	0.35	99
SIM 2021	n <sub>E</sub>	0.23	94
	n <sub>W</sub>	0.38	86
	n <sub>M</sub>	0.32	99
BER 2020	n <sub>E</sub>	0.18	96
	n <sub>W</sub>	0.29	95
	n <sub>M</sub>	0.14	99
BER 2021	n <sub>E</sub>	0.16	96
	n <sub>W</sub>	0.26	94
	n <sub>M</sub>	0.86	96

#### **REFERENCES**

- Alvarez, C., Bégin, C., Savard, M. M., Dinis, L., Marion, J., Smirnoff, A., & Bégin, Y. (2018). Relevance of using whole-ring stable isotopes of black spruce trees in the perspective of climate reconstruction. *Dendrochronologia*, *50*, 64–69. https://doi.org/10.1016/j.dendro.2018.05.004
- Ameray, A., Cavard, X., & Bergeron, Y. (2023). Climate change may increase Quebec boreal forest productivity in high latitudes by shifting its current composition. *Frontiers in Forests and Global Change*, 6. https://doi.org/10.3389/ffgc.2023.1020305
- Andreu-Hayles, L., Lévesque, M., Guerrieri, R., Siegwolf, R. T., & Körner, C. (2022). Limits and strengths of tree-ring stable isotopes. In Stable isotopes in tree rings: Inferring physiological, climatic and environmental responses (Vol. 8). Springer International Publishing. https://doi.org/10.1007/978-3-030-92698-4
- Antonucci, S., Rossi, S., Deslauriers, A., Lombardi, F., Marchetti, M., & Tognetti, R. (2015). Synchronisms and correlations of spring phenology between apical and lateral meristems in two boreal conifers. *Tree Physiology*, *35*(10), 1086–1094. https://doi.org/10.1093/treephys/tpv077
- Arora, R. (2018). Mechanism of freeze-thaw injury and recovery: *A cool retrospective and warming up to new ideas. Plant Science, 270*, 301–313. https://doi.org/10.1016/j.plantsci.2018.03.002
- Baldocchi, D. D. (2020). How eddy covariance flux measurements have contributed to our understanding of Global Change Biology. *Global Change Biology*, *26*(1), 242–260. https://doi.org/10.1111/gcb.14807
- Balducci, L., Cuny, H. E., Rathgeber, C. B. K., Deslauriers, A., Giovannelli, A., & Rossi, S. (2016).

  Compensatory mechanisms mitigate the effect of warming and drought on wood formation.

  Plant, Cell & Environment, 39(6), 1338–1352. https://doi.org/10.1111/pce.12689
- Balducci, L., Deslauriers, A., De Barba, D., Rossi, S., Houle, D., Bergeron, Y., & Morin, H. (2021). Influence of soil warming and N-addition on sap flux density and stem radius variation in boreal stands in Quebec, Canada. *Ecohydrology*, *14*(2), e2261. https://doi.org/10.1002/eco.2261
- Ballantyne, A. P., Miller, J. B., & Tans, P. P. (2010). Apparent seasonal cycle in isotopic discrimination of carbon in the atmosphere and biosphere due to vapor pressure deficit. *Global Biogeochemical Cycles*, *24*(3), 2009GB003623. https://doi.org/10.1029/2009GB003623
- Barbour, M. M. (2007). Stable oxygen isotope composition of plant tissue: A review. *Functional Plant Biology*, *34*(2), 83. https://doi.org/10.1071/FP06228
- Barbour, M. M., & Farquhar, G. D. (2000). Relative humidity- and ABA-induced variation in carbon and oxygen isotope ratios of cotton leaves. *Plant, Cell & Environment*, *23*(5), 473–485. https://doi.org/10.1046/j.1365-3040.2000.00575.x

- Barbour, M. M., Roden, J. S., Farquhar, G. D., & Ehleringer, J. R. (2004). Expressing leaf water and cellulose oxygen isotope ratios as enrichment above source water reveals evidence of a P clet effect. *Oecologia*, 138(3), 426–435. https://doi.org/10.1007/s00442-003-1449-3
- Barbour, M. M., Schurr, U., Henry, B. K., Wong, S. C., & Farquhar, G. D. (2000). Variation in the Oxygen Isotope Ratio of Phloem Sap Sucrose from Castor Bean. Evidence in Support of the Péclet Effect. *Plant Physiology*, *123*(2), 671–680.
- Barbour, M. M., Walcroft, A. S., & Farquhar, G. D. (2002). Seasonal variation in  $\delta$ 13C and  $\delta$ 18O of cellulose from growth rings of Pinus radiata. *Plant, Cell & Environment*, *25*(11), 1483–1499. https://doi.org/10.1046/j.0016-8025.2002.00931.x
- Barçante Ladvocat Cintra, B., Gloor, M., Boom, A., Schöngart, J., Locosselli, G. M., & Brienen, R. (2019). Contrasting controls on tree ring isotope variation for Amazon floodplain and terra firme trees. *Tree Physiology*, *39*(5), 845–860. https://doi.org/10.1093/treephys/tpz009
- Beer, C., Reichstein, M., Tomelleri, E., Ciais, P., Jung, M., Carvalhais, N., Rödenbeck, C., Arain, M. A., Baldocchi, D., Bonan, G. B., Bondeau, A., Cescatti, A., Lasslop, G., Lindroth, A., Lomas, M., Luyssaert, S., Margolis, H., Oleson, K. W., Roupsard, O., ... Papale, D. (2010). Terrestrial Gross Carbon Dioxide Uptake: Global Distribution and Covariation with Climate. *Science*, *329*(5993), 834–838. https://doi.org/10.1126/science.1184984
- Bégin, C., Gingras, M., Savard, M. M., Marion, J., Nicault, A., & Bégin, Y. (2015). Assessing tree-ring carbon and oxygen stable isotopes for climate reconstruction in the Canadian northeastern boreal forest. *Palaeogeography, Palaeoclimatology, Palaeoecology, 423*, 91–101. https://doi.org/10.1016/j.palaeo.2015.01.021
- Belien, Evelyn, Rossi, Sergio, Morin, Hubert, & Deslauriers, Annie. (2012). Xylogenesis in black spruce subjected to a rain exclusion in the field. *Canadian Journal of Forest Research*, 42(7), 1306–1315.
- Belmecheri, S., & Lavergne, A. (2020). Compiled records of atmospheric CO2 concentrations and stable carbon isotopes to reconstruct climate and derive plant ecophysiological indices from tree rings. *Dendrochronologia*, 63, 125748. https://doi.org/10.1016/j.dendro.2020.125748
- Belmecheri, S., Wright, W. E., Szejner, P., Morino, K. A., & Monson, R. K. (2018). Carbon and oxygen isotope fractionations in tree rings reveal interactions between cambial phenology and seasonal climate. *Plant, Cell & Environment*, *41*(12), 2758–2772. https://doi.org/10.1111/pce.13401
- Bonan, G. B. (2008). Forests and Climate Change: Forcings, Feedbacks, and the Climate Benefits of Forests. *Science*, *320*(5882), 1444–1449. https://doi.org/10.1126/science.1155121
- Bortolami, G. C., Ricci, B., & Susella, G. F. (1979). *ISOTOPE HYDROLOGY OF THE VAL CORSAGLIA MARITIME ALPS, PIEDMONT, ITALY*.
- Bozonnet, C., Saudreau, M., Badel, E., Améglio, T., & Charrier, G. (2024). Freeze dehydration vs supercooling in tree stems: Physical and physiological modelling. *Tree Physiology*, 44(1), tpad117. https://doi.org/10.1093/treephys/tpad117

- Brienen, R. J. W., Wanek, W., & Hietz, P. (2011). Stable carbon isotopes in tree rings indicate improved water use efficiency and drought responses of a tropical dry forest tree species. *Trees*, 25(1), 103–113. https://doi.org/10.1007/s00468-010-0474-1
- Briffa. (1990). Basic chronology statistics and assessment. *Methods of Dendrochronology*. https://cir.nii.ac.jp/crid/1571980075394451072
- Buckley, T. N. (2017). Modeling Stomatal Conductance. *Plant Physiology*, 174(2), 572–582. https://doi.org/10.1104/pp.16.01772
- Burke, M. J., Gusta, L. V., Quamme, H. A., Weiser, C. J., & Li, P. H. (1976). Freezing and Injury in Plants. Annual Review of Plant Biology, 27(Volume 27, 1976), 507–528. https://doi.org/10.1146/annurev.pp.27.060176.002451
- Buttò, V., Rossi, S., Deslauriers, A., & Morin, H. (2019). Is size an issue of time? Relationship between the duration of xylem development and cell traits. *Annals of Botany*, 123(7), 1257–1265. https://doi.org/10.1093/aob/mcz032
- Buttò, V., Rozenberg, P., Deslauriers, A., Rossi, S., & Morin, H. (2021). Environmental and developmental factors driving xylem anatomy and micro-density in black spruce. *New Phytologist*, *230*(3), 957–971. https://doi.org/10.1111/nph.17223
- Cabon, A., Fernández-de-Uña, L., Gea-Izquierdo, G., Meinzer, F. C., Woodruff, D. R., Martínez-Vilalta, J., & De Cáceres, M. (2020). Water potential control of turgor-driven tracheid enlargement in Scots pine at its xeric distribution edge. *New Phytologist*, *225*(1), 209–221. https://doi.org/10.1111/nph.16146
- Carbone, M. S., Czimczik, C. I., Keenan, T. F., Murakami, P. F., Pederson, N., Schaberg, P. G., Xu, X., & Richardson, A. D. (2013). Age, allocation and availability of nonstructural carbon in mature red maple trees. *New Phytologist*, 200(4), 1145–1155. https://doi.org/10.1111/nph.12448
- Carrer, M., Von Arx, G., Castagneri, D., & Petit, G. (2015). Distilling allometric and environmental information from time series of conduit size: The standardization issue and its relationship to tree hydraulic architecture. *Tree Physiology*, *35*(1), 27–33. https://doi.org/10.1093/treephys/tpu108
- Cartenì, F., Balducci, L., Dupont, A., Salucci, E., Néron, V., Mazzoleni, S., & Deslauriers, A. (2023). Phenocab: A new phenological model based on carbon balance in boreal conifers. *New Phytologist*, 239(2), 592–605. https://doi.org/10.1111/nph.18974
- Cartenì, F., Deslauriers, A., Rossi, S., Morin, H., De Micco, V., Mazzoleni, S., & Giannino, F. (2018). The Physiological Mechanisms Behind the Earlywood-To-Latewood Transition: A Process-Based Modeling Approach. *Frontiers in Plant Science*, *9*, 1053. https://doi.org/10.3389/fpls.2018.01053
- Castagneri, D., Battipaglia, G., Von Arx, G., Pacheco, A., & Carrer, M. (2018). Tree-ring anatomy and carbon isotope ratio show both direct and legacy effects of climate on bimodal xylem formation in Pinus pinea. *Tree Physiology*, 38(8), 1098–1109. https://doi.org/10.1093/treephys/tpy036

- Castagneri, D., Fonti, P., Von Arx, G., & Carrer, M. (2017). How does climate influence xylem morphogenesis over the growing season? Insights from long-term intra-ring anatomy in *Picea abies. Annals of Botany*, mcw274. https://doi.org/10.1093/aob/mcw274
- Cernusak, L. A., Barbour, M. M., Arndt, S. K., Cheesman, A. W., English, N. B., Feild, T. S., Helliker, B. R., Holloway-Phillips, M. M., Holtum, J. A. M., Kahmen, A., Mcinerney, F. A., Munksgaard, N. C., Simonin, K. A., Song, X., Stuart-Williams, H., West, J. B., & Farquhar, G. D. (2016). Stable isotopes in leaf water of terrestrial plants. *Plant Cell and Environment*, *39*(5), 1087–1102. https://doi.org/10.1111/pce.12703
- Cernusak LA, Farquhar GD, Pate JS (2005) Environmental and physiological controls over oxygen and carbon isotope composition of Tasmanian blue gum, Eucalyptus globulus. Tree Physiol 25:129–146.
- Charrier, G., & Améglio, T. (2024). Dynamic modeling of stem water content during the dormant period in walnut trees. *Tree Physiology*, 44(1), tpad128. https://doi.org/10.1093/treephys/tpad128
- Charrier, G., Cochard, H., & Améglio, T. (2013). Evaluation of the impact of frost resistances on potential altitudinal limit of trees. *Tree Physiology*, *33*(9), 891–902. https://doi.org/10.1093/treephys/tpt062
- Charrier G, Améglio T (2011) The timing of leaf fall affects cold acclimation by interactions with air temperature through water and carbohydrate contents. Environ Exp Bot 72:351–357.
- Chave, J., Coomes, D., Jansen, S., Lewis, S. L., Swenson, N. G., & Zanne, A. E. (2009). Towards a worldwide wood economics spectrum. *Ecology Letters*, 12(4), 351–366. https://doi.org/10.1111/j.1461-0248.2009.01285.x
- Cuny, H. E., & Rathgeber, C. B. K. (2016). Xylogenesis: Coniferous Trees of Temperate Forests Are Listening to the Climate Tale during the Growing Season But Only Remember the Last Words!1. *Plant Physiology*, *171*(1), 306–317. https://doi.org/10.1104/pp.16.00037
- Cuny, H. E., Rathgeber, C. B. K., Frank, D., Fonti, P., & Fournier, M. (2014). Kinetics of tracheid development explain conifer tree-ring structure. *New Phytologist*, 203(4), 1231–1241. https://doi.org/10.1111/nph.12871
- Cuny, H. E., Rathgeber, C. B. K., Frank, D., Fonti, P., Mäkinen, H., Prislan, P., Rossi, S., del Castillo, E. M., Campelo, F., Vavrčík, H., Camarero, J. J., Bryukhanova, M. V., Jyske, T., Gričar, J., Gryc, V., De Luis, M., Vieira, J., Čufar, K., Kirdyanov, A. V., ... Fournier, M. (2015). Woody biomass production lags stem-girth increase by over one month in coniferous forests. *Nature Plants*, *1*(11), 15160. https://doi.org/10.1038/nplants.2015.160
- Cuny, H. E., Rathgeber, C. B. K., Kiessé, T. S., Hartmann, F. P., Barbeito, I., & Fournier, M. (2013).

  Generalized additive models reveal the intrinsic complexity of wood formation dynamics. *Journal of Experimental Botany*, 64(7), 1983–1994. https://doi.org/10.1093/jxb/ert057
- Danis, P. A., Masson-Delmotte, V., Stievenard, M., Guillemin, M. T., Daux, V., Naveau, Ph., & Von Grafenstein, U. (2006). Reconstruction of past precipitation  $\delta$ 180 using tree-ring cellulose  $\delta$ 180

- and  $\delta$ 13C: A calibration study near Lac d'Annecy, France. *Earth and Planetary Science Letters*, 243(3–4), 439–448. https://doi.org/10.1016/j.epsl.2006.01.023
- Dao, M. C. E., Rossi, S., Walsh, D., Morin, H., & Houle, D. (2015). A 6-Year-Long Manipulation with Soil Warming and Canopy Nitrogen Additions does not Affect Xylem Phenology and Cell Production of Mature Black Spruce. *Frontiers in Plant Science*, 6. https://doi.org/10.3389/fpls.2015.00877
- Deslauriers, A., Beaulieu, M., Balducci, L., Giovannelli, A., Gagnon, M. J., & Rossi, S. (2014). Impact of warming and drought on carbon balance related to wood formation in black spruce. *Annals of Botany*, 114(2), 335–345. https://doi.org/10.1093/aob/mcu111
- Deslauriers, A., Fournier, M.-P., Cartenì, F., & Mackay, J. (2019). Phenological shifts in conifer species stressed by spruce budworm defoliation. *Tree Physiology*, *39*(4), 590–605. https://doi.org/10.1093/treephys/tpy135
- Deslauriers, A., Giovannelli, A., Rossi, S., Castro, G., Fragnelli, G., & Traversi, L. (2009). Intra-annual cambial activity and carbon availability in stem of poplar. *Tree Physiology*, *29*(10), 1223–1235. https://doi.org/10.1093/treephys/tpp061
- Deslauriers, A., Huang, J.-G., Balducci, L., Beaulieu, M., & Rossi, S. (2016). The Contribution of Carbon and Water in Modulating Wood Formation in Black Spruce Saplings. *Plant Physiology*, *170*(4), 2072–2084. https://doi.org/10.1104/pp.15.01525
- Deslauriers, A., & Morin, H. (2005). Intra-annual tracheid production in balsam fir stems and the effect of meteorological variables. *Trees*, *19*(4), 402–408. https://doi.org/10.1007/s00468-004-0398-8
- Deslauriers, Morin, Hubert, & Bégin, Yves. (2003). Cellular phenology of annual ring formation of Abies balsamea (L.) Mill. In the 1 Québec boreal forest (Canada). *Can. J. For. Res.*, *33*, 190-200.
- Dietze, M. C., Sala, A., Carbone, M. S., Czimczik, C. I., Mantooth, J. A., Richardson, A. D., & Vargas, R. (2014). Nonstructural Carbon in Woody Plants. *Annual Review of Plant Biology*, 65(1), 667–687. https://doi.org/10.1146/annurev-arplant-050213-040054
- Dodd, J. P., Patterson, W. P., Holmden, C., & Brasseur, J. M. (2008). Robotic micromilling of tree-rings: A new tool for obtaining subseasonal environmental isotope records. *Chemical Geology*, 252(1–2), 21–30. https://doi.org/10.1016/j.chemgeo.2008.01.021
- Dominguez, P. G., & Niittylä, T. (2022). Mobile forms of carbon in trees: Metabolism and transport. *Tree Physiology*, 42(3), 458–487. https://doi.org/10.1093/treephys/tpab123
- D'Orangeville, L., Houle, D., Duchesne, L., Phillips, R. P., Bergeron, Y., & Kneeshaw, D. (2018). Beneficial effects of climate warming on boreal tree growth may be transitory. *Nature Communications*, 9(1), 3213. https://doi.org/10.1038/s41467-018-05705-4
- Drew, D., & Downes, G. (2015). A model of stem growth and wood formation in Pinus radiata. *Trees, 29*. https://doi.org/10.1007/s00468-015-1216-1

- Durzan, D. J., & Steward, F. C. (1967). The nitrogen metabolism of picea glauca (moench) voss and pinus banksiana lamb. As influenced by mineral nutrition. *Canadian Journal of Botany*, 45(5), 695–710. https://doi.org/10.1139/b67-077
- Epstein, S., Yapp, C. J., & Hall, J. H. (1976). The determination of the D/H ratio of non-exchangeable hydrogen in cellulose extracted from aquatic and land plants. *Earth and Planetary Science Letters*, 30(2), 241–251. https://doi.org/10.1016/0012-821X(76)90251-X
- Fajstavr, M., Paschová, Z., Giagli, K., Vavrčík, H., Gryc, V., & Urban, J. (2018). Auxin (IAA) and soluble carbohydrate seasonal dynamics monitored during xylogenesis and phloemogenesis in Scots pine. *iForest Biogeosciences and Forestry*, 11(5), 553–562. https://doi.org/10.3832/ifor2734-011
- Farquhar, G. D., Barbour, M. M., & Henry, B. K. (1998). Interpretation of oxygen isotope composition of leaf material. In *Stable Isotopes*. Garland Science.
- Farquhar, G. D., & Ehleringer. (1989). CARBON ISOTOPE DISCRIMINATION AND PHOTOSYNTHESIS. *Plant Physio*, *40*, 503–537.
- Farquhar, G. D., Ehleringer, J. R., & Hubick, K. T. (1989). CARBON ISOTOPE DISCRIMINATION AND PHOTOSYNTHESIS. *Annual Reviews of Plant Physiology, Plant Molecular Biology, 40*, 503–537.
- Farquhar, G. D., & Lloyd, J. (1993). 5—Carbon and Oxygen Isotope Effects in the Exchange of Carbon Dioxide between Terrestrial Plants and the Atmosphere. In J. R. Ehleringer, A. E. Hall, & G. D. Farquhar (Eds.), *Stable Isotopes and Plant Carbon-water Relations* (pp. 47–70). Academic Press. https://doi.org/10.1016/B978-0-08-091801-3.50011-8
- Farquhar, G. D., O'Leary, M., & Berry, J. (1982). On the Relationship Between Carbon Isotope
  Discrimination and the Intercellular Carbon Dioxide Concentration in Leaves. *Functional Plant Biology*, *9*(2), 121. https://doi.org/10.1071/PP9820121
- Farquhar, G. D., & Sharkey, T. D. (1982). Stomatal Conductance and Photosynthesis. *Annual Review of Plant Physiology*, *33*(1), 317–345. https://doi.org/10.1146/annurev.pp.33.060182.001533
- Fernández-de-Uña, L., Rossi, S., Aranda, I., Fonti, P., González-González, B. D., Cañellas, I., & Gealzquierdo, G. (2017). Xylem and Leaf Functional Adjustments to Drought in Pinus sylvestris and Quercus pyrenaica at Their Elevational Boundary. *Frontiers in Plant Science*, 8. https://doi.org/10.3389/fpls.2017.01200
- Fichtler, E., Helle, G., & Worbes, M. (2010). Stable-Carbon Isotope Time Series from Tropical Tree Rings Indicate a Precipitation Signal. *Tree-Ring Research*, 66(1), 35–49. https://doi.org/10.3959/2008-20.1
- Flexas, J., Diaz-Espejo, A., Gago, J., Gallé, A., Galmés, J., Gulías, J., & Medrano, H. (2013). Photosynthetic limitations in Mediterranean plants: A review. *Environmental and Experimental Botany*, 103, 12–23. https://doi.org/10.1016/j.envexpbot.2013.09.002

- Fonti, M., Vaganov, E., Wirth, C., Shashkin, A., Astrakhantseva, N., & Schulze, E.-D. (2018). Age-Effect on Intra-Annual δ13C-Variability within Scots Pine Tree-Rings from Central Siberia. *Forests*, *9*(6), 364. https://doi.org/10.3390/f9060364
- Fonti, P., Von Arx, G., García-González, I., Eilmann, B., Sass-Klaassen, U., Gärtner, H., & Eckstein, D. (2010). Studying global change through investigation of the plastic responses of xylem anatomy in tree rings. *New Phytologist*, 185(1), 42–53. https://doi.org/10.1111/j.1469-8137.2009.03030.x
- Frank, D. C., Poulter, B., Saurer, M., Esper, J., Huntingford, C., Helle, G., Treydte, K., Zimmermann, N. E., Schleser, G. H., Ahlström, A., Ciais, P., Friedlingstein, P., Levis, S., Lomas, M., Sitch, S., Viovy, N., Andreu-Hayles, L., Bednarz, Z., Berninger, F., ... Weigl, M. (2015). Water-use efficiency and transpiration across European forests during the Anthropocene. *Nature Climate Change*, *5*(6), 579–583. https://doi.org/10.1038/nclimate2614
- Fu, P.-L., Grießinger, J., Gebrekirstos, A., Fan, Z.-X., & Bräuning, A. (2017a). Earlywood and Latewood Stable Carbon and Oxygen Isotope Variations in Two Pine Species in Southwestern China during the Recent Decades. *Frontiers in Plant Science*, 7. https://doi.org/10.3389/fpls.2016.02050
- Gauthier, S., Bernier, P., Kuuluvainen, T., Shvidenko, A. Z., & Schepaschenko, D. G. (2015). Boreal forest health and global change. *Science*, *349*(6250), 819–822. https://doi.org/10.1126/science.aaa9092
- Gebrekirstos, A., Worbes, M., Teketay, D., Fetene, M., & Mitlöhner, R. (2009). Stable carbon isotope ratios in tree rings of co-occurring species from semi-arid tropics in Africa: Patterns and climatic signals. *Global and Planetary Change*, 66(3–4), 253–260. https://doi.org/10.1016/j.gloplacha.2009.01.002
- Gessler, A., Brandes, E., Buchmann, N., Helle, G., Rennenberg, H., & Barnard, R. L. (2009). Tracing carbon and oxygen isotope signals from newly assimilated sugars in the leaves to the tree-ring archive. *Plant, Cell & Environment*, 32(7), 780–795. https://doi.org/10.1111/j.1365-3040.2009.01957.x
- Gessler A, Brandes E, Keitel C, Boda S, Kayler ZE, Granier A, Barbour M, Farquhar GD, Treydte K (2013)

  The oxygen isotope enrichment of leaf-exported assimilates does it always reflect lamina leaf water enrichment? New Phytol 200:144–157.
- Gessler, A., Ferrio, J. P., Hommel, R., Treydte, K., Werner, R. A., & Monson, R. K. (2014). Stable isotopes in tree rings: Towards a mechanistic understanding of isotope fractionation and mixing processes from the leaves to the wood. *Tree Physiology*, *34*(8), 796–818. https://doi.org/10.1093/treephys/tpu040
- Gessler, A., Tcherkez, G., Peuke, A. D., Ghashghaie, J., & Farquhar, G. D. (2008). Experimental evidence for diel variations of the carbon isotope composition in leaf, stem and phloem sap organic matter in Ricinus communis. *Plant, Cell & Environment*, *31*(7), 941–953. https://doi.org/10.1111/j.1365-3040.2008.01806.x
- Giguère-Croteau, C., Boucher, É., Bergeron, Y., Girardin, M. P., Drobyshev, I., Silva, L. C. R., Hélie, J.-F., & Garneau, M. (2019). North America's oldest boreal trees are more efficient water users due to increased [CO2], but do not grow faster. *Proceedings of the National Academy of Sciences*, 116(7), 2749–2754. https://doi.org/10.1073/pnas.1816686116

- Giovannelli, A., Emiliani, G., Traversi, M. L., Deslauriers, A., & Rossi, S. (2011). Sampling cambial region and mature xylem for non structural carbohydrates and starch analyses. *Dendrochronologia*, 29(3), 177–182. https://doi.org/10.1016/j.dendro.2011.01.001
- Gleixner, G., & Schmidt, H.-L. (1997). Carbon Isotope Effects on the Fructose-1,6-bisphosphate Aldolase Reaction, Origin for Non-statistical 13C Distributions in Carbohydrates\*. *Journal of Biological Chemistry*, 272(9), 5382–5387. https://doi.org/10.1074/jbc.272.9.5382
- Grams, T. E. E., Kozovits, A. R., Häberle, K.-H., Matyssek, R., & Dawson, T. E. (2007). Combining? <sup>13</sup> C and? <sup>18</sup> O analyses to unravel competition, CO <sub>2</sub> and O <sub>3</sub> effects on the physiological performance of different-aged trees. *Plant, Cell & Environment, 30*(8), 1023–1034. https://doi.org/10.1111/j.1365-3040.2007.01696.x
- Gričar, J., Prislan, P., Gryc, V., Vavr ik, H., De Luis, M., & Ufar, K. (2014). Plastic and locally adapted phenology in cambial seasonality and production of xylem and phloem cells in Picea abies from temperate environments. *Tree Physiology*, *34*(8), 869–881. https://doi.org/10.1093/treephys/tpu026
- Grissino-Mayer, H. D. (2003). A Manual and Tutorial for the Proper Use of an Increment Borer. https://repository.arizona.edu/handle/10150/262572
- Guiot, J., Boucher, E., & Gea-Izquierdo, G. (2014). Process models and model-data fusion in dendroecology. *Frontiers in Ecology and Evolution*, 2. https://doi.org/10.3389/fevo.2014.00052
- Gurskaya, M. A., & Shiyatov, S. G. (2006). Distribution of frost injuries in the wood of conifers. *Russian Journal of Ecology*, *37*(1), 7–12. https://doi.org/10.1134/S1067413606010024
- Hansen, J., & Beck, E. (1990). The fate and path of assimilation products in the stem of 8-year-old Scots pine (Pinus sylvestris L.) trees. *Trees*, 4(1), 16–21. https://doi.org/10.1007/BF00226235
- Hartmann, H., & Trumbore, S. (2016). Understanding the roles of nonstructural carbohydrates in forest trees from what we can measure to what we want to know. *New Phytologist*, *211*(2), 386–403. https://doi.org/10.1111/nph.13955
- Heinrich, S., Dippold, M. A., Werner, C., Wiesenberg, G. L. B., Kuzyakov, Y., & Glaser, B. (2015). Allocation of freshly assimilated carbon into primary and secondary metabolites after in situ <sup>13</sup> C pulse labelling of Norway spruce ( *Picea abies* ). *Tree Physiology*, tpv083. https://doi.org/10.1093/treephys/tpv083
- Helama, S., Arppe, L., Hyvönen, J., Mielikäinen, K., & Oinonen, M. (2018). Isoscapes of plant  $\delta^{13}C$  in the northern forests: Addressing the question of inter-tree and -site variability in *Pinus sylvestris* L. tree rings from Finnish Lapland. *GEOCHEMICAL JOURNAL*, *52*(4), 287–298. https://doi.org/10.2343/geochemj.2.0507
- Hélie, J., & Hillaire-Marcel, C. (2021). Designing working standards for stable H, C, and O isotope measurements in CO  $_2$  and H  $_2$  O. *Rapid Communications in Mass Spectrometry*, *35*(5), e9008. https://doi.org/10.1002/rcm.9008

- Helle G, Pauly M, Heinrich I, Schollän K, Balanzategui D, & Schürheck L. (2022). Stable Isotope Signatures of Wood, its Constituents and Methods of Cellulose Extraction. In *Stable Isotopes in Tree Rings* (Vol. 8). Tree Physiology.
- Helle, G., & Schleser, G. H. (2004). Beyond CO2-fixation by Rubisco—An interpretation of 13C/12C variations in tree rings from novel intra-seasonal studies on broad-leaf trees. *Plant, Cell and Environment*, 27(3), 367–380. https://doi.org/10.1111/j.0016-8025.2003.01159.x
- Hilasvuori, E., Berninger, F., Sonninen, E., Tuomenvirta, H., & Jungner, H. (2009). Stability of climate signal in carbon and oxygen isotope records and ring width from Scots pine (Pinus sylvestris L.) in Finland. *Journal of Quaternary Science*, *24*(5), 469–480. https://doi.org/10.1002/jqs.1260
- Hill, S. A., Waterhouse, J. S., Field, E. M., Switsur, V. R., & Ap Rees, T. (1995). Rapid recycling of triose phosphates in oak stem tissue. *Plant, Cell & Environment*, *18*(8), 931–936. https://doi.org/10.1111/j.1365-3040.1995.tb00603.x
- Hsiao, T. C. (1973). Plant Responses to Water Stress. *Annual Review of Plant Biology, 24*(Volume 24, 1973), 519–570. https://doi.org/10.1146/annurev.pp.24.060173.002511
- Hultine, K. R., & Marshall, J. D. (2000). Altitude trends in conifer leaf morphology and stable carbon isotope composition. *Oecologia*, 123(1), 32–40. https://doi.org/10.1007/s004420050986
- Kagawa, A., Sugimoto, A., & Maximov, T. C. (2006). 13CO2 pulse-labelling of photoassimilates reveals carbon allocation within and between tree rings. *Plant, Cell and Environment, 29*(8), 1571–1584. https://doi.org/10.1111/j.1365-3040.2006.01533.x
- Keitel, C., Adams, M. A., Holst, T., Matzarakis, A., Mayer, H., Rennenberg, H., & GEßLER, A. (2003).

  Carbon and oxygen isotope composition of organic compounds in the phloem sap provides a short-term measure for stomatal conductance of European beech ( *Fagus sylvatica* L.). *Plant, Cell & Environment*, 26(7), 1157–1168. https://doi.org/10.1046/j.1365-3040.2003.01040.x
- Klein, T., Hemming, D., Lin, T., Grünzweig, J. M., Maseyk, K., Rotenberg, E., & Yakir, D. (2005). Association between tree-ring and needle  $\delta$ 13C and leaf gas exchange in Pinus halepensis under semi-arid conditions. *Oecologia*, 144(1), 45–54. https://doi.org/10.1007/s00442-005-0002-y
- Klein, T., & Hoch, G. (2015). Tree carbon allocation dynamics determined using a carbon mass balance approach. *New Phytologist*, 205(1), 147–159. https://doi.org/10.1111/nph.12993
- Körner, C. (2003). Carbon limitation in trees. *Journal of Ecology*, *91*(1), 4–17. https://doi.org/10.1046/j.1365-2745.2003.00742.x
- Kurz, W. A., Stinson, G., & Rampley, G. (2008). Could increased boreal forest ecosystem productivity offset carbon losses from increased disturbances? *Philosophical Transactions of the Royal Society B: Biological Sciences*, 363(1501), 2261–2269. https://doi.org/10.1098/rstb.2007.2198
- Leavitt, S. W. (2010). Tree-ring C–H–O isotope variability and sampling. *Science of The Total Environment*, 408(22), 5244–5253. https://doi.org/10.1016/j.scitotenv.2010.07.057

- Leland, C., Andreu-Hayles, L., Cook, E. R., Anchukaitis, K. J., Byambasuren, O., Davi, N., Hessl, A., Martin-Benito, D., Nachin, B., & Pederson, N. (2023). Impacts of climate and tree morphology on tree-ring stable isotopes in central Mongolia. *Tree Physiology*, *43*(4), 539–555. https://doi.org/10.1093/treephys/tpac142
- Lévesque, M., Siegwolf, R., Saurer, M., Eilmann, B., & Rigling, A. (2014). Increased water-use efficiency does not lead to enhanced tree growth under xeric and mesic conditions. *New Phytologist*, 203(1), 94–109. https://doi.org/10.1111/nph.12772
- Li, J., Wang, G., Liu, X., Han, J., Liu, M., & Liu, X. (2009). Variations in carbon isotope ratios of C3 plants and distribution of C4 plants along an altitudinal transect on the eastern slope of Mount Gongga. *Science in China Series D: Earth Sciences*, *52*, 1714–1723. https://doi.org/10.1007/s11430-009-0170-4
- Lipavská, H., Svobodová, H., & Albrechtová, J. (2000). Annual dynamics of the content of non-structural saccharides in the context of structural development of vegetative buds of Norway spruce. *Journal of Plant Physiology*, 157(4), 365–373. https://doi.org/10.1016/S0176-1617(00)80021-8
- Loader, N. J., McCarroll, D., Barker, S., Jalkanen, R., & Grudd, H. (2017). Inter-annual carbon isotope analysis of tree-rings by laser ablation. *Chemical Geology*, 466, 323–326. https://doi.org/10.1016/j.chemgeo.2017.06.021
- Luo Y-H, Sternberg LDSL (1992) Hydrogen and Oxygen Isotopic Fractionation During Heterotrophic Cellulose Synthesis. J Exp Bot 43:47–50.
- MacNeill, G. J., Mehrpouyan, S., Minow, M. A. A., Patterson, J. A., Tetlow, I. J., & Emes, M. J. (2017). Starch as a source, starch as a sink: The bifunctional role of starch in carbon allocation. *Journal of Experimental Botany*, 68(16), 4433–4453. https://doi.org/10.1093/jxb/erx291
- Marchand, W., Girardin, M. P., Hartmann, H., Depardieu, C., Isabel, N., Gauthier, S., Boucher, É., & Bergeron, Y. (2020). Strong overestimation of water-use efficiency responses to rising CO 2 in tree-ring studies. *Global Change Biology*, *January*, 1–21. https://doi.org/10.1111/gcb.15166
- Martin-Benito, D., Anchukaitis, K., Evans, M., Del Río, M., Beeckman, H., & Cañellas, I. (2017). Effects of Drought on Xylem Anatomy and Water-Use Efficiency of Two Co-Occurring Pine Species. *Forests*, 8(9), 332. https://doi.org/10.3390/f8090332
- Martin-Benito, D., Beeckman, H., & Cañellas, I. (2013). Influence of drought on tree rings and tracheid features of Pinus nigra and Pinus sylvestris in a mesic Mediterranean forest. *European Journal of Forest Research*, 132(1), 33–45. https://doi.org/10.1007/s10342-012-0652-3
- Martínez-Sancho, E., Cernusak, L. A., Fonti, P., Gregori, A., Ullrich, B., Pannatier, E. G., Gessler, A., Lehmann, M. M., Saurer, M., & Treydte, K. (2023). Unenriched xylem water contribution during cellulose synthesis influenced by atmospheric demand governs the intra-annual tree-ring δ180 signature. *New Phytologist*, 240(5), 1743–1757. https://doi.org/10.1111/nph.19278
- Martínez-Sancho, E., Treydte, K., Lehmann, M. M., Rigling, A., & Fonti, P. (2022). Drought impacts on tree carbon sequestration and water use evidence from intra-annual tree-ring characteristics. *New Phytologist*, 236(1), 58–70. https://doi.org/10.1111/nph.18224

- Martínez-Sancho, E., Treydte, K., Lehmann, M. M., Rigling, A., & Fonti, P. (2022). Drought impacts on tree carbon sequestration and water use evidence from intra-annual tree-ring characteristics. *New Phytologist*, 236(1), 58–70. https://doi.org/10.1111/nph.18224
- McCarroll, D., & Loader, N. J. (2004). Stable isotopes in tree rings. *Quaternary Science Reviews*, 23(7–8), 771–801. https://doi.org/10.1016/j.quascirev.2003.06.017
- Namvar, S., Boucher, É., Deslauriers, A., Morin, H., & Savard, M. M. (2024). Monitoring weekly δ 13C variations along the cambium-xylem continuum in the Canadian eastern boreal forest. *Tree Physiology*, tpae136. https://doi.org/10.1093/treephys/tpae136
- Naulier, M., Savard, M. M., Bégin, C., Marion, J., Arseneault, D., & Bégin, Y. (2014). Carbon and oxygen isotopes of lakeshore black spruce trees in northeastern Canada as proxies for climatic reconstruction. *Chemical Geology*, *374–375*, 37–43. https://doi.org/10.1016/j.chemgeo.2014.02.031
- Nilsson, L.-O. (1997). Manipulation of conventional forest management practices to increase forest growth—Results from the Skogaby project. *Forest Ecology and Management*, *91*(1), 53–60. https://doi.org/10.1016/S0378-1127(96)03888-1
- Offermann, C., Ferrio, J. P., Holst, J., Grote, R., Siegwolf, R., Kayler, Z., & Gessler, A. (2011). The long way down—Are carbon and oxygen isotope signals in the tree ring uncoupled from canopy physiological processes? *Tree Physiology*, *31*(10), 1088–1102. https://doi.org/10.1093/treephys/tpr093
- Ogée, J., Barbour, M. M., Wingate, L., Bert, D., Bosc, A., Stievenard, M., Lambrot, C., Pierre, M., Bariac, T., Loustau, D., & Dewar, R. C. (2009). A single-substrate model to interpret intra-annual stable isotope signals in tree-ring cellulose. *Plant, Cell & Environment*, 32(8), 1071–1090. https://doi.org/10.1111/j.1365-3040.2009.01989.x
- Ortega, J. K. E. (2010). Plant Cell Growth in Tissue. *Plant Physiology*, *154*(3), 1244–1253. https://doi.org/10.1104/pp.110.162644
- Palacio, S., Hoch, G., Sala, A., Körner, C., & Millard, P. (2014). Does carbon storage limit tree growth? New Phytologist, 201(4), 1096–1100. https://doi.org/10.1111/nph.12602
- Pan, Y., Birdsey, R. A., Fang, J., Houghton, R., Kauppi, P. E., Kurz, W. A., Phillips, O. L., Shvidenko, A., Lewis, S. L., Canadell, J. G., Ciais, P., Jackson, R. B., Pacala, S. W., McGuire, A. D., Piao, S., Rautiainen, A., Sitch, S., & Hayes, D. (2011). A Large and Persistent Carbon Sink in the World's Forests. *Science*, *333*(6045), 988–993. https://doi.org/10.1126/science.1201609
- Peñuelas, J., Canadell, J. G., & Ogaya, R. (2011). Increased water-use efficiency during the 20th century did not translate into enhanced tree growth. *Global Ecology and Biogeography*, 20(4), 597–608. https://doi.org/10.1111/j.1466-8238.2010.00608.x
- Perrin, M., Rossi, S., & Isabel, N. (2017). Synchronisms between bud and cambium phenology in black spruce: Early-flushing provenances exhibit early xylem formation. *Tree Physiology*, *37*, 1–11. https://doi.org/10.1093/treephys/tpx019

- Piao, S., Liu, Q., Chen, A., Janssens, I. A., Fu, Y., Dai, J., Liu, L., Lian, X., Shen, M., & Zhu, X. (2019). Plant phenology and global climate change: Current progresses and challenges. *Global Change Biology*, 25(6), 1922–1940. https://doi.org/10.1111/gcb.14619
- Piper, F. I. (2020). Decoupling between growth rate and storage remobilization in broadleaf temperate tree species. *Functional Ecology*, *34*(6), 1180–1192. https://doi.org/10.1111/1365-2435.13552
- Poage, M. A., & Chamberlain, C. P. (2001). Empirical Relationships Between Elevation and the Stable Isotope Composition of Precipitation and Surface Waters: Considerations for Studies of Paleoelevation Change. *American Journal of Science*, 301(1), 1–15. https://doi.org/10.2475/ajs.301.1.1
- Pons, T. L., & Helle, G. (2011). Identification of anatomically non-distinct annual rings in tropical trees using stable isotopes. *Trees*, *25*(1), 83–93. https://doi.org/10.1007/s00468-010-0527-5
- Porté, A., & Loustau, D. (2001). Seasonal and interannual variations in carbon isotope discrimination in a maritime pine (Pinus pinaster) stand assessed from the isotopic composition of cellulose in annual rings. *Tree Physiology*, 21(12–13), 861–868. https://doi.org/10.1093/treephys/21.12-13.861
- Rademacher, T., Fonti, P., LeMoine, J. M., Fonti, M. V., Bowles, F., Chen, Y., Eckes-Shephard, A. H., Friend, A. D., & Richardson, A. D. (2022). Insights into source/sink controls on wood formation and photosynthesis from a stem chilling experiment in mature red maple. *New Phytologist*, *236*(4), 1296–1309. https://doi.org/10.1111/nph.18421
- Raffalli-Delerce, G., Masson-Delmotte, V., Dupouey, J. L., Stievenard, M., Breda, N., & Moisselin, J. M. (2004). Reconstruction of summer droughts using tree-ring cellulose isotopes: A calibration study with living oaks from Brittany (western France). *Tellus B*, *56*(2), 160–174. https://doi.org/10.1111/j.1600-0889.2004.00086.x
- Rathgeber, C. B. K., Pérez-de-Lis Gonzalo, Fernández-de-Uña Laura, Fonti Patrick, Rossi Sergio, Treydte Kerstin, Gessler Arthur, Deslauriers Annie, V. Fonti Marina, & Ponton téphane. (2022).

  Anatomical, Developmental and Physiological Bases of Tree-Ring Formation in Relation to Environmental Factors. In *Stable Isotopes in Tree Rings* (Vol. 8). Tree Physiology. https://doi.org/10.1007/978-3-030-92698-4\_3
- Richardson, A. D., Carbone, M. S., Keenan, T. F., Czimczik, C. I., Hollinger, D. Y., Murakami, P., Schaberg, P. G., & Xu, X. (2013). Seasonal dynamics and age of stemwood nonstructural carbohydrates in temperate forest trees. *New Phytologist*, 197(3), 850–861. https://doi.org/10.1111/nph.12042
- Rinne, K. T., Saurer, M., Kirdyanov, A. V., Loader, N. J., Bryukhanova, M. V., Werner, R. A., & Siegwolf, R. T. W. (2015). The relationship between needle sugar carbon isotope ratios and tree rings of larch in Siberia. *Tree Physiology*, tpv096. https://doi.org/10.1093/treephys/tpv096
- Rinne-Garmston, K. T., Tang, Y., Sahlstedt, E., Adamczyk, B., Saurer, M., Salmon, Y., Carrasco, M. del R. D., Hölttä, T., Lehmann, M. M., Mo, L., & Young, G. H. F. (2023). Drivers of intra-seasonal δ13C signal in tree-rings of Pinus sylvestris as indicated by compound-specific and laser ablation isotope analysis. *Plant, Cell & Environment*, *46*(9), 2649–2666. https://doi.org/10.1111/pce.14636

- Roden, J. S., & Ehleringer, J. R. (1999). Hydrogen and oxygen isotope ratios of tree-ring cellulose for riparian trees grown long-term under hydroponically controlled environments. *Oecologia*, 121(4), 467–477. https://doi.org/10.1007/s004420050953
- Roden, J. S., & Farquhar, G. D. (2012). A controlled test of the dual-isotope approach for the interpretation of stable carbon and oxygen isotope ratio variation in tree rings. *Tree Physiology*, 32(4), 490–503. https://doi.org/10.1093/treephys/tps019
- Roden, J. S., Johnstone, J. A., & Dawson, T. E. (2009). Intra-annual variation in the stable oxygen and carbon isotope ratios of cellulose in tree rings of coast redwood (Sequoia sempervirens). *The Holocene*, 19(2), 189–197. https://doi.org/10.1177/0959683608098959
- Roden, J. S., Johnstone, J. A., & Dawson, T. E. (2011). Regional And Watershed-Scale Coherence In the Stable-Oxygen and Carbon Isotope Ratio Time Series In Tree Rings Of Coast Redwood (Sequoia sempervirens). *Tree-Ring Research*, 67(2), 71–86. https://doi.org/10.3959/2010-4.1
- Roden, J. S., Lin, G., & Ehleringer, J. R. (2000). A mechanistic model for interpretation of hydrogen and oxygen isotope ratios in tree-ring cellulose. *Geochimica et Cosmochimica Acta*, *64*(1), 21–35. https://doi.org/10.1016/S0016-7037(99)00195-7
- Rossi, S., Anfodillo, T., Čufar, K., Cuny, H. E., Deslauriers, A., Fonti, P., Frank, D., Gričar, J., Gruber, A., King, G. M., Krause, C., Morin, H., Oberhuber, W., Prislan, P., & Rathgeber, C. B. K. (2013). A meta-analysis of cambium phenology and growth: Linear and non-linear patterns in conifers of the northern hemisphere. *Annals of Botany*, *112*(9), 1911–1920. https://doi.org/10.1093/aob/mct243
- Rossi, S., Deslauriers, A., & Anfodillo, T. (2006). Assessment of Cambial Activity and Xylogenesis by Microsampling Tree Species: An Example at the Alpine Timberline. *IAWA Journal*, *27*(4), 383–394. https://doi.org/10.1163/22941932-90000161
- Rossi, S., Deslauriers, A., Anfodillo, T., & Carraro, V. (2007). Evidence of threshold temperatures for xylogenesis in conifers at high altitudes. *Oecologia*, *152*(1), 1–12. https://doi.org/10.1007/s00442-006-0625-7
- Rossi, S., Deslauriers, A., Anfodillo, T., Morin, H., Saracino, A., Motta, R., & Borghetti, M. (2006). Conifers in cold environments synchronize maximum growth rate of tree-ring formation with day length. *New Phytologist*, *170*(2), 301–310. https://doi.org/10.1111/j.1469-8137.2006.01660.x
- Rossi, S., Girard, M.-J., & Morin, H. (2014). Lengthening of the duration of xylogenesis engenders disproportionate increases in xylem production. *Global Change Biology*, *20*(7), 2261–2271. https://doi.org/10.1111/gcb.12470
- Rossi, S., Morin, H., Deslauriers, A., & Plourde, P.-Y. (2011). Predicting xylem phenology in black spruce under climate warming. *Global Change Biology*, *17*(1), 614–625. https://doi.org/10.1111/j.1365-2486.2010.02191.x
- Sala, A., Woodruff, D. R., & Meinzer, F. C. (2012). Carbon dynamics in trees: Feast or famine? *Tree Physiology*, 32(6), 764–775. https://doi.org/10.1093/treephys/tpr143

- Sarris, D., Siegwolf, R., & Körner, C. (2013). Inter- and intra-annual stable carbon and oxygen isotope signals in response to drought in Mediterranean pines. *Agricultural and Forest Meteorology*, *168*, 59–68. https://doi.org/10.1016/j.agrformet.2012.08.007
- Sass-Klaassen, U., Poole, I., Wils, T., Helle, G., Schleser, G. H., & Bergen, P. F. van. (2005). Carbon and Oxygen Isotope Dendrochronology in Sub-Fossil Bog Oak Tree Rings—A Preliminary Study. *IAWA Journal*, 26(1), 121–136. https://doi.org/10.1163/22941932-90001607
- Saurer, M., Sahlstedt, E., Rinne-Garmston, K., Lehmann, M., Oettli, M., Gessler, A., & Treydte, K. (2022). Progress in high-resolution isotope-ratio analysis of tree rings using laser ablation. *Tree Physiology*, 43. https://doi.org/10.1093/treephys/tpac141
- Saurer, M., Sahlstedt, E., Rinne-Garmston, K. T., Lehmann, M. M., Oettli, M., Gessler, A., & Treydte, K. (2023). Progress in high-resolution isotope-ratio analysis of tree rings using laser ablation. *Tree Physiology*, 43(5), 694–705. https://doi.org/10.1093/treephys/tpac141
- Saurer, M., Siegwolf, R. T. W., & Schweingruber, F. H. (2004). Carbon isotope discrimination indicates improving water-use efficiency of trees in northern Eurasia over the last 100 years. *Global Change Biology*, 10(12), 2109–2120. https://doi.org/10.1111/j.1365-2486.2004.00869.x
- Saurer, M., & Voelker, S. (2022). Intrinsic Water-Use Efficiency Derived from Stable Carbon Isotopes of Tree-Rings. In R. T. W. Siegwolf, J. R. Brooks, J. Roden, & M. Saurer (Eds.), *Stable Isotopes in Tree Rings: Inferring Physiological, Climatic and Environmental Responses* (pp. 481–498). Springer International Publishing. https://doi.org/10.1007/978-3-030-92698-4\_17
- Savard, M. M., & Daux, V. (2020). An overview on isotopic divergences causes for instability of tree-ring isotopes and climate correlations. *Climate of the Past*, *16*(4), 1223–1243. https://doi.org/10.5194/cp-16-1223-2020
- Scheidegger, Y., Saurer, M., Bahn, M., & Siegwolf, R. (2000a). Linking stable oxygen and carbon isotopes with stomatal conductance and photosynthetic capacity: A conceptual model. *Oecologia*, 125(3), 350–357. https://doi.org/10.1007/s004420000466
- Schiestl-Aalto, P., Ryhti, K., Mäkelä, A., Peltoniemi, M., Bäck, J., & Kulmala, L. (2019). Analysis of the NSC Storage Dynamics in Tree Organs Reveals the Allocation to Belowground Symbionts in the Framework of Whole Tree Carbon Balance. *Frontiers in Forests and Global Change*, *2*, 17. https://doi.org/10.3389/ffgc.2019.00017
- Schollaen, K., Heinrich, I., & Helle, G. (2014). UV -laser-based microscopic dissection of tree rings a novel sampling tool for  $\delta$  <sup>13</sup> C and  $\delta$  <sup>18</sup> O studies. *New Phytologist*, 201(3), 1045–1055. https://doi.org/10.1111/nph.12587
- Schulze, B., Wirth, C., Linke, P., Brand, W. A., Kuhlmann, I., Horna, V., & Schulze, E.-D. (2004). Laser ablation-combustion-GC-IRMS—a new method for online analysis of intra-annual variation of δ13C in tree rings. *Tree Physiology*, *24*(11), 1193–1201. https://doi.org/10.1093/treephys/24.11.1193
- Schweingruber, F. H., Börner, A., & Schulze, E.-D. (2007). *Atlas of Woody Plant Stems: Evolution, Structure, and Environmental Modifications*. Springer Science & Business Media.

- Siegwolf, R. T. W., Brooks, J. R., Roden, J., & Saurer, M. (Eds.). (2022). Stable Isotopes in Tree Rings: Inferring Physiological, Climatic and Environmental Responses (Vol. 8). Springer International Publishing. https://doi.org/10.1007/978-3-030-92698-4
- Siegwolf, R. T. W., Lehmann, M., Goldsmith, G., (Sidorova), O. C., Mirande-Ney, C., (Timoveeva), G. G., Weigt, R., & Saurer, M. (2021). The dual C and O isotope gas exchange model: A concept review for understanding plant responses to the environment and its application in tree rings. https://doi.org/10.22541/au.163844646.68129291/v1
- Siegwolf, R. T. W., Lehmann, M. M., Goldsmith, G. R., Churakova (Sidorova), O. V., Mirande-Ney, C., Timoveeva, G., Weigt, R. B., & Saurer, M. (2023). Updating the dual C and O isotope—Gasexchange model: A concept to understand plant responses to the environment and its implications for tree rings. *Plant, Cell & Environment*, 46(9), 2606–2627. https://doi.org/10.1111/pce.14630
- Silvestro, R., Mencuccini, M., García-Valdés, R., Antonucci, S., Arzac, A., Biondi, F., Buttò, V., Camarero, J. J., Campelo, F., Cochard, H., Čufar, K., Cuny, H. E., De Luis, M., Deslauriers, A., Drolet, G., Fonti, M. V., Fonti, P., Giovannelli, A., Gričar, J., ... Rossi, S. (2024). Partial asynchrony of coniferous forest carbon sources and sinks at the intra-annual time scale. *Nature Communications*, *15*(1), 6169. https://doi.org/10.1038/s41467-024-49494-5
- Silvestro, R., Zeng, Q., Buttò, V., Sylvain, J.-D., Drolet, G., Mencuccini, M., Thiffault, N., Yuan, S., & Rossi, S. (2023). A longer wood growing season does not lead to higher carbon sequestration. *Scientific Reports*, *13*(1), 4059. https://doi.org/10.1038/s41598-023-31336-x
- Simard, S., Giovannelli, A., Treydte, K., Traversi, M. L., King, G. M., Frank, D., & Fonti, P. (2013). Intraannual dynamics of non-structural carbohydrates in the cambium of mature conifer trees reflects radial growth demands. *Tree Physiology*, *33*(9), 913–923. https://doi.org/10.1093/treephys/tpt075
- Skene, D. S. (1972). The Kinetics of Tracheid Development in Tsuga canadensis Carr. And its Relation to Tree Vigour. *Annals of Botany*, *36*(1), 179–187. https://doi.org/10.1093/oxfordjournals.aob.a084570
- Sleptsov, I. V., Mikhailov, V. V., Rozhina, S. M., & Kershengolts, B. M. (2023). The year-round dynamic of metabolites accumulation in Pinus sylvestris needles in permafrost zone. *Trees*, *37*(2), 285–296. https://doi.org/10.1007/s00468-022-02346-5
- Song, X., Clark, K. S., & Helliker, B. R. (2014). Interpreting species-specific variation in tree-ring oxygen isotope ratios among three temperate forest trees. *Plant, Cell & Environment*, *37*(9), 2169–2182. https://doi.org/10.1111/pce.12317
- Song, X., Farquhar, G. D., Gessler, A., & Barbour, M. M. (2014). Turnover time of the non-structural carbohydrate pool influences  $\delta^{18}$  O of leaf cellulose. *Plant, Cell & Environment*, *37*(11), 2500–2507. https://doi.org/10.1111/pce.12309
- Soudant, A., Loader, N. J., Bäck, J., Levula, J., & Kljun, N. (2016). Intra-annual variability of wood formation and δ13C in tree-rings at Hyytiälä, Finland. *Agricultural and Forest Meteorology*, 224, 17–29. https://doi.org/10.1016/j.agrformet.2016.04.015

- Sprenger, M., Leistert, H., Gimbel, K., & Weiler, M. (2016). Illuminating hydrological processes at the soil-vegetation-atmosphere interface with water stable isotopes. *Reviews of Geophysics*, *54*(3), 674–704. https://doi.org/10.1002/2015RG000515
- Steppe, K., Sterck, F., & Deslauriers, A. (2015). Diel growth dynamics in tree stems: Linking anatomy and ecophysiology. *Trends in Plant Science*, *20*(6), 335–343. https://doi.org/10.1016/j.tplants.2015.03.015
- Sternberg LDSLO (2009) Oxygen stable isotope ratios of tree-ring cellulose: the next phase of understanding. New Phytol 181:553–562.
- Sternberg, L. D. S. L., Deniro, M. J., & Savidge, R. A. (1986). Oxygen Isotope Exchange between Metabolites and Water during Biochemical Reactions Leading to Cellulose Synthesis 1. *Plant Physiology*, 82(2), 423–427.
- Szejner, P., Clute, T., Anderson, E., Evans, M. N., & Hu, J. (2020). Reduction in lumen area is associated with the  $\delta^{18}$  O exchange between sugars and source water during cellulose synthesis. *New Phytologist*, 226(6), 1583–1593. https://doi.org/10.1111/nph.16484
- Szymczak, S., Joachimski, M. M., Bräuning, A., Hetzer, T., & Kuhlemann, J. (2012). A 560 yr summer temperature reconstruction for the Western Mediterranean basin based on stable carbon isotopes from <i&gt;Pinus nigra&lt;/i&gt; ssp. &lt;i&gt;laricio&lt;/i&gt; (Corsica/France). https://doi.org/10.5194/cpd-8-2111-2012
- Tans, P. P., & Mook, W. G. (1980). Past atmospheric CO2 levels and the 13C/12C ratios in tree rings. *Tellus*, 32(3), 268–283. https://doi.org/10.1111/j.2153-3490.1980.tb00954.x
- Teets, D. A. (2003). Predicting Sunrise and Sunset Times. *The College Mathematics Journal*, *34*(4), 317. https://doi.org/10.2307/3595771
- Thomas, F. M., Rzepecki, A., Lücke, A., Wiekenkamp, I., Rabbel, I., Pütz, T., & Neuwirth, B. (2018). Growth and wood isotopic signature of Norway spruce (*Picea abies*) along a small-scale gradient of soil moisture. *Tree Physiology*, 38(12), 1855–1870. https://doi.org/10.1093/treephys/tpy100
- Tixier, A., Gambetta, G. A., Godfrey, J., Orozco, J., & Zwieniecki, M. A. (2019). Non-structural Carbohydrates in Dormant Woody Perennials; The Tale of Winter Survival and Spring Arrival. *Frontiers in Forests and Global Change*, *2*, 18. https://doi.org/10.3389/ffgc.2019.00018
- Treydte, K., Boda, S., Graf Pannatier, E., Fonti, P., Frank, D., Ullrich, B., Saurer, M., Siegwolf, R., Battipaglia, G., Werner, W., & Gessler, A. (2014). Seasonal transfer of oxygen isotopes from precipitation and soil to the tree ring: Source water versus needle water enrichment. *New Phytologist*, 202(3), 772–783. https://doi.org/10.1111/nph.12741
- Turcotte, A., Morin, H., Krause, C., Deslauriers, A., & Thibeault-Martel, M. (2009). The timing of spring rehydration and its relation with the onset of wood formation in black spruce. *Agricultural and Forest Meteorology*, *149*(9), 1403–1409. https://doi.org/10.1016/j.agrformet.2009.03.010

- Turcotte, A., Rossi, S., Deslauriers, A., Krause, C., & Morin, H. (2011). Dynamics of Depletion and Replenishment of Water Storage in Stem and Roots of Black Spruce Measured by Dendrometers. *Frontiers in Plant Science*, 2. https://doi.org/10.3389/fpls.2011.00021
- Vaganov, E. A. (1990). The traheidogram method in tree-ring analysis and its application. In: Cook ER, Kairiuktis LA (eds) Methods of dendrochronology. Applications in the environmental sciences. 63–75.
- Vaganov, E. A., Schulze, E.-D., Skomarkova, M. V., Knohl, A., Brand, W. A., & Roscher, C. (2009). Intraannual variability of anatomical structure and  $\delta$ 13C values within tree rings of spruce and pine in alpine, temperate and boreal Europe. *Oecologia*, *161*(4), 729–745. https://doi.org/10.1007/s00442-009-1421-y
- Verheyden, A., Helle, G., Schleser, G. H., Dehairs, F., Beeckman, H., & Koedam, N. (2004). Annual cyclicity in high-resolution stable carbon and oxygen isotope ratios in the wood of the mangrove tree *Rhizophora mucronata*. *Plant, Cell & Environment*, *27*(12), 1525–1536. https://doi.org/10.1111/j.1365-3040.2004.01258.x
- Verlinden, M. S., Fichot, R., Broeckx, L. S., Vanholme, B., Boerjan, W., & Ceulemans, R. (2015). Carbon isotope compositions ( $\delta^{13}$  C) of leaf, wood and holocellulose differ among genotypes of poplar and between previous land uses in a short-rotation biomass plantation. *Plant, Cell & Environment*, 38(1), 144–156. https://doi.org/10.1111/pce.12383
- Vieira, J., Carvalho, A., & Campelo, F. (2020). Tree Growth Under Climate Change: Evidence From Xylogenesis Timings and Kinetics. *Frontiers in Plant Science*, *11*, 90. https://doi.org/10.3389/fpls.2020.00090
- Voelker, S. L., Brooks, J. R., Meinzer, F. C., Anderson, R., Bader, M. K. F., Battipaglia, G., Becklin, K. M., Beerling, D., Bert, D., Betancourt, J. L., Dawson, T. E., Domec, J. C., Guyette, R. P., K??rner, C., Leavitt, S. W., Linder, S., Marshall, J. D., Mildner, M., Og??e, J., ... Wingate, L. (2016). A dynamic leaf gas-exchange strategy is conserved in woody plants under changing ambient CO2: Evidence from carbon isotope discrimination in paleo and CO2 enrichment studies. *Global Change Biology*, 22, 889–902. https://doi.org/10.1111/gcb.13102
- Von Arx, G., Archer, S. R., & Hughes, M. K. (2012). Long-term functional plasticity in plant hydraulic architecture in response to supplemental moisture. *Annals of Botany*, *109*(6), 1091–1100. https://doi.org/10.1093/aob/mcs030
- Von Arx, G., Arzac, A., Fonti, P., Frank, D., Zweifel, R., Rigling, A., Galiano, L., Gessler, A., & Olano, J. M. (2017). Responses of sapwood ray parenchyma and non-structural carbohydrates of *Pinus sylvestris* to drought and long-term irrigation. *Functional Ecology*, *31*(7), 1371–1382. https://doi.org/10.1111/1365-2435.12860
- Warren, C., McGrath, J., & Adams, M. (2001). Water availability and carbon isotope discrimination in conifers. Oecologia 127: 476-486. *Oecologia*, 127, 476–486. https://doi.org/10.1007/s004420000609
- Warren, C. R., & Adams, M. A. (2004). What determines rates of photosynthesis per unit nitrogen in Eucalyptus seedlings? *Functional Plant Biology*, *31*(12), 1169. https://doi.org/10.1071/FP04115

- Waterhouse, J. S., Switsur, V. R., Barker, A. C., Carter, A. H. C., & Robertson, I. (2002). Oxygen and hydrogen isotope ratios in tree rings: How well do models predict observed values? *Earth and Planetary Science Letters*, 201(2), 421–430. https://doi.org/10.1016/S0012-821X(02)00724-0
- Way, D. A., & Oren, R. (2010). Differential responses to changes in growth temperature between trees from different functional groups and biomes: A review and synthesis of data. *Tree Physiology*, 30(6), 669–688. https://doi.org/10.1093/treephys/tpq015
- Wigley, T. M. L., Briffa, K. R., & Jones, P. D. (1984). On the Average Value of Correlated Time Series, with Applications in Dendroclimatology and Hydrometeorology. *Journal of Applied Meteorology and Climatology*, 23(2), 201–213. https://doi.org/10.1175/1520-0450(1984)023<0201:OTAVOC>2.0.CO;2
- Wiley, E., & Helliker, B. (2012). A re-evaluation of carbon storage in trees lends greater support for carbon limitation to growth. *New Phytologist*, *195*(2), 285–289. https://doi.org/10.1111/j.1469-8137.2012.04180.x
- Willmott, C., & Matsuura, K. (2005). Advantages of the mean absolute error (MAE) over the root mean square error (RMSE) in assessing average model performance. *Climate Research*, *30*, 79–82. https://doi.org/10.3354/cr030079
- Wood, S. (2006). Generalized Additive Models: An Introduction with R.Chapman and Hall/CRC, Boca Raton, FL.
- Xi, Y., Zhang, W., Wei, F., Fang, Z., & Fensholt, R. (2024). Boreal tree species diversity increases with global warming but is reversed by extremes. *Nature Plants*, *10*(10), 1473–1483. https://doi.org/10.1038/s41477-024-01794-w
- Xu, G., Liu, X., Hu, J., Dorado-Liñán, I., Gagen, M., Szejner, P., Chen, T., & Trouet, V. (2022). Intra-annual tree-ring δ18O and δ13C reveal a trade-off between isotopic source and humidity in moist environments. *Tree Physiology*, tpac076. https://doi.org/10.1093/treephys/tpac076
- Yang, Z., Liu, J., Tischer, S. V., Christmann, A., Windisch, W., Schnyder, H., & Grill, E. (2016). Leveraging abscisic acid receptors for efficient water use in Arabidopsis. *Proceedings of the National Academy of Sciences*, 113(24), 6791–6796. https://doi.org/10.1073/pnas.1601954113
- Ye, Y., Liu, Y., Ren, M., Cai, Q., Sun, C., Li, Q., Song, H., Ye, M., & Zhang, T. (2023). Responses of Tree Growth and Intrinsic Water Use Efficiency to Climate Factors and Human Activities in Upper Reaches of Tarim River in Alaer, Xinjiang, China. *Forests*, *14*(9), Article 9. https://doi.org/10.3390/f14091873
- Young, G. H. F., Demmler, J. C., Gunnarson, B. E., Kirchhefer, A. J., Loader, N. J., & McCarroll, D. (2011). Age trends in tree ring growth and isotopic archives: A case study of Pinus sylvestris L. from northwestern Norway. *Global Biogeochemical Cycles*, 25(2). https://doi.org/10.1029/2010GB003913
- Ziaco, E., Biondi, F., & Heinrich, I. (2016). Wood Cellular Dendroclimatology: Testing New Proxies in Great Basin Bristlecone Pine. *Frontiers in Plant Science*, 7. https://doi.org/10.3389/fpls.2016.01602

Zuidema, P. A., Poulter, B., & Frank, D. C. (2018). A Wood Biology Agenda to Support Global Vegetation Modelling. *Trends in Plant Science*, *23*(11), 1006–1015. https://doi.org/10.1016/j.tplants.2018.08.003